UNIVERSIDAD POLITÉCNICA SALESIANA

LA GRANJA 44

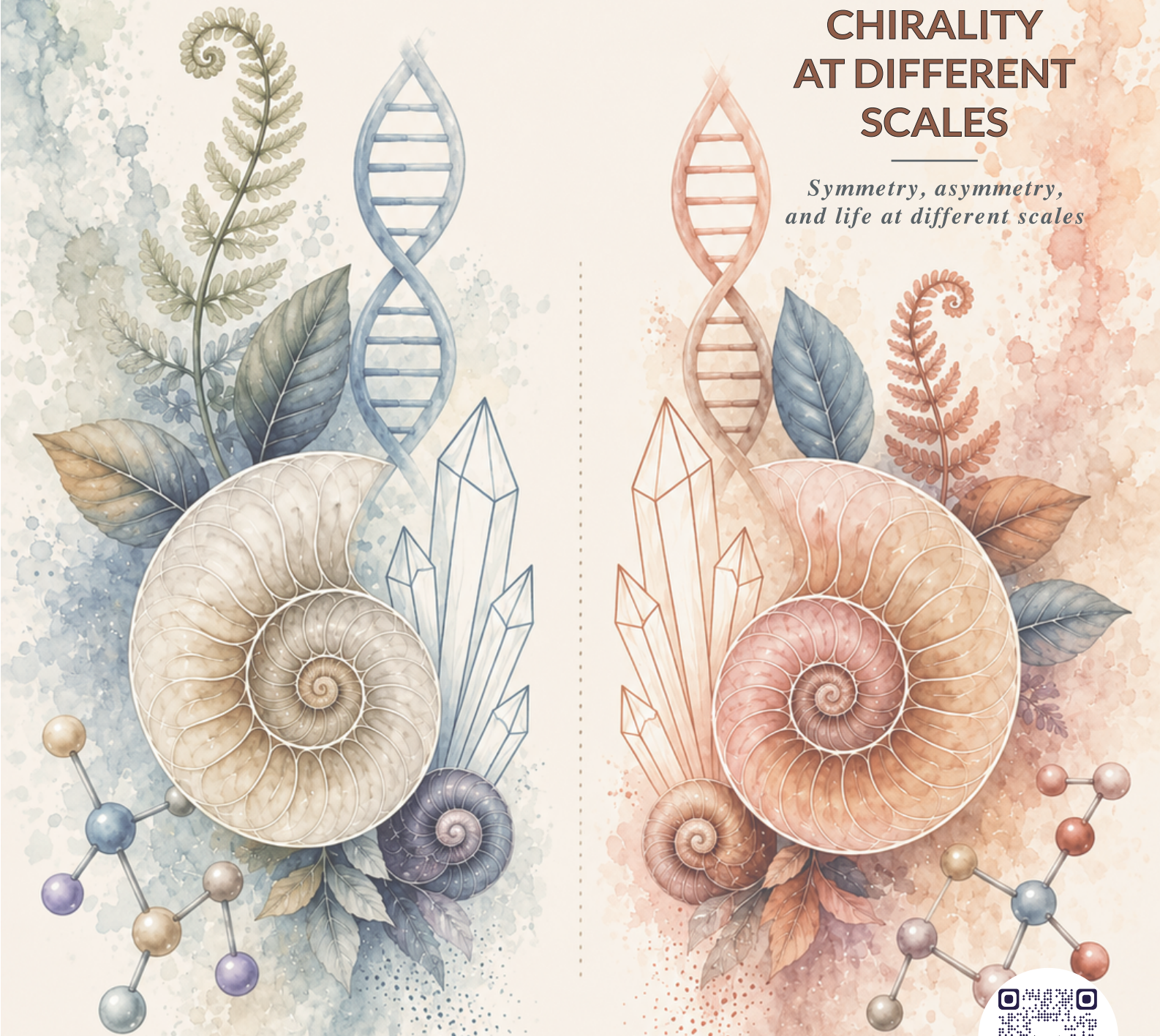
THE LIFE SCIENCE JOURNAL

Num. (2)

SPECIAL ISSUE

CHIRALITY AT DIFFERENT SCALES

Symmetry, asymmetry, and life at different scales



ISSN impress:1390-3799 / ISSN electronic:1390-8596

La Granja: Journal of Life Sciences. • Volume 44 • Number 2 • September 2026 – February 2027. A semiannual journal of Life Sciences of the Universidad Politécnica Salesiana of Ecuador. An international bilingual publication devoted to studies related to environmental, earth, agricultural, biological, and life sciences, as well as their cross-cutting areas of knowledge. The ideas and opinions expressed in the contributions are the sole responsibility of the authors.

Editorial Board

Editors-in-Chief
Dr. Ignacio de los Ríos,
Universidad Politécnica de Madrid, España
Dra. Sheila Serrano Vincenti,
Universidad Politécnica Salesiana, Ecuador

Guest Editors of the Special Issue of Chirality across scales

Dr. Alejandro Heredia Barbero,
Universidad Nacional Autónoma de México
Dr. Igor Bdikin,
Universidade de Aveiro, Portugal
MSc. Betsaida Lucinda Ávila Suárez,
Universidad Nacional Autónoma de México
Dra. María Noble Terán,
Universidad Autónoma del Estado de Morelos, México
Dr. Hugo Iván Cruz Rosas,
Universidad Autónoma del Estado de Morelos, México

Section Editors

Earth sciences
Dr. Thomas Condom,
Institut de Recherche Pour Le Développement, Francia
Dr. César Iván Álvarez,
University of Augsburg, Alemania
Dr. Charles Cachipuendo,
Universidad Politécnica Salesiana, Ecuador

Agricultural and Veterinary Sciences
Dra. Nora Mestorino,
Universidad Nacional de La Plata, Argentina.
Dra. Nancy Bonifáz,
Universidad Politécnica Salesiana, Ecuador.
Dra. Narcisa Relqueme,
Universidad Politécnica Salesiana, Ecuador.

Biological, Biotechnological, Chemical and related Sciences
Dr. Paco Noriega,
Universidad Politécnica Salesiana, Ecuador.
Dr. Lorenzo Guerrini,
Universita di Firenze, Italia.
Dr. Alejandro Heredia Barbero,
Universidad Nacional Autónoma de México (UNAM), México.
Dr. Elena Coyago,
Universidad Politécnica Salesiana, Ecuador.

Environmental Sciences
Dr. Jorge G Figueroa,
Universidad Técnica Particular de Loja (UTPL), Ecuador.
Dra. María Rocío Rodríguez,
Universidad de Cádiz, España.

Final Photo
Geometries of Life
Autor: Jonathan González Chuqui

Ethics and Bioethics Committee
Dra. Gladys Bustamante,
Universidad Mayor de San Andrés, Bolivia.
Comité Iberoamericano de Ética (CIEB)
Dr. Ángel Acevedo-Duque,
Universidad Autónoma de Chile, Chile.
Dra. Elena Coyago,
Universidad Politécnica Salesiana, Ecuador.

International coeditor in English
Dr. Lorenzo Guerrini,
Universita di Firenze, Italia.

International Coeditor in Portuguese
Dra. Rocio Elizabeth Contero Callay,
Universidad Politécnica Salesiana, Ecuador.

Publication Board
Dr. Juan Cárdenas Tapia PRESIDENT
Dr. José Juncosa Blasco ABYA-YALA
Dr. Esteban Inga VICE CHANCELLOR FOR RESEARCH
Dr. Angel Torres-Toukoumidis EDITOR OF UNIVERSITAS
Dr. Jaime Padilla Verdugo EDITOR OF ALTERIDAD
Dra. Sheila Serrano Vincenti EDITOR OF LA GRANJA
Dr (c). Jorge Cueva Estrada EDITOR OF RETOS
Dr. John Calle Sigüencia EDITOR OF INGENIUS
Dra. Floralba Aguilar Gordón EDITOR OF SOPHIA
Dra. Betty Rodas Soto EDITOR OF UTOPÍA
Dra. Mónica Ruiz Vásquez EDITOR OF NOTI-UPS
Dr. Jorge Altamirano Sánchez EDITOR JOURNAL CÁTEDRA UNESCO
MSc. David Armendáriz González EDITOR WEB
Dr. Angel Torres-Toukoumidis EDITOR GENERAL

Technical Board
Lcda. María José Cabrera (Marcalyc Technique)
Lcdo. Christian Arpi (Community Manager Coordinator)
MSc. Mariana Luna (Editorial Assistant)
Dr. Danny Vargas (Assistant Editor)

Publications Service
Hernán Hermosa (General Coordination)
Marco Gutiérrez (OJS Support)
Mariana Luna (Layout)
Adriana Curiel (Translator)

Publisher
Editorial Abya-Yala (Quito, Ecuador)
12 de Octubre Ave. N-422 and Wilson St.
Block A, UPS Quito, Ecuador
P.O. Box 17-12-719
Phone: (+593-2) 3962800 ext. 2638
Email: editorial@abyayala.org

Cover and Back Cover Photo
"Chirality as an interplay of symmetry and asymmetry across different scales of nature. The mirror-image compositions integrate biological, crystalline, and molecular forms to represent how handedness emerges from inert matter to life."
Authors: Guest Editors

Copyright: La Granja: Journal of Life Sciences, Universidad Politécnica Salesiana. Total or partial reproduction of this journal is permitted provided that the source is cited.

La Granja: Revista de Ciencias de la Vida

Volume 44, Number 2, September 2026 – February 2027

ISSN print 1390-3799 • ISSN electronic 1390-8596

The management of La Granja is carried out using the following parameters:

- The journal uses the academic anti-plagiarism system iThenticate Professional Plagiarism Prevention
- The items have an identification code (*Digital Object Identifier*) doi
- The editorial process is managed through the *Open Journal System* OJS Open Journal Systems

It is an open access publication licensed under *Creative Commons*

CC BY NC SA

The *copyright* and *postprint* usage policies are published in the *Sherpa/Romeo* Self-Archiving Policy Repository.

The articles in this edition can be consulted at `https://lagranja.ups.edu.ec/`

ABYA YALA | UNIVERSIDAD POLITÉCNICA SALESIANA

Universidad Politécnica Salesiana del Ecuador

LA GRANJA, is indexed in the following databases and scientific information systems:

SELECTIVE INTERNATIONAL DATABASES

Scopus®

INDEXED IN EMERGING SOURCES CITATION INDEX CLARIVATE ANALYTICS

SciELO

Google scholar

EuroPub Directory of Academic and Scientific Journals

BASE

JOURNAL EVALUATION PLATFORMS

MIAR

CABELLS SCHOLARLY ANALYTICS

DIRECTORIOS SELECTIVOS

latindex

Journal Seeker Research Bible

AcademicKeys UNLOCKING ACADEMIC CAREERS

SELECTIVE NEWSPAPER ARCHIVES

redalyc.org

REDIB Red Iberoamericana de Innovación y Conocimiento Científico

OPEN ACCESS SCIENTIFIC LITERATURE SEARCH ENGINES

DOAJ DIRECTORY OF OPEN ACCESS JOURNALS

EXALEAD

PUBLISHERS' COPYRIGHT POLICIES AND SELF-ARCHIVING

SHERPA/RoMEO

Other Bibliographic Databases

Dialnet

Catalogue of International University Libraries

American University of Sharjah 1997

Universiteit van Pretoria
University of Pretoria
Yunibesithi ya Pretoria

Maastricht University

Erasmus Universiteit Rotterdam

Hanzehogeschool Groningen

University of Skövde

Bishop Grosseteste University

DePaul University College of Law

Bethune-Cookman University 1923 1904 1872 2007

Université Sainte Anne

Plymouth State University

DePaul University

Franklin College

University of Nebraska Omaha

Southwestern University

Texas A&M University San Antonio

Simpson University

AUT University

Claremont McKenna College

ExLibris Primo

University of the West

Universidad de Navarra

Muhlenberg College

Franklin & Marshall College

Tyndale University College & Seminary

The University of North Carolina Greensboro

UNC Charlotte

Advisory Board

Dr. Guillermo Marcillo, University of Illinois Urbana Champaign, EEUU
Dr. Alessandro Medici, Universita di Ferrara, Italia
Dr. John Mejía, Universidad de Nevada, Estados Unidos
Dra. Enrica Caporali, Universita di Firenze, Italia
Dr. Ankit Singla, Ministry Office of Agriculture, Co-operation and Farmers Welfare, India Government
Dra. Paola VitaFinzi, Universita di Pavia, Italia
Dr. Geovanni Vidari,Universita di Pavia, Italia
Dr. Flavio Contreras-Torres, Universidad Autónoma de México, México
Dr. Miguel A. Altieri, University of California, EEUU
Dra. Clara Inés Nicholls, University of California, EEUU
Dr. Jaime Vadell Adrover, Universidad de las Islas Baleares, España
Dra. Janeth Patricia Muñoz Eraso, Pontificia Universidad Javeriana, Colombia.
Dr. Marcos Villacís, Escuela Politécnica Nacional, Ecuador
Dra. Silvia Perez Damonte, Universidad de Buenos Aires, Argentina
Dr. Fernando Funes Monzote, Universidad de Matanzas, Cuba
Dra. Alessandra Guerrini, Universita di Ferrara, Italia
Dr. Giovanni Bernacchia,Universita di Ferrara, Italia
Proff. León Escobar Moreira, SYNAPTRONIC, EEUU
Dr. Lorenzo Guerrini, Universita di Firenze, Italia
Dr. José Luis Santos. International CLIVAR Project Office, China
Dr. Solveig Tosi,Universita di Pavia, Italia
Dra. Priscila dos Santos Silva, Universidad de Sao Paulo, Brasil
Dra. Connie Gallardo Vela, Universidad de Sao Paulo, Brasil
Dr. Thomas Condom, Institut de Recherche Pour Le Développement, Francia
Dr. Leonardo Basile, Escuela Politécnica Nacional, Ecuador
Dra. Claudinéia Brazil, Faculdade Dom Bosco de Porto Alegre, Brasil
Dr. Alejandro Fontana, Universidad de Piura, Perú
Dra. Adriana Sánchez Urdaneta, Universidad de Zulia, Venezuela
Dr. Emmanuel Donkor, Kwame Nkrumah University of Science and Technology, West Africa
Dr. Jorge Palomeque Santiago, Instituto Mexicano del Petróleo, México
Dr. Alejandro Heredia Barbero, Universidad Nacional Autónoma de México, Facultad de Ciencias
Dr. Carlos Hernandez Medina, Centro Universitario Municipal Camajuaní, Cuba
Dr. Daniel A. Lowy, Northern Virginia Community College, EEUU
Dr. László Palcsu, Institute of Nuclear Research of the Hungarian Academy of Sciences,Hungría
Dr. Marjan Temovski, Institute of Nuclear Research of the Hungarian Academy of Sciences, Hungría
Dr. Elemer Laszlo, Institute of Nuclear Research of the Hungarian Academy of Sciences,Hungría
Dr. Pablo Marini, Universidad Nacional de Rosario, Argentina
Dr. Antonio Panico Università degli Studi Pegaso, Italia
Dr. Fernando Bimbela, Univerdidad Publica de Navarra, España
Dr. Panagiotis Kechagiopoulos, University of Aberdeen, Reino Unido.
Dr. Carlo Visconti, Politecnico di Milano, Italia
Dra. Marta Elena Alonso, Universidad de León, España
Dra. Alison Hanlon, University College Dublin, Irlanda
Dr. Mehmood Ali, NED University of Engineering and Technology, Pakistán
Dra. Ana Teodoro, Universidade do Porto, Portugal

International Reviewers Board

Dr. Guillermo Marcillo, University of Illinois Urbana Champaign, EE.UU.
Dr. Antonio Panico Università degli Studi Pegaso, Italia
Dr. John Mejía, Universidad de Nevada, EE.UU.
Dra. Enrica Caporali, Universita di Firenze, Italia
Dra. Nancy Bonifáz, Universidad Politécnica Salesiana, Ecuador
Dra. Paola VitaFinzi, Universita di Pavia, Italia
Dr. Flavio Contreras-Torres, Universidad Autónoma de México, México
Dr. Alejandro Heredia Barbero, Universidad Nacional Autónoma de México (UNAM), México
Proff. León Escobar Moreira, SYNAPTRONIC, EE.UU.
Dr.Geovanni Vidari,Universita di Pavia, Italia
Dra. Lorena Meneses, Pontificia Universidad Católica del Ecuador, Ecuador
Dr. Fernando Funes Monzote, Universidad de Matanzas, Cuba
Dr. Nicolás Vásquez, Escuela Politécnica Nacional, Ecuador
Dr. Giovanni Bernacchia,Universita di Ferrara, Italia
Dr. Juan H. Avellaneda Cevallos, Universidad Técnica Estatal de Quevedo Ecuador
Dr. Lorenzo Guerrini, Universita di Firenze, Italia
Dr. José Luis Santos, International CLIVAR Project Office, China
Dr. Solveig Tosi, Universita di Pavia, Italia
Dra. Pamela Jaramillo, Mikuna-Food Science and Technology, Ecuador
Dr. Juan Enrique Tacoronte, Universidad Central del Ecuador, Ecuador
Dra. Mercy Bordor, Escuela Politécnica del Litoral
Dr. Christian Domínguez, Universidad Politécnica Salesiana, Ecuador
MSc. Laura Huachi, Universidad Politécnica Salesiana
Dra. Priscila dos Santos Silva, Universidad de Sao Paulo, Brasil
Dr. Pablo Marini, Universidad Nacional de Rosario, Argentina
Dra. Claudineia Brazil, Universidad de Don Bosco de Puerto Alegre, Brasil
Dra. Adriana Sánchez Urdaneta, Universidad de Zulia, Venezuela
MSc. Bernardo Navarrete, Instituto Nacional de Investigaciones Agropecuarias-INIAP, Ecuador
Dr. Jorge Palomeque Santiago, Instituto Mexicano del Petróleo, México
Dr. Antonio Panico Università degli Studi Pegaso, Italia
MSc. Patricio Yánez Moretta, Universidad Internacional del Ecuador, Ecuador
Dr. Emmanuel Donkor, Kwame Nkrumah University of Science and Technology, West Africa
Dr. Carlos Hernandez Medina, Centro Universitario Municipal Camajuaní, Cuba
Dr. Daniel A. Lowy, Northern Virginia Community College, EE.UU.
Dr. Marjan Temovski, Institute of Nuclear Research of the Hungarian Academy of Sciences, Hungría
Dr. Elemer Laszlo, Institute of Nuclear Research of the Hungarian Academy of Sciences,Hungría
Dr. Manuel Maldonado, Escuela Politécnica del Ejército, Ecuador.
Dr. Mehmood Ali, NED University of Engineering and Technology, Pakistán
Dr. Oscar Peña Cáceres, Universidad Nacional de Piura, Perú
Dra. Ana Teodoro, Universidade do Porto, Portugal
Dr. Panagiotis Kechagiopoulos, University of Aberdeen, Reino Unido
Dr. Carlo Visconti, Politecnico di Milano, Italia
Dr. Fernando Bimbela, Universidad Pública de Navarra, España
Dra. Marta Elena Alonso, Universidad de León, España
Dra. Alison Hanlon, University College Dublin, Irlanda
Dr. Sabino Armenise, Universidad Rey Juan Carlos, España
Dr. Jesús Evaristo Tumi Quispe, Universidad Nacional del Altiplano, Perú

Reviewers Volume 44 Number 2

Revisores Richard Alcides Molina Alvarez, Universidade Federal de Roraima, Brasil.
Gabriela Méndez, Universidad Politécnica Salesiana, Ecuador.
Jaime Naranjo-Morán, Universidad Politécnica Salesiana, Ecuador.
Paco Fernando Noriega-Rivera, Universidad Politécnica Salesiana, Ecuador.
Ulbio Alcívar-Cedeño, Universidad Técnica de Manabí, Ecuador.
Johana Meneses Morillo, Universidad Politécnica Salesiana, Ecuador.
Jorge Toro, Universidad de Investigación de Tecnología Experimental Yachay, Ecuador.
Paul Esteban Bravo López, Universidad del Azuay,
Instituto de Estudios de Régimen Seccional del Ecuador (IERSE), Ecuador.
Fredy Cuarán, Universidad Politécnica Salesiana, Ecuador.
Roxanna Palma, Universidad Técnica Estatal de Quevedo, Ecuador.
Ximena Borja, Universidad Politécnica Salesiana, Ecuador.
René Parra, Universidad San Francisco de Quito, Ecuador.
Cristian Zambrano, Instituto Nacional de Investigaciones Agropecuarias (INIAP), Ecuador.
Rosita Graciela Espinoza Gavilanes, Universidad Politécnica Salesiana, Ecuador.
Mario Guadalupe González Pérez, Universidad de Guadalajara, México.
William Sacher, Universidad Andina Simón Bolívar, Ecuador.
Daniel Acosta-Avalos, Centro Brasileiro de Pesquisas Físicas (CBPF), Brasil.
Yolanda Marina Vargas Rodríguez, Universidad Nacional Autónoma de México, México.
María Soledad Córdova Aguilar, Universidad Nacional Autónoma de México, México.
Héctor Vázquez López, Universidad Nacional Autónoma de México, México.
Hugo I. Cruz Rosas, Universidad Autónoma del Estado de Morelos, México.
María Eugenia Noble Terán, Universidad Autónoma del Estado de Morelos, México.

The Editorial Board would like to express its deep gratitude to the peer reviewers who contributed their time and expertise to ensure the scientific quality of the articles published in this issue.

Index

Editorial 8

Special issue: Quality of life, development and social responsibility, climate change and the environment

Environmental transformations in Latin America, a critical review of the sustainable practices in the territories 13
Mayel Castillo, Lina Alfonso, Daniel Valderrama and Néstor Pachón.

The role of NEAZDP on social mobility of poverty in Yobe State of Nigeria 33
Mohammed Sanusi Sadiq and Isiyaku Jawa Grema.

Development of an Instrument Based on the EGCI Model to Measure Sustainable Water Use Practices among Citizens 64
Jessica Müller, Angel Acevedo, Montserrat Sánchez, Irma Verges and Rina Álvarez.

Critical points and socio-ecological dynamics of tomato *(Solanum lycopersicum L.)* cultivation in low-tech greenhouse systems in Colombia 76
Jessica Müller, Angel Acevedo, Montserrat Sánchez, Irma Verges and Rina Álvarez.

Earth Sciences

Meteorological variability and its impact on agricultural activities in the Ecuadorian Amazon in Pastaza (2011–2021) 97
Brigitte Leiva, Julia Maza and Reni Vinocunga.

Agricultural Sciences

Quantitative analysis of crop richness and monoculture adoption in Ecuador 114
Cristian Vasco and Lourdes Caisaguano.

***In vitro* propagation of banana *(Musa spp.)* by somatic embryogenesis** 128
Jessenia Lucero, Jorge Manzano, Iliana Loaiza and Yamile Orellana.

Effects of lead and chromium on germination and root architecture of *Typha latifolia* (Typhaceae) seedlings 145
Renato Oquendo, Loiret Fernández, Galo Pabón and Lucía Vásquez.

Biotechnology

Valorization of banana peel *(Musa paradisiaca)* as a raw material for biopolymer production 160
Jimena Taco, Ronald Jiménez and Maria Soto.

Optimization of the acid hydrolysis factors for obtaining glucose from banana, cacao, African palm, and sugarcane bagasse residues 171
Mónica F. Abril, Angélica M. Vele and Verónica Pinos

Guidelines 184

La granja:
Revista de
Ciencias de la Vida

Editorial

ABYA YALA | UNIVERSIDAD POLITÉCNICA SALESIANA

Dear reader,

Since the pioneering experiments of Louis Pasteur, conducted in collaboration with Marie Laurent in the nineteenth century, chirality has captivated scientific, artistic, and philosophical thought. By observing crystals derived from tartaric acid, Laurent and Pasteur distinguished mirror-image forms and opened a window onto one of the most profound problems in science: the preference for one symmetry over another in matter. In living systems, this asymmetry is clearly manifested, as certain molecular forms predominate over their mirror images and acquire specific functions. Chirality can be recognized at multiple scales, from subatomic particles to biological systems and cosmological structures. This special issue of *La Granja: Revista de Ciencias de la Vida*, in collaboration with the *Institute of Nuclear Sciences of the National Autonomous University of Mexico (UNAM), the Chemical Research Center of the Autonomous University of the State of Morelos (UAEM), Mexico, the Faculty of Sciences of the National Autonomous University of Mexico (UNAM)*, and the *Interdisciplinary Research Network on Chirality (RiiQ)*, explores some of its multiple facets and its role in the organization of matter and living systems.

The study of chiral symmetry breaking in crystalline systems has provided a robust theoretical and experimental model for understanding how asymmetry may have emerged before the origin of life. The crystallization of $NaClO_3$, an achiral compound in solution that forms enantiomorphic conglomerates, demonstrates that chirality can emerge at the supramolecular level from simple systems. This phenomenon is addressed in the manuscript by Cruz-Rosas, H. et al., "*Chiral Symmetry Breaking in $NaClO_3$ Crystals as a Model for the Study of Biological Homochirality*," which analyzes experimental conditions that allow a system initially lacking chiral preference to transition toward states of high enantiomeric purity.

Processes such as secondary nucleation and Viedma deracemization show that local fluctuations, coupled with dissolution and crystallization cycles induced by mechanical or thermal energy, can amplify an asymmetry without necessarily requiring an initial external bias. These nonequilibrium processes offer plausible scenarios for understanding how an initially racemic prebiotic chemistry could have evolved toward chiral preferences. However, the transition between this physicochemical asymmetry and its fixation in self-replicating systems remains an open question. Were crystalline processes decisive in biasing chemical evolution, or did they act jointly with other physical mechanisms?

Biological homochirality, particularly the predominance of L-amino acids in protein synthesis, has traditionally been considered a characteristic property of life. However, as Díaz Aguilar, J. et

La Granja:*Revista de Ciencias de la Vida* 44(2) 2026: 8-12
©2026, Universidad Politécnica Salesiana, Ecuador.

al. explain in "*A Look at* D*-Amino Acids in Living Organisms*," this view has been enriched by the discovery of essential functions performed by D-enantiomers in different organisms.

D-amino acids such as D-alanine and D-glutamate are fundamental components of bacterial peptidoglycan, whereas D-serine and D-aspartate perform relevant functions in mammals. This coexistence raises a central question: how do organisms preserve the chiral fidelity of their proteome while selectively using the opposite enantiomer? Enzymatic mechanisms such as D-aminoacyl-*tRNA* deacylases contribute to this control. Rather than absolute homochirality at all levels, life thus reveals a scenario in which homochirality and heterochirality can functionally coexist.

At a higher level of complexity, chirality is also manifested in the organization of genetic information. The work by Rios-Willars et al., "*Tendency Toward Functional Asymmetry and Microsatellite-Induced Helical Chirality in Staphylococcus aureus*," explores this dimension through the analysis of repetitive sequences or microsatellites. The differences observed in the distribution of motifs such as ATAT, AGAG, and ACAC suggest a reorganization of repetitive architecture with possible structural and evolutionary implications. This asymmetry introduces a spatial and conformational dimension into genome organization that transcends its description as a simple linear sequence.

We currently have more tools available to understand chiral symmetry breaking and its amplification, yet we have still not unraveled why asymmetry appears so persistently in nature. Is the chiral preference of biological systems the consequence of initial fluctuations amplified through nonlinear and autocatalytic processes, or does it reflect more fundamental asymmetries in the laws of physics, such as parity violation in the weak interaction? The answer may lie at the convergence of different levels of explanation.

This search resonates with the work of Germinal Cocho Gil† and Thomas Buhse†, two leading figures in the study of complexity and chirality, whom we miss and remember with admiration in these pages. Their contributions broadened our understanding of irreversibility, symmetry breaking, and the emergence of order in chemical and biological systems.

In this context, the Interdisciplinary Network for Research on Chirality in Mexico constitutes a space for dialogue and collaboration among those who study these phenomena from different disciplines. Its annual meeting, which this year will be held at the Institute of Nuclear Sciences of UNAM on November 12, 2026, represents an opportunity to share ideas and chart new avenues of research. This special issue of *La Granja* contributes to this effort by providing a platform for disseminating knowledge and stimulating debate.

As living beings, we embody symmetry breaking in our cells, amino acids, proteins, and in the helical structure of DNA. Molecular asymmetry is not merely a geometric curiosity: it is intimately linked to the organization and functionality of life. However, life is also a dynamic and fragile process. When it ends, the slow process of racemization begins; the molecular orientation associated with function fades, and the system once again moves toward thermodynamic equilibrium. The amino acids that once formed part of active proteins progressively tend toward racemic states, like an echo of the prebiotic chemistry of the early Earth from which they emerged.

©2026, Universidad Politécnica Salesiana, Ecuador.

Chirality at different scales confronts us with questions that span physics, chemistry, and biology, and invites us to reflect on the relationship between elementary particles, life, and the cosmos; between order and equilibrium; between functional asymmetry and thermodynamic symmetry. This special issue of *La Granja* does not seek to offer definitive answers, but rather to delineate some of the frontiers that our academic community continues to explore. In this sense, it constitutes an invitation to critically examine one of the most persistent questions in science: how, from matter and its interactions, could the organization that gave rise to life have emerged?

Following the three manuscripts in the special section on chirality, the issue opens to seven miscellaneous articles in the life sciences. Although diverse, they share the same purpose: to transform rigorous observation into knowledge capable of explaining the complexity of living systems and guiding their care. Watersheds, reserves, native species, and foods thus trace a continuity between fundamental research, conservation, and innovation.

Two studies highlight the need for continuous observation of environmental changes. First, Raúl Moreno and María Flores analyze the Wawayme River watershed in Ecuador, where the reduction in vegetation cover associated with mining activities modifies the hydrological response and demonstrates that changes in land use directly affect water availability and dynamics. The study emphasizes the importance of combining monitoring, mitigation, and conservation with actions that strengthen the resilience of local communities.

Meanwhile, Jaime Enrique Maza, Hugo Anazco, Darwin Poma, and Alex Luna study the Arenillas Ecological Reserve. The analysis identifies high-risk areas near roads and productive activities and confirms that protecting the interior of a reserve is insufficient if its boundaries are not managed. Conservation requires protecting adjacent areas, reducing anthropogenic pressures, and maintaining connectivity with other natural remnants.

Regional biodiversity, in turn, is presented as a source of knowledge and added value. Laura Scalvenzi, Sting Luna Fox, and Matteo Radice optimize a freeze-dried extract of *Ilex guayusa* rich in caffeine. Ultrasound-assisted aqueous extraction and product characterization provide a technological basis for developing ingredients intended for energy drinks. The study shows how an Amazonian resource can generate added value when innovation is grounded in rigorous and responsible processes.

Likewise, Johana Meneses, Stephanie Moncayo, María Elena Maldonado, and Ramiro Acurio evaluate extracts of *Vaccinium floribundum* against *Staphylococcus saprophyticus*. The marked antimicrobial activity observed *in vitro* links the phenolic and anthocyanin richness of mortiño with a promising response. The study broadens the scientific horizon of an Andean species of cultural and productive relevance.

Food systems complete this journey. David Vivanco, Haydee Rodríguez, Raúl Siche, and David Callirgos optimize the drying of Muscat of Alexandria grapes. Indirect solar drying reduces processing time and maintains high acceptability, demonstrating that the use of mathematical models can improve efficiency without compromising quality. This approach offers relevant alternatives for agri-food chains seeking to make better use of solar energy.

Likewise, Luis David Jarquín-Izaguirre, Luisa

La Granja:*Revista de Ciencias de la Vida* 44(2) 2026: 8-12
©2026, Universidad Politécnica Salesiana, Ecuador.

Fernanda Correa Díaz, and Saúl Alejandro Jarquín-Izaguirre review the management of *Zabrotes subfasciatus* in common bean. The integration of cultural, physical, chemical, and plant-breeding methods emerges as the most robust strategy for protecting stored grains and reducing dependence on insecticides. Monitoring, resistant varieties, and producer training are essential for food security.

Environmental quality is also expressed through what is not always visible. The study conducted in Espíndola by David del Pozo, María de los Ángeles Álvarez, and Bryan Valle found concentrations of settleable particulate matter below the regulatory limit, but confirmed the presence of heavy metals. Compliance with a standard, therefore, should not be interpreted as the absence of risk. Strengthening air-quality monitoring in rural communities will make it possible to identify at an early stage the effects of vehicular emissions and extractive activities, areas in which information remains limited.

Taken together, this issue articulates two complementary perspectives within the life sciences. The special section on chirality investigates the fundamental asymmetries involved in the organization of matter and biological systems; the miscellaneous section extends this same commitment to understanding toward concrete challenges involving territories, biodiversity, food production, and environmental quality. From molecular architecture to watershed dynamics or forest conservation, the works brought together here confirm that life can only be understood through dialogue across scales, disciplines, and contexts. With this issue, *La Granja* renews its commitment to plural, rigorous, and context-sensitive science, capable of posing fundamental questions while simultaneously providing tools for building healthier, more sustainable, and more resilient futures.

Sincerely,

PhD. Ignacio de los Ríos
Universidad Politécnica de Madrid, España
EDITOR-IN-CHIEF

PhD. Sheila Serrano Vincenti
Universidad Politécnica Salesiana, Ecuador
EDITOR-IN-CHIEF

PhD. Alejandro Heredia Barbero
Universidad Nacional Autónoma de México
GUEST EDITOR

PhD. Igor Bdikin
Universidade de Aveiro, Portugal
GUEST EDITOR

MSc. Betsaida Lucinda Ávila Suárez
Universidad Nacional Autónoma de México
GUEST EDITOR

PhD. María Noble Terán
Universidad Autónoma del Estado de Morelos, México
GUEST EDITOR

PhD. Hugo Iván Cruz Rosas
Universidad Autónoma del Estado de Morelos, México
GUEST EDITOR

©2026, Universidad Politécnica Salesiana, Ecuador.

LA GRANJA:*Revista de Ciencias de la Vida* 44(2) 2026: 8-12
©2026, Universidad Politécnica Salesiana, Ecuador.

La Granja: Revista de Ciencias de la Vida
pISSN:1390-3799; eISSN:1390-8596
https://doi.org/10.17163/lgr.n44.2026.01

Special Issue / Edición Especial
Chirality across scales

Chiral symmetry breaking in $NaClO_3$ crystals as a model for the study of biological homochirality

Ruptura de la simetría quiral en cristales de $NaClO_3$ como modelo para el estudio de la homoquiralidad biológica

Hugo I. Cruz-Rosas*[1,4], María E. Noble-Terán[2,4], José-Manuel Cruz[3,4], Heidi García Quintana[2], Marleen Alejandra Chávez Vidal[2], Fátima del C. Ramírez Hernández[2] and Thomas Buhse[2,4,†]

[1]*Facultad de Ciencias. Universidad Nacional Autónoma de México. [https://ror.org/01tmp8f25]*
[2]*Centro de Investigaciones Químicas – IICBA, Universidad Autónoma del Estado de Morelos, Cuernavaca, Morelos, México. [https://ror.org/03rzb4f20]*
[3]*Facultad de Ciencias en Física y Matemáticas, Universidad Autónoma de Chiapas, Tuxtla Gutiérrez, Chiapas, México. [https://ror.org/04eexme77]*
[4]*Red Interdisciplinaria de Investigaciones en Quiralidad (RiiQ), México.*

*Corresponding author: quetzal@ciencias.unam.mx

Article received on March 26th, 2026. Accepted, after review, on July 06th, 2026. Published on September 1st, 2026.

Abstract

Living systems are composed of chiral molecules. In the absence of asymmetric influences, chemical reactions that generate chiral molecules produce statistically equivalent proportions of left- and right-handed enantiomers (the racemic state). However, biological systems exhibit a marked preference for one enantiomer over the other. The paradigmatic example is the predominant use of L-amino acids in protein synthesis and D-pentose sugars in the synthesis of nucleic acids (DNA and RNA). The asymmetric crystallization mechanisms of sodium chlorate ($NaClO_3$) provide an experimental model for investigating the possible origin of this molecular asymmetry and its relevance to living systems. In this article, we review the mechanisms responsible for the formation of chiral $NaClO_3$ crystals, including amplification and deracemization processes, as well as their potential applications in the production of enantiomerically pure compounds. We also examine the relationship between the chiral asymmetry observed in these inorganic systems and biological homochirality. Finally, we discuss the hypothesis that asymmetric crystallization processes may have occurred on the prebiotic Earth and influenced the molecular dynamics associated with the origin of life. We conclude that $NaClO_3$-based systems provide a useful model for understanding the physical mechanisms capable of generating and amplifying chiral asymmetries from initially symmetric conditions.

Keywords: Homochirality, asymmetric crystallization, deracemization, sodium chlorate ($NaClO_3$), origin of life.

©2026, Universidad Politécnica Salesiana, Ecuador.

Resumen

Los seres vivos están constituidos por moléculas quirales. En ausencia de influencias asimétricas, las reacciones químicas que producen moléculas quirales generan proporciones estadísticamente equivalentes de los enantiómeros izquierdo y derecho (estado racémico). Sin embargo, los sistemas biológicos muestran una marcada preferencia por uno de los enantiómeros. El caso paradigmático es el uso predominante de aminoácidos levógiros (L) en la síntesis de proteínas y de azúcares pentosas dextrógiras (D) en la síntesis de ácidos nucleicos (DNA y RNA). Los mecanismos de cristalización asimétrica del clorato de sodio ($NaClO_3$) constituyen un modelo experimental para estudiar el posible origen de esta asimetría molecular y su relevancia para los sistemas biológicos. En el presente artículo revisamos los mecanismos responsables de la formación de cristales quirales de $NaClO_3$, incluyendo los procesos de amplificación y desracemización, así como sus posibles aplicaciones en la obtención de compuestos enantioméricamente puros. Asimismo, analizamos la relación entre la asimetría observada en estos sistemas inorgánicos y la homoquiralidad biológica. Finalmente, discutimos la hipótesis de que procesos de cristalización asimétrica pudieron ocurrir en la Tierra prebiótica e influir en la dinámica molecular asociada con el origen de la vida. Concluimos que los sistemas basados en $NaClO_3$ constituyen un modelo útil para comprender los mecanismos físicos capaces de generar y amplificar asimetrías quirales a partir de condiciones inicialmente simétricas.

Palabras clave: Homoquiralidad, cristalización asimétrica, desracemización, clorato de sodio ($NaClO_3$), origen de la vida.

Suggested citation: Cruz-Rosas, H. I., et al. (2026). Chiral symmetry breaking in $NaClO_3$ crystals as a model for the study of biological homochirality. La Granja: Revista de Ciencias de la Vida. Vol. 44(2):13-26. https://doi.org/10.17163/lgr.n44.2026.01.

Orcid IDs:

Hugo I. Cruz-Rosas: https://orcid.org/0000-0003-2451-544X
María E. Noble-Terán: https://orcid.org/0000-0002-6435-5551
José-Manuel Cruz: https://orcid.org/0000-0003-3306-5137
Heidi García Quintana: https://orcid.org/0009-0009-1879-0649
Marleen Alejandra Chávez Vidal: https://orcid.org/0009-0006-9550-8561
Fátima del C. Ramírez Hernández: https://orcid.org/0009-0009-2852-1709
Thomas Buhse: https://orcid.org/0000-0001-5082-0873

©2026, Universidad Politécnica Salesiana, Ecuador.

1 Introduction

Chirality is a fundamental geometric property wherein an object or system exists in two distinct configurations that are non-superimposable mirror images of each other, precisely analogous to the structural relationship between a left and a right hand (See Figure 1).

In the case of chiral molecules and crystals, these forms are known as enantiomers. Experimentally, enantiomers can be distinguished by their interaction with plane-polarized light, as they rotate the plane of polarization in opposite directions. This property is denoted as $(+)$ or $(-)$, depending on whether the rotation is clockwise or counterclockwise, respectively. Historically, this phenomenon gave rise to the terms levorotatory (L) and dextrorotatory (D); however, in modern chemistry, the designations L and D do not describe optical rotation but instead correspond to a relative structural nomenclature based on the Fischer projection of glyceraldehyde. In contrast, the absolute configuration of a chiral molecule is defined using the R/S (*rectus/sinister*) system, which is assigned according to the Cahn–Ingold–Prelog priority rules (Cleaves, 2023). These rules establish the priority of substituents around a chiral center based on the atomic number (Z) of the atoms directly bonded to it. In the event of a tie, the next atoms along the chain are progressively compared until a difference is found, determining the spatial arrangement of the groups around the chiral center.



Figure 1. Chirality is prominently expressed in gastropod anatomy through the direction of shell coiling. The dextral (right-handed) coiling of the shell in most snail species defines a chiral asymmetry, as individuals with sinistral (left-handed) shell coiling are less common. This reversal in shell coiling is caused by mutations that alter the animal's anatomy from the earliest cleavage stages of embryonic development.

©2026, Universidad Politécnica Salesiana, Ecuador.

Figure 2 illustrates the assignment of the R/S absolute configuration for lactic acid according to these rules. In both enantiomers, the substituent with the lowest priority is $-$H ($Z = 1$), which is oriented away from the observer. Moving upward in priority, $-CH_3$ is followed by $-CO_2H$. This assignment arises because the atoms directly bonded to the chiral center (the α-carbon) are identical, as both substituents possess a carbon atom with $Z = 6$. To resolve this tie, the next atoms in the chain are compared: hydrogen has $Z = 1$, whereas oxygen has $Z = 8$. Consequently, $-CH_3$ (carbon bonded to H, H, H) holds a lower priority than $-CO_2H$ (carbon bonded to O, O, H). Finally, $-$OH is the substituent with the highest priority because the oxygen atom directly bonded to the chiral center has $Z = 8$. Thus, the overall priority order is OH $>$ CO_2H $>$ CH_3 $>$ H. Based on this sequence, the orientation OH $\rightarrow$ CO_2H $\rightarrow$ CH_3 traced in a counterclockwise direction corresponds to the S configuration, whereas a clockwise sequence corresponds to the R configuration.

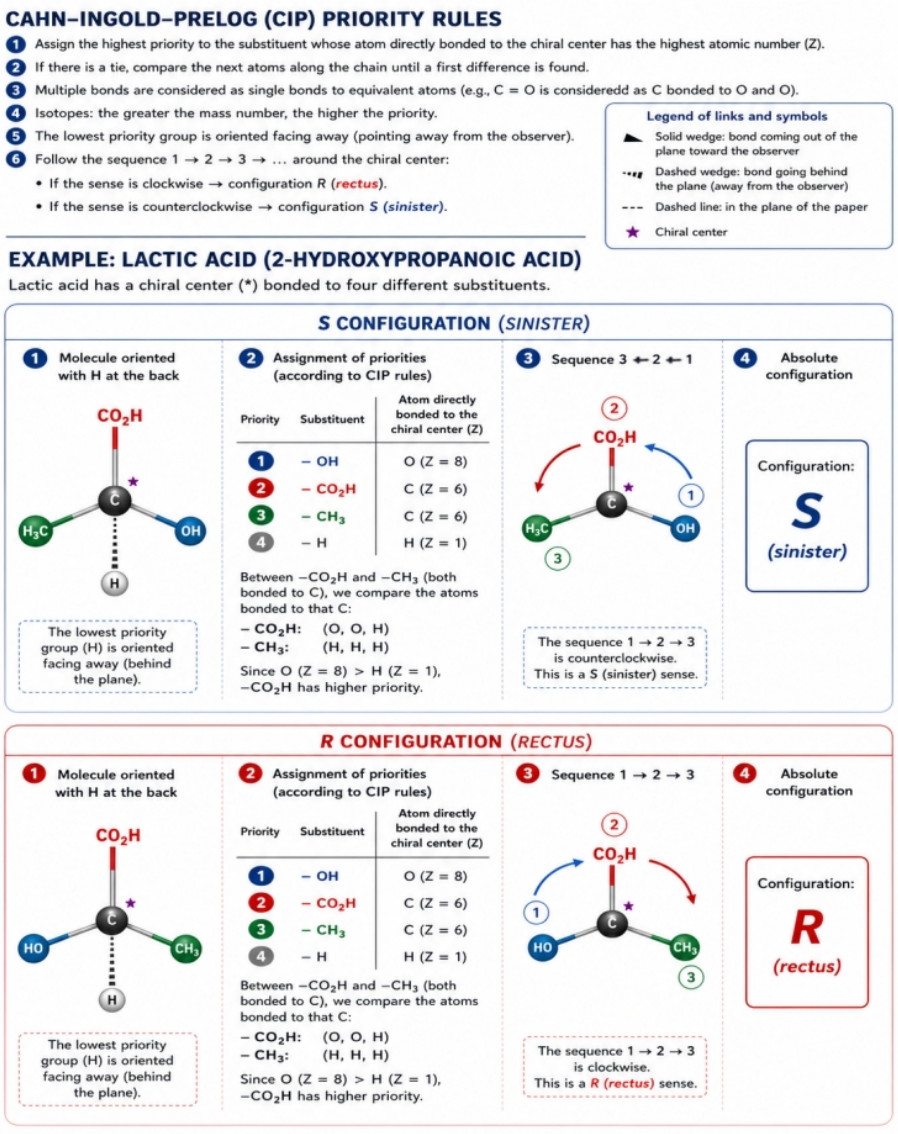


Figure 2. Assignment of the R/S absolute configuration for lactic acid according to Cahn–Ingold–Prelog priority rules.

©2026, Universidad Politécnica Salesiana, Ecuador.

In biological systems, homochirality is a property of functional asymmetry associated with the flow of information at the cellular level (Carroll, 2009; Cruz-Rosas et al., 2020). It is a distinctive characteristic of life that extends across different levels of biological organization (Cruz-Rosas et al., 2022; Inaki et al., 2016). During the synthesis of informational biopolymers, ribosomes recognize only *L*-amino acids (except glycine, which is achiral), whereas RNA polymerase and DNA polymerase recognize only nucleotides containing *D*-ribose and *D*-deoxyribose—a phenomenon strictly referred to as biohomochirality. Nevertheless, the presence of *D*-amino acids and *L*-sugars has been reported to play important roles in certain biological processes (Bitchagno et al., 2022; Forsman and Leino, 2011; Fuchs et al., 2005; Genchi, 2017). Conversely, the synthesis of mirror proteins and mirror nucleic acids—achieved by polymerizing *D*-amino acids and *L*-nucleotides—has been accomplished only under laboratory conditions, requiring synthetic mirror enzymes (Harrison et al., 2023; Young et al., 2019).

Thus, the strict homochirality involved in the synthesis of proteins and nucleic acids is not maintained universally outside these core processes. However, the preferential use of one enantiomer over the other remains a consistent characteristic of biological systems (Franco-Rodríguez et al., 2023). Interestingly, inorganic systems also exhibit chiral asymmetry, displaying biases toward either right-handed or left-handed configurations that range from the weak interactions within atoms to the rotation of spiral galaxies like the Milky Way (Pavlov and Klabunovskii, 2014), thereby demonstrating that chiral asymmetry is a widespread feature of nature.

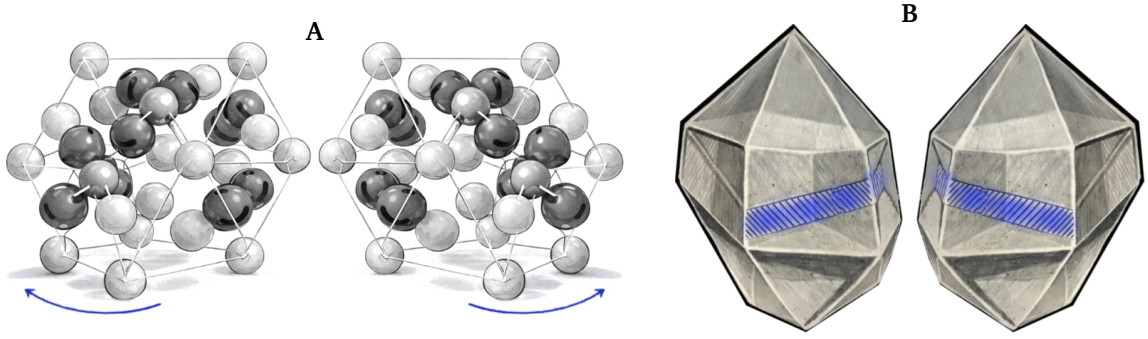


Figure 3. Schematic illustration of chirality observed in crystals. A) Enantiomorphs in which chirality emerges because of the spatial arrangement of the chemical units. B) Enantiomorphs in which chirality is observed as inclined striations on the surface of one of the crystal faces.

The stable, disordered, and most probable state of a chiral system is the racemic state, which represents an equimolar mixture of both enantiomers (50 % left-handed and 50 % right-handed). Consequently, biohomochirality represents a distinct state of molecular asymmetry and order in biology. Even non-living biological systems, such as viruses, must be homochiral to interact with the cells they infect. In crystalline systems composed of inorganic compounds, where molecular order follows a periodic pattern, chirality does not necessarily reside in the individual chemical units; instead, it emerges as a collective property of the spatial arrangement of the crystal lattice and its space group symmetry (Flack, 2003; Valentín-Pérez et al., 2022). These arrangements can manifest as helices rotating either clockwise or counterclockwise, as seen in sodium chlorate ($NaClO_3$) (Dickinson and Goodhue, 1921), or as striations on crystal faces that incline to the left or right relative to the observer, as observed in the hemihedral faces of sodium tartrate (Gal, 2011) (Figure 3).

In these cases, each crystal form is the mirror image of the other and is referred to as an enantiomorph (Flack, 2003). Notably, this chirality occurs at the supramolecular level, largely independent of the chirality of the units constituting the lattice. This is exemplified by sodium chlorate, an achiral molecule that gives rise to a chiral helical lattice,

©2026, Universidad Politécnica Salesiana, Ecuador.

further demonstrating that chirality is an emergent property determined by the spatial arrangement of a system's components. Therefore, chirality can be observed at different levels of organization in nature without necessarily being present at the preceding level.

The emergence of chirality in a molecular system depends on physicochemical forces and processes that may have operated on the prebiotic Earth, influencing the origin or the earliest evolutionary stages of life and determining, from a very early stage, the subsequent development toward present-day biohomochirality. Therefore, studying these forces and processes may provide important insights into the mechanisms that led to the emergence of living systems. Furthermore, research focused on the pathways that induce chiral asymmetry is interesting for understanding the origin and functioning of biological processes, with implications that are not only theoretical but also highly practical.

An example of this is the development of medical therapies based on the fact that biohomochirality represents a fundamental structural order enabling stereospecific recognition among biomolecules. This principle has been exploited in the design of chiral nanomaterials capable of selectively recognizing molecular structures of biomedical interest, with applications in diagnostics, targeted drug delivery, and medical therapies (Sun et al., 2026; Zhao et al., 2024). The development of enantiomerically specific drugs is also an area of research based on molecular chirality, aiming to minimize adverse effects while enhancing physiological activity through the stereoisomer with the appropriate biological action (Nguyen et al., 2006).

To achieve these objectives, various research groups employ simple molecular models, such as the formation of chiral crystals to understand the mechanisms by which chiral symmetry breaking can be induced and to investigate their implications for biology. On this basis, the present study highlights the relevance of investigating the crystallization of $NaClO_3$ and the mechanisms underlying its chiral symmetry breaking as a simple and useful experimental model for approaching the possible asymmetric conditions under which the earliest living systems were assembled.

2 Sodium Chlorate ($NaClO_3$): An Experimental Model

Sodium chlorate is an achiral inorganic salt that crystallizes to form chiral conglomerates. This chirality does not reside in the individual chemical units but rather emerges because of the three-dimensional arrangement of the Na^+ and ClO_3^- ions within the crystal lattice. Specifically, the crystal belongs to a chiral space group ($P2_13$), in which the structural units are arranged along helical axes, giving rise to left- or right-handed enantiomorphic structures (Buhse et al., 2021; Flack, 2003; Florent et al., 2023). An important consequence of this arrangement is that the crystals exhibit optical activity; i.e., they are capable of rotating the plane of plane-polarized light. As a result, when observed through polarized filters, crystals of opposite handedness interact differently with light, allowing opposite chiral conglomerates to be visually distinguished.

If the polarizing plates are initially crossed (their polarization planes oriented perpendicularly to each other at $90°$) and the upper plate (analyzer) is rotated to the right, the polarized light passes through the crystal mixture, causing the L-crystals of $NaClO_3$ to appear brighter than the D-crystals. Conversely, if the analyzer is rotated to the left, the appearance of the conglomerates is reversed, and the D-crystals appear brighter. This phenomenon is illustrated in Figure 4, where the arrows indicate clockwise and counterclockwise rotations and the corresponding effect on the pair of crystals. The lower images show the appearance of the L and D conglomerates, respectively, because each enantiomorph interacts differently with the direction of the polarized light passing through the crystal mixture. There is no direct relationship between the clockwise or counterclockwise rotation of the analyzer and the chirality of each enantiomorph. Therefore, this method does not determine the absolute configuration of each conglomerate but rather serves as a technique for distinguishing between left- and right-handed crystals, as well as from achiral crystals (Niinomi et al., 2014).

A particularly interesting feature of $NaClO_3$ crystallization is that when a supersaturated solution is prepared from previously formed crystals—whether composed exclusively of left-handed crystals, right-handed crystals, or a racemic mixture—

La Granja: *Revista de Ciencias de la Vida* 44(2) 2026:13-26.
©2026, Universidad Politécnica Salesiana, Ecuador.

the chirality associated with the crystal lattice is entirely lost upon dissolution. Consequently, the formation of new crystals from this solution yields a racemic mixture. This demonstrates that the racemate is the natural equilibrium state of the system's dynamics, to which it recurrently returns. Under certain conditions, however, this equilibrium can be broken, leading to non-racemic growth and the clear predominance of one of the enantiomorphic crystal forms (Buhse et al., 2021; Noble-Terán et al., 2023).

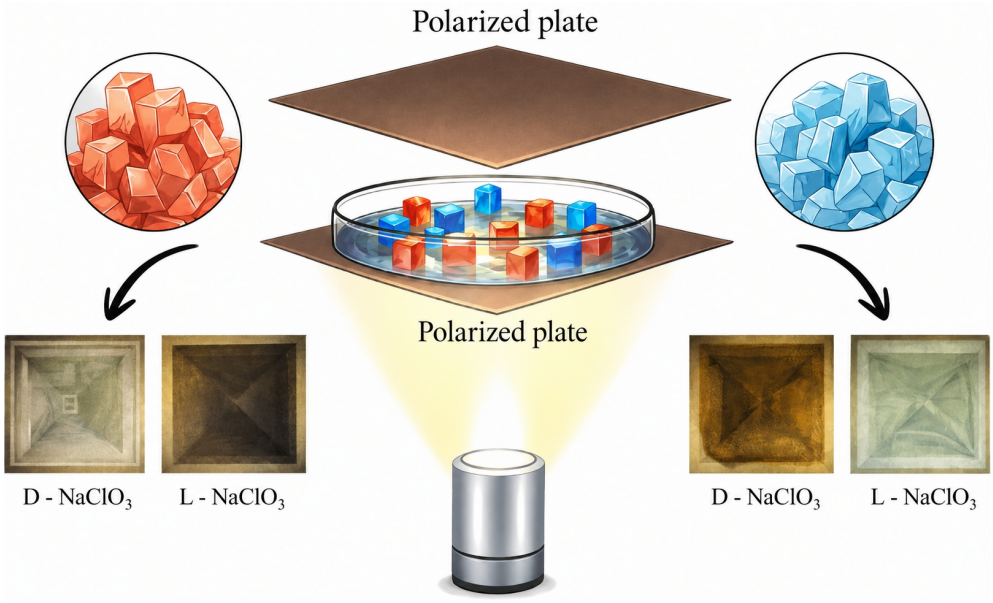


Figure 4. Asymmetric interaction of L- and D-$NaClO_3$ crystals with plane-polarized light. When the upper polarizing plate is rotated clockwise (to the right) relative to the lower polarizing plate, the L-$NaClO_3$ crystals appear brighter. When the upper polarizing plate is rotated counterclockwise (to the left), the D-$NaClO_3$ crystals appear brighter. Original image: Heidi García Quintana. Colors are for illustrative purposes only.

3 Chiral Symmetry Breaking and Non-Racemic Growth

Non-racemic growth refers to any process that results in a significant excess of one enantiomer over the other (in this case, one enantiomorphic crystal form of a given handedness over the other). Both stochastic (random) and deterministic mechanisms can cause this phenomenon.

3.1 The Effect of Spontaneous Conglomeration and Viedma Ripening

Viedma ripening operates through the spontaneous formation of chiral crystals resulting from a dynamic process of conglomeration, fragmentation, and recycling, in which a chiral nucleus induces the incorporation (adsorption) of structural units compatible with the configuration of the growing enantiomorph, thereby giving rise to crystals with a defined chirality. Under static conditions, the crystallization of $NaClO_3$ produces left-handed and right-handed conglomerates in a symmetric (racemic) state. From this spontaneous conglomeration, the Viedma ripening mechanism (Viedma, 2005) makes it possible to obtain a homochiral crystal population (100 % enantiomorphs of the same handedness) from a supersaturated racemic solution.

The system is subjected to a continuous cycle of dissolution and growth of the crystal conglomerates. This process can be induced in two ways. The first involves the mechanical fragmentation of crystals through the presence of glass beads that act as a grinding medium under continuous stirring, causing the smaller, less stable conglomerates to dissolve preferentially. This favors an Ostwald ri-

©2026, Universidad Politécnica Salesiana, Ecuador.

pening process, in which the dissolved material is incorporated into the larger crystals, thereby promoting their growth (Noorduin et al., 2009). The second approach involves thermal fluctuations, in which cycles of heating and cooling induce crystal dissolution and growth, respectively (Noorduin et al., 2008).

The key to this mechanism lies in the fact that $NaClO_3$ ions transition from the crystal phase into the aqueous phase during dissolution and are subsequently adsorbed again by either of the two enantiomorphic crystal forms. This solid–liquid–solid interconversion is reversible and exhibits no preference for the formation of crystals of a particular chirality, since $NaClO_3$ is achiral in solution and its ionic units (Na^+ and ClO_3^-) can be incorporated into either enantiomorph. However, owing to stochastic fluctuations, a slight excess of one handedness may arise at a given moment. As the cycles of crystal dissolution and growth continue, the enantiomorph present in greater abundance has a higher probability of adsorbing the ions released by crystals that have dissolved after reaching a size below the critical threshold (Noorduin et al., 2008). This dynamic constitutes a symmetry-breaking process in the formation of the two enantiomorphs and establishes a positive feedback loop that ultimately leads to the complete disappearance of the minority enantiomorph and the formation of a homochiral crystal population (Noble-Terán et al., 2023).

The Viedma mechanism is stochastic, giving rise to homochiral populations of either the left-handed or the right-handed enantiomorph following a binomial probability distribution, without preference for either handedness (Kondepudi et al., 1990; Viedma, 2005) (Figure 5). However, it is possible to control the direction of chiral symmetry breaking, thereby making the system deterministic, either by applying unidirectional stirring to the solution (Ribó et al., 2001) or by using chiral initiators, also referred to as chiral seeds, such as crystals of the same compound or molecules dissolved in the medium (Putman and Armstrong, 2022). In this context, controlling the handedness of the resulting homochiral state has implications that are not only theoretical for the origin of life but also practical, for example, in the food and pharmaceutical industries.

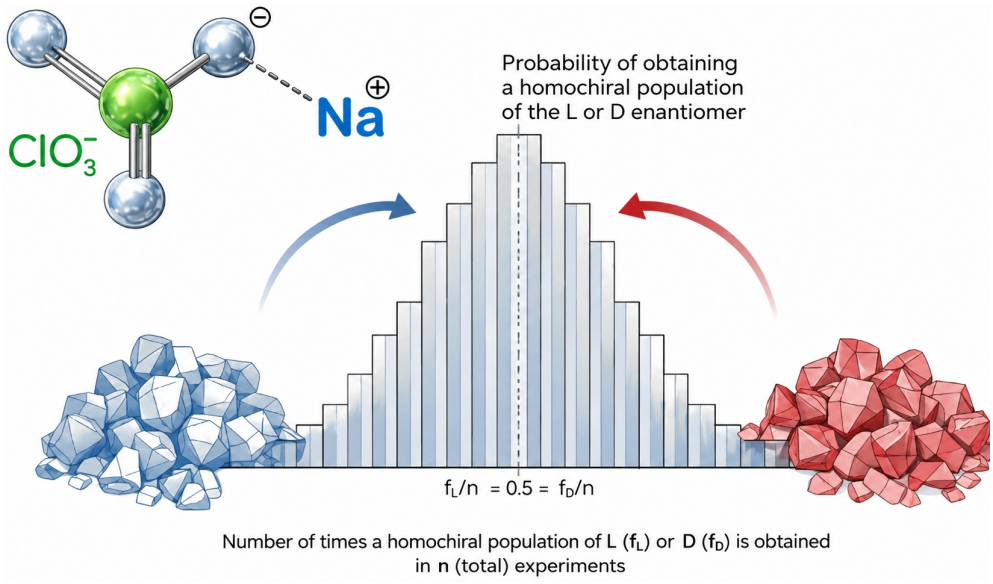


Figure 5. Example of a binomial distribution. An idealized histogram is shown with symmetric probabilities of obtaining homochiral populations of left-handed and right-handed crystals, each having a maximum probability of 50 %. Colors are for illustrative purposes only.

©2026, Universidad Politécnica Salesiana, Ecuador.

3.2 Chiral Symmetry Breaking by Secondary Nucleation

This mechanism, observed in salts such as $NaClO_3$, is based on the growth of crystals from previously formed crystals. During primary nucleation, the stochastic formation of the first crystals gives rise to a racemic mixture (Kondepudi et al., 1990). As the initial crystals continue to grow in solution, they may induce secondary nucleation: small fragments detached from the parent crystals act as new crystallization nuclei, inheriting their structure and, consequently, their chirality (Noorduin et al., 2008).

This mechanism may constitute a source of asymmetry if either a left-handed or a right-handed crystal becomes slightly larger or more active by incorporating more ions into its crystal lattice, thereby generating more secondary nuclei of the same chirality. These newly formed crystals, in turn, generate additional crystallization nuclei with the same handedness, thus establishing an autocatalytic process. This cascade effect can rapidly lead to the predominance of a single enantiomorph in the crystallization medium. Under appropriate conditions, these mechanisms can produce crystal populations with enantiomeric purities approaching $100\,\%$ (Viedma, 2005).

4 Some Implications for the Pharmaceutical and Food Industries

In the pharmaceutical industry, the production of enantiomerically pure substances is important because biological systems exhibit stereospecific recognition and utilization of chiral molecules. Consequently, enantiomers of the same drug may display different pharmacological properties. There are several examples, one of the most famous being thalidomide, which causes severe malformations during embryonic development if the S-enantiomer is administered; however, both enantiomers interconvert under physiological conditions, undergoing *in vivo* racemization, which makes it difficult to use them as enantiomerically pure compounds (Hutt and Tan, 1996). Another example is ibuprofen, where the S-enantiomer is the physiologically active form in humans (and, in general, in mammals). This anti-inflammatory drug can be obtained as a racemate, in which the R-enantiomer (right-handed) is physiologically inactive but is converted to the S-enantiomer in blood plasma. If the racemic mixture is administered, the effective dose increases because the R-enantiomer is partially converted to the active S-form in the body by liver enzymes, which can potentially lead to kidney damage (Nguyen et al., 2006).

In many cases, enantiopure drugs are obtained through enantioselective synthesis or chiral resolution. From an alternative perspective, chiral crystallization processes can be explored as potential methods for the separation of enantiomers; however, most chiral organic compounds, including ibuprofen, crystallize as racemic compounds (where both S- and R-ibuprofen are part of the same crystal lattice) rather than as enantiomeric aggregates, which limits the direct application of these methods. Research into the mechanisms of asymmetric nucleation, such as the Viedma mechanism or secondary crystallization, remains an open field for the development of industrial processes aimed at obtaining aggregates of these substances with high enantiomeric purity.

In the food industry, a similar situation occurs because sensory chemoreceptors recognize chiral molecules differently depending on the specific enantiomer. Since smell and taste are closely linked, there are numerous examples starting with the classic case of limonene, where it is often claimed that $S(-)$-limonene is perceived as the scent of lemon, while $R(+)$-limonene is recognized as the scent of orange (Brenna et al., 2003). However, the validity of this widely cited example has been questioned. In a study on aroma characteristics, it is argued that $R(+)$-limonene is actually the primary terpene present in the essential oil of all citrus fruits (including both lemons and oranges), and that the $S(-)$-limonene historically obtained from lemon peel may have been contaminated with citral. This contamination likely produced the reported lemon aroma—making it an artifact of the experimental method used—an error that has since persisted in the scientific literature (Sell, 2014).

Leaving the debate about limonene aside for now, chiral organic molecules are consistently found in asymmetric proportions within living organisms. Menthol, obtained from certain species of

©2026, Universidad Politécnica Salesiana, Ecuador.

herbaceous plants of the genus *Mentha*, is naturally produced as $(-)$-menthol, which corresponds to the $(1R, 3R, 4S)$ configuration because the molecule possesses three chiral centers. This notation indicates that each of the three chiral centers has an absolute configuration of R or S, describing the three-dimensional arrangement of substituents around each center; for menthol, this structural complexity results in 8 stereoisomers. $(-)$-Menthol is responsible for the characteristic mint flavor and cooling sensation when recognized by sensory chemoreceptors in the mucous membranes. Conversely, $(+)$-menthol, which corresponds to the $(1S, 3S, 4R)$ configuration, is perceived as having an artificial, medicine-like flavor and actively interferes with the receptor recognition of $(-)$-menthol when both are present together. Although the extraction of $(-)$-menthol from peppermint oil (primarily from the species *Mentha canadensis*) remains the primary source of this monoterpenoid, its industrial synthesis can occur via chiral precursors such as $(+)$-limonene, or achiral precursors such as β-pinene, followed by isolation of the pure compound through the crystallization of $(-)$-menthol (Kamatou et al., 2013). In this regard, research into the mechanisms of crystal formation with high enantiomeric purity—such as Viedma ripening or secondary crystallization—represents an active field that could lead to new, economically feasible industrial processes.

5 Implications for the Origin of Biological Chirality

Regarding the origin of biohomochirality, both the Viedma mechanism and secondary nucleation demonstrate that simple processes based on crystallization–dissolution cycles and statistical fluctuations can lead to homochiral states in inorganic systems. This may imply the existence of sites or local environments exhibiting chiral asymmetry on mineral surfaces of the prebiotic Earth, or within the environments in which the earliest living systems assembled and began their evolutionary process. The transfer of chiral bias from inorganic crystals to organic molecules such as amino acids and sugars constitutes a field of research that can be framed within Curie's principle of symmetry: "When certain causes produce certain effects, the symmetry elements of the causes must be found in the effects produced" (quoted by Chalmers, 1970). Accordingly, inorganic chiral asymmetry would impose geometric constraints on molecular dynamics, biasing organic molecular systems toward one of the enantiomers.

The chiral symmetry breaking observed during $NaClO_3$ crystallization demonstrates that simple processes, independent of biological dynamics, can generate homochiral states. This asymmetry in inorganic systems may have contributed to determining biological chiral asymmetry under one of two general scenarios: first, as a condition preceding the origin of life; or second, as an environmental factor that influenced evolutionary processes during the earliest stages following the emergence of living systems. In both cases, one hypothesis linking these phenomena to life proposes that chiral crystals may have acted as the earliest agents of selection and amplification of molecular chirality, either before or after the origin of life.

The non-racemic growth of chiral minerals or prebiotic organic compounds (such as amino acids that crystallize as conglomerates) may have provided the earliest local environments on the primitive Earth with a significant enantiomeric excess. Unlike other hypotheses, such as molecular panspermia (Bonner, 1991; Bonner and Rubenstein, 1987; Rubenstein et al., 1983) or the Oparin–Haldane hypothesis (Schopf, 2024), chiral symmetry breaking during $NaClO_3$ crystallization did not require cosmic radiation or a source of circularly polarized light to induce asymmetric growth; statistical fluctuations and amplification alone were sufficient.

One of the simplest proposed mechanisms is that crystal surfaces exhibiting chiral asymmetry may have functioned as reaction surfaces, displaying asymmetric interactions based on molecular geometric affinities with one enantiomer of organic molecules. For example, a homochiral crystal could preferentially promote the binding and polymerization of amino acids, in this case *L*-amino acids, or sugars such as *D*-ribose and *D*-deoxyribose. This process could have led to the formation of the first oligopeptides or oligonucleotides with a chiral bias, which, once molecular life became autonomous, perpetuated this initial asymmetry (Vogl, 2011).

Several research groups have reported the se-

©2026, Universidad Politécnica Salesiana, Ecuador.

lective adsorption of one enantiomer by mineral surfaces exhibiting chiral asymmetry. Examples include the preferential adsorption of *L*-amino acids onto mineral surfaces such as calcite (Hazen et al., 2001) and the selective adsorption of *D*-ribose onto mineral surfaces (Delidovich et al., 2014).

Along the same lines, cross-amplification may also have played an important role. A slight excess of *L*-amino acids or *D*-ribose, perhaps generated by a homochiral population of inorganic crystals, could subsequently have been amplified by other mechanisms, such as asymmetric catalysis on mineral surfaces or autocatalytic reaction systems such as the Soai reaction, ultimately leading to the homochirality observed in living systems today (Barron, 2008).

6 Conclusion: Inorganic Asymmetry and Biological Asymmetry

The crystallization of $NaClO_3$ into enantiomorphic conglomerates demonstrates that chirality can emerge at the supramolecular level from an achiral molecular system. Furthermore, secondary nucleation and Viedma ripening demonstrate that an initially racemic condition can generate a state of pure homochirality through simple physicochemical processes (crystallization, dissolution, mechanical energy, or thermal energy). No initial external asymmetric influence is required; only statistical fluctuations are sufficient. These processes may therefore represent an abiotic mechanism capable of inducing chiral symmetry breaking in organic molecules, particularly in amino acids and pentose sugars (such as ribose and deoxyribose), thereby determining the chiral bias observed in biological systems.

Therefore, it is plausible that on the prebiotic Earth, mineral surfaces subjected to cycles of humidity and temperature, or hydrothermal systems, experienced crystallization processes analogous to Viedma ripening, which acted as the turning point that biased the system toward the predominance of *L*-amino acids or *D*-sugars. Although these mechanisms explain the generation and amplification of chiral asymmetry in simple physical systems, the transition toward its incorporation and fixation in self-replicating chemical systems remains an open question in studies on the origin of life. Nevertheless, the scenario presented here may have formed part of the process that transformed the asymmetry of abiotic chemistry into the functional asymmetry of living organisms, the latter in the sense that organisms maintain their fundamental biological processes because they are organized on the basis of their homochiral state (Cruz-Rosas et al., 2022; Cruz-Rosas and Miramontes, 2021).

Acknowledgments

The authors would like to express their deepest gratitude to their mentor, colleague, and friend Thomas Buhse, who passed away during the preparation of this manuscript. They also thank the two anonymous reviewers for their valuable comments and suggestions, which greatly contributed to improving the initial version of this work.
Furthermore, they are grateful to the entire editorial team of *La Granja* for their professional academic and editorial management of this article. This work was supported by the Basic Science Research Project CBF-2025-G-28, entitled "Kinetics and Dynamics of Viedma-Type Deracemization: Fundamentals of Spontaneous Chiral Symmetry Breaking", funded by the Secretariat of Science, Humanities, Technology and Innovation (SECIHTI), Mexico.

Declaration on the Use of Artificial Intelligence

The authors DECLARE that, during the preparation of the article entitled "Chiral Symmetry Breaking in $NaClO_3$ Crystals as a Model for the Study of Biological Homochirality," generative artificial intelligence tools were used exclusively to generate and/or edit the images accompanying this manuscript. The final version of these visual elements is the result of manual editing by the authors. These tools were not used for data analysis or interpretation, generation of results, formulation of conclusions, or as a substitute for the authors' academic and scientific judgment.

The authors assume full responsibility for the content, originality, integrity, and final version of the article.

©2026, Universidad Politécnica Salesiana, Ecuador.

Author Contributions

H.I.C.R.: Conceptualization, supervision, visualization, writing–original draft, writing–review and editing. **M.E.N.T.:** Supervision, visualization, writing–review and editing. **J.M.C.:** Supervision, visualization, writing–review and editing. **H.G.Q.:** Visualization, writing–review and editing. **M.A.C.V.:** Visualization, writing–review and editing. **F.C.R.H.:** Visualization, writing–review and editing. **T.B.:** Supervision, visualization, writing–review and editing.

References

Barron, L. D. (2008). Chirality and life. *Space Science Reviews*, *135*, 187–201. Online: https://doi.org/10.1007/s11214-007-9254-7

Bitchagno, G. T. M., Nchiozem-Ngnitedem, V.-A., Melchert, D., and Fobofou, S. A. (2022). Demystifying racemic natural products in the homochiral world. *Nature Reviews Chemistry*, *6*, 806–822. Online: https://doi.org/10.1038/s41570-022-00431-4

Bonner, W. A. (1991). Terrestrial and extraterrestrial sources of molecular homochirality. *Origins of Life and Evolution of Biospheres*, *21*(5), 407–420. Online: https://doi.org/10.1007/BF01808311

Bonner, W. A., and Rubenstein, E. (1987). Supernovae, neutron stars and biomolecular chirality. *BioSystems*, *20*(1), 99–111. Online: https://doi.org/10.1016/0303-2647(87)90025-6

Brenna, E., Fuganti, C., and Serra, S. (2003). Enantioselective perception of chiral odorants. *Tetrahedron: Asymmetry*, *14*, 1–42. Online: https://doi.org/10.1016/S0957-4166(02)00713-9

Buhse, T., Cruz, J.-M., Noble-Terán, M. E., Hochberg, D., Ribó, J. M., Crusats, J., and Micheau, J.-C. (2021). Spontaneous deracemizations. *Chemical Reviews*, *121*, 2147–2229. Online: https://doi.org/10.1021/acs.chemrev.0c00819

Carroll, J. D. (2009). A new definition of life. *Chirality*, *21*(3), 354–358. Online: https://doi.org/10.1002/chir.20590

Chalmers, A. F. (1970). Curie's principle. *The British Journal for the Philosophy of Science*, *21*, 133–148. Online: https://doi.org/10.1093/bjps/21.2.133

Cleaves, H. J. (2023). Cahn–ingold–prelog rules. En *Encyclopedia of astrobiology* (pp. 450–450). Cham: Springer. Online: https://doi.org/10.1007/978-3-662-65093-6_295

Cruz-Rosas, H. I., and Miramontes, P. (2021). Spatial information in the emergence of life. *Frontiers in Genetics*, *12*, 672780. Online: https://doi.org/10.3389/fgene.2021.672780

Cruz-Rosas, H. I., Noble-Terán, M. E., Cruz, J. M., and Buhse, T. (2022). Quiralidad biológica: la asimetría funcional de la vida. *Inventio, la génesis de la cultura universitaria en Morelos*, *18*(45), 1–9. Online: https://doi.org/10.30973/inventio/2022.18.45/3

Cruz-Rosas, H. I., Riquelme, F., Ramírez-Padrón, A., Buhse, T., Cocho, G., and Miramontes, P. (2020). Molecular shape as a key source of prebiotic information. *Journal of Theoretical Biology*, *499*, 110316. Online: https://doi.org/10.1016/j.jtbi.2020.110316

Delidovich, I. V., Simonov, A. N., Taran, O. P., and Parmon, V. N. (2014). Catalytic formation of monosaccharides: from the formose reaction towards selective synthesis. *ChemSusChem*, *7*, 1833–1846. Online: https://doi.org/10.1002/cssc.201400040

Dickinson, R. G., and Goodhue, E. A. (1921). The crystal structures of sodium chlorate and sodium bromate. *Journal of the American Chemical Society*, *43*, 2045–2055. Online: https://doi.org/10.1021/ja01442a008

Flack, H. D. (2003). Chiral and achiral crystal structures. *Helvetica Chimica Acta*, *86*, 905–921. Online: https://doi.org/10.1002/hlca.200390109

Florent, S. R., Couvrat, N., Bilot, C., Marinel, S., Malo, S., and Coquerel, G. F. (2023). *The solid solution between $NaClO_3$ and $NaBrO_3$ revisited.* Online: https://doi.org/10.20944/preprints202306.1610.v1 (Preprint)

Forsman, J. J., and Leino, R. (2011). L-pentoses in biological and medicinal applications. *Chemical Reviews*, *111*, 3334–3357. Online: https://doi.org/10.1021/cr1002563

©2026, Universidad Politécnica Salesiana, Ecuador.

Franco-Rodríguez, F. C., Gonzáles-Morales, H., Heredia-Barbero, A., Montoya, L., and Reyes-Medina, Y. (2023). Quiralidad en las ciencias naturales: un acercamiento a distintas escalas. *LA GRANJA. Revista de Ciencias de la Vida*, *37*, 8–22. Online: https://doi.org/10.17163/lgr.n37.2023.01

Fuchs, S. A., Berger, R., Klomp, L. W. J., and de Koning, T. J. (2005). D-amino acids in the central nervous system in health and disease. *Molecular Genetics and Metabolism*, *85*, 168–180. Online: https://doi.org/10.1016/j.ymgme.2005.03.003

Gal, J. (2011). Louis pasteur, language, and molecular chirality. i. background and dissymmetry. *Chirality*, *23*, 1–16. Online: https://doi.org/10.1002/chir.20866

Genchi, G. (2017). An overview on D-amino acids. *Amino Acids*, *49*, 1521–1533. Online: https://doi.org/10.1007/s00726-017-2459-5

Harrison, K., Mackay, A. S., Kambanis, L., Maxwell, J. W. C., and Payne, R. J. (2023). Synthesis and applications of mirror-image proteins. *Nature Reviews Chemistry*, *7*, 383–404. Online: https://doi.org/10.1038/s41570-023-00493-y

Hazen, R. M., Filley, T. R., and Goodfriend, G. A. (2001). Selective adsorption of L- and D-amino acids on calcite: implications for biochemical homochirality. *Proceedings of the National Academy of Sciences of the United States of America*, *98*(10), 5487–5490. Online: https://doi.org/10.1073/pnas.101085998

Hutt, A. J., and Tan, S. C. (1996). Drug chirality and its clinical significance. *Drugs*, *52*, 1–12. Online: https://doi.org/10.2165/00003495-199600525-00003

Inaki, M., Liu, J., and Matsuno, K. (2016). Cell chirality: its origin and roles in left–right asymmetric development. *Philosophical Transactions of the Royal Society B: Biological Sciences*, *371*, 20150403. Online: https://doi.org/10.1098/rstb.2015.0403

Kamatou, G. P. P., Vermaak, I., Viljoen, A. M., and Lawrence, B. M. (2013). Menthol: a simple monoterpene with remarkable biological properties. *Phytochemistry*, *96*, 15–25. Online: https://doi.org/10.1016/j.phytochem.2013.08.005

Kondepudi, D. K., Kaufman, R. J., and Singh, N. (1990). Chiral symmetry breaking in sodium chlorate crystallization. *Science*, *250*, 975–976. Online: https://doi.org/10.1126/science.250.4983.975

Nguyen, L. A., He, H., and Pham-Huy, C. (2006). Chiral drugs: an overview. *International Journal of Biomedical Science*, *2*(2), 85–100. Online: https://pubmed.ncbi.nlm.nih.gov/23674971/

Niinomi, H., Miura, H., Kimura, Y., Uwaha, M., Katsuno, H., Harada, S., ... Tsukamoto, K. (2014). Emergence and amplification of chirality via achiral–chiral polymorphic transformation in sodium chlorate solution growth. *Crystal Growth & Design*, *14*, 3596–3602. Online: https://doi.org/10.1021/cg500527t

Noble-Terán, M. E., Cruz, J., Cruz-Rosas, H. I., Buhse, T., and Micheau, J. (2023). A complex reaction network model for spontaneous mirror symmetry breaking in viedma deracemizations. *ChemPhysChem*, *24*, e202300318. Online: https://doi.org/10.1002/cphc.202300318

Noorduin, W. L., Meekes, H., van Enckevort, W. J. P., Millemaggi, A., Leeman, M., Kaptein, B., ... Vlieg, E. (2008). Complete deracemization by attrition-enhanced ostwald ripening elucidated. *Angewandte Chemie International Edition*, *47*, 6445–6447. Online: https://doi.org/10.1002/anie.200801846

Noorduin, W. L., Vlieg, E., Kellogg, R. M., and Kaptein, B. (2009). From ostwald ripening to single chirality. *Angewandte Chemie International Edition*, *48*, 9600–9606. Online: https://doi.org/10.1002/anie.200905215

Pavlov, V., and Klabunovskii, E. (2014). Homochirality origin in nature: possible versions. *Current Organic Chemistry*, *18*(1), 93–114. Online: https://doi.org/10.2174/1385272813179990033

Putman, J. I., and Armstrong, D. W. (2022). Recent advances in the field of chiral crystallization. *Chirality*, *34*, 1338–1354. Online: https://doi.org/10.1002/chir.23492

Ribó, J. M., Crusats, J., Sagués, F., Claret, J., and Rubires, R. (2001). Chiral sign induction by vortices during the formation of mesophases in stirred solutions. *Science*, *292*, 2063–2066. Online: https://doi.org/10.1126/science.1060835

©2026, Universidad Politécnica Salesiana, Ecuador.

Rubenstein, E., Bonner, W. A., Noyes, H. P., and Brown, G. S. (1983). Supernovae and life. *Nature*, *306*(5939), 118. Online: https://doi.org/10.1038/306118a0

Schopf, J. W. (2024). Pioneers of origin of life studies—darwin, oparin, haldane, miller, oró—and the oldest known records of life. *Life*, *14*(10), 1345. Online: https://doi.org/10.3390/life14101345

Sell, C. S. (2014). Analysis and characterisation of odour. En *Chemistry and the sense of smell* (pp. 188–208). Chichester: John Wiley & Sons, Ltd. Online: https://doi.org/10.1002/9781118522981.ch3

Sun, L., Zhang, Y., Yang, Z., Zhang, Y., Dong, Q., Zhang, Z., and Zhang, Q. (2026). Recent advances in synthesis and biomedical applications of structurally chiral plasmonic nanomaterials. *Coordination Chemistry Reviews*, *556*, 217660. Online: https://doi.org/10.1016/j.ccr.2026.217660

Valentín-Pérez, A., Rosa, P., Hillard, E. A., and Giorgi, M. (2022). Chirality determination in crystals. *Chirality*, *34*, 163–181. Online: https://doi.org/10.1002/chir.23377

Viedma, C. (2005). Chiral symmetry breaking during crystallization: complete chiral purity induced by nonlinear autocatalysis and recycling. *Physical Review Letters*, *94*, 065504. Online: https://doi.org/10.1103/PhysRevLett.94.065504

Vogl, O. (2011). Chiral crystallization and the origin of chiral life on earth. *Journal of Polymer Science Part A: Polymer Chemistry*, *49*, 1299–1308. Online: https://doi.org/10.1002/pola.24548

Young, B. E., Kundu, N., and Sczepanski, J. T. (2019). Mirror-image oligonucleotides: history and emerging applications. *Chemistry – A European Journal*, *25*, 7981–7990. Online: https://doi.org/10.1002/chem.201900149

Zhao, L.-X., Chen, L.-L., Cheng, D., Wu, T.-Y., Fan, Y.-G., and Wang, Z.-Y. (2024). Potential application prospects of biomolecule-modified two-dimensional chiral nanomaterials in biomedicine. *ACS Biomaterials Science & Engineering*, *10*, 2022–2040. Online: https://doi.org/10.1021/acsbiomaterials.3c01871

©2026, Universidad Politécnica Salesiana, Ecuador.

La Granja: Revista de Ciencias de la Vida
pISSN:1390-3799; eISSN:1390-8596
https://doi.org/10.17163/lgr.n44.2026.02

Special Issue / Edición Especial
Chirality across scales

A look at *D*-Amino Acids in living beings

Una mirada a los *D*-aminoácidos en los seres vivos

Josué Fabián Díaz Aguilar* and Mario Israel Hernández Alva

Laboratorio de Evolución Química, Instituto de Ciencias Nucleares, Posgrado en Ciencias Biológicas, Universidad Nacional Autónoma de México. [https://ror.org/01tmp8f25]

*Corresponding author: josue.diaz@correo.nucleares.unam.mx

Article received on March 26th, 2026. Accepted, after review, on June 22nd, 2026. Published on September 1st, 2026.

Abstract

The predominance of L-amino acids in biological systems has long been considered a defining feature of life. However, accumulating evidence over the past decades has demonstrated that D-amino acids are not merely biochemical anomalies, but biologically relevant molecules with diverse and essential functions across all domains of life. This review summarizes current knowledge on the distribution, biosynthesis, metabolism, and physiological roles of D-amino acids, highlighting their significance in microbial, animal, and evolutionary contexts. In bacteria, D-amino acids such as D-alanine and D-glutamate are integral components of peptidoglycan, contributing to cell wall integrity and resistance to proteolytic degradation. Beyond structural roles, several noncanonical D-amino acids act as signaling molecules to biofilm formation and microbial community dynamics. In eukaryotes, particularly in mammals, D-serine and D-aspartate have emerged as key neuromodulators involved in synaptic plasticity, neurodevelopment, and endocrine regulation, with growing implications in neurological and psychiatric disorders. Furthermore, the coexistence of functional D-amino acids with the largely L-based proteome raises fundamental questions about the origin and maintenance of biological homochirality. Mechanisms such as stereospecific aminoacyl-*tRNA* synthetases and D-aminoacyl-*tRNA* deacylases actively preserve proteomic homochirality while allowing selective utilization of D-amino acids in specialized pathways. Overall, D-amino acids represent a crucial yet historically underappreciated dimension of biological chemistry, with implications ranging from microbial physiology to neuroscience and the origin of life.

Keywords: Enantiomers, amino acids' evolution, homochirality, biofilm, racemase, peptidoglycan.

©2026, Universidad Politécnica Salesiana, Ecuador.

Resumen

La predominancia de los L-aminoácidos en los sistemas biológicos se ha considerado durante mucho tiempo como una característica definitoria de la vida. Sin embargo, la evidencia acumulada en las últimas décadas ha demostrado que los D-aminoácidos no son solo anomalías bioquímicas, sino moléculas biológicamente relevantes con funciones diversas y esenciales en todos los dominios de la vida. Esta revisión resume el conocimiento actual sobre la distribución, biosíntesis, metabolismo y funciones fisiológicas de los D-aminoácidos, destacando su importancia en contextos microbianos, animales y evolutivos. Los D-aminoácidos como la D-alanina y el D-glutamato en las bacterias son componentes integrales del peptidoglicano, contribuyendo a la integridad de la pared celular y a la resistencia a la degradación proteolítica. Más allá de sus funciones estructurales, varios D-aminoácidos actúan como moléculas de señalización para la formación de *biofilms* y la dinámica de las comunidades microbianas. En los eucariontes, particularmente en los mamíferos, han surgido la D-serina y el D-aspartato como neuromoduladores clave implicados en el neurodesarrollo y la regulación endocrina, con implicaciones crecientes en trastornos neurológicos y psiquiátricos. Además, la coexistencia de D-aminoácidos funcionales con un proteoma mayoritariamente basado en L-aminoácidos plantea preguntas fundamentales sobre el origen y el mantenimiento de la homoquiralidad biológica. Los mecanismos como las D-aminoacil-*tRNA* desaciclasas preservan activamente la homoquiralidad del proteoma, al tiempo que permiten la utilización selectiva de D-aminoácidos en rutas especializadas. En conjunto, los D-aminoácidos representan una dimensión crucial, aunque históricamente subestimada, de la química biológica, con implicaciones que van desde la fisiología microbiana hasta la neurociencia y el origen de la vida.

Palabras clave: Enantiómeros, evolución de aminoácidos, homoquiralidad, biofilm, racemasa, peptidoglicano.

Suggested citation: Díaz-Aguilar, J. F. and Hernández-Alva, M. I. (2026). A look at *D*-Amino Acids in living beings. La Granja: Revista de Ciencias de la Vida. Vol. 44(2):27-41. https://doi.org/10.17163/lgr.n44.2026.02.

Orcid IDs:

Josué Fabián Díaz Aguilar: https://orcid.org/0000-0003-0004-1577
Mario Israel Hernández Alva: https://orcid.org/0009-0004-8719-1109

©2026, Universidad Politécnica Salesiana, Ecuador.

Introduction

Proteins constitute one of the most abundant biomolecules in living organisms. The protein system performs structural, catalytic, signaling, storage, and immune defense functions (Sasabe and Suzuki, 2018). All proteins are composed of basic units known as amino acids, which are linked together to form chains called peptides. Upon folding, these peptides acquire a three-dimensional conformation that often corresponds to the active form known as protein. However, in most instances, several polypeptide chains associate through oligomerization to achieve the fully active state. These building blocks comprise a set of 20 α-amino acids, all sharing a common structure consisting of a central carbon atom (α-carbon) bonded to four substituents: an amino group, a carboxyl group, a hydrogen atom, and a variable side chain known as the R group (Alberts et al., 2015).

The α-carbon forms a chiral center, except in glycine, because the four substituents can adopt two possible spatial arrangements, giving rise to the *L*- (left-handed) and *D*- (right-handed) optical isomers, commonly referred to as enantiomers. The *D*- or *L*- nomenclature is assigned by comparing the Fischer projection of these molecules with that of glyceraldehyde: if the $-$OH group (or $-NH_3^+$ in amino acids) is positioned on the right, the molecule is classified as the *D*-enantiomer, whereas if it is located on the left, it is classified as the *L*-enantiomer.

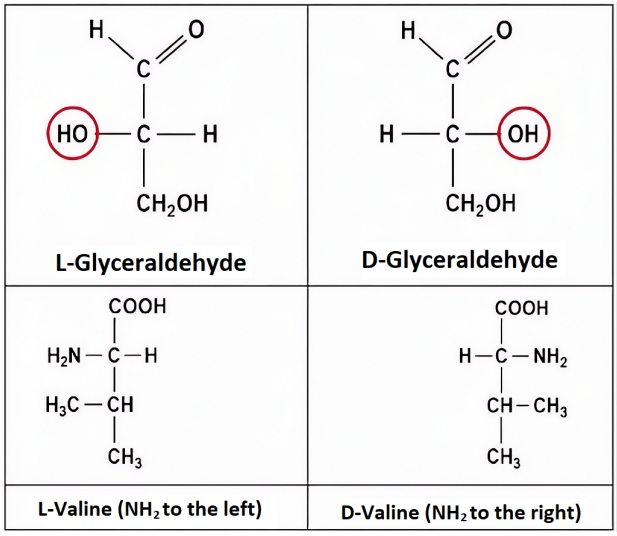


Figure 1. *D/L* designation of chiral molecules using Fischer projections. In glyceraldehyde (top), the *L* configuration is assigned when the hydroxyl group ($-$OH) attached to the chiral carbon is located on the left side of the Fischer projection, whereas the *D* configuration corresponds to its location on the right. This criterion constitutes the historical reference for the relative *D/L* nomenclature used for carbohydrates and amino acids. Using valine as an example (bottom), the *L* configuration has the amino group ($-NH_2$) positioned on the left side of the α-carbon, whereas in the *D* configuration this group is located on the right. Note that the $-$OH and $-NH_2$ groups exhibit the same relative orientation in their respective Fischer projections. Thus, the *D/L* designation expresses a structural relationship to glyceraldehyde and does not necessarily indicate the direction of optical rotation of plane-polarized light.

Only one of the two enantiomers is incorporated into proteins: *L*-amino acids. Consequently, proteins are considered a homochiral system (Du et al., 2023; Sasabe and Suzuki, 2018). For many years, it was widely assumed that homochirality extended to all biological functions involving amino acids, leading to the belief that *D*-amino acids lacked biological relevance (Blackmond, 2010). However, advances in analytical techniques, particularly enantioselective chromatography (Kobayashi, 2019), enabled the detection of *D*-amino acids in bacterial cultures. These findings demonstrated that *D*-amino acids are naturally present in living organisms, where they perform physiological functions distinct from those associated with proteins (Pollegioni et al., 2025).

©2026, Universidad Politécnica Salesiana, Ecuador.

Since their initial discovery, *D*-amino acids have also been identified in eukaryotes, ranging from yeasts to the mammalian nervous system (Fuchs et al., 2005), considerably expanding the range of biological functions attributed to these molecules. Their roles at multiple biological levels continue to be investigated, and although much of their metabolism remains poorly understood, they have attracted considerable interest in fields such as microbiology, neuroscience, endocrinology, and biotechnology (Du et al., 2023).

D-amino acids in bacteria

The first compelling evidence for the biological role of *D*-amino acids emerged from studies of the bacterial cell wall, a structure shared by all bacteria. The bacterial cell wall consists of peptidoglycan, a polymeric network composed of glycosidic linkages between *N*-acetylglucosamine (NAG) and *N*-acetylmuramic acid (NAM), cross-linked by peptides containing primarily *D*-alanine (*D*-Ala) and *D*-glutamate (*D*-Glu) residues (Cava et al., 2011). These amino acids serve as anchoring points for adjacent peptidoglycan strands by forming short peptide bridges between *D*-Ala residues. The extensive cross-linking of these chains provides the bacterial cell wall with remarkable mechanical rigidity (Figure 2). In addition to their structural role, *D*-amino acid residues protect bacteria against proteases and other components of the host immune system that are unable to recognize these enantiomers as substrates. Consequently, *D*-amino acids have become attractive targets for the development of novel antibodies and antimicrobial agents (Sanchez et al., 2014).

The establishment of bacterial colonies is frequently accompanied by the formation of extracellular multicellular structures known as biofilms. These structures are composed primarily of amyloid protein fibers and polysaccharides, providing a protective environment that supports the multicellular proliferation of bacteria such as *Bacillus subtilis* (Kolodkin-Gal et al., 2010), where they are shielded from host immune defenses during infection. *D*-amino acids within the peptidoglycan also contribute to biofilm attachment, providing mechanical stability and facilitating bacterial movement through the extracellular matrix (Su et al., 2022).

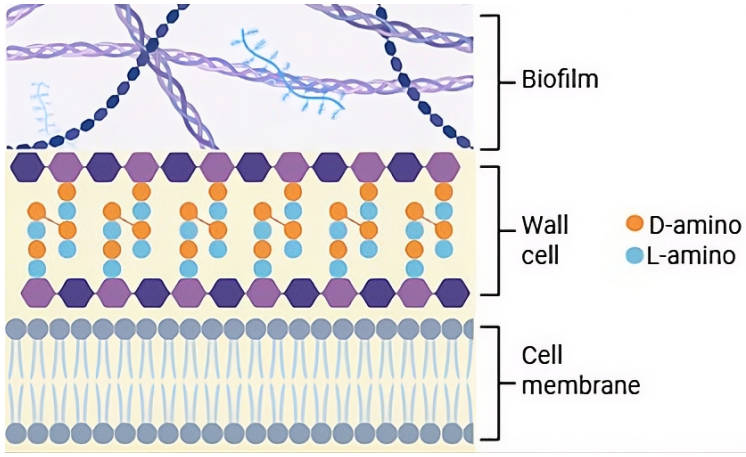


Figure 2. Structure of the bacterial peptidoglycan cell wall composed of sugar chains cross-linked by peptides containing *D*-Ala and *D*-Glu residues. The incorporation of *D*-amino acids enhances cell wall rigidity and promotes adhesion to extracellular biofilm structures, including TasA amyloid proteins (Sasabe and Suzuki, 2018).

Beyond their structural function, *D*-amino acids also exert regulatory roles within biofilms (Roesch et al., 2003), promoting cyst dispersal (exit from the dormant phase) and accelerating bacterial proliferation. Although these regulatory mechanisms remain under investigation, studies on *Staphylococcus aureus* and *Pseudomonas aeruginosa* have demonstrated that increasing the concentration of *D*-amino acids such as *D*-leucine (*D*-Leu), *D*-methionine (*D*-Met), *D*-tryptophan (*D*-Trp), and *D*-tyrosine (*D*-Tyr)

©2026, Universidad Politécnica Salesiana, Ecuador.

promotes the disassembly of TasA amyloid fibers, one of the principal structural components of bacterial biofilms (Kolodkin-Gal et al., 2010).

The replacement of *D*-Ala residues in peptidoglycan has been extensively investigated and can be readily achieved by enriching the culture medium with alternative *D*-amino acids. This substitution reduces or inhibits the anchoring of the peptidoglycan cell wall to TasA proteins within the biofilm matrix (Ramón-Pérez et al., 2014). Among these compounds, *D*-Leu, *D*-Met, *D*-Trp, and *D*-Tyr exhibit the greatest inhibitory effects on bacterial biofilm formation and are currently being investigated as potential therapeutic agents against bacterial infections (Su et al., 2022). Furthermore, supplementation with *D*-amino acids such as *D*-Met and *D*-Trp has been shown to enhance the efficacy of antibiotics, including ciprofloxacin and vancomycin by increasing bacterial permeability and improving molecular recognition (Cava et al., 2011; Sanchez et al., 2014).

Lactic Acid Bacteria and D-Amino Acid Metabolism

The primary biological source of *D*-amino acids is their synthesis through racemases (Radkov and Moe, 2014), a family of enzymes whose function is to recognize an *L*-amino acid and convert it into its corresponding *D*-enantiomer. However, these enzymes have also been shown to catalyze the reverse reaction, converting *D*-amino acids into their *L*-enantiomers (Mutaguchi et al., 2018). Racemases are not exclusive to bacteria, as they have been identified in several animal groups (Fuchs et al., 2005; Ollivaux et al., 2014). Nevertheless, bacteria remain the group in which the enzymes involved in *D*-amino acid metabolism have been most thoroughly characterized. The best-studied enzyme of this family is alanine racemase (*AlaR*) (Kobayashi et al., 2015; Rubinstein and Major, 2010), which serves as the primary source of *D*-alanine (*D*-Ala) for the peptidoglycan cell wall. Enzymes capable of racemizing other amino acids have also been identified, including aspartate racemase (*AspR*) and glutamate racemase (*GluR*) (Glavas and Tanner, 1999).

Lactic acid bacteria comprise a large group of sugar-fermenting microorganisms of considerable industrial importance and are also natural members of the intestinal microbiota (Kobayashi, 2019; Sasabe and Suzuki, 2018). This group of bacteria has been shown to release large amounts of *D*-amino acids into the surrounding medium, predominantly *D*-Ala, but also *D*-leucine (*D*-Leu), *D*-valine (*D*-Val), and *D*-methionine (*D*-Met) (Mutaguchi et al., 2016). Owing to their high production of racemic amino acids during fermentation processes, lactic acid bacteria have attracted considerable interest for industrial applications and large-scale production (Kato et al., 2011).

Enzymatic studies on *D*-amino acid production in lactic acid bacteria have revealed that several racemases are not specific to a single R side chain, as many of them recognize more than one substrate, thereby synthesizing multiple *D*-amino acids from their corresponding *L*-enantiomers. For example, isoleucine racemase (*IsoR*) isolated from *Lactobacillus* sp. (Mutaguchi et al., 2018) exhibits low specificity toward aliphatic amino acids and is capable of racemizing not only *L*-isoleucine (*L*-Ile) but also *L*-leucine (*L*-Leu), *L*-valine (*L*-Val), *L*-norvaline (*L*-Nva), and *L*-norleucine (*L*-Nle). A similar case is lysine racemase (*LysR*) isolated from *Oenococcus oeni* (Kato et al., 2012), which has been shown not only to catalyze the racemization of lysine to *D*-lysine (*D*-Lys), but also to synthesize *D*-arginine (*D*-Arg) and *D*-ornithine (*D*-Orn), two other positively charged amino acids.

Racemases are not the only enzymes involved in *D*-amino acid synthesis. *D*-amino acid aminotransferases (DAATs) constitute another family of enzymes that synthesize *D*-amino acids by transferring an amino group to sugar (Kobayashi, 2019; Martinez-Carrion and Jenkins, 1965). The reaction mechanism begins with the recognition of an α-keto acid; during transamination, the carbonyl group is replaced by an amino group. These enzymes are considered to exhibit a certain degree of substrate specificity through the recognition of R side chains (Shilova et al., 2023). Nevertheless, it has been widely demonstrated that several DAATs can catalyze the transamination of amino acids bearing different types of R side chains, enabling bacteria to produce multiple *D*-amino acids using a single enzyme, including *D*-Val, *D*-Leu, *D*-Nva, and *D*-Met (Tanizawa et al., 1989). An even more remarkable example is the DAAT characterized in the hyperthermophi-

©2026, Universidad Politécnica Salesiana, Ecuador.

lic bacterium *Thermotoga maritima*, whose DAAT is capable of catalyzing the synthesis of *D*-alanine (*D*-Ala), *D*-glutamine (*D*-Gln), *D*-aspartate (*D*-Asp), and *D*-cysteine (*D*-Cys) (Yu et al., 2024), thereby recognizing substrates with R side chains of markedly different chemical characteristics.

Archaea and D-Amino Acids

The case of Archaea, the second major domain of prokaryotes and the lineage from which eukaryotes originated, should also be considered (Stevens and Warnecke, 2023). Archaea are unicellular organisms that possess a cell wall less dense than that of bacteria, known as pseudopeptidoglycan. This structure also consists of a matrix of short peptides linked to polysaccharides; however, very few of these peptides contain *D*-amino acids (Sasabe and Suzuki, 2018; Yu et al., 2024). The incorporation of *D*-alanine (*D*-Ala) and *D*-glutamate (*D*-Glu) into pseudopeptidoglycan may occur; however, these additions are considered to result from the availability of these molecules in the surrounding environment. Detection of these *D*-amino acids is infrequent and is thought to originate primarily from microbial communities, such as those inhabiting marine sediments (Imachi et al., 2024).

Because they are considered metabolic anomalies, enzymes associated with *D*-amino acids in archaea are generally regarded as catabolic. Several enzymes capable of recognizing *D*-amino acids have been identified, including alanine racemase (*AlaR*) and an amino acid dehydrogenase exhibiting activity toward *D*-alanine (*D*-Ala) and *D*-proline (*D*-Pro) as substrates (Nagata et al., 1999). These enzymes are believed to function in the elimination of *D*-amino acids that may accumulate because of the coexistence with *D*-amino acid-producing bacteria, such as lactic acid bacteria. Within archaeal metabolism, there is little evidence supporting the endogenous production of *D*-enantiomers. More recently, a possible pathway for the synthesis of α-keto acids has been described. These molecules are precursors of sugars and serve as substrates for DAAT enzymes in the biosynthesis of *D*-amino acids (Sasabe and Suzuki, 2018; Yu et al., 2024).

D-Amino Acids in Eukaryotes

Following the discovery of *D*-alanine (*D*-Ala) in bacteria, evidence of other *D*-amino acids was gradually found in numerous biological processes in eukaryotes as well. In the mid-1960s, *D*-amino acids were identified in several animal species. *D*-serine (*D*-Ser) was first isolated in *Bombyx mori* (Srinivasan et al., 1962), the silkworm, where it promotes chrysalis formation and moth metamorphosis. During the following decades, amino acids such as *D*-Ala, *D*-methionine (*D*-Met), and *D*-glutamate (*D*-Glu) were isolated from numerous marine invertebrates (Preston, 1985). *D*-Ala and *D*-aspartate (*D*-Asp) were detected in the muscle tissues of mollusks such as *Octopus vulgaris* (Abe et al., 2005), and during embryonic development in echinoderms such as *Paracentrotus lividus* (D'Aniello et al., 1990).

The presence of free *D*-amino acids in the blood of marine organisms serves as a buffering system against the osmotic pressure of seawater, since the protonatable groups of amino acids such as *D*-Ala have been shown to function as physiological buffers (D'Aniello et al., 1990). This buffering activity is regulated by *D*-amino acid oxidases (DAAO), which catalyze the conversion of *D*-amino acids into α-keto acids (Yoshimura et al., 2016), thereby regulating the concentration of these molecules within tissues. DAAOs exhibit high specificity toward *D*-Ala. DAAOs with affinity for *D*-Asp and *D*-Met have also been described; however, this affinity does not appear to be exclusive, as they are capable of catabolizing other *D*-amino acids to a lesser extent (Preston, 1985).

Plants have also been shown to incorporate *D*-amino acids into multiple physiological and developmental processes. Within the glaucophyte algae, a group associated with the origin of the kingdom Plantae, the physiology includes several *D*-amino acids, among which *D*-Ala and *D*-Glu have been identified (Palmer et al., 2004). The presence of *D*-amino acids in plants was originally attributed to the rhizosphere microenvironment, where coexistence with bacterial communities enriches the surrounding medium with these molecules, representing approximately 3–5 % of the total amino acid content (Pollegioni et al., 2025).

©2026, Universidad Politécnica Salesiana, Ecuador.

The study of the physiology of these molecules began with their detection in most fruits, where *D*-Ala, *D*-arginine (*D*-Arg), *D*-Asp, and *D*-Glu were isolated (Pollegioni et al., 2025), and subsequently associated with seed development. In the early 1990s, *D*-Met was found not to be restricted to the roots; rather, it undergoes active transport to other plant tissues, suggesting its involvement in physiological functions (Du et al., 2023). Receptors for *D*-Asp and *D*-Ala have been identified that promote ethylene production, a phytohormone responsible for radicle development during germination and root maturation (Du et al., 2023; Kolukisaoglu, 2020). Finally, the production of peptidoglycan within chloroplast cell walls has been associated with an ancestral trait shared between cyanobacteria and the chloroplasts of angiosperms, providing evidence supporting the endosymbiotic theory of this organelle (Tran et al., 2023).

Within the fungal kingdom, *D*-amino acids are generally not synthesized. A particular case is that of yeasts, which, by coexisting with lactic acid-fermenting bacteria, have evolved metabolic pathways that exploit the abundance of these molecules in their environment (Kato et al., 2011; Mutaguchi et al., 2016). In *Saccharomyces cerevisiae*, enzymatic complexes of amino acid dehydratases (AmDH) have been described. These enzymes are lyases that convert amino acids such as *D*-threonine (*D*-Thr) and *D*-serine (*D*-Ser) into sugars (Gogami et al., 2011). One of these enzymes is serine dehydratase (*SerDH*), which recognizes both *D*- and *L*-serine as substrates and converts them into trioses, exhibiting a preferential affinity for *D*-Ser (Ito et al., 2008).

This affinity suggests an ecological adaptation. As discussed previously, fermentative environments typically contain high concentrations of *D*-amino acids due to the activity of lactic acid bacteria. In environments where both microorganisms coexist, yeasts, like some archaea, can utilize *D*-amino acids as substrates for the production of pyruvate and oxaloacetate, which subsequently enter the Krebs cycle (Mutaguchi et al., 2016) (Figure 3).

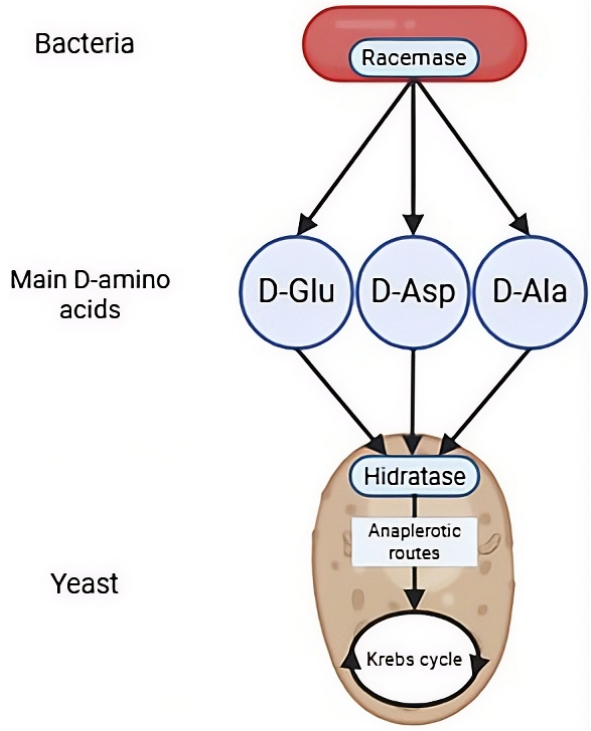


Figure 3. Anabolism of *D*-amino acids by racemase enzymes (AAr) in lactic acid bacteria. *D*-amino acids are released into the extracellular medium as regulators of biofilm formation. Catabolism of *D*-amino acids by yeasts for the synthesis of Krebs cycle metabolites (anaplerotic pathways) (Mutaguchi et al., 2016).

©2026, Universidad Politécnica Salesiana, Ecuador.

Mammalian Nervous System and D-Amino Acids

D-amino acids have been identified in the nervous and endocrine systems of mammals. These animals possess highly complex nervous systems, from which amino acids such as *D*-serine (*D*-Ser) and *D*-aspartate (*D*-Asp) have been isolated (Fuchs et al., 2005), and enzymatic complexes involved in their metabolism have also been described (Sasabe and Suzuki, 2018). *D*-Ser has been demonstrated to act as a promoter of synaptic transmission as well as dendrite formation. Deficiency in the production of this molecule has been associated with impaired cognitive abilities and linked to diseases such as Alzheimer's disease (Li-Zhen and Xing-Zu, 2003; Ni et al., 2023).

The production of this amino acid is highly concentrated in the brain, particularly in astrocytes. These cells contain enzymatic complexes composed of serine racemase (*SerR*) and *SerDH* (Suzuki et al., 2015), thereby regulating local *D*-Ser levels while simultaneously producing energy. This amino acid plays a central role in the development of motor and spatial abilities. During embryonic development of the cerebellum, *D*-Ser is present at high concentrations, which decline to minimal levels in adulthood (Nagata et al., 1994). Regulation of *D*-Ser levels is mediated by *D*-amino acid oxidase (DAAO). This enzyme exhibits low expression at birth and during postnatal development, with its activity increasing during adulthood, thereby maintaining *D*-Ser concentrations at minimal levels. DAAO activity has been reported to be concentrated in the base of the cerebellum and the spinal cord, maintaining *D*-Ser production localized within the central nervous system (Sasabe et al., 2014).

D-Asp is another amino acid widely found in the mammalian nervous system and has been attributed several endocrine functions, particularly during cellular differentiation (Furuchi and Homma, 2005). Its presence in glandular tissue stimulates the production of testosterone in the testes and of oxytocin, vasopressin, and prolactin in the pituitary gland (Wang et al., 2000). As observed for *D*-Ser, *D*-Asp is associated with neuronal plasticity, displaying peak activity during embryonic development followed by a marked decline after birth. Dietary supplementation with *D*-Asp has been shown to provide benefits for neuronal plasticity (Errico et al., 2011). This amino acid has also been incorporated into the cosmetic industry as an anti-aging additive, as its absorption through the skin has been associated with an antioxidant effect on collagen in dermal cells (Mutaguchi et al., 2016).

As in the case of *D*-Ser, *D*-Asp production is associated with the enzyme aspartate racemase (*AspR*), which has been shown to catalyze the racemization reaction in both directions, from *L*- to *D*- and from *D*- to *L*- (Matsuda et al., 2015). However, *D*-Asp production cannot be attributed exclusively to this enzyme. Studies employing targeted mutagenesis have successfully inactivated the *AspR* enzyme, resulting in reduced *D*-Asp levels in mice without completely abolishing its production (Kobayashi, 2019), thereby demonstrating the existence of additional biosynthetic pathways. The explanation for these alternative pathways was found in the low substrate specificity of certain racemases, such as *SerR*, whose activity has also been shown to synthesize *D*-Asp from the corresponding *L*-enantiomer (Ito et al., 2016).

Several enantioselective enzymes for *D*-amino acids are present in the nervous system. In the case of *SerR*, several of these enzymes are capable of recognizing multiple *D*-amino acids. Another example is the ionotropic *L*-glutamate receptors (NMDARs), which have been shown to exhibit affinity for *D*-Ser, *D*-Asp, and glycine (*Gly*) (Mothet et al., 2000). Consequently, maintaining tight regulation of *D*-amino acid levels is essential. Excessive activation of NMDARs or the inactivation of DAAO enzymes results in the accumulation of *D*-amino acids, which has been shown to induce cytotoxicity that, within the brain, may ultimately lead to schizophrenia (Sasabe et al., 2007).

Homochiral Proteins in a Heterochiral System

In the absence of sources of asymmetry, the products of an abiotic chemical reaction generate a racemic mixture: chiral molecules such as amino acids are produced in equivalent amounts. This does not occur in protein systems because of the active function of enzymes themselves, which synthesize, recognize, and are composed of *L*-amino acids. There-

©2026, Universidad Politécnica Salesiana, Ecuador.

fore, the exclusive use of *L*-amino acids in proteins can be considered the result of a dynamic equilibrium (Du et al., 2023).

As discussed throughout this review, the presence of *D*-amino acids in living organisms is strictly regulated by enzymes, including racemases, *D*-amino acid aminotransferases, *D*-amino acid oxidases, and *D*-amino acid dehydratases (Molla et al., 2020; Ollivaux et al., 2014). Because of these regulatory mechanisms, *D*-amino acids are rarely found in proteins. Their occurrence is generally associated with post-translational modifications that take place in the polypeptide chain, since they are only exceptionally incorporated by the ribosome during the elongation process (Alberts et al., 2015). Amino acids reach the ribosome attached to a transfer RNA (*tRNA*), which recognizes the nucleotide sequence that determines the identity of each amino acid.

To prevent the incorporation of *D*-amino acids into *tRNAs*, two regulatory mechanisms, or chirality checkpoints, have been described (Kuncha et al., 2019). The first is the stereoselectivity of aminoacyl-*tRNA* synthetases (*aaRS*s), the enzymes responsible for attaching amino acids to their corresponding *tRNAs*. These enzymes exhibit a chiral preference for *L*-amino acids; however, substrate recognition may occasionally fail, resulting in the attachment of *D*-enantiomers (Prathapan, 2025). These errors are corrected by the second checkpoint, the *D*-aminoacyl-*tRNA* deacylases (*DTD*) (Bhatt et al., 2016; Jani and Pappachan, 2022). These enzymes recognize the chirality of amino acids attached to *tRNAs* and hydrolyze the ester bond when *D*-amino acids have been mistakenly charged, thereby eliminating aminoacylation errors.

DTD activity is enantiospecific and therefore acts exclusively on *D*-amino acids. It has been demonstrated, however, that this recognition is biased in the particular case of glycine, an achiral amino acid (Calendar, 2017). Because glycine lacks chirality, *DTD* can recognize glycyl-*tRNA* ($tRNA^{Gly}$) as a substrate and hydrolyze the aminoacyl bond despite the correct amino acid being attached. Evidence indicates that this bias is prevented by the elongation factor *EF-Tu*, which forms a complex with $tRNA^{Gly}$, thereby shielding glycine from recognition and hydrolysis by *DTD* (Kuncha et al., 2019).

Evolution Toward Homochirality

Life is intrinsically linked to planet Earth; its origin and evolution modified the Earth's crust so profoundly that the planet cannot be understood without considering the intervention of the biosphere (Cintas, 2013). Biological activity is the reason why *D*-amino acids are scarce in nature, as enzymatic activity continuously recycles these molecules into other metabolites. However, such enzymatic barriers did not exist on the primitive Earth. During the first millions of years, the formation of organic molecules under abiotic conditions produced racemic mixtures of *D*- and *L*-amino acids, making both enantiomers available during the processes of chemical evolution.

Two major abiotic mechanisms have been proposed to explain the selection of one enantiomer before the emergence of life on Earth. On the one hand, deterministic hypotheses attribute chiral preference to physical and chemical biases analogous to those occurring throughout the universe and within Earth's geochemistry. On the other hand, stochastic hypotheses propose that symmetry breaking originated from local fluctuations or contingencies, whose effects were subsequently amplified until significant enantiomeric differences were established (Malloy et al., 2025).

Within the deterministic framework, parity violation in the electroweak interaction predicts minimal energy differences between enantiomers, suggesting a systematic bias favoring *L*-amino acids and *D*-sugars (Malloy et al., 2025). Although these differences are far too small to account for homochirality by themselves, they may have been reinforced in environments where heavy metal centers generated chiral coordination complexes capable of discriminating between *L*- and *D*-enantiomers during the abiotic formation of peptides. One example of this mechanism involves Cu(II) and the oxygen-evolving complex (OEC), in which intrinsically chiral copper structures promote spin polarization during electron transfer in hydrogen production, thereby benefiting from the chirality of the material (Cintas, 2013; Garcés-Pineda et al., 2025).

In this context, the salt-induced peptide formation (SIPF) mechanism, proposed as a general pathway for amino acid condensation in primitive

©2026, Universidad Politécnica Salesiana, Ecuador.

oceans rich in NaCl and Cu(II), not only overcomes the thermodynamic and kinetic barriers associated with peptide formation in aqueous environments, but also provides a scenario in which the structure of metal complexes could slightly favor the incorporation of *L*-amino acids, thereby offering a plausible explanation for the origin of biological homochirality (Cintas, 2013).

Another deterministic perspective shifts the origin of chirality to interstellar space and early meteoritic bombardment. The synthesis of amino acids in interstellar ice analogs exposed to ultraviolet radiation has been documented, as has their presence in comets and meteorites. In meteorites such as *Murchison*, mixtures containing dozens of amino acids with small enantiomeric excesses have been identified, suggesting a possible extraterrestrial source of molecular asymmetry (Jakschitz and Rode, 2012). These imbalances may have resulted from circularly polarized radiation in star-forming regions, capable of inducing photochemical asymmetry in previously racemic mixtures. Consequently, the primitive Earth may have inherited a slight chiral bias in the organic material delivered from space (Jakschitz and Rode, 2012).

In contrast, stochastic hypotheses argue that the universe does not inherently "prefer" one handedness over the other, and that the choice between *L*- and *D*-enantiomers may ultimately have been a historical accident (Malloy et al., 2025). The so-called chance hypothesis envisions a scenario in which a slight imbalance between enantiomers, arising from random fluctuations, stochastic crystal nucleation, or spontaneous resolution within a particular microenvironment, became fixed because that specific molecular ensemble participated in the earliest cycles of chemical self-organization and replication (Malloy et al., 2025).

However, without an amplification mechanism, such fluctuations would tend to return to a racemic state. This is where the autocatalytic models with mutual antagonism proposed by Frank (1953) and subsequently developed in recent studies become relevant. In these models, each enantiomer catalyzes its own formation while simultaneously reacting with its mirror image to produce an inactive compound, allowing even a minute initial excess to grow until an almost enantiopure population is achieved. The Soai reaction (Soai et al., 1995), an autocatalytic alkylation capable of amplifying minimal enantiomeric excesses to values approaching optical purity, has become the experimental paradigm of this behavior (Jakschitz and Rode, 2012; Hanopolskyi et al., 2021).

From a physical perspective, crystallization processes and phase behavior provide alternative pathways for symmetry breaking and amplification. In systems that crystallize as conglomerates, the combination of dissolution, recrystallization, and mechanical attrition may lead to the complete disappearance of one enantiomer from the solid phase. Conversely, in systems forming racemic crystals, eutectic models demonstrate that the coexistence of racemic solids and pure enantiomorphic crystals establishes very high enantiomeric excesses in solution (Malloy et al., 2025). Experiments involving amino acids and copolymerization models have further shown that these dynamics can interact with surface self-assembly processes to generate highly non-random oligomer distributions from racemic mixtures, thereby providing a bridge between phase chemistry and the emergence of homochiral peptide structures.

Finally, these physicochemical processes are complemented by biological fixation mechanisms. Modern protein biosynthesis exhibits extremely high chiral selectivity: the molecular machinery composed of aminoacyl-*tRNA* synthetases and the ribosomal peptidyl transferase center discriminates very efficiently against *D*-amino acids, making their incorporation into proteins through natural biosynthetic pathways virtually impossible (Jakschitz and Rode, 2012). This suggests that, once a certain degree of enrichment in *L*-amino acids and *D*-sugars had been achieved through the combined action of deterministic and stochastic mechanisms, evolution fixed this preference by integrating chirality into the very core of translation and replication (Blackmond, 2010). Thus, current theories regarding the emergence of homochirality converge on the view that small initial asymmetries, whether dictated by physical laws, statistical chance, or the intrinsic dynamics of chemical networks, were progressively amplified and channeled by increasingly complex chemical systems until they became encoded within the molecular machinery of life as it exists today.

©2026, Universidad Politécnica Salesiana, Ecuador.

Conclusions

The statement that living organisms constitute a homochiral system is not entirely accurate. Amino acid homochirality is a condition that applies to proteins, but it is not a universal rule for organisms. As highlighted throughout this review, *D*-amino acids perform multiple biological functions, among which hormonal functions are particularly noteworthy, providing a high degree of specificity within these systems owing to the stereoselectivity of these molecules. The homochiral nature of proteins and the use of *D*-enantiomers in other biological systems are tightly regulated by proteins themselves, which actively function as stereoselective determinants, directing the use of *L*-amino acids as the basis for protein synthesis and *D*-amino acids as signaling molecules.

Acknowledgments

This work was made possible through the support of Dr. Alejandro Heredia Barbero and the Institute of Nuclear Sciences (*Instituto de Ciencias Nucleares*) at the National Autonomous University of Mexico (UNAM). We thank the Marcos Rosenbaum Information and Library Unit for providing access to the information used during this research. We also acknowledge the Secretariat of Science, Humanities, Technology and Innovation (Secihti) project CF-2023-I-2604, the UNAM project DGAPA-PAPIIT IN21425, and the Graduate Program in Biological Sciences at UNAM for supporting our academic development.

Declaration on the Use of Artificial Intelligence

The authors DECLARE that, during the preparation of the article entitled " A look at *D*-Amino Acids in living beings", no generative artificial intelligence tools or automated assistance systems were used for the writing, analysis, data interpretation, content generation, translation, or editing of the manuscript.

The authors assume full responsibility for the content, originality, integrity, and final version of the article.

Author Contributions

J.F.D.A.: Conceptualization, investigation, project administration, resources, supervision, visualization, writing–original draft, writing–review and editing. **M.I.H.A.:** Conceptualization, investigation, resources, software, visualization, writing–original draft, writing–review and editing.

References

Abe, H., Yoshikawa, N., Sarower, M. G., and Okada, S. (2005). Physiological function and metabolism of free D-alanine in aquatic animals. *Biological and Pharmaceutical Bulletin*, *28*(9), 1571–1577. Online: https://doi.org/10.1248/bpb.28.1571

Alberts, B., Johnson, A., Lewis, J., Morgan, D., Raff, M., Roberts, K., and Walter, P. (2015). *Molecular biology of the cell* (6ta ed.). Reino Unido: Garland Science Taylor & Francis Group.

Bhatt, T. K., Soni, R., and Sharma, D. (2016). Recent updates on D-tyr-trna^{Tyr} deacylase (dtd): An enzyme essential for fidelity and quality of protein synthesis. *Frontiers in Cell and Developmental Biology*, *4*, 3. Online: https://doi.org/10.3389/fcell.2016.00032

Blackmond, D. G. (2010). The origin of biological homochirality. *Cold Spring Harbor Perspectives in Biology*, *2*(5), a002147. Online: https://doi.org/10.1101/cshperspect.a002147

Calendar, R. (2017). D-tyrosyl-trna deacylase: A new function. *Trends in Biochemical Sciences*, *42*(9), 684–686. Online: https://doi.org/10.1016/j.tibs.2017.06.012

Cava, F., Lam, H., De Pedro, M. A., and Waldor, M. K. (2011). Emerging knowledge of regulatory roles of D-amino acids in bacteria. *Cellular and Molecular Life Sciences*, *68*(5), 817–831. Online: https://doi.org/10.1007/s00018-010-0571-8

Cintas, P. (Ed.). (2013). *Biochirality: Origins, evolution and molecular recognition*. Berlin, Heidelberg: Springer Berlin Heidelberg. Online: https://doi.org/10.1007/978-3-642-37626-9

D'Aniello, A., Nardi, G., Cipollaro, M., Pischetola, M., and Padula, L. (1990). Occurrence of D-alanine in the eggs and the developing embryo

©2026, Universidad Politécnica Salesiana, Ecuador.

of the sea urchin *Paracentrotus lividus*. *Comparative Biochemistry and Physiology Part B: Comparative Biochemistry*, *97*(2), 291–294. Online: https://doi.org/10.1016/0305-0491(90)90283-Y

Du, S., Wey, M., and Armstrong, D. W. (2023). D-amino acids in biological systems. *Chirality*, *35*(7), 508–534. Online: https://doi.org/10.1002/chir.23562

Errico, F., Nisticò, R., Napolitano, F., Mazzola, C., Astone, D., Pisapia, T., … Usiello, A. (2011). Increased D-aspartate brain content rescues hippocampal age-related synaptic plasticity deterioration of mice. *Neurobiology of Aging*, *32*(12), 2229–2243. Online: https://doi.org/10.1016/j.neurobiolaging.2010.01.002

Frank, F. C. (1953). On spontaneous asymmetric synthesis. *Biochimica et Biophysica Acta*, *11*, 459–463. Online: https://doi.org/10.1016/0006-3002(53)90082-1

Fuchs, S. A., Berger, R., Klomp, L. W. J., and De Koning, T. J. (2005). D-amino acids in the central nervous system in health and disease. *Molecular Genetics and Metabolism*, *85*(3), 168–180. Online: https://doi.org/10.1016/j.ymgme.2005.03.003

Furuchi, T., and Homma, H. (2005). Free D-aspartate in mammals. *Biological and Pharmaceutical Bulletin*, *28*(9), 1566–1570. Online: https://doi.org/10.1248/bpb.28.1566

Garcés-Pineda, F. A., Yu, J., Mesa, C. A., Plana-Ruiz, S., Ruano, D., Liang, Y., … Galán-Mascarós, J. R. (2025). Operando evidence on the chirality-enhanced oxygen evolution reaction in intrinsically chiral electrocatalysts. *Chemical Science*, *16*(14), 5475–5482. Online: https://doi.org/10.1039/D4SC07927B

Glavas, S., and Tanner, M. E. (1999). Catalytic acid/base residues of glutamate racemase. *Biochemistry*, *38*(13), 4106–4113. Online: https://doi.org/10.1021/bi982663n

Gogami, Y., Okada, K., and Oikawa, T. (2011). High-performance liquid chromatography analysis of naturally occurring D-amino acids in sake. *Journal of Chromatography B*, *879*(30), 3259–3267. Online: https://doi.org/10.1016/j.jchromb.2011.04.006

Hanopolskyi, A. I., Smaliak, V. A., Novichkov, A. I., and Semenov, S. N. (2021). Autocatalysis: Kinetics, mechanisms and design. *ChemSystemsChem*, *3*(4), e2000026. Online: https://doi.org/10.1002/syst.202000026

Imachi, H., Nobu, M. K., Kato, S., Takaki, Y., Miyazaki, M., Miyata, M., … Takai, K. (2024). *Promethearchaeum syntrophicum* gen. nov., sp. nov., an anaerobic, obligately syntrophic archaeon, the first isolate of the lineage 'asgard' archaea, and proposal of the new archaeal phylum promethearchaeota phyl. nov. and kingdom promethearchaeati regn. nov. *International Journal of Systematic and Evolutionary Microbiology*, *74*(1). Online: https://doi.org/10.1099/ijsem.0.006435

Ito, T., Hayashida, M., Kobayashi, S., Muto, N., Hayashi, A., Yoshimura, T., and Mori, H. (2016). Serine racemase is involved in D-aspartate biosynthesis. *Journal of Biochemistry (Tokyo)*, *160*(6), 345–353. Online: https://doi.org/10.1093/jb/mvw043

Ito, T., Hemmi, H., Kataoka, K., Mukai, Y., and Yoshimura, T. (2008). A novel zinc-dependent D-serine dehydratase from *Saccharomyces cerevisiae*. *Biochemical Journal*, *409*(2), 399–406. Online: https://doi.org/10.1042/BJ20070642

Jakschitz, T. A. E., and Rode, B. M. (2012). Chemical evolution from simple inorganic compounds to chiral peptides. *Chemical Society Reviews*, *41*(16), 5484–5507. Online: https://doi.org/10.1039/c2cs35073d

Jani, J., and Pappachan, A. (2022). A review on quality control agents of protein translation – the role of trans-editing proteins. *International Journal of Biological Macromolecules*, *199*, 252–263. Online: https://doi.org/10.1016/j.ijbiomac.2021.12.176

Kato, S., Hemmi, H., and Yoshimura, T. (2012). Lysine racemase from a lactic acid bacterium, *Oenococcus oeni*: structural basis of substrate specificity. *Journal of Biochemistry (Tokyo)*, *152*(6), 505–508. Online: https://doi.org/10.1093/jb/mvs120

Kato, S., Ishihara, T., Hemmi, H., Kobayashi, H., and Yoshimura, T. (2011). Alterations in D-amino acid concentrations and microbial community structures during the fermentation of red and

©2026, Universidad Politécnica Salesiana, Ecuador.

white wines. *Journal of Bioscience and Bioengineering*, *111*(1), 104–108. Online: https://doi.org/10.1016/j.jbiosc.2010.08.019

Kobayashi, J. (2019). D-amino acids and lactic acid bacteria. *Microorganisms*, *7*(12), 690. Online: https://doi.org/10.3390/microorganisms7120690

Kobayashi, J., Yukimoto, J., Shimizu, Y., Ohmori, T., Suzuki, H., Doi, K., and Ohshima, T. (2015). Characterization of *Lactobacillus salivarius* alanine racemase: short-chain carboxylate-activation and the role of a131. *SpringerPlus*, *4*, 639. Online: https://doi.org/10.1186/s40064-015-1335-6

Kolodkin-Gal, I., Romero, D., Cao, S., Clardy, J., Kolter, R., and Losick, R. (2010). D-amino acids trigger biofilm disassembly. *Science*, *328*(5978), 627–629. Online: https://doi.org/10.1126/science.1188628

Kolukisaoglu, Ü. (2020). D-amino acids in plants: Sources, metabolism, and functions. *International Journal of Molecular Sciences*, *21*(15), 5421. Online: https://doi.org/10.3390/ijms21155421

Kuncha, S. K., Kruparani, S. P., and Sankaranarayanan, R. (2019). Chiral checkpoints during protein biosynthesis. *Journal of Biological Chemistry*, *294*(45), 16535–16548. Online: https://doi.org/10.1074/jbc.REV119.008166

Li-Zhen, W., and Xing-Zu, Z. (2003). Spatiotemporal relationships among D-serine, serine racemase, and D-amino acid oxidase during mouse postnatal development. *Acta Pharmacologica Sinica*, *24*(10), 965–974.

Malloy, J. F., Millsaps, C., Narasimhan, K., Slocombe, L., Mathis, C., Cronin, L., and Walker, S. I. (2025). *The emergence of chirality from metabolism.* Online: https://doi.org/10.48550/arXiv.2505.01056 (arXiv preprint arXiv:2505.01056)

Martinez-Carrion, M., and Jenkins, W. T. (1965). D-alanine-D-glutamate transaminase. *Journal of Biological Chemistry*, *240*(9), 3538–3546. Online: https://doi.org/10.1016/S0021-9258(18)97177-2

Matsuda, S., Katane, M., Maeda, K., Kaneko, Y., Saitoh, Y., Miyamoto, T., … Homma, H. (2015). Biosynthesis of D-aspartate in mammals: the rat and human homologs of mouse aspartate racemase are not responsible for the biosynthesis of D-aspartate. *Amino Acids*, *47*(5), 975–985. Online: https://doi.org/10.1007/s00726-015-1926-0

Molla, G., Chaves-Sanjuan, A., Savinelli, A., Nardini, M., and Pollegioni, L. (2020). Structure and kinetic properties of human D-aspartate oxidase, the enzyme-controlling D-aspartate levels in brain. *FASEB Journal*, *34*(1), 1182–1197. Online: https://doi.org/10.1096/fj.201901703R

Mothet, J.-P., Parent, A. T., Wolosker, H., Brady, R. O., Linden, D. J., Ferris, C. D., … Snyder, S. H. (2000). D-serine is an endogenous ligand for the glycine site of the *N*-methyl-D-aspartate receptor. *Proceedings of the National Academy of Sciences*, *97*(9), 4926–4931. Online: https://doi.org/10.1073/pnas.97.9.4926

Mutaguchi, Y., Kasuga, K., and Kojima, I. (2018). Production of D-branched-chain amino acids by lactic acid bacteria carrying homologs to isoleucine 2-epimerase of *Lactobacillus buchneri*. *Frontiers in Microbiology*, *9*, 1540. Online: https://doi.org/10.3389/fmicb.2018.01540

Mutaguchi, Y., Kobayashi, J., Oikawa, T., and Ohshima, T. (2016). D-amino acids in fermentative foods. En T. Yoshimura, T. Nishikawa, and H. Homma (Eds.), *D-amino acids* (pp. 341–357). Tokyo: Springer Japan. Online: https://doi.org/10.1007/978-4-431-56077-7_22

Nagata, Y., Horiike, K., and Maeda, T. (1994). Distribution of free D-serine in vertebrate brains. *Brain Research*, *634*(2), 291–295. Online: https://doi.org/10.1016/0006-8993(94)91932-1

Nagata, Y., Tanaka, K., Iida, T., Kera, Y., Yamada, R., Nakajima, Y., … Kawaguchi-Nagata, K. (1999). Occurrence of D-amino acids in a few archaea and dehydrogenase activities in hyperthermophile *Pyrobaculum islandicum*. *Biochimica et Biophysica Acta (BBA) - Protein Structure and Molecular Enzymology*, *1435*(1–2), 160–166. Online: https://doi.org/10.1016/S0167-4838(99)00208-3

Ni, X., Inoue, R., Wu, Y., Yoshida, T., Yaku, K., Nakagawa, T., … Mori, H. (2023). Regional contributions of D-serine to alzheimer's disease pathology in male app$^{NL-G-F/NL-G-F}$ mice. *Frontiers in Aging Neuroscience*, *15*, 1211067. Online: https://doi.org/10.3389/fnagi.2023.1211067

©2026, Universidad Politécnica Salesiana, Ecuador.

Ollivaux, C., Soyez, D., and Toullec, J. (2014). Biogenesis of D-amino acid containing peptides/proteins: where, when and how? *Journal of Peptide Science*, *20*(8), 595–612. Online: https://doi.org/10.1002/psc.2637

Palmer, J. D., Soltis, D. E., and Chase, M. W. (2004). The plant tree of life: an overview and some points of view. *American Journal of Botany*, *91*(10), 1437–1445. Online: https://doi.org/10.3732/ajb.91.10.1437

Pollegioni, L., Kustrimovic, N., Piubelli, L., Rosini, E., Rabattoni, V., and Sacchi, S. (2025). D-amino acids: new functional insights. *The FEBS Journal*, *292*(18), 4395–4417. Online: https://doi.org/10.1111/febs.70083

Prathapan, P. (2025). Aminoacyl-trna synthetase: A 'semiotic enzyme'. *European Journal of Medical Genetics*, *77*, 105041. Online: https://doi.org/10.1016/j.ejmg.2025.105041

Preston, R. L. (1985). Distribution and transport of D-amino acids in marine invertebrates. *MDI Biological Laboratory Bulletin*, *25*, 1–3.

Radkov, A. D., and Moe, L. A. (2014). Bacterial synthesis of D-amino acids. *Applied Microbiology and Biotechnology*, *98*(12), 5363–5374. Online: https://doi.org/10.1007/s00253-014-5726-3

Ramón-Pérez, M. L., Diaz-Cedillo, F., Ibarra, J. A., Torales-Cardeña, A., Rodríguez-Martínez, S., Jan-Roblero, J., ... Cancino-Diaz, J. C. (2014). D-amino acids inhibit biofilm formation in *Staphylococcus epidermidis* strains from ocular infections. *Journal of Medical Microbiology*, *63*(10), 1369–1376. Online: https://doi.org/10.1099/jmm.0.075796-0

Roesch, P. L., Redford, P., Batchelet, S., Moritz, R. L., Pellet, S., Haugen, B. J., ... Welch, R. A. (2003). Uropathogenic *Escherichia coli* use D-serine deaminase to modulate infection of the murine urinary tract. *Molecular Microbiology*, *49*(1), 55–67. Online: https://doi.org/10.1046/j.1365-2958.2003.03543.x

Rubinstein, A., and Major, D. T. (2010). Understanding catalytic specificity in alanine racemase from quantum mechanical and molecular mechanical simulations of the arginine 219 mutant. *Biochemistry*, *49*(18), 3957–3964. Online: https://doi.org/10.1021/bi1002629

Sanchez, C. J., Akers, K. S., Romano, D. R., Woodbury, R. L., Hardy, S. K., Murray, C. K., and Wenke, J. C. (2014). D-amino acids enhance the activity of antimicrobials against biofilms of clinical wound isolates of *Staphylococcus aureus* and *Pseudomonas aeruginosa*. *Antimicrobial Agents and Chemotherapy*, *58*(8), 4353–4361. Online: https://doi.org/10.1128/AAC.02468-14

Sasabe, J., Chiba, T., Yamada, M., Okamoto, K., Nishimoto, I., Matsuoka, M., and Aiso, S. (2007). D-serine is a key determinant of glutamate toxicity in amyotrophic lateral sclerosis. *The EMBO Journal*, *26*(18), 4149–4159. Online: https://doi.org/10.1038/sj.emboj.7601840

Sasabe, J., and Suzuki, M. (2018). Distinctive roles of D-amino acids in the homochiral world: Chirality of amino acids modulates mammalian physiology and pathology. *The Keio Journal of Medicine*, *68*(1), 1–16. Online: https://doi.org/10.2302/kjm.2018-0001-IR

Sasabe, J., Suzuki, M., Imanishi, N., and Aiso, S. (2014). Activity of D-amino acid oxidase is widespread in the human central nervous system. *Frontiers in Synaptic Neuroscience*, *6*, 14. Online: https://doi.org/10.3389/fnsyn.2014.00014

Shilova, S. A., Khrenova, M. G., Matyuta, I. O., Nikolaeva, A. Y., Rakitina, T. V., Klyachko, N. L., ... Bezsudnova, E. Y. (2023). To the understanding of catalysis by D-amino acid transaminases: A case study of the enzyme from *Aminobacterium colombiense*. *Molecules*, *28*(5), 2109. Online: https://doi.org/10.3390/molecules28052109

Soai, K., Shibata, T., Morioka, H., and Choji, K. (1995). Asymmetric autocatalysis and amplification of enantiomeric excess of a chiral molecule. *Nature*, *378*(6559), 767–768. Online: https://doi.org/10.1038/378767a0

Srinivasan, N. G., Corrigan, J. J., and Meister, A. (1962). D-serine in the blood of the silkworm *Bombyx mori* and other lepidoptera. *Journal of Biological Chemistry*, *237*(12), 3844–3845.

Stevens, K. M., and Warnecke, T. (2023). Histone variants in archaea – an undiscovered country. *Seminars in Cell and Developmental Biology*, *135*, 50–58. Online: https://doi.org/10.1016/j.semcdb.2022.02.016

©2026, Universidad Politécnica Salesiana, Ecuador.

Su, X., Cheng, X., Wang, Y., and Luo, J. (2022). Effect of different D-amino acids on biofilm formation of mixed microorganisms. *Water Science and Technology*, *85*(1), 116–124. Online: https://doi.org/10.2166/wst.2021.623

Suzuki, M., Sasabe, J., Miyoshi, Y., Kuwasako, K., Muto, Y., Hamase, K., … Aiso, S. (2015). Glycolytic flux controls D-serine synthesis through glyceraldehyde-3-phosphate dehydrogenase in astrocytes. *Proceedings of the National Academy of Sciences*, *112*(17), E2217–E2224. Online: https://doi.org/10.1073/pnas.1416117112

Tanizawa, K., Masu, Y., Asano, S., Tanaka, H., and Soda, K. (1989). Thermostable D-amino acid aminotransferase from a thermophilic *Bacillus* species. purification, characterization, and active site sequence determination. *Journal of Biological Chemistry*, *264*(5), 2445–2449.

Tran, X., Keskin, E., Winkler, P., Braun, M., and Kolukisaoglu, Ü. (2023). The chloroplast envelope of angiosperms contains a peptidoglycan layer. *Cells*, *12*(4), 563. Online: https://doi.org/10.3390/cells12040563

Wang, H., Wolosker, H., Pevsner, J., Snyder, S., and Selkoe, D. (2000). Regulation of rat magnocellular neurosecretory system by D-aspartate: evidence for biological role(s) of a naturally occurring free D-amino acid in mammals. *Journal of Endocrinology*, *167*(2), 247–252. Online: https://doi.org/10.1677/joe.0.1670247

Yoshimura, T., Nishikawa, T., and Homma, H. (Eds.). (2016). D-*amino acids*. Tokyo: Springer Japan. Online: https://doi.org/10.1007/978-4-431-56077-7

Yu, Y., Liu, N.-H., Teng, Z.-J., Chen, Y., Wang, P., Zhang, Y.-Z., … Zhang, Y.-Q. (2024). Evidence for archaeal metabolism of D-amino acids in the deep marine sediments. *Science of The Total Environment*, *948*, 174723. Online: https://doi.org/10.1016/j.scitotenv.2024.174723

©2026, Universidad Politécnica Salesiana, Ecuador.

La Granja: Revista de Ciencias de la Vida
pISSN:1390-3799; eISSN:1390-8596
https://doi.org/10.17163/lgr.n44.2026.03

Special Issue / Edición Especial
Chirality across scales

CC BY NC SA

Tendency to Functional Asymmetry and Microsatellite-Induced Helical Chirality in *Staphylococcus aureus*

Tendencia a la asimetría funcional y quiralidad helicoidal inducida por microsatélites en *Staphylococcus aureus*

Ernesto Ríos-Willars[1], María Magdalena Delabra-Salinas*[2] and Mónica Itzel García Martínez[1]

[1]*Universidad Autónoma de Coahuila. Facultad de Sistemas Unidad Saltillo. Coahuila-México. [https://ror.org/00dpnh189]*
[2]*Universidad Autónoma de Coahuila. Facultad de Enfermería Unidad Saltillo. Coahuila-México. [https://ror.org/00dpnh189]*

*Corresponding author: magdalena-delabra-salinas@uadec.edu.mx

Article received on March 2nd, 2026. Accepted, after review, on July 30th, 2026. Published on September 1st, 2026.

Abstract

Staphylococcus aureus exhibits a microsatellite-rich genomic architecture that can induce functional asymmetries and helical chirality biases. We analyzed four genomes reported in the NCBI database and quantified ATAT, ACAC, and AGAG repetitive motifs in all genes using the MFind tool and surface plots. Reproducible differences in peak and valley topography between genomes were revealed, with a consistent pattern of similarity in Gn2–Gn4 and a marked deviation in Gn1. While ATAT predominated in Gn2–Gn4, Gn1 showed an atypical enrichment of ACAC. This change in the dominant motif, together with the displacement of maxima between genomes, suggests variation in the local arrangement of repeats compatible with chiral effects (asymmetries between strands, inverted repeats, and possible transitions between mirror patterns). Such configurations are plausible modulators of regulatory directionality, secondary structure formation, and recombination propensity. Methodologically, we highlight that the length of the regions and genes analyzed can influence the metric used. In the analysis of three motifs in four genomes, the observed patterns offer an initial comparative map of chiral dimension in the repetitive architecture of *S. aureus* and motivate mechanistic analyses that integrate structural and functional evidence to quantify the contribution of chirality to genomic variation between lineages. Genomes, microsatellite quantification tables, and calculations of the proposed chirality change trend index are available at https://www.usegalaxy.org/u/rioswillars/h/s-aureus-microsatellite.

Keywords: *Staphylococcus aureus*, chirality, microsatellite, genome.

©2026, Universidad Politécnica Salesiana, Ecuador.

Resumen

Staphylococcus aureus presenta una distribución genómica rica en microsatélites, lo que puede inducir asimetrías funcionales y sesgos de quiralidad helicoidal. Se analizaron cuatro genomas reportados en la base de datos NCBI y se cuantificaron los motivos repetitivos ATAT, ACAC y AGAG en todos los genes mediante la herramienta MFind y los gráficos de superficie. Se observaron diferencias reproducibles en la topografía de picos y valles entre genomas, con un patrón consistente de similitud en Gn2–Gn4 y un marcado desvío en Gn1. Mientras que ATAT predominó en Gn2–Gn4, Gn1 mostró un enriquecimiento atípico de ACAC. Este cambio en el motivo dominante, junto con el desplazamiento de máximos entre genomas, sugiere una variación en la disposición local de las repeticiones compatible con efectos quirales (asimetrías entre hebras, repeticiones invertidas y posibles transiciones entre patrones en espejo). Tales configuraciones son plausibles moduladoras de la direccionalidad regulatoria, de la formación de estructuras secundarias y de la propensión a la recombinación. Metodológicamente, se destaca que la métrica empleada puede verse influida por la longitud de las regiones y de los genes analizados. En el análisis de tres motivos en cuatro genomas, los patrones observados ofrecen un mapa comparativo inicial de la dimensión quiral en la arquitectura repetitiva de *S. aureus* y motivan análisis mecanísticos que integren evidencia estructural y funcional para cuantificar la contribución de la quiralidad a la variación genómica entre linajes. Se ponen a disposición los genomas, las tablas de cuantificación de microsatélites y los cálculos del índice propuesto de tendencia al cambio de quiralidad: https://www.usegalaxy.org/u/rioswillars/h/s-aureus-microsatellite.

Palabras clave: *Staphylococcus aureus*, quiralidad, microsatélite, genoma.

Suggested citation: Ríos-Willars, E., Delabra-Salinas, M. and García-Martínez, M. (2026). Tendency to Functional Asymmetry and Microsatellite-Induced Helical Chirality in *Staphylococcus aureus*. La Granja: Revista de Ciencias de la Vida. Vol. 44(2):42-58. https://doi.org/10.17163/lgr.n44.2026.03.

Orcid IDs:

Ernesto Ríos-Willars: https://orcid.org/0000-0002-7157-8884
María Magdalena Delabra-Salinas: https://orcid.org/0000-0002-4467-191X
Mónica Itzel García Martínez: https://orcid.org/0009-0000-2869-9747

©2026, Universidad Politécnica Salesiana, Ecuador.

1 Introduction

Staphylococcus aureus is a spherical Gram-positive bacterium that forms grape-like clusters. It is well known for its ability to cause a wide range of infections in humans, ranging from minor skin infections to severe diseases such as sepsis and endocarditis (Larkin et al., 2009; Gherardi, 2023; Tong et al., 2015). It has been isolated from wastewater, water, and contaminated soils (Heaton et al., 2020; Ramos et al., 2022). The genomic study of this bacterium is important because it supports bioinformatic approaches aimed at preventing infections in both animals and humans. In this context, microsatellites are repeated nucleotide sequences present in DNA; in bacteria, they occur in lower abundance than in other organisms because they are generally subject to mutational pressure that favors their elimination. Nevertheless, they are commonly found in regions of the bacterial genome where they contribute adaptive capabilities through evolution and natural selection. Among the main characteristics of *S. aureus* are its pathogenicity and virulence, as it employs a variety of factors, including toxin production, to cause infections. These toxins can trigger severe immune responses, such as fever and shock (Oliveira et al., 2018; Ahmad-Mansour et al., 2021). Additionally, *S. aureus* exhibits antibiotic resistance, which constitutes one of its most concerning characteristics. Examples include methicillin-resistant *S. aureus* (MRSA) and vancomycin-resistant *S. aureus* (VRSA). This resistance complicates the treatment of infections and represents a growing problem in hospitals (Archer, 1998; Idrees et al., 2021). Associated infections: *S. aureus* is responsible for infections affecting multiple body systems, including skin infections, osteomyelitis, endocarditis, pneumonia, and others (Kwiecinski and Horswill, 2020). Furthermore, it is widely present in dust, feces, surfaces, and bedding on pig and poultry farms; the levels of staphylococci in air and dust can be very high near livestock buildings (Pedersen et al., 2024; Gladding et al., 2020; George et al., 2020) or animal housing facilities. In humans, it is a pathogen commonly associated with diabetic foot infections, contributing significantly to patient morbidity and mortality. This microorganism is the pathogen most frequently isolated from diabetic foot infections (Shettigar and Murali, 2020). Among its various toxins and virulence factors are TSST-1, leukocidins, enterotoxins, and exfoliatins, which play a crucial role in the colonization and infection of diabetic foot wounds (Dunyach-Remy et al., 2016). *S. aureus* strains isolated from diabetic foot ulcers can induce a significant inflammatory response, which is influenced by glucose levels and their metabolites (Wu et al., 2023). Regarding the relationship between *S. aureus* infection and wounds, it is known that this bacterium can induce an altered inflammatory response in the host, thereby inhibiting wound healing. For example, the induction of *miR-15b-5p* by *S. aureus* can suppress the inflammatory response and negatively affect healing (Ramirez et al., 2018). Farm dust may contain MRSA (methicillin-resistant *S. aureus*) and disperse over hundreds of meters, increasing the exposure of farmers, nearby residents, and their homes to resistant bacteria (Crespo-Piazuelo and Lawlor, 2021; Wang et al., 2023). Open, moist wounds containing necrotic tissue, created or enlarged by the screwworm, favor colonization by *S. aureus* and other pathogenic bacteria (Sayhood et al., 2022).

On the other hand, microsatellites in bacteria are short tandemly repeated DNA sequences, also known as simple sequence repeats (SSRs), consisting of nucleotide motifs ranging from one to six base pairs. These sequences are highly mutable and are distributed throughout different locations in the bacterial genome. They are important genetic markers because their high mutation rate contributes to genetic variability and the evolution of the microbial genome (Saeed et al., 2016). In pathogenic bacteria, microsatellite instability can regulate gene expression through phase variation, a mechanism that enables rapid and reversible changes in phenotype expression, as observed in other microorganisms (Martin et al., 2005). However, bacteria exhibit a mutational bias toward microsatellite repeat contraction, which may lead to their extinction in the absence of natural selection, unlike eukaryotes, in which microsatellite repeats tend to expand (Metzgar et al., 2002). In the research conducted in this study, no studies related to microsatellites in *S. aureus* were found; however, in *Escherichia coli*, between 1.75 % and 2.85 % of all microsatellites have been identified as compound microsatellites, consisting of two or more adjacent repeat motifs. These compound microsatellites are significantly overrepresented in bacterial genomes. Although less common, bacterial microsatellites may play an important role in gene regulation and contribute adaptive

©2026, Universidad Politécnica Salesiana, Ecuador.

functional variability. This suggests that, although mutational pressure tends to eliminate them, those that persist may be maintained by selection because of their adaptive functions (Srivastava et al., 2019).

The bacterial genome consists of double-stranded right-handed B-DNA; this is the fundamental chemical chirality shared with other living organisms (Winogradoff et al., 2021; Yu et al., 2025). The right-handed double helix determines the formation of DNA crossovers between DNA segments and the stabilization of positive and negative supercoils (Timsit and Várnai, 2010). The chirality of right-handed versus left-handed crossovers modulates the physical stability of DNA and may have influenced the evolutionary selection that maintains predominantly negatively supercoiled genomes in mesophilic bacteria. At the enzymatic level, topoisomerases, such as DNA gyrase, recognize and capture DNA crossovers of a specific chirality in order to introduce or relax supercoils (Vayssières et al., 2024).

Finally, microsatellites can alter the three-dimensional architecture of DNA because, although they do not change its chemical chirality, they induce torsional stress, which may favor structural features such as A-DNA (compact, more tightly wound), Z-DNA (left-handed helix, opposite chirality), hairpin loops, cruciform structures, and strand slippage (Gadgil et al., 2020; Bagshaw, 2017). This does not alter the chemical chirality, but it does modify the helical conformation, causing certain DNA regions to behave differently because of their geometry, flexibility, or torsional properties (Bacolla et al., 2008). For example, the ATAT microsatellite is extremely flexible and therefore adopts slight curvatures, whereas ACAC and CGCG are more rigid, favoring an alternating geometry (Song et al., 2021).

In pathogens such as *S. aureus*, the spatial and structural instability of microsatellites is not merely a genomic artifact but rather acts as contingency loci that drive phase variation (Brooks and Jefferson, 2014). Conformational changes derived from chirality and torsional stress, such as the formation of loop structures or minidumbbells in tetranucleotide repeats such as ACAC, increase the rate of strand slippage during DNA replication (Harhay et al., 2019). This architectural reconfiguration facilitates reversible mutations (insertions/deletions) that rapidly switch gene expression on or off. Biologically, these structural differences enable human strains such as MRSA to adapt their virulence by controlling key processes such as biofilm formation (through the *ica* operon) to evade antibiotics or by modulating the regulatory system to survive as a "Trojan horse" within host macrophages (Gor et al., 2021). Therefore, the term "atypical case" in the context of microsatellite analysis refers to genomic arrangements that, by deviating from their standard chirality and geometry, confer greater phenotypic plasticity in terms of resistance and infectivity to certain lineages.

In this context, this research investigates the microsatellites identified in *Staphylococcus aureus* genomes reported in the NCBI database (Sayers et al., 2025) over different years. Subsequently, this information is used to estimate changes in genome chirality.

2 Materials and Methods

Four *S. aureus* genomes were downloaded, herein referred to as Gn1, Gn2, Gn3, and Gn4. General information on these genomes is provided below.

The Gn1 genome (strain MRSA_TCH60) is registered in the NCBI database by Baylor College of Medicine from a human skin sample (*Homo sapiens*). Clinically, TCH60 is a reference genome representative of the CC30-ST30-IV lineage. This clonal complex (CC30/ST30) has epidemiological importance because it descends from the pandemic phage 80/81 strain and has evolved into the "Southwest Pacific clone," a highly virulent and globally distributed community-associated MRSA variant responsible for severe invasive infections (Essien et al., 2022; Guillén et al., 2024). Bioinformatically, the assembly and validation of this strain were performed using Clusterflock (Narechania et al., 2016). A size of 2.8 megabases and two chromosomes are reported. It has a GC content of 33 %, as well as 2790 genes, of which 2700 are identified as protein-coding. It was sequenced using Illumina 454 GS FLX technology. The annotation details were registered on August 28, 2013. This record is accessible through the following link: https://www.ncbi.nlm.nih.gov/datasets/genome/GCA_000159535.2/

©2026, Universidad Politécnica Salesiana, Ecuador.

The genome designated Gn2 (strain MRSA252) is described below. It is a 2.9-megabase genome with a GC content of 33 %. Clinically, this strain is representative of the hospital epidemic clone EMRSA-16 (sequence type ST36) and was originally isolated from a case of fatal septicemia. Whole-genome analysis demonstrated that it is a highly divergent lineage characterized by rapid evolution toward virulence and multidrug resistance driven by the acquisition of mobile genetic elements, such as the type II SCC*mec* chromosomal cassette and multiple prophages (Holden et al., 2004). In the NCBI database, based on metadata from an animal-associated habitat, it is reported as corresponding to an original collection from 1998. In this case, 2746 genes were identified, of which 2656 were considered protein-coding. This record is publicly available at: https://www.ncbi.nlm.nih.gov/datasets/genome/GCA_000011505.1/

The genome designated Gn3 (strain CC239-MRSA-III var) corresponds to an isolate from a human host (*Homo sapiens*) in Trinidad and Tobago. Clinically, this lineage belongs to Clonal Complex 239 (CC239), one of the most widely distributed hospital epidemic clones worldwide and highly prevalent in clinical samples from the Caribbean islands. Its genome was sequenced and registered by the Leibniz Institute of Photonic Technology (Monecke et al., 2023). Oxford Nanopore MinION sequencing technology was used on June 5, 2023. A total of 3152 genes are reported, of which 2940 were identified as protein-coding. The GC content is 32.5 %, and the genome size is 3.1 megabases. This record is accessible through the following link: https://www.ncbi.nlm.nih.gov/datasets/genome/GCA_030252755.1/

Finally, the genome designated Gn4 (strain HP20814-043) was analyzed. It has a size of 2.9 megabases and a GC content of 33 %. Clinically, it represents a linezolid-resistant isolate obtained from a patient with cystic fibrosis (*Homo sapiens*) at the University of Iowa Hospitals and Clinics, United States. Evolutionary analysis of this strain reveals profound adaptation under antibiotic stress, and the deletion of the DNA repair genes (*mutS* and *mutL*), which confers a hypermutable phenotype suitable for studying tandem-repeat variation. Its bioinformatic validation was processed according to RefSeq database representation strategies (Tatusova et al., 2015). A total of 2860 genes were reported in this genome, of which 2631 were identified as protein-coding. This genome is available at the following link: https://www.ncbi.nlm.nih.gov/datasets/genome/GCF_030409015.1

The exclusive selection of the tetranucleotide motifs ATAT, AGAG, and ACAC is based on thermodynamic considerations associated with the phase-variation mechanism. Microsatellites involved in strand-slippage events have been documented to be rich in adenine and thymine (A/T), which facilitates the local "melting" of the DNA double helix and produces hypermutability (Zhou et al., 2014). Unlike sequences composed exclusively of guanine and cytosine, such as CGCG, which exhibit high thermal stability that severely restricts their local opening, the ATAT, AGAG, and ACAC motifs combine the requirements necessary to permit this melting with a diversity of topological behaviors. Repetitions of these microsatellites act as a key evolutionary driver of the rapid adaptation and survival of pathogenic bacteria (Saeed et al., 2016); therefore, this specific selection of A/T-rich motifs is ecologically representative and consistent with the low GC content, approximately 33 %, characteristic of the *S. aureus* genome.

The processing method used for microsatellite analysis consisted of applying the MFind tool (Rios-Willars and Chirinos-Arias, 2024). Unlike generic methods based on multiple sequence alignment (MSA), MFind employs a parallel-processing "sliding window" algorithm that performs an exact count of motifs independently of their position. Additionally, its selection was based on the fact that it is a freely available tool with a simple graphical interface, whose computational efficiency allows complete genomes to be explored on conventional computer equipment without requiring supercomputing infrastructure. The MFind software is available in the author's GitHub repository: https://github.com/riosew/Mfind

Given the problem, a sequence PS in length ρ containing the subsequences (SP) to be searched is provided. $SP = \{SP_1 \dots SP_n\}$ and the set of sequences is $S = \{1 \dots N\}$ where N is the number of sequences in the set. Given an SP_x of size k, the problem size TP is defined as:

©2026, Universidad Politécnica Salesiana, Ecuador.

$$TP = (\rho - k)N \quad (1)$$

The number of operations N_e indicates the number of windows in each sequence of S with size k and is defined as:

$$N_e = \sum_{1}^{TP} \sum_{1}^{OC} (Ct + 1) \quad (2)$$

Where (Ct) is the hit counter and (OC) is the number of subsequences matching within the sliding window. The search process is executed through parallel iterations programmed in Java to maximize the use of hardware resources and reduce execution time. Six simultaneous evaluations are performed per iteration. This process produces a database consisting of the microsatellite count for each gene, which is subsequently used to generate graphs and conduct statistical analyses with Minitab 16 software. Subsequently, to quantify the tendency of a DNA region to adopt alternative helical conformations, the Chirality Change Propensity Index (IQZ) was defined. This index integrates three independent sequence-derived components: GC content, the presence of alternating purine–pyrimidine patterns, and the density of repetitive microsatellites. Each of these factors is associated with physicochemical and structural properties that favor the local transition from the B-DNA conformation to alternative states, such as Z-DNA.

The index is expressed as:

$$IQZ = w_1 \cdot GC_score + w_2 \cdot Alt_score + w_3 \cdot MS_score \quad (3)$$

Where:

$$GC_score = \frac{\%GC}{100} \quad (4)$$

This represents the proportion of G and C bases in the analyzed region. Regions with higher GC content exhibit greater torsional rigidity and a greater propensity to stabilize the Z-DNA conformation.

Alt_score is the number of bases forming alternating purine–pyrimidine patterns divided by the total sequence length, in this case, the gene being analyzed. This quantifies the proportion of bases organized into repeated alternating patterns, for example, ATAT and ACAC, which reduces the energy required for helicity inversion.

Finally:

$$MS_score = \frac{\text{Total length of microsatellites}}{Lmax} \quad (5)$$

This estimates the torsional effect resulting from the presence of microsatellites. The variable $Lmax$ corresponds to the maximum expected size of these repetitions for normalization purposes; the maximum number of *hits* counted by the MFind tool among the analyzed genes was used.

The coefficients w_1, w_2 and w_3 allow the relative contribution of each parameter to be adjusted. In this study, values of $w_1 = 0.4$, $w_2 = 0.4$ and $w_3 = 0.2$, were used, assigning greater weight to GC content and purine–pyrimidine alternation, which are the most relevant predictors of the transition to Z-DNA. This index provides a normalized measurement between 0 and 1, thereby facilitating comparisons among different genomic regions and allowing the identification of segments with a high propensity to modify their helical architecture.

3 Results and Discussion

The location of microsatellites in the bacterial genome is generally specific to functional regions, suggesting that they have evolved under selection to perform specific functions. In *S. aureus*, these functions may be related to its ability to cause skin infections and, consequently, diabetic foot wounds. The results obtained are described below. Figure 1 illustrates the surface generated from the analysis of the ATAT, AGAG, and ACAC microsatellites in genome 1 (Gn1). A peak is observed in the upper-right corner, corresponding to the highest microsatellite count values (*hits*) per gene in the genome.

Likewise, a decline is observed in the lower-left corner, suggesting that the microsatellites tend to disappear jointly in this region. Finally, there is a prominent flat region in the center of the surface, where it can be observed that, while the AGAG and ACAC microsatellites increase, the ATAT microsatellite remains absent. Regarding the distribution, Figure 2 shows the box plots of the three variables, in which outliers are observed for ATAT and ACAC. These correspond to genes that exhibited an extraordinary number of microsatellites and, at the same time, constitute the origin of the peak in the surface plot.

©2026, Universidad Politécnica Salesiana, Ecuador.

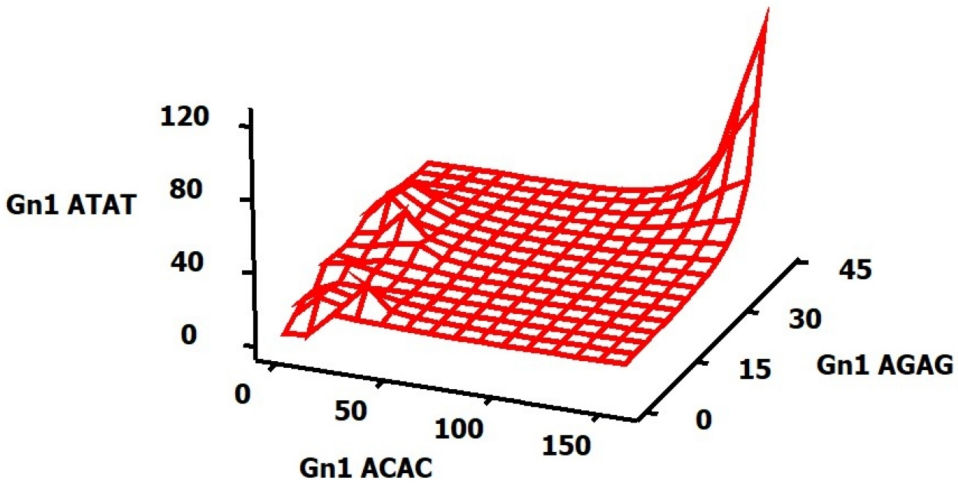


Figure 1. Surface plot of microsatellites in the Gn1 genome of *S. aureus*. The vertical axis represents the frequency of the ATAT motif as a function of the co-occurrence of the ACAC and AGAG motifs. The peaks indicate genes with an anomalous joint accumulation of these tetranucleotides.

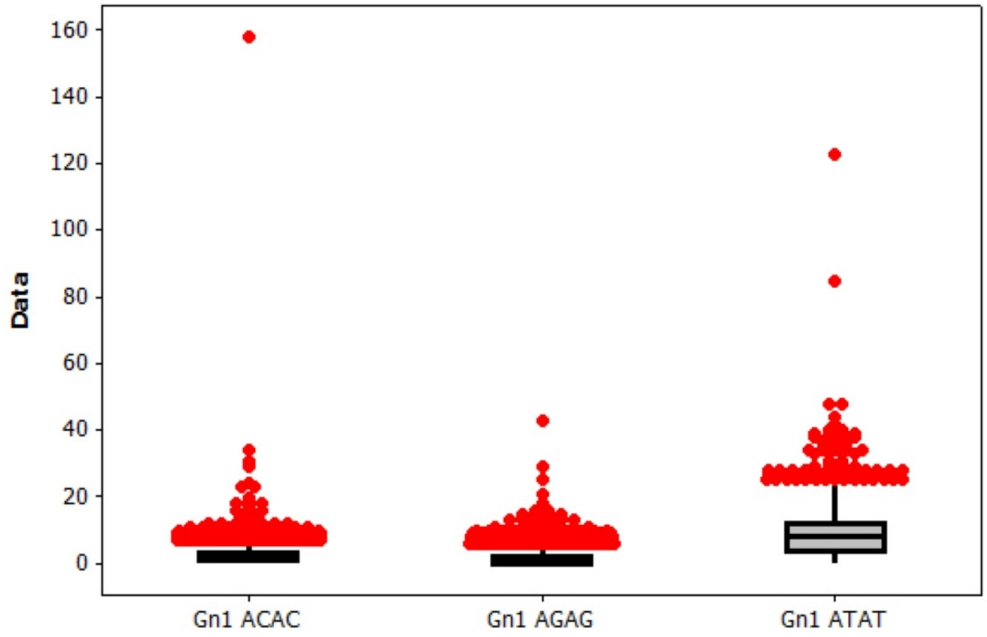


Figure 2. Box plot of the frequencies of the ACAC, AGAG, and ATAT motifs in the genes of the Gn1 genome. Individual points outside the whiskers represent genes that possess an extraordinary number of microsatellites compared with the central tendency of the genome.

©2026, Universidad Politécnica Salesiana, Ecuador.

In the analysis of Gn2, a surface plot of the ATAT, ACAC, and AGAG variables was obtained. Figure 3 shows the surface, in which a peak can be observed near the right edge. Likewise, another peak is observed near the central region. This suggests a redistribution of the genome and the corresponding relocation of microsatellites. A valley or flat region of smaller extent than that observed in the previous result can also be seen. This also indicates microsatellite dispersion.

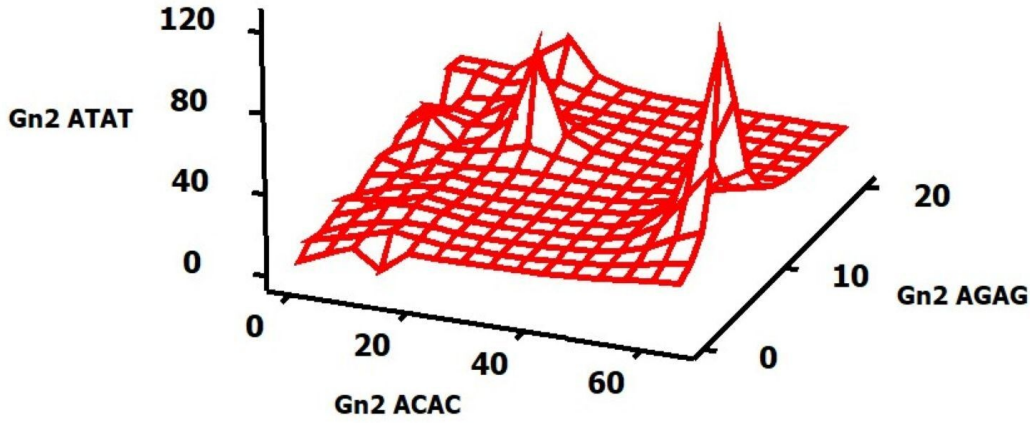


Figure 3. Surface plot of microsatellites in the Gn2 genome of *S. aureus*. The vertical axis represents the frequency of the ATAT motif as a function of the co-occurrence of the ACAC and AGAG motifs. The peaks indicate genes with an anomalous joint accumulation of these tetranucleotides.

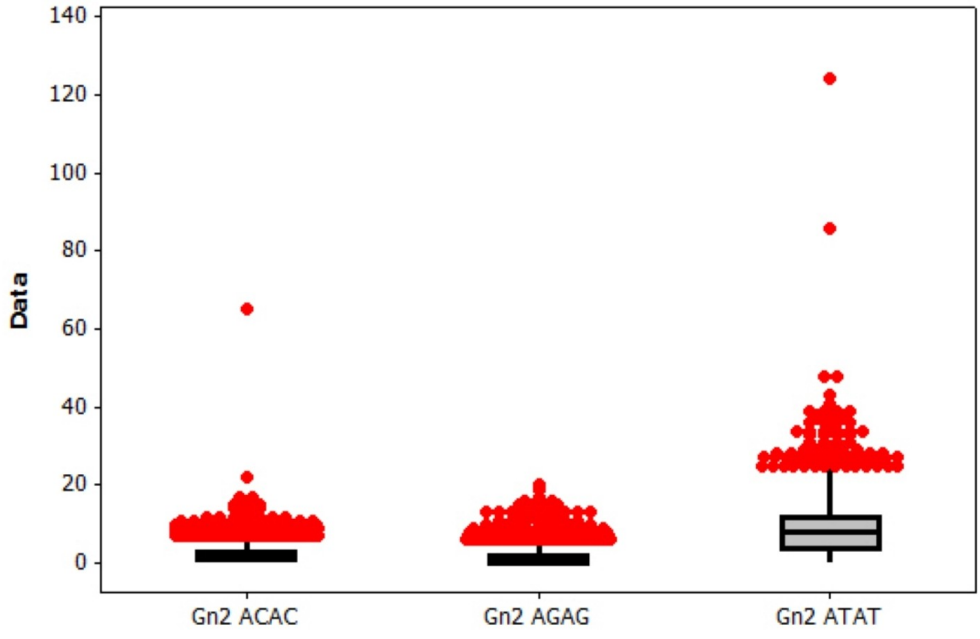


Figure 4. Box plot of the frequencies of the ACAC, AGAG, and ATAT motifs in the genes of the Gn2 genome. Individual points outside the whiskers represent genes that possess an extraordinary number of microsatellites compared with the central tendency of the genome.

©2026, Universidad Politécnica Salesiana, Ecuador.

On the other hand, the box plot in Figure 4, corresponding to the microsatellites in Gn2, illustrates the findings. Outliers can be observed for ATAT, which in turn generate the peaks observed in the surface plot. It should be noted that, for AGAG and ACAC, most points are located near zero, indicating that most Gn2 genes contain few or no microsatellites of this type.

Regarding Gn3, a surface plot of the ATAT, AGAG, and ACAC variables was also obtained. Figure 5 illustrates this representation.

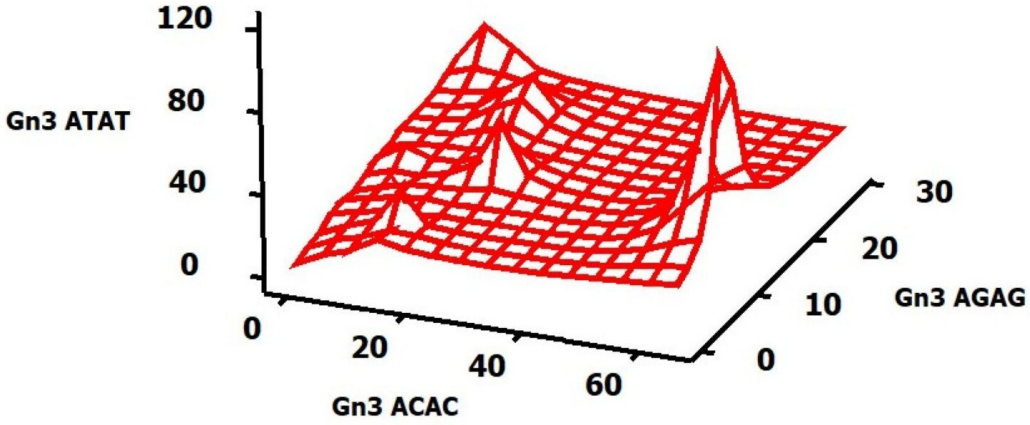


Figure 5. Surface plot of microsatellites in the Gn3 genome of *S. aureus*. The vertical axis represents the frequency of the ATAT motif as a function of the co-occurrence of the ACAC and AGAG motifs. The peaks indicate genes with an anomalous joint accumulation of these tetranucleotides.

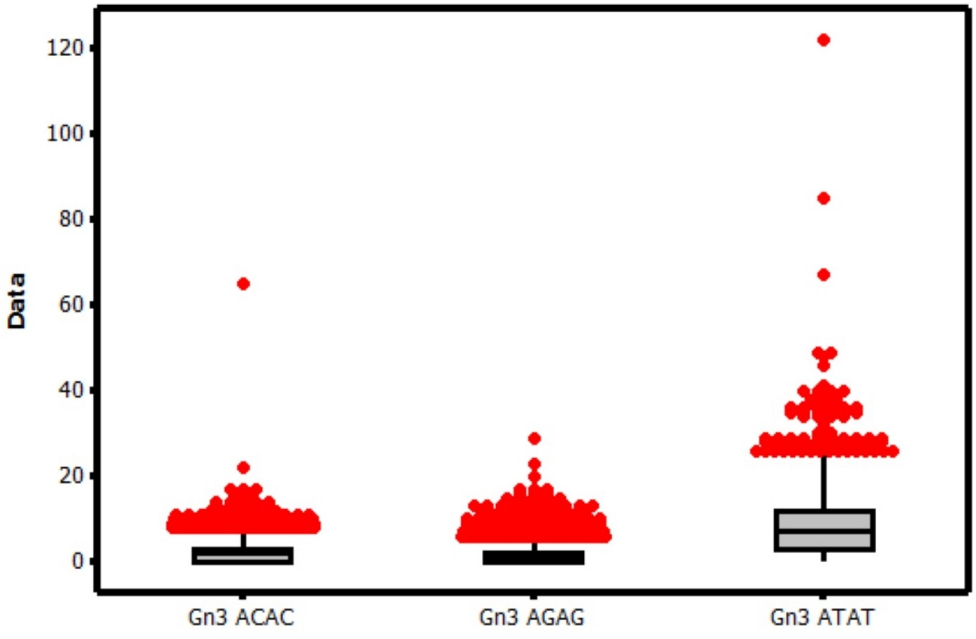


Figure 6. Box plot of the frequencies of the ACAC, AGAG, and ATAT motifs in the genes of the Gn3 genome. Individual points outside the whiskers represent genes that possess an extraordinary number of microsatellites compared with the central tendency of the genome.

La Granja: *Revista de Ciencias de la Vida* 44(2) 2026:42-58.
©2026, Universidad Politécnica Salesiana, Ecuador.

Similar features are observed compared with the previous figure; however, differences indicating changes in the microsatellites are also present. For example, the location of the central peaks in the image. Figure 6 below illustrates this distribution using a box plot.

Scattered points corresponding to ATAT and AGAG are observed in the figure. This indicates that other genes, compared with the previous genome, contain a greater number of microsatellites. Finally, for Gn4, Figure 7 shows the surface plot corresponding to the three microsatellites: ATAT, AGAG, and ACAC.

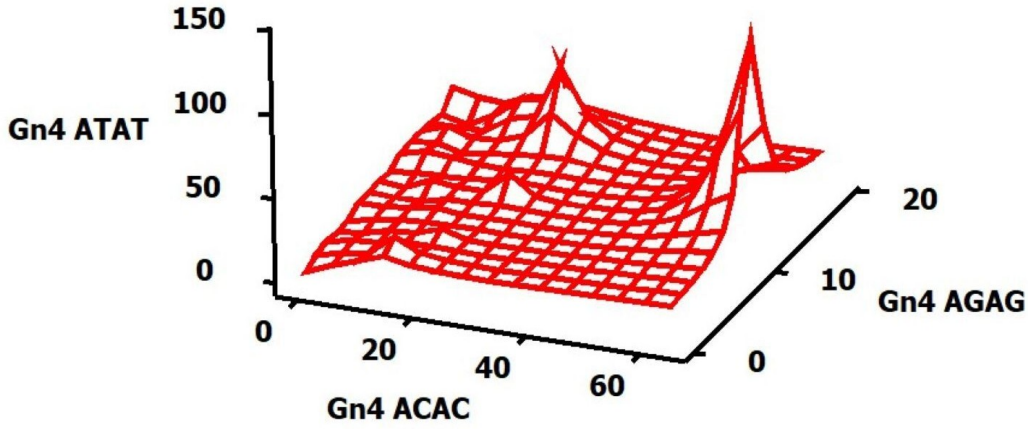


Figure 7. Surface plot of microsatellites in the Gn4 genome of *S. aureus*. The vertical axis represents the frequency of the ATAT motif as a function of the co-occurrence of the ACAC and AGAG motifs. The peaks indicate genes with an anomalous joint accumulation of these tetranucleotides.

It is noteworthy that a peak is present on the right side, although at a location closer to the upper corner. This suggests new microsatellite arrangements. Likewise, the peak near the upper-left corner exhibits a greater elevation than that of the previous genome. On the other hand, Figure 8 shows the box plot of this genome for microsatellite counts.

The microsatellite count for AGAG remained practically below those of the other motifs, with no outliers. The distribution also changed for ACAC. In addition, ATAT appears to be increasing in abundance compared with the other genomes. Table 1 below presents the descriptive statistics for the mean, minimum, and maximum values of the three variables in the Gn1, Gn2, Gn3, and Gn4 genomes. It is noteworthy that, in all cases, the mean values of the ATAT variable are higher. This indicates a greater presence of ATAT microsatellites in all cases. However, the highest value was observed in the Gn1 genome for the ACAC variable, with a value of 158.

Regarding the results obtained, a folder containing the Gn1, Gn2, Gn3, and Gn4 genomes in .fna format is available for download on the Galaxy platform. Likewise, the .csv files generated from the processing performed with the MFind tool for each microsatellite in the genomes are made available. Thus, for example, the files Gn1 ACAC.csv, Gn1 ATAT.csv, and Gn1 AGAG.csv are available for download for genome 1. Three .csv files corresponding to each of the remaining genomes are presented below. The tables corresponding to the calculation of the IQZ for each genome are also included. Available at: https://www.usegalaxy.org/u/rioswillars/h/s-aureus-microsatellite.

©2026, Universidad Politécnica Salesiana, Ecuador.

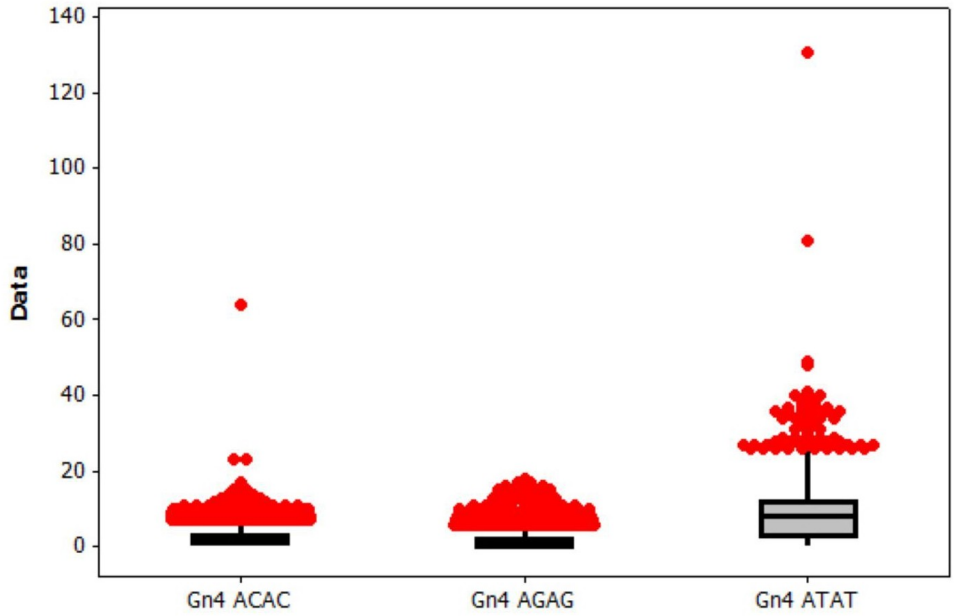


Figure 8. Box plot of the frequencies of the ACAC, AGAG, and ATAT motifs in the genes of the Gn4 genome. Individual points outside the whiskers represent genes that possess an extraordinary number of microsatellites compared with the central tendency of the genome.

Table 1. Descriptive statistics of the ATAT, AGAG, and ACAC variables in the Gn1, Gn2, Gn3, and Gn4 genomes.

Genome	Variable	Mean	SD	Min	Max
Gn1	ACAC	2.47	4.03	0	158
Gn1	AGAG	1.5688	2.4365	0	43
Gn1	ATAT	8.722	7.286	0	123
Gn2	ACAC	2.3752	2.7245	0	65
Gn2	AGAG	1.5338	2.2454	0	20
Gn2	ATAT	8.705	7.26	0	124
Gn3	ACAC	2.3016	2.6768	0	65
Gn3	AGAG	1.5826	2.348	0	29
Gn3	ATAT	8.618	7.36	0	122
Gn4	ACAC	2.3844	2.7234	0	64
Gn4	AGAG	1.5654	2.2614	0	18
Gn4	ATAT	8.484	7.162	0	131

In this study, we calculated the IQZ composite index for four *Staphylococcus aureus* genomes (Gn1–Gn4) using three normalized components: GC_norm, Alt_Score, and MS_score, weighted at 0.4, 0.4, and 0.2, respectively. This combination integrates nucleotide composition (GC_norm) with quantitative metrics derived from hit patterns (Alt_Score and MS_score), thereby providing a unified metric for sequence prioritization. The IQZ calculation was applied to all genes in each genome, and quantification tables were generated. In all cases, we observed that the highest IQZ values were

©2026, Universidad Politécnica Salesiana, Ecuador.

associated with segments that simultaneously exhibited moderate to high GC profiles, together with a high microsatellite count in terms of both density and relative prominence. This indicates that IQZ prioritizes regions in which pattern-based metrics and GC composition converge.

In Gn1, the sequences with the highest IQZ correspond to extended regions with high Alt_Score (a metric of pattern density per unit length) and high MS_score (a metric of normalized intragenomic prominence). In Gn2 and Gn3, the maximum IQZ values exhibit similar behavior: the top candidates combine GC_norm values above the average, a favorable hits-to-length ratio, and remarkable relative prominence within the genome. In Gn4, the profile of the maximum IQZ values is consistent with that of Gn2 and Gn3, reinforcing the reproducibility of the composite criterion across different genomic contexts of *S. aureus*. Comparatively among genomes, although MS_score is intrinsically intragenomic (normalized to the maximum value within each file), the structure of IQZ allows the qualitative assessment of the robustness of priority regions in each genome. Furthermore, the stability of the IQZ ranking under moderate variations in GC_norm suggests that the pattern-based metrics (Alt_Score and MS_score) adequately capture both the density and the prominence of the motifs, thereby avoiding excessive bias due to nucleotide composition.

For traceability and practical use, Table 2 presents the lists of the five sequences (genes) with the highest IQZ values for each genome (Gn1–Gn4). These lists support the conclusions presented above and provide a basis for subsequent decisions, such as experimental validation, probe/primer design, or annotation prioritization. Additionally, Figure 9 presents a visual representation of the IQZ index for the sequences of each genome. Overall, IQZ behaves as a synthetic and stable metric for highlighting candidate genomic segments by integrating GC composition and the quantitative metrics of the pattern in a balanced manner.

Table 2. List of the five genes with the highest IQZ values in each genome.

Dataset	seq num	Gene length	Total hits	ACAC hits	AGAG hits	ATAT hits	IQZ
Gn1	1861	31303	324	158	43	123	0.35334
Gn1	1337	74	1	0	1	0	0.270888
Gn1	1325	76	1	0	1	0	0.269038
Gn1	1336	76	1	0	1	0	0.269038
Gn1	1391	72	2	2	0	0	0.262346
Gn2	1447	32241	195	65	6	124	0.34976
Gn2	172	7176	121	22	13	86	0.277447
Gn2	1967	84	2	2	0	0	0.27348
Gn2	1929	89	3	2	1	0	0.27274
Gn2	1983	74	1	1	0	0	0.271296
Gn3	1519	31266	196	65	9	122	0.349261
Gn3	194	7176	120	22	13	85	0.275793
Gn3	2043	84	2	2	0	0	0.273469
Gn3	2060	74	1	1	0	0	0.271291
Gn3	624	76	1	0	1	0	0.269441
Gn4	1491	31875	205	64	10	131	0.348869
Gn4	1962	84	2	2	0	0	0.27338
Gn4	1914	89	3	2	1	0	0.27259
Gn4	1978	74	1	1	0	0	0.271246
Gn4	174	7176	119	23	15	81	0.270445

©2026, Universidad Politécnica Salesiana, Ecuador.

It is noteworthy that the length of the region is strongly associated with the IQZ (correlation of 0.98, $p = 0.00$). Longer regions tend to exhibit higher IQZ values. This is consistent with the fact that IQZ includes components that depend on both the number of hits and the sequence length, as well as the associated normalization procedures.

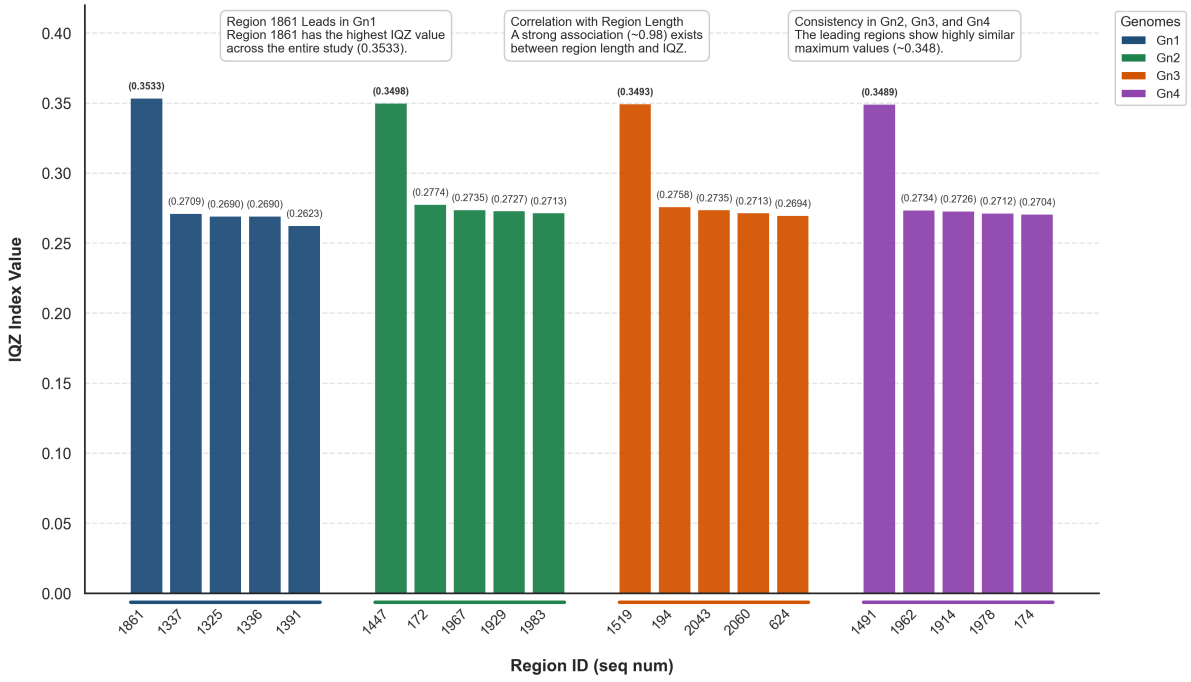


Figure 9. Comparison of the Chirality Change Propensity Index (IQZ) for the five genes with the highest values in each genome. The graph illustrates the magnitude of the index grouped by genome, allowing the differences in the distribution of the maximum values of the Gn1 genome to be observed relative to the remaining lineages.

Finally, the electronic folder on the Galaxy platform mentioned above contains tables showing the calculations for the *MS_score*, *Alt_score*, *GC_norm* and *IQZ* metrics for each of the genes in the Gn1, Gn2, Gn3 and Gn4 genomes.

4 Conclusions

Microsatellite analysis is a strategy for understanding the evolution and adaptation of organisms of interest. In this study, four *S. aureus* genomes were described in detail by analyzing each of their genes and identifying and counting the ATAT, AGAG, and ACAC microsatellites using the MFind tool, a freely available software package that can be downloaded and executed in Java and is available on GitHub. Among the findings, Gn1 exhibited clear differences compared with the other three genomes. Whereas Gn2, Gn3, and Gn4 displayed similarities that allowed comparable regions to be identified in the surface plots, the peaks and valleys of the plots were located at different positions, suggesting a reorganization of the genetic information. On the other hand, microsatellite counts were higher for the ATAT motif in the Gn2, Gn3, and Gn4 genomes, whereas Gn1 represented an exception, in which the maximum value was observed for the ACAC variable, with a value of 158. This indicates an atypical case due to the presence of this number of microsatellites within a gene of this genome.

Finally, this work provides an overview of microsatellites in four reported *S. aureus* genomes, this bacterium being the species most commonly identified in studies of wounds in humans and farm animals. In addition, this study characterizes the organization of repetitive motifs in the four *Staphy-*

©2026, Universidad Politécnica Salesiana, Ecuador.

lococcus aureus genomes analyzed, focusing on the chirality of the patterns and their variation among genomes. The comparative profiles show that Gn1 differs from the behavior observed in Gn2–Gn4, not only because of the predominant motif but also because of the displacement of peaks and valleys in the density surfaces, suggesting chirally relevant differences in the local arrangement of the repeats. In Gn2–Gn4, the ATAT motif predominates, whereas Gn1 exhibits an atypical enrichment of the ACAC motif. This asymmetry in the predominant motif, together with the displacement of maxima among genomes, is consistent with a reconfiguration of the repetitive architecture with a chiral component (differences in relative orientations and possible transitions between mirror motifs along the genome). Such patterns may affect genomic directionality and plasticity, insofar as inverted or strand-biased repeats modulate properties such as secondary structure formation or the propensity for recombination events.

The interpretation of these findings should consider certain limitations: only three motifs (ATAT, AGAG, and ACAC) were evaluated, the metrics depend on the size of the analyzed region, and the MFind detection tool was employed. Future studies should incorporate an index based on three-dimensional simulations because, unlike the current statistical predictive index (IQZ), which is based on a linear (2D) sequence, a 3D simulation would allow the torsional stress energy to be measured accurately and confirm whether alternating chirality induces the folding of secondary structures *in vivo*. Such biophysical validation is crucial because these three-dimensional conformational changes promote polymerase slippage and activate the phase-variation switch that regulates virulence and adaptation in *S. aureus*. Overall, this study provides a comparative map highlighting the chiral dimension of *S. aureus* microsatellites and motivates mechanistic analyses to quantify their contribution to genomic variation among lineages. In this regard, future studies should determine whether these regions occur in specific genomic areas, such as low-complexity regions, or whether they are distributed in a delimited manner within them.

Acknowledgments

The authors wish to thank the Faculty of Systems of the Autonomous University of Coahuila, Saltillo Campus, for the assistance provided during the development of this work.

Funding

The authors would like to thank the IPICyT National Supercomputing Center for supporting this research with computing time grant TKII-E-1024-I-011024-47.

Declaration on the use of artificial intelligence

The authors DECLARE that, during the preparation of the article entitled "Tendency to Functional Asymmetry and Microsatellite-Induced Helical Chirality in *Staphylococcus aureus*", no generative artificial intelligence tools or automated assistance systems were used for the writing, analysis, data interpretation, content generation, translation, or editing of the manuscript.

The authors assume full responsibility for the content, originality, integrity, and final version of the article.

Author's contribution

E.R.W.: Conceptualization, Investigation, Methodology, Software. **M.M.D.S.:** Writing – original draft, Investigation, Data curation. **M.I.G.M.:** Writing – review & editing.

References

Ahmad-Mansour, N., Loubet, P., Pouget, C., Dunyach-Remy, C., Sotto, A., Lavigne, J.-P., and Molle, V. (2021). Staphylococcus aureus toxins: An update on their pathogenic properties and potential treatments. *Toxins*, *13*(10), 677. Online: https://doi.org/10.3390/toxins13100677

Archer, G. L. (1998). Staphylococcus aureus: A well–armed pathogen. *Clinical Infectious Diseases*, *26*(5),

©2026, Universidad Politécnica Salesiana, Ecuador.

1179–1181. Online: https://doi.org/10.1086/520289

Bacolla, A., Larson, J. E., Collins, J. R., Li, J., Milosavljevic, A., Stenson, P. D., ... Wells, R. D. (2008). Abundance and length of simple repeats in vertebrate genomes are determined by their structural properties. *Genome Research*, *18*(10), 1545–1553. Online: https://doi.org/10.1101/gr.078303.108

Bagshaw, A. T. M. (2017). Functional mechanisms of microsatellite adn in eukaryotic genomes. *Genome Biology and Evolution*, *9*(9), 2428–2443. Online: https://doi.org/10.1093/gbe/evx164

Brooks, J., and Jefferson, K. (2014). Phase variation of poly-n-acetylglucosamine expression in staphylococcus aureus. *PLoS Pathogens*, *10*(7), e1004292. Online: https://doi.org/10.1371/journal.ppat.1004292

Crespo-Piazuelo, D., and Lawlor, P. G. (2021). Livestock-associated methicillin-resistant staphylococcus aureus (la-mrsa) prevalence in humans in close contact with animals and measures to reduce on-farm colonisation. *Irish Veterinary Journal*, *74*(1), 21. Online: https://doi.org/10.1186/s13620-021-00200-7

Dunyach-Remy, C., Ngba Essebe, C., Sotto, A., and Lavigne, J.-P. (2016). Staphylococcus aureus toxins and diabetic foot ulcers: Role in pathogenesis and interest in diagnosis. *Toxins*, *8*(7), 209. Online: https://doi.org/10.3390/toxins8070209

Essien, U. C., Boswihi, S. S., Agbakoba, N. R., and Udo, E. E. (2022). Description of methicillin-susceptible staphylococcus aureus clonal complex 30 related to the pandemic phage type 80/81 isolated from patients in three tertiary hospitals in jos, north central nigeria. *Medical Principles and Practice*, *31*, 269–275. Online: https://doi.org/10.1159/000524755

Gadgil, R. Y., Romer, E. J., Goodman, C. C., Rider, S. D., Damewood, F. J., Barthelemy, J. R., ... Leffak, M. (2020). Replication stress at microsatellites causes dna double-strand breaks and break-induced replication. *Journal of Biological Chemistry*, *295*(45), 15378–15397. Online: https://doi.org/10.1074/jbc.RA120.013495

George, A. N., Stewart, J. R., Evans, J. C., and Gibson, J. M. (2020). Risk of antibiotic-resistant staphylococcus aureus dispersion from hog farms: A critical review. *Risk Analysis*, *40*(8), 1645–1665. Online: https://doi.org/10.1111/risa.13495

Gherardi, G. (2023). Staphylococcus aureus infection: Pathogenesis and antimicrobial resistance. *International Journal of Molecular Sciences*, *24*(9), 8182. Online: https://doi.org/10.3390/ijms24098182

Gladding, T. L., Rolph, C. A., Gwyther, C. L., Kinnersley, R., Walsh, K., and Tyrrel, S. (2020). Concentration and composition of bioaerosol emissions from intensive farms: Pig and poultry livestock. *Journal of Environmental Management*, *272*, 111052. Online: https://doi.org/10.1016/j.jenvman.2020.111052

Gor, V., Ohniwa, R., and Morikawa, K. (2021). No change, no life? what we know about phase variation in staphylococcus aureus. *Microorganisms*, *9*(2), 244. Online: https://doi.org/10.3390/microorganisms9020244

Guillén, R., Salinas, C., Mendoza-Álvarez, A., Rubio Rodríguez, L. A., Díaz-de Usera, A., Lorenzo-Salazar, J. M., ... Rodríguez, F. (2024). Genomic epidemiology of the primary methicillin-resistant staphylococcus aureus clones causing invasive infections in paraguayan children. *Microbiology Spectrum*, *12*(2), e03012-23. Online: https://doi.org/10.1128/spectrum.03012-23

Harhay, G., Harhay, D., Bono, J., Capik, S., Dedonder, K., Apley, M., ... Smith, T. (2019). A computational method to quantify the effects of slipped strand mispairing on bacterial tetranucleotide repeats. *Scientific Reports*, *9*, 17192. Online: https://doi.org/10.1038/s41598-019-53866-z

Heaton, C. J., Gerbig, G. R., Sensius, L. D., Patel, V., and Smith, T. C. (2020). Staphylococcus aureus epidemiology in wildlife: A systematic review. *Antibiotics*, *9*(2), 89. Online: https://doi.org/10.3390/antibiotics9020089

Holden, M. T. G., Feil, E. J., Lindsay, J. A., Peacock, S. J., Day, N. P. J., Enright, M. C., ... Parkhill, J. (2004). Complete genomes of two clinical staphylococcus aureus strains: Evidence for the rapid evolution of virulence and drug resistance. *Proceedings of the National Academy of Sciences*, *101*(26), 9786–9791. Online: https://doi.org/10.1073/pnas.0402521101

©2026, Universidad Politécnica Salesiana, Ecuador.

Idrees, M., Sawant, S., Karodia, N., and Rahman, A. (2021). Staphylococcus aureus biofilm: Morphology, genetics, pathogenesis and treatment strategies. *International Journal of Environmental Research and Public Health*, *18*(14), 7602. Online: https://doi.org/10.3390/ijerph18147602

Kwiecinski, J. M., and Horswill, A. R. (2020). Staphylococcus aureus bloodstream infections: pathogenesis and regulatory mechanisms. *Current Opinion in Microbiology*, *53*, 51–60. Online: https://doi.org/10.1016/j.mib.2020.02.005

Larkin, E., Carman, R., Krakauer, T., and Stiles, B. (2009). Staphylococcus aureus: The toxic presence of a pathogen extraordinaire. *Current Medicinal Chemistry*, *16*(30), 4003–4019. Online: https://doi.org/10.2174/092986709789352321

Martin, P., Makepeace, K., Hill, S. A., Hood, D. W., and Moxon, E. R. (2005). Microsatellite instability regulates transcription factor binding and gene expression. *Proceedings of the National Academy of Sciences*, *102*(10), 3800–3804. Online: https://doi.org/10.1073/pnas.0406805102

Metzgar, D., Liu, L., Hansen, C., Dybvig, K., and Wills, C. (2002). Domain-level differences in microsatellite distribution and content result from different relative rates of insertion and deletion mutations. *Genome Research*, *12*(3), 408–413. Online: https://doi.org/10.1101/gr.198602

Monecke, S., Akpaka, P. E., Smith, M. R., Unakal, C. G., Thoms Rodriguez, C.-A., Ashraph, K., … Ehricht, R. (2023). Clonal complexes distribution of staphylococcus aureus isolates from clinical samples from the caribbean islands. *Antibiotics*, *12*(6), 1050. Online: https://doi.org/10.3390/antibiotics12061050

Narechania, A., Baker, R., DeSalle, R., Mathema, B., Kolokotronis, S.-O., Kreiswirth, B., and Planet, P. J. (2016). Clusterflock: a flocking algorithm for isolating congruent phylogenomic datasets. *GigaScience*, *5*(1), 43. Online: https://doi.org/10.1186/s13742-016-0152-3

Oliveira, D., Borges, A., and Simões, M. (2018). Staphylococcus aureus toxins and their molecular activity in infectious diseases. *Toxins*, *10*(6), 252. Online: https://doi.org/10.3390/toxins10060252

Pedersen, K., Nielsen, M. W., Fertner, M. E., Espinosa-Gongora, C., and Bækbo, P. (2024). Development of livestock-associated methicillin-resistant staphylococcus aureus (la-mrsa) loads in pigs and pig stables during the fattening period. *Veterinary Sciences*, *11*(11), 558. Online: https://doi.org/10.3390/vetsci11110558

Ramirez, H. A., Pastar, I., Jozic, I., Stojadinovic, O., Stone, R. C., Ojeh, N., … Tomic-Canic, M. (2018). Staphylococcus aureus triggers induction of mir-15b-5p to diminish dna repair and deregulate inflammatory response in diabetic foot ulcers. *Journal of Investigative Dermatology*, *138*(5), 1187–1196. Online: https://doi.org/10.1016/j.jid.2017.11.038

Ramos, B., Rosalino, L. M., Palmeira, J. D., Torres, R. T., and Cunha, M. V. (2022). Antimicrobial resistance in commensal staphylococcus aureus from wild ungulates is driven by agricultural land cover and livestock farming. *Environmental Pollution*, *303*, 119116. Online: https://doi.org/10.1016/j.envpol.2022.119116

Rios-Willars, E., and Chirinos-Arias, M. C. (2024). Mfind: a tool for dna barcode analysis in angiosperms and its relationship with microsatellites using a sliding window algorithm. *Planta*, *259*(6), 134. Online: https://doi.org/10.1007/s00425-024-04420-3

Saeed, A. F., Wang, R., and Wang, S. (2016). Microsatellites in pursuit of microbial genome evolution. *Frontiers in Microbiology*, *6*, 1462. Online: https://doi.org/10.3389/fmicb.2015.01462

Sayers, E. W., Beck, J., Bolton, E. E., Brister, J. R., Chan, J., Connor, R., … Pruitt, K. D. (2025). Database resources of the national center for biotechnology information in 2025. *Nucleic Acids Research*, *53*(D1), D20–D29. Online: https://doi.org/10.1093/nar/gkae979

Sayhood, M. H., Mohammed, A. L., Abdulhameed, M. F., and Jori, M. M. (2022). Classical and molecular identification of staphylococcus aureus isolated from infestation cattle wounds with myiasis in basrah governorate, iraq. *Iraqi Journal of Veterinary Sciences*, *36*(3), 641–646. Online: https://doi.org/10.33899/ijvs.2021.131196.1930

Shettigar, K., and Murali, T. S. (2020). Virulence factors and clonal diversity of staphylococcus

©2026, Universidad Politécnica Salesiana, Ecuador.

aureus in colonization and wound infection with emphasis on diabetic foot infection. *European Journal of Clinical Microbiology & Infectious Diseases*, *39*(12), 2235–2246. Online: https://doi.org/10.1007/s10096-020-03984-8

Song, X., Yang, T., Zhang, X., Yuan, Y., Yan, X., Wei, Y., … Zhou, C. (2021). Comparison of the microsatellite distribution patterns in the genomes of euarchontoglires at the taxonomic level. *Frontiers in Genetics*, *12*, 622724. Online: https://doi.org/10.3389/fgene.2021.622724

Srivastava, D., Ahmad, M. M., Shamim, M., Maurya, R., Srivastava, N., Pandey, P., … Siddiqui, M. H. (2019). Modulation of gene expression by microsatellites in microbes. En *New and future developments in microbial biotechnology and bioengineering* (pp. 209–218). Elsevier. Online: https://doi.org/10.1016/B978-0-444-63503-7.00012-7

Tatusova, T., Ciufo, S., Fedorov, B., O'Neill, K., and Tolstoy, I. (2015). Refseq microbial genomes database: new representation and annotation strategy. *Nucleic Acids Research*, *43*(7), 3872–3872. Online: https://doi.org/10.1093/nar/gkv278

Timsit, Y., and Várnai, P. (2010). Helical chirality: a link between local interactions and global topology in dna. *PLoS ONE*, *5*(2), e9326. Online: https://doi.org/10.1371/journal.pone.0009326

Tong, S. Y. C., Davis, J. S., Eichenberger, E., Holland, T. L., and Fowler, V. G. (2015). Staphylococcus aureus infections: Epidemiology, pathophysiology, clinical manifestations, and management. *Clinical Microbiology Reviews*, *28*(3), 603–661. Online: https://doi.org/10.1128/CMR.00134-14

Vayssières, M., Marechal, N., Yun, L., Lopez Duran, B., Murugasamy, N. K., Fogg, J. M., … Lamour, V. (2024). Structural basis of dna crossover capture by escherichia coli dna gyrase. *Science*, *384*(6692), 227–232. Online: https://doi.org/10.1126/science.adl5899

Wang, Y., Zhang, P., Wu, J., Chen, S., Jin, Y., Long, J., … Yang, H. (2023). Transmission of livestock-associated methicillin-resistant staphylococcus aureus between animals, environment, and humans in the farm. *Environmental Science and Pollution Research*, *30*(37), 86521–86539. Online: https://doi.org/10.1007/s11356-023-28532-7

Winogradoff, D., Li, P., Joshi, H., Quednau, L., Maffeo, C., and Aksimentiev, A. (2021). Chiral systems made from dna. *Advanced Science*, *8*(5), 2003113. Online: https://doi.org/10.1002/advs.202003113

Wu, Y., Chen, T., Wang, Y., Huang, M., Wang, Y., and Luo, Z. (2023). New insight into the virulence and inflammatory response of staphylococcus aureus strains isolated from diabetic foot ulcers. *Frontiers in Cellular and Infection Microbiology*, *13*, 1234994. Online: https://doi.org/10.3389/fcimb.2023.1234994

Yu, S., Xie, Y., Jiao, Y., Li, N., and Ding, B. (2025). Nucleic acid-based chiral nanostructures and their biomedical applications. *Nanoscale Horizons*, *10*(9), 1802–1814. Online: https://doi.org/10.1039/D5NH00140D

Zhou, K., Aertsen, A., and Michiels, C. (2014). The role of variable dna tandem repeats in bacterial adaptation. *FEMS Microbiology Reviews*, *38*(1), 119–141. Online: https://doi.org/10.1111/1574-6976.12036

©2026, Universidad Politécnica Salesiana, Ecuador.

La Granja:
Revista de
Ciencias de la Vida

pISSN:1390-3799; eISSN:1390-8596

https://doi.org/10.17163/lgr.n44.2026.04

Artículo científico / Scientific paper

Earth Sciences

Hydrological variability due to changes in land cover in the Wawayme river basin caused by mining activities, Ecuador

Variabilidad hidrológica por cambio de cobertura de suelo en la cuenca del río Wawayme debido a actividades mineras, Ecuador

Raúl Andrés Moreno Farfán[1] and María Z. Flores López[2]

[1]*Universidad Estatal Península de Santa Elena (UPSE), La Libertad, Santa Elena, Ecuador. [https://ror.org/01k410495]*
[2]*Universidad Autónoma de Baja California Sur, México. [https://ror.org/01046sm89]*

*Corresponding author: rmoreno320@upse.edu.ec

Article received on February 1st, 2025. Accepted, after review, on December 11th, 2025. Published on September 1st, 2026.

Abstract

This study evaluates the hydrological effects resulting from changes in land use and land cover in the Wawayme River basin, Ecuador. The research was conducted through: 1) multitemporal analysis of vegetation cover between 2013 and 2020, using supervised classification with the SCP plugin in QGIS; and 2) comparative hydrological modeling of scenarios for 2015–2020, using the TETIS distributed hydrological model. Hydrological parameters were estimated based on available meteorological data, terrain characteristics, and edaphic properties. As a result, we obtained a decrease of 14.35 % in primary vegetated areas and an increase of 13.86 % in primary non-vegetated areas; and an increase in simulated flow and volume in the basin of 0.002 $m^3\ s^{-1}$ and 0.196 Hm^3, respectively, evidencing a variability in the hydrological behavior of the basin. The limited availability of meteorological and hydrological data is a recurrent challenge in the region. However, the applied methodology highlights the importance of monitoring and managing water resources in areas with extractive activities. This study underlines the need to implement mitigation and conservation measures that minimize environmental impacts and favor the resilience of local communities.

Keywords: Land cover and land use, hydrologic modeling, watershed, mining, environment.

©2026, Universidad Politécnica Salesiana, Ecuador.

Resumen

Este estudio evalúa los efectos hidrológicos derivados de cambios en el uso y cobertura del suelo en la cuenca del río Wawayme, Ecuador. La investigación se desarrolló mediante: 1) análisis multitemporal de cobertura vegetal entre 2013-2020 utilizando clasificación supervisada con el plug-in SCP en QGIS; y 2) modelación hidrológica comparativa de escenarios 2015-2020 empleando el modelo hidrológico distribuido TETIS. Los parámetros hidrológicos se estimaron a partir de datos meteorológicos, características del terreno y propiedades edáficas disponibles. Como resultado se obtuvo una disminución de áreas primariamente vegetadas de 14,35 % y un aumento de áreas primariamente no vegetales de 13,86 %; y un aumento del caudal y volumen simulado en la cuenca de 0,002 $m^3\ s^{-1}$ y 0,196 Hm^3 respectivamente, evidenciando una variabilidad en el comportamiento hidrológico de la cuenca. La limitada disponibilidad de datos meteorológicos e hidrológicos constituye un desafío recurrente en la región. No obstante, la metodología aplicada resalta la importancia de monitorear y gestionar de manera adecuada los recursos hídricos en zonas con actividades extractivas. Este estudio subraya la necesidad de implementar medidas de mitigación y conservación que minimicen los impactos ambientales y favorezcan la resiliencia de las comunidades locales.

Palabras clave: Cobertura y uso del suelo, modelación hidrológica, cuenca hidrográfica, minería, ambiente.

Suggested citation: Moreno, R. and Flores, M. (2026). Hydrological variability due to changes in land cover in the Wawayme river basin caused by mining activities, Ecuador. La Granja: Revista de Ciencias de la Vida. Vol. 44(2):59-77. https://doi.org/10.17163/lgr.n44.2026.04.

Orcid IDs:

Raúl Andrés Moreno Farfán: https://orcid.org/0000-0001-8194-8386
María Z. Flores López: https://orcid.org/0000-0002-8446-9951

©2026, Universidad Politécnica Salesiana, Ecuador.

1 Introduction

The global hydrological cycle is undergoing significant modifications as a result of alterations in terrestrial ecosystems. At a global scale, river basins are increasingly facing water availability challenges due to the degradation of their natural conditions. The overexploitation of natural resources, land cover change, and climate change are key drivers reducing both the quantity and availability of water resources, leading to more frequent flood events and increased water stress (Angulo and Saavedra, 2018). Furthermore, it is difficult to conceive of any human activity on land that does not involve soil disturbance or modifications to the upper soil layers, often replacing ecosystems that once contributed to the formation of fertile soils with others that do not (Daily and Ehrlich, 1992).

This ecosystem transformation is particularly relevant in regions characterized by high biodiversity and environmental fragility, such as the Amazon, where alterations in vegetation cover can have significant impacts on regional and local hydrological regimes (Nobre et al., 2016). Recent studies demonstrate that the conversion of natural land covers into anthropized areas can substantially alter runoff, infiltration, and evapotranspiration patterns, thereby generating imbalances in watershed hydrological behavior (Siswanto and Francés, 2019; Fang and Fan, 2021).

Within this context, economic development is often accompanied by activities such as the exploitation of non-renewable resources, particularly mining. In this regard, Ecuador has increased its position as a mining destination by 26 % (Ministerio de Energía y Minas, 2022), reflecting new strategies and regulatory frameworks that mark a shift for a country traditionally reliant on oil and agricultural exports. Major mining projects such as Mirador and Fruta del Norte are currently in operation, while others—including Loma Larga, Curipamba, La Plata, and Cascabel—are expected to enter production in the future (Moreno Farfán, 2022).

Although these developments are consistent with economic growth objectives, it is important to know that mining activities have generated problematic situations due to their inherent impacts (Vásconez and Torres, 2018). Large-scale extractive projects have not been exempted from controversy, particularly regarding concerns over the violation of human rights and the rights of nature (Angelo and Sempere, 2018). This issue becomes especially critical given the location of many of these projects within ecosystems of high ecological value and biodiversity—such as the Ecuadorian Amazon—where inadequate planning and overexploitation of natural resources may lead to severe environmental impacts, particularly affecting water resources.

In recent decades, accelerated soil degradation driven by anthropogenic activities has significantly altered the Earth's surface (de Jong et al., 2021), with nearly three-quarters of it having been modified over the last millennium. At present, addressing global sustainability challenges—such as climate change mitigation, biodiversity loss, and food sovereignty—has become a main concern. These challenges are directly linked to land use and land cover changes, as unsustainable practices can severely affect carbon sources and sinks, lead to habitat loss, and undermine the capacity to sustain food production (Winkler et al., 2021).

Consequently, economic activities such as agriculture, oil extraction, and mining are the main drivers of deforestation in the Ecuadorian Amazon, resulting in biodiversity loss, extensive forest clearing—reaching approximately 50 000 ha $year^{-1}$—and continuous soil degradation (Custode and Sourdat, 1986; Bustamante et al., 1993; Giraldo et al., 2013). For example, in Ecuador, the agricultural and forestry sectors expanded by 45 % over a 37-year period, while mining-affected areas exceeded 7 000 ha by 2021 (Paz, 2024). According to the National Institute of Agricultural Research (INIAP, 2018), soil loss in the country ranges from 30 to 50 t ha^{-1} $year^{-1}$ in foothill areas with slopes greater than 25 %. In areas with slopes between 12 % and 25 %, erosion ranges from 10 to 30 t ha^{-1} $year^{-1}$, while in areas with slopes below 12 %—which comprise much of the Ecuadorian Amazon—erosion is estimated between 5 and 10 t ha^{-1} $year^{-1}$ (Suquilanda, 2008).

Before addressing the relevance of land use and land cover within the hydrological regime, it is essential to define these concepts. Land cover refers to the biophysical surface observed on the Earth, focusing on vegetation and anthropogenic elements.

©2026, Universidad Politécnica Salesiana, Ecuador.

Land use, in contrast, is characterized by the arrangements, activities, and inputs undertaken by humans on a given land cover to produce, modify, or maintain it (FAO, 2005).

In a relatively short period, environmental degradation caused by changes in land use and land cover has become a major global concern, attracting increasing attention from researchers. These changes pose a significant threat to watershed sustainability, as they are directly associated with increased water stress, higher frequency of flood events—due to their influence on water supply at the basin scale, where deforestation tends to increase streamflow as a result of reduced evapotranspiration—and alterations in erosion rates and sediment production (Angulo and Saavedra, 2018; Siswanto and Francés, 2019).

Dingman (2014) highlights that vegetation is a key determinant of the hydrological cycle, as it regulates evapotranspiration, infiltration, runoff, interception, and transpiration processes. Vegetation cover plays a fundamental role—alongside precipitation, topography, and other factors—in soil water recharge and runoff formation, directly influencing: (1) net precipitation reaching the soil surface; (2) soil infiltration rates; (3) soil moisture redistribution; and (4) evapotranspiration losses (Pascual, 2002).

Vegetation introduces a bidirectional sub-cycle within the hydrological system due to two main processes: (1) it interferes with the downward flux of precipitation through interception and evaporation losses, modifying the redistribution of fall according to soil infiltration capacity; and (2) it contributes to upward water flux through transpiration, by extracting water stored in soil layers and releasing it into the atmosphere as water vapor (Pascual, 2002).

In summary: (1) vegetation directly influences the water cycle, particularly in the dynamics of water storage surfaces, as it interacts with both the atmosphere and the soil; and (2) as a biological system, it consumes water necessary for its vital functions, forming what Barceló Coll et al. (2000) describe as the soil–vegetation–atmosphere system (Pascual, 2002).

Regarding the role of forests (forest soils and tree cover) in the hydrological cycle, Mintegui Aguirre and Robredo Sánchez (2008) note that they regulate water movement within watersheds by reducing runoff velocity and enhancing infiltration. They also directly influence the horizontal component of the hydrological cycle (transpiration) and interact with precipitation by intercepting vertical rainfall and facilitating the formation of horizontal precipitation processes such as condensation and fog formation.

Additionally, Mintegui Aguirre and Robredo Sánchez (1994) emphasize that: (1) vegetation cover acts as a stabilizing factor in watersheds during extreme rainfall events, mitigating torrential effects and functioning as a natural regulator of water resources; (2) it promotes biological stability and ecosystem regeneration processes, thus playing a conservation role; and (3) it prevents soil loss by reducing the impact of various erosion processes.

In this sense, soils with well-developed vegetation cover maintain sufficient levels of organic matter, improving soil structure and enhancing infiltration capacity. The root systems of forest species create preferential pathways that increase infiltration compared to agricultural soils, thereby contributing more significantly to subsurface runoff (Prats et al., 2011).

According to the FAO, global deforestation rates reached approximately 10 million hectares per year between 2015 and 2020. In Ecuador, the most recent data from the Ministry of Environment, Water and Ecological Transition (2018) indicate an annual loss of approximately 94 353 hectares of forest, a considerable figure compared to other countries in the region (Montaño, 2021). Historically, land use changes in the Amazon have been driven by increasing demand for agricultural products and non-renewable resources (Nobre et al., 2016). Ecuador is no exception, as these activities have been key drivers of deforestation, soil degradation, and the continuous loss of soil resources (Instituto Nacional de Investigaciones Agropecuarias (INIAP), 2018).

©2026, Universidad Politécnica Salesiana, Ecuador.

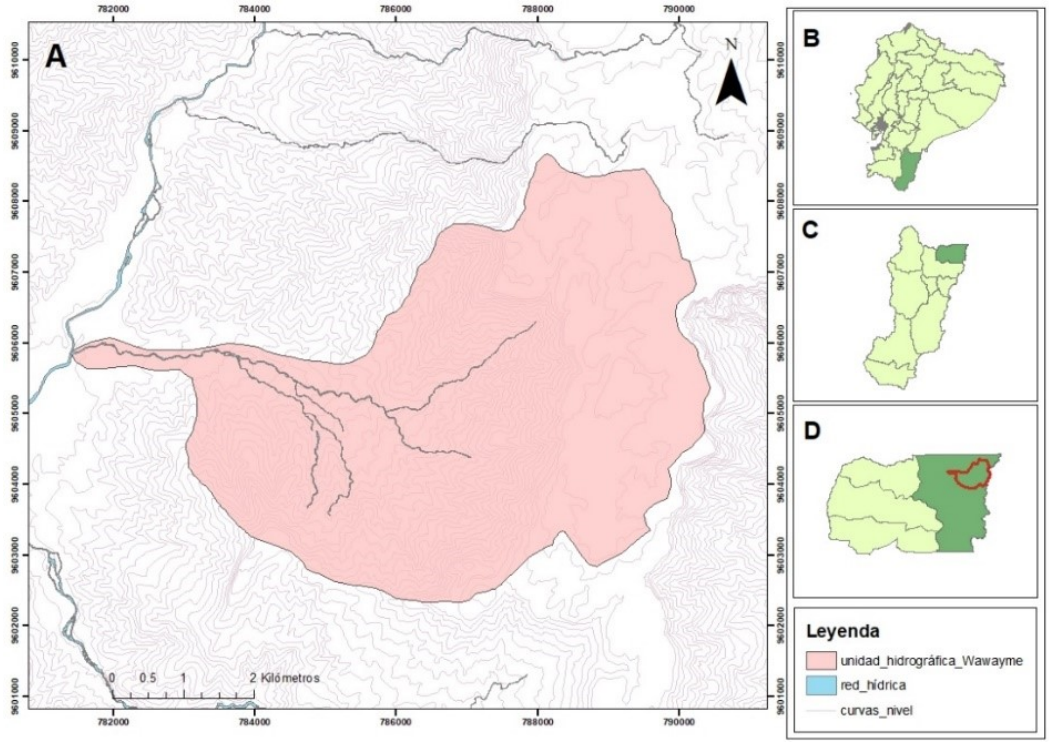


Figure 1. A: Location of the Wawayme River watershed; B: Location of Zamora Chinchipe Province within the Republic of Ecuador; C: Location of El Pangui canton within Zamora Chinchipe Province; and D: Location of the watershed within Tundayme parish, El Pangui canton.

Based on the foregoing, the present study aims to determine the variability in the hydrological balance resulting from changes in land use and land cover within the Wawayme River watershed (Figure 1), located in Zamora Chinchipe Province, Ecuador. This is achieved through geospatial analysis (using the SCP plugin and its post-processing methodology) and hydrological modeling (using the TETIS software). The specific objectives include: (1) quantifying changes in vegetation cover between 2013 and 2020 using remote sensing techniques; (2) implementing a hydrological model to simulate comparative scenarios; and (3) evaluating changes in hydrological regimes associated with the identified alterations in vegetation cover.

2 Materials and Methods

This research adopts a methodological approach that integrates geospatial analysis techniques and hydrological modeling. The methodology is structured into three main components. The first addresses: (1) the climatic and watershed characterization of the study area; (2) the initial operations and methodology used for satellite image classification; and (3) the estimation of TETIS parameters required for the execution of the hydrological model.

2.1 Climatic and Watershed Characterization

Initially, it was considered essential to carry out the climatic characterization of the study area by identifying climatic trends and extreme events, based on data recorded from two conventional meteorological stations located near the study area and operated by the National Institute of Meteorology and Hydrology (INAMHI). It should be noted that these stations are not located within the study watershed; however, they are the closest available (approximately 60 km in a straight line) and provide a more extensive temporal dataset.

The collected precipitation data were processed according to the available temporal scale (monthly

©2026, Universidad Politécnica Salesiana, Ecuador.

records from 1990 to 2017), allowing the calculation of Mean Monthly Precipitation values for each station over the available periods. The precipitation regime was identified as bimodal, with peak rainfall occurring between March and July, and lower precipitation during the remaining months of the year.

Further analysis of maximum 24-hour precipitation and the average maximum for each period revealed several years in which values exceeded the average (Figure 2), suggesting that the area has experienced flood events that could potentially recur in future periods.

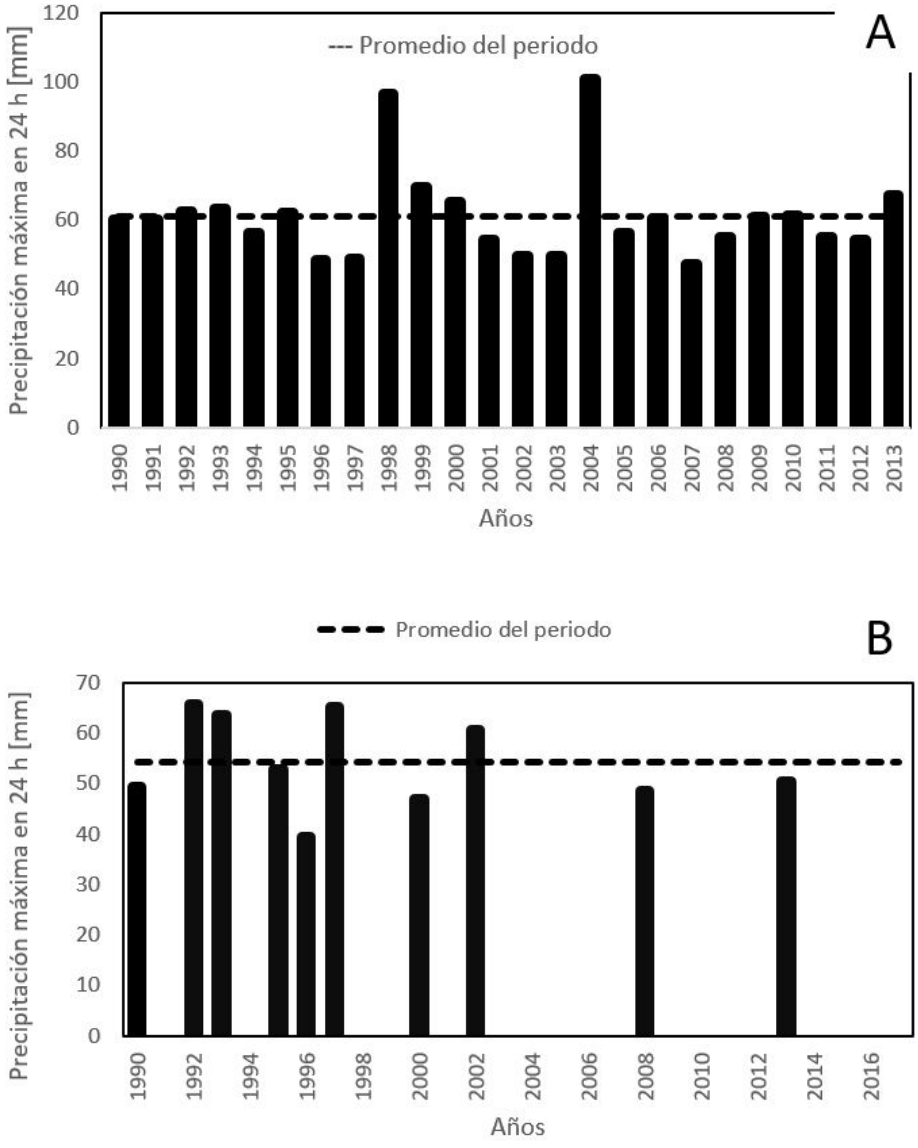


Figure 2. A) Annual maximum 24-hour precipitation recorded at the Gualaquiza meteorological station (INAMHI) for the 1990–2013 period. The dashed line represents the mean value for the study period. Years without bars indicate periods with no available records due to missing data in the INAMHI database. B) Annual maximum 24-hour precipitation recorded at the El Pangui meteorological station (INAMHI) for the 1990–2016 period. The dashed line represents the mean value for the study period. The years 2006 and 2016 are not represented by bars due to the absence of recorded data for those periods. Source: Authors' own elaboration.

La Granja: *Revista de Ciencias de la Vida* 44(2) 2026:59-77.
©2026, Universidad Politécnica Salesiana, Ecuador.

Temperature analysis indicates a mean annual temperature of 23.2 °C, a maximum annual temperature of 28.6 °C, and a minimum annual temperature of 18.11 °C, with the warmest months occurring between October and March. Finally, the analysis of potential evapotranspiration (PET) using the Thornthwaite method yielded an average value of 1 211.65 mm, with higher values observed from October to January.

Regarding the characterization of the Wawayme River watershed, the process begins with the acquisition of a Digital Elevation Model (DEM) (30 × 30 m resolution) downloaded from NASA's Earth Data server (Figure 3), using QGIS software and the SRTM Downloader plugin. Geographic Information Systems (GIS) were employed as the primary tools for data processing and analysis.

The morphometric parameters of the watershed reveal characteristics associated with a moderately torrential hydrological response. In particular, the shape indices (Kc = 1.43; Ff = 0.34) indicate a tendency toward sustained flood generation rather than abrupt responses. In terms of relief, the mean slope (S = 32.12 %) and mean elevation (Hm = 1 648.22 m.a.s.l.) classify the basin as mountainous, which directly influences runoff dynamics and erosion processes. The drainage system exhibits a stream order of 5 and a concentration time (tc = 25.12 min), suggesting that the entire watershed contributes relatively rapidly to runoff processes, thereby favoring the occurrence of peak discharges during intense precipitation events.

Finally, the analysis of the hypsometric curve indicates that the watershed is in a transitional stage between juvenile and mature phases. This is reflected in the altitudinal distribution, where approximately 35 % of the area lies above 1 900 m.a.s.l., suggesting the persistence of active erosive processes. This interpretation is further supported by the altimetric frequency histogram, which shows that the largest proportion of the watershed area is concentrated on the elevation range of 1 900 to 2 080 m.a.s.l.

2.2 Image Classification Methodology

For analyzing changes in vegetation cover, a supervised classification methodology was implemented using the Semi-Automatic Classification Plugin (SCP) in QGIS. This approach enables the identification and quantification of land cover transformations based on multitemporal satellite imagery. Initially, two complete Landsat 8 images dated April 27, 2013, and September 12, 2020—covering southern Ecuador and northern Peru—were used. These images were downloaded from the United States Geological Survey (USGS) Earth Explorer portal and include nine bands from the Operational Land Imager (OLI) sensor and two bands from the Thermal Infrared Sensor (TIRS).

It is important to note that the images correspond to Level 1T (L1T) products, meaning that they have undergone systematic radiometric correction, as well as orthorectification and terrain correction.

Table 1. Data set showing the monthly variation in evapotranspiration across four types of vegetation cover.

Code	Land Use	January	February	March	April	May	June	July	August	September	October	November	December	Interception
1	Native forest	1.00	1.00	1.00	1.00	1.00	1.00	1.00	1.00	1.00	1.00	1.00	1.00	4.00
2	Shrub vegetation	0.70	0.70	0.75	0.88	0.98	0.95	0.75	0.70	0.70	0.70	0.70	0.70	0.00
3	Grasslands	0.40	0.40	0.50	0.75	0.95	0.90	0.50	0.40	0.40	0.40	0.40	0.40	5.00
4	Anthropogenic infrastructure	0.20	0.20	0.20	0.20	0.20	0.20	0.20	0.20	0.20	0.20	0.20	0.20	1.00

©2026, Universidad Politécnica Salesiana, Ecuador.

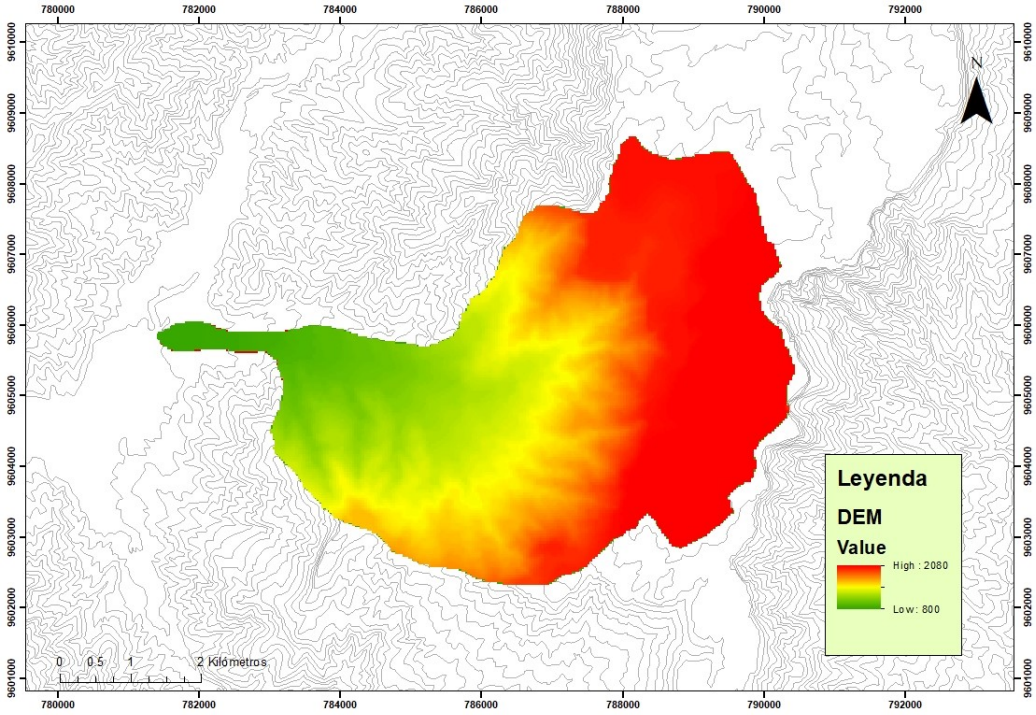


Figure 3. Digital Elevation Model of the Wawayme River watershed

Subsequently, using the Semi-Automatic Classification Plugin (SCP) in QGIS and through the combination of spectral bands, land cover changes within the study area were quantified, including the application of preprocessing steps prior to classification. For this study, the (FAO, 2005) classification system was adopted, which includes distinctions at three levels (primary, secondary, and tertiary). The primary level is particularly relevant for this research, as it establishes a dichotomous classification to determine the presence or absence of vegetation (Table 1).

2.3 Hydrological Modeling

To evaluate the influence of land cover changes on hydrological response, the TETIS model was implemented. This is a distributed conceptual model that allows the simulation of watershed behavior under different land use scenarios. The modeling process included parameterization, calibration, and validation stages.

The TETIS model, developed by the Department of Hydraulic Engineering and Environment at the Polytechnic University of Valencia, is a rainfall–runoff tank-type model that maintains water balance in each grid cell of the system. Its structure enables the integrated representation of hydrological processes such as interception, surface storage, infiltration, evapotranspiration, percolation, and groundwater recharge, among others (Instituto de Ingeniería del Agua y Medio Ambiente (IIAMA), 2021). Furthermore, this model can be applied both to the analysis of extreme events—such as floods and erosion processes—using minute or hourly time steps, and to water resource availability studies at a daily scale, making it a versatile tool for hydrological simulation in watersheds.

According to Barrientos et al. (2020), the model can analyze changes in watershed runoff by considering the effects of intensive forestry and/or climate change through the simulation of different land use and climate scenarios. Their findings indicate that runoff can be significantly influenced by reductions in precipitation and increases in evapotranspiration.

©2026, Universidad Politécnica Salesiana, Ecuador.

In this regard, Rodríguez-Lloveras et al. (2015) highlight that this approach allows for the estimation of runoff rates and sediment yield based on historical changes in land use and vegetation, concluding that land management and land use are decisive factors in watershed hydrological behavior, particularly in relation to erosion and sediment yield. Additionally, appropriate land use management can mitigate the adverse impacts of climate change on the hydrological cycle (Fang and Fan, 2021).

TETIS requires a set of initial parameters, which can be grouped into: (1) parameters derived from the DEM (elevation, slope, flow direction, flow accumulation, and hill slope velocity); (2) parameters derived from edaphic, hydrogeological, and geomorphological properties (static storage, infiltration capacity, percolation capacity, among others); and (3) parameters derived from land use and land cover.

The first raster input for the hydrological model is the Digital Elevation Model (DEM). In this study, a DEM (30 $\times$ 30 m resolution) previously downloaded from NASA's Earth Explorer server (Figure 3) was used. It is important to note that, after acquisition, surface imperfections were corrected using the "Fill sinks" tool. From this dataset, slope, flow direction, flow accumulation, and hill slope velocity layers were derived.

Parameters derived from edaphic, hydrogeological, and geomorphological properties include: (1) static storage, referring to water within the watershed that is lost through evapotranspiration and does not contribute to runoff; (2) infiltration capacity, defined as the rate at which water enters the soil through its surface and dependent on the different soil types present in the watershed; and (3) percolation capacity, referring to the downward movement of water through the soil toward the aquifer via the unsaturated zone, associated with subsurface structure and geological and geomorphological characteristics.

These parameters were estimated as a function of altitude (empirical relationship), due to the absence of observed data for watershed, following the methodology proposed by Terán (2017). For example, static storage values were estimated at approximately 200 mm at 5 000 m.a.s.l., and around 350 mm at 2 000 m.a.s.l.

The land cover dataset was derived from the geopedological database of the project "Thematic Cartography Survey at 1:25,000 Scale, Lots 1 and 2," conducted by the Ministry of Agriculture and Livestock (MAG) through the MAGAP-PRAT executing unit within the SIGTIERRAS program (2015) (Figure 4A), as well as from the Landsat 8 image dated September 12, 2020 (Figure 4B). Four land cover types were identified within the watershed: (1) native forest; (2) shrub vegetation; (3) grasslands; and (4) anthropogenic infrastructure.

Another input required by the TETIS model corresponds to the temporal variation of evapotranspiration, which includes the month-to-month variation for each vegetation cover type present in the watershed. This data set consists of thirteen columns: the first column corresponds to January values, the twelfth to December, and each row represents a specific vegetation cover type identified within the basin.

Due to the absence of monthly values for the vegetation factor in the present study, reference values from similar vegetation covers were adopted, following the FAO methodology and the study conducted by Tejada Espinoza (2016) in the implementation of the TETIS model in the Carraixet ravine watershed (Table 1).

Regarding the event file, this input corresponds to precipitation, evaporation, and discharge data, representing a rainfall event over a specific period. For the present study, monthly data derived from the meteorological and hydrological station described in the section on climatic and watershed characterization were used, covering the period from February 2012 to June 2015.

Finally, within the modeling process, it is necessary to perform a calibration (using the previously described data files), which aims to achieve a closer approximation to reality by adjusting and combining parameters. In this stage, the objective was to obtain appropriate values for each evaluation criterion (RMSE and Nash–Sutcliffe efficiency), as well as to improve the fit between the peak flows of the hydrograph.

©2026, Universidad Politécnica Salesiana, Ecuador.

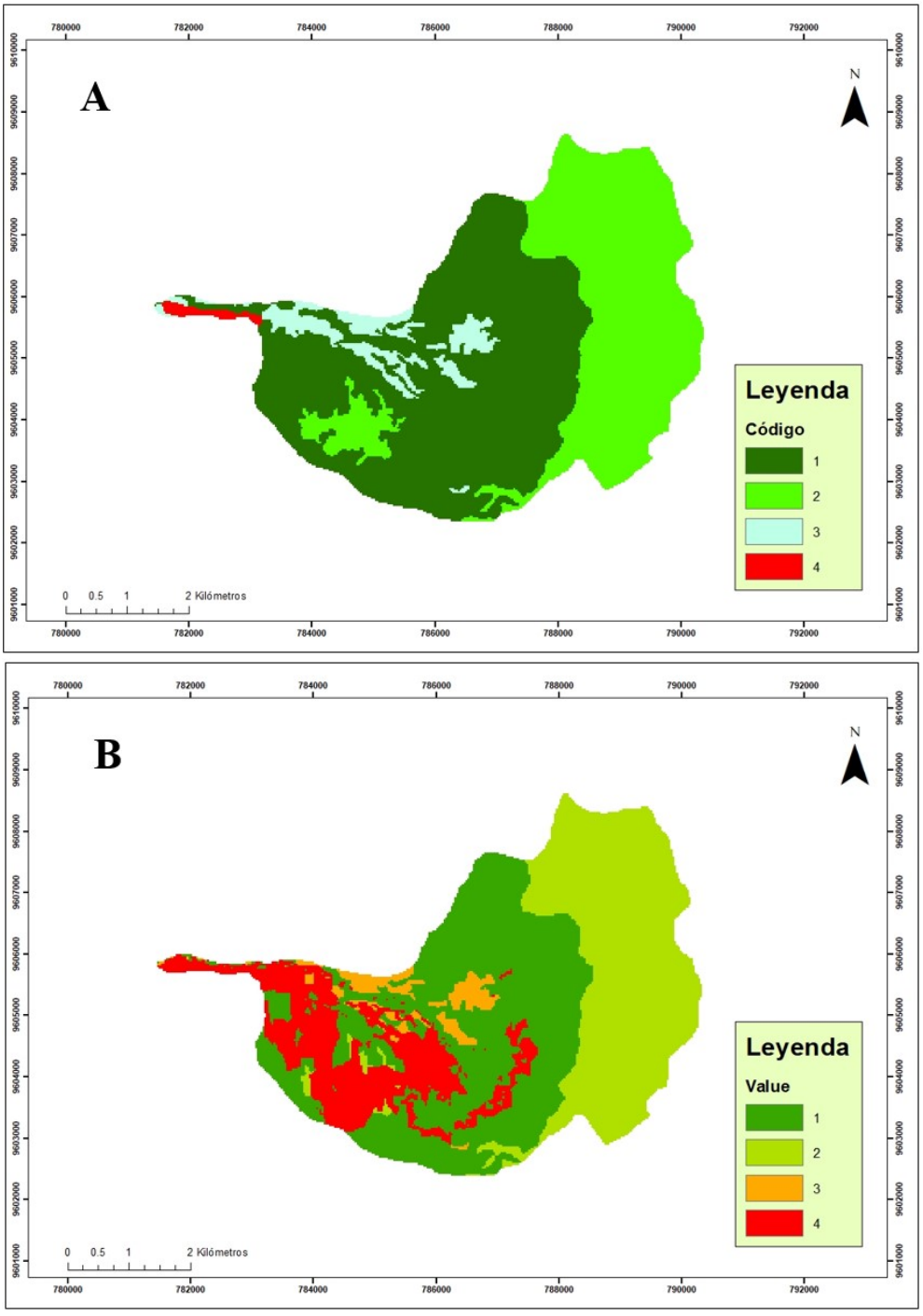


Figure 4. A) Land cover map for 2015, derived from the geopedological database of the SIGTIERRAS Project – MAG (2015). B) Land cover map for 2020, obtained through supervised classification of a Landsat 8 image. In both maps, the colors represent the following land cover classes: code 1 (dark green) = native forest; code 2 (light green) = shrub vegetation; code 3 (orange/light blue) = grasslands; and code 4 (red) = anthropogenic infrastructure. Since monthly values for the vegetation factor were not available, values from similar vegetation cover types were adopted following the methodology proposed by the Food and Agriculture Organization (FAO) and the study conducted by Tejada Espinoza (2016) on the implementation of the TETIS model in the Carraixet Ravine watershed (Table 1).

©2026, Universidad Politécnica Salesiana, Ecuador.

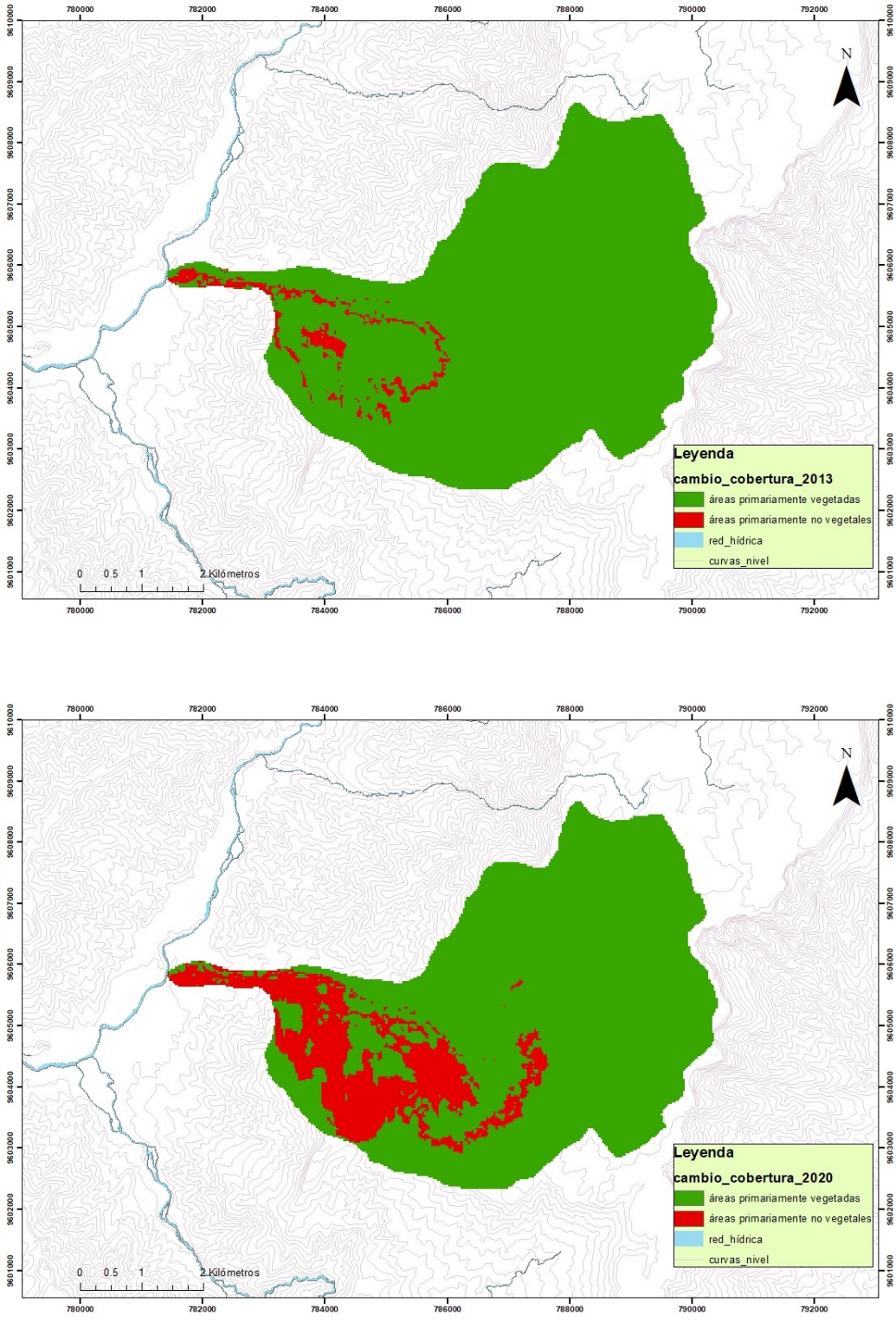


Figure 5. Land cover classification for the years 2013 and 2020.

©2026, Universidad Politécnica Salesiana, Ecuador.

3 Results and Discussion

This section presents the results of: (1) the assessment of land cover change in the Wawayme River watershed; (2) the hydrological modeling, in which observed and simulated discharges are obtained as a function of land use and land cover changes; and (3) the discussion of the findings of this study.

3.1 Results of Land Cover Change Assessment

The analysis began with two classifications based on satellite images corresponding to the years 2013 and 2020. The 2013 classification was used as the reference image, while the 2020 classification represented the updated scenario. This process was carried out using the SCP plugin and its post-processing method (land cover), which enabled the calculation of the number of pixels transitioning from one class to another.

The results show a decrease in primarily vegetated areas (PVA) from 28.43 km^2 in 2013 to 24.34 km^2 in 2020, representing a loss of 14.35 %. Conversely, primarily non-vegetated areas (PNVA) increased from 1 km^2 in 2013 to 5.08 km^2 in 2020, corresponding to an increase of 13.86 % (Table 2, Figure 5).

Additionally, Figure 7 presents a multitemporal comparison that more clearly illustrates the land use and land cover changes occurring within the watershed. The analysis of land cover changes reveals a significant transformation of the landscape, where areas of native vegetation are being primarily replaced by mining infrastructure and degraded lands. This transition represents a concerning pattern from an ecological perspective, as primary vegetation performs critical hydrological functions that are now being compromised.

Table 2. Land use and land cover change analysis in the Wawayme River watershed, years 2013 and 2020.

New \ Reference	**Primarily Vegetated Areas (PVA)**	**Primarily Non-Vegetated Areas (PNVA)**	**TOTAL 2013**
Primarily Vegetated Areas (PVA)	24.21	4.22	28.43
Primarily Non-Vegetated Areas (PNVA)	0.14	0.86	1.00
TOTAL 2020	24.34	5.08	29.42

3.2 Hydrological Modeling

It is well established that distributed hydrological models are useful for simulating scenarios that determine the influence of specific parameters. In this research the main objective is to assess the influence of land use and land cover changes on discharge at the gauging point.

The hydrographs resulting from the simulations for the years 2015 and 2020 show variations in simulated discharge ($m^3\ s^{-1}$) and simulated volume (Hm^3) over a period of 43 800 minutes (monthly data) (Figure 6). The results indicate: (1) a maximum observed discharge of 5.6 $m^3\ s^{-1}$ and an observed volume of 217.4 Hm^3 (for both scenarios); (2) a maximum simulated discharge of 5.7 $m^3\ s^{-1}$ for both the 2015 and 2020 scenarios; (3) simulated volumes of 186.5 Hm^3 (2015 scenario) and 186.7 Hm^3 (2020 scenario); and (4) an RMSE value of 1.01 and a Nash–Sutcliffe efficiency index of 0.03 (for both scenarios) (Table 3).

The Root Mean Square Error (RMSE) allows quantifying the magnitude of the deviation between simulated and observed values, ranging from zero to positive infinity. A value of zero indicates a perfect fit, whereas larger values reflect a poorer model performance. For both simulations, an RMSE value of 1.009 was obtained, which represents an adequate level of agreement (Cabrera, 2012).

Regarding the Nash–Sutcliffe efficiency criterion—one of the most widely used metrics in hydrology—it measures how much of the variability in the observed data is captured by the simulation. For both scenarios, a value of 0.0350 was obtained,

©2026, Universidad Politécnica Salesiana, Ecuador.

which is close to the mean benchmark value (E = 0). Additionally, during model calibration, efforts were made to improve the fit of the peak flows in the hydrograph, which influenced the resulting Nash–Sutcliffe efficiency value (Cabrera, 2012).

One of the conditions highlighted by the results in relation to determining greater variability in the hydrological balance due to changes in land use and land cover is the limited availability of meteorological and hydrological data—a recurrent issue in Ecuador, particularly in Amazonian watersheds. For the present study, a design was implemented in which variability in simulated discharges and volumes is observed, showing an increase in maximum simulated discharge of 0.002 $m^3\ s^{-1}$ and 0.196 Hm^3 in simulated volume when comparing the 2020 scenario with that of 2015.

In the case of an applied hydrological study, a larger amount of hydrological data and greater temporal resolution (e.g., daily values) over at least one complete hydrological cycle would be required. This should include information on precipitation, stream flow measurements, evapotranspiration, among others, to determine the hydrological behavior of the watershed more accurately.

Additionally, field-based data on the initial parameters required by the model such as static storage, infiltration capacity, and percolation would be necessary.

3.3 Discussion

Given the differences observed between discharge and volume increases obtained from the respective model simulations, it is evident that the watershed exhibits variability in its hydrological characteristics, derived from spatial changes in land use and land cover (Figure 4). This information is relevant due to: (1) the environmental risk associated with the reduction of vegetated areas and the consequent increase in stream flow in natural channels due to decreased evapotranspiration; (2) the occurrence of marked flood events; (3) the intensification of water deficit; and (4) the need for ecosystem conservation and erosion control.

In this context, based on the findings of the present study and the provisions outlined in the National Climate Change Adaptation Plan of Ecuador (2023–2027) (MAATE, 2023), it is imperative to improve monitoring, data management, and access to hydrological and water-related information. This would enhance the resilience of populations located within the direct and indirect areas of influence of extractive projects, as well as reduce the risk of economic losses associated with climate variability. Understanding and predicting the factors that modulate such variations requires strengthening, expanding, and improving hydrological and meteorological monitoring, as well as data management and accessibility. This may be achieved through actions such as equipment acquisition, the implementation of strategic action plans, and the development of policies related to the collection, management, and exchange of climate information in the short, medium, and long term.

Furthermore, it is essential to establish inclusive and transparent governance in water resource management, involving all stakeholders to implement mitigation and conservation measures addressing environmental risks associated with such activities, while also strengthening community resilience.

It is important to note that, given the limitations in input data (monthly records, distant meteorological stations, and estimated soil parameters), the absolute discharge values should be interpreted with caution. The associated uncertainty is estimated at $\pm$20–30 % (Beven, 2012). Therefore, the main contribution of this study lies in the relative comparison between scenarios (a change of +0.02 $m^3\ s^{-1}$ between 2015 and 2020), rather than in the absolute modeled values. Although this difference is small in absolute terms, it represents an increase that could be amplified during periods of higher precipitation.

Finally, while the analysis of vegetation cover change using remote sensing constitutes the most robust component of this study (due to its objectivity and replicability), hydrological modeling—despite its limitations—serves the purpose of translating these spatial changes into projected hydrological consequences. The model results should be interpreted as indicators of trends (i.e., direction of change) rather than precise predictions. Nevertheless, the methodology presented is replicable and can be improved as higher-quality input data become available.

©2026, Universidad Politécnica Salesiana, Ecuador.

Table 3. Results. A: Simulation corresponding to the year 2015; B: Simulation corresponding to the year 2020.

A			B		
Description	**Value**	**Unit**	**Description**	**Value**	**Unit**
Maximum observed discharge	5.6	$m^3\ s^{-1}$	Maximum observed discharge	5.6	$m^3\ s^{-1}$
Maximum simulated discharge	5.7	$m^3\ s^{-1}$	Maximum simulated discharge	5.7	$m^3\ s^{-1}$
RMSE	1.010		RMSE	1.010	
Observed volume	217.4	Hm^3	Observed volume	217.4	Hm^3
Simulated volume	186.5	Hm^3	Simulated volume	186.7	Hm^3
Nash–Sutcliffe Efficiency (NSE)	0.035		Nash–Sutcliffe Efficiency (NSE)	0.035	
Accumulated area	23.909	km^2	Accumulated area	23.909	km^2

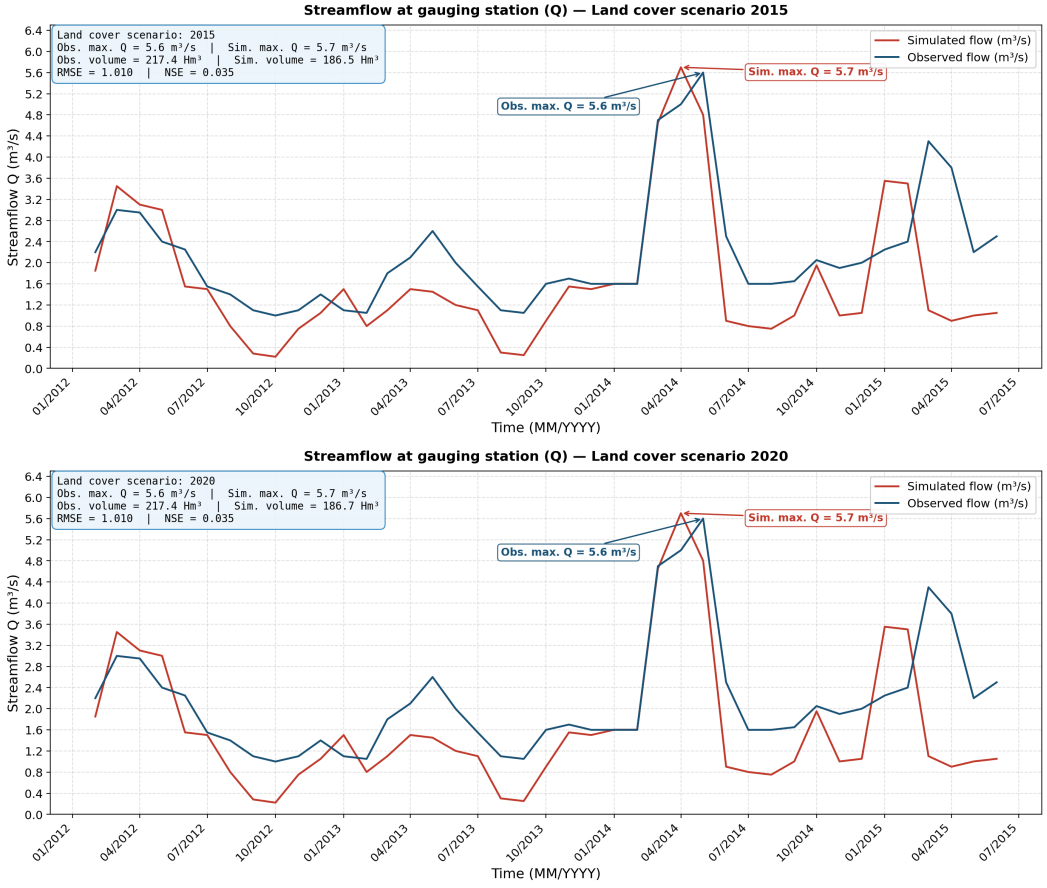
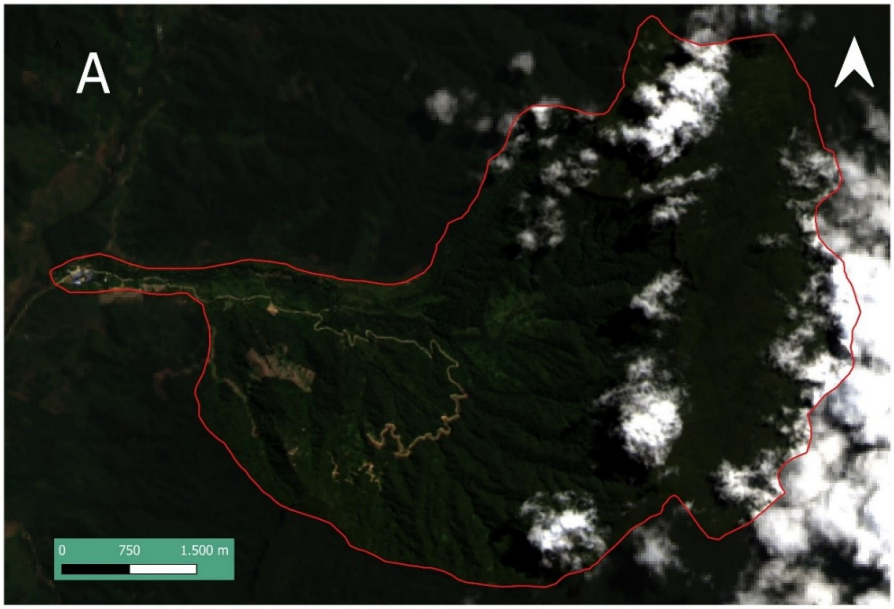
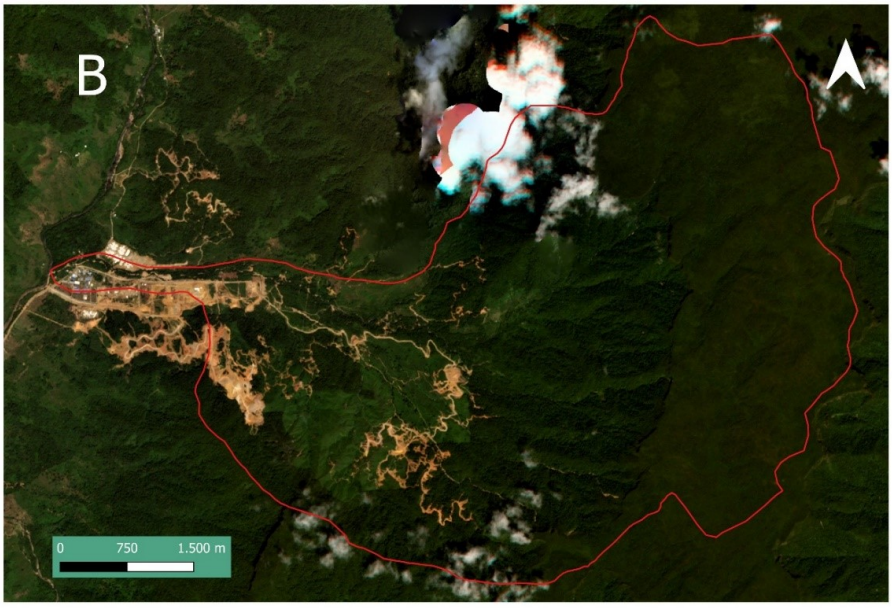


Figure 6. Hydrological charts resulting from the simulations for the years 2015 and 2020

©2026, Universidad Politécnica Salesiana, Ecuador.





©2026, Universidad Politécnica Salesiana, Ecuador.



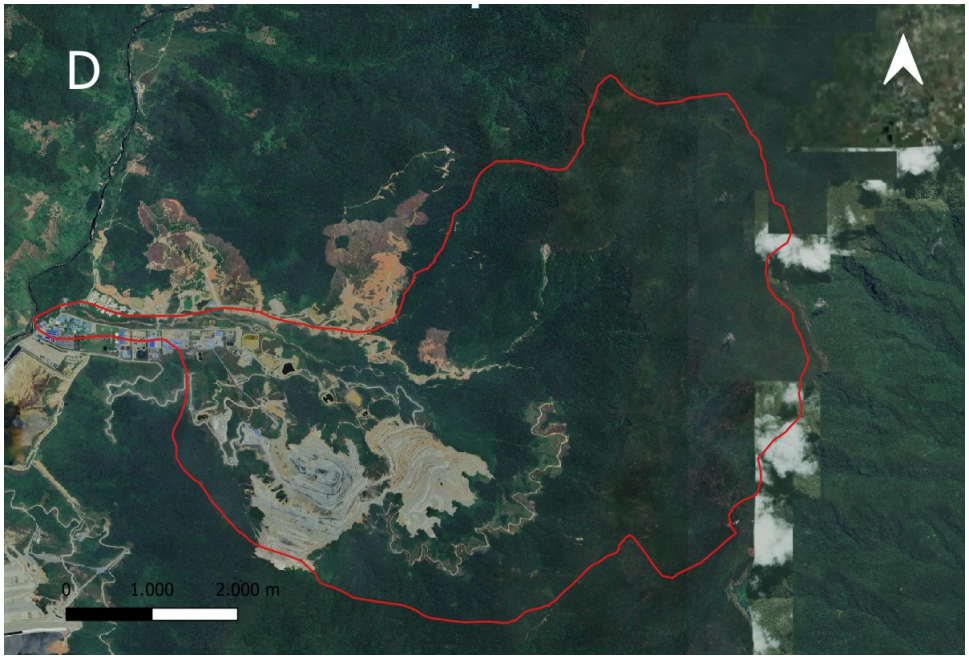


Figure 7. A (2013): The watershed was predominantly covered by dense vegetation, with only minimal anthropogenic disturbance observed at its western edge. B (2015): Areas of bare soil became clearly visible in the central-western sector. Mining infrastructure was evident along the western margin, indicating the onset of significant land disturbance. C (2020): A substantial expansion of the disturbed area was observed. An open-pit mine was clearly identifiable in the central part of the watershed, characterized by extensive exposed soil. Mining infrastructure had become well established along the western margin, while green vegetation remained predominant in the eastern sector. D (2025): The open-pit mine dominated the central-southern portion of the watershed, with well-defined extraction benches clearly visible. Degraded areas had expanded northward across the basin. Although the eastern sector retained forest cover, increasing anthropogenic pressure was evident.

©2026, Universidad Politécnica Salesiana, Ecuador.

4 Conclusions

The implementation of the distributed conceptual hydrological simulation model TETIS allows identifying the variability in the hydrological balance as a function of changes in land use and land cover. Specifically, an increase in maximum discharge and simulated volume of 0.002 $m^3\ s^{-1}$ and 0.196 Hm^3, respectively, was determined when comparing the scenarios for the years 2015 and 2020. Furthermore, model calibration enabled a better fit between observed and simulated data series—particularly in achieving an appropriate adjustment of peak flows in the hydrographs—yielding satisfactory results for the RMSE and Nash–Sutcliffe objective functions.

By applying the FAO (2005) classification system through the SCP plugin and its post-processing methodology, land cover changes in the watershed were assessed. The results indicate a decrease of 14.35 % in primarily vegetated areas and an increase of 13.86 % in primarily non-vegetated areas between 2013 and 2020, as evidenced by the corresponding multitemporal comparison.

Consequently, considering that the watershed is located within unique ecosystems of high biological diversity (Ecuadorian Amazon region), it is essential to implement adequate extractive management practices. A lack of planning and the overexploitation of natural resources may lead to severe environmental alterations, particularly affecting water resources. Therefore, the applied methodology highlights the issues associated with the reduction in vegetation cover, reflected partly through hydrological variability.

Likewise, it is important to evaluate the effectiveness of current regulatory frameworks for watershed protection in mining areas of Ecuador, and to propose improvements based on scientific evidence as part of public policy strategies in the region. In this sense, this research serves as a starting point from which appropriate measures should be developed to minimize risks associated with flood events and their environmental impacts.

Finally, future research lines are proposed as follows: (1) the implementation of high temporal resolution hydrometeorological monitoring networks within the watershed; (2) the evaluation of the effectiveness of mitigation measures implemented by the mining project; (3) the development of water quality studies to complement the quantitative analysis; (4) the extension of the analysis to other Amazonian watersheds with similar mining activities; and (5) the development of predictive models incorporating climate change scenarios.

Declaration on the use of artificial intelligence

The authors DECLARE that, during the preparation of the article entitled "Hydrological Variability Due to Land Cover Change in the Wawayme River Basin Associated with Mining Activities, Ecuador", no generative artificial intelligence tools or automated assistance systems were used for the writing, analysis, data interpretation, content generation, translation, or editing of the manuscript.

The authors assume full responsibility for the content, originality, integrity, and final version of the article.

Author's contribution

R.A.M.F.: Conceptualization, formal analysis, investigation, methodology, resources, software, visualization, writing – original draft. **M.Z.F.L.:** Investigation, supervision, validation, writing – review and editing.

References

Angelo, J., and Sempere, F. (2018). Extracción minera y derechos humanos: Impactos adversos y caminos hacia un desarrollo sostenible. *Revista Internacional de Cooperación y Desarrollo*, *5*, 105–123. Online: https://doi.org/10.21500/23825014.3598

Angulo, M. A., and Saavedra, O. C. (2018). Modelación hidrológica de la cuenca maylanco utilizando hec-hms. *Investigación y Desarrollo*, *18*, 53–67. Online: https://doi.org/10.23881/idupbo.018.1-4i

©2026, Universidad Politécnica Salesiana, Ecuador.

Barceló Coll, J., Nicolás Rodrigo, G., Sabater García, B., and Sánchez Tamés, R. (2000). *Fisiología vegetal* (9.ª ed.). Ediciones Pirámide. Online: https://n9.cl/kqk4d0

Barrientos, G., et al. (2020). *Evaluación de cambios en la escorrentía bajo escenarios de uso de suelo.* Online: https://www.researchgate.net (Disponible en ResearchGate)

Beven, K. J. (2012). *Rainfall-runoff modelling: The primer* (2.ª ed.). John Wiley & Sons. Online: https://doi.org/10.1002/9781119951001

Bustamante, T., Espinoza, M., Ruiz, L., Trujillo, J., and Uquillas, J. (1993). *Retos de la amazonía*. Quito, Ecuador: Abya-Yala. Online: https://n9.cl/d32rk

Cabrera, J. (2012). Calibración de modelos hidrológicos. *Instituto para la Mitigación de los Efectos del Fenómeno El Niño, Universidad Nacional de Ingeniería, Facultad de Ingeniería Civil, Perú*, *1*(1).

Custode, E., and Sourdat, M. (1986). Paisajes y suelos de la amazonía ecuatoriana: entre la conservación y la explotación. *Revista del Banco Central del Ecuador*, *8*, 325–337.

Daily, G. C., and Ehrlich, P. R. (1992). Population, sustainability, and earth's carrying capacity. *BioScience*, *42*, 761–771. Online: https://doi.org/10.2307/1311995

de Jong, L., De Bruin, S., Knoop, J., and van Vliet, J. (2021). Understanding land-use change conflict: a systematic review of case studies. *Journal of Land Use Science*, *16*, 223–239. Online: https://doi.org/10.1080/1747423X.2021.1933226

Dingman, S. L. (2014). *Physical hydrology* (3.ª ed.). Waveland Press. Online: https://www.waveland.com/browse.php?t=382

Fang, H., and Fan, Z. (2021). Effects of land use/cover change on hydrological processes. *Environmental Earth Sciences*, *80*, 1–15. Online: https://doi.org/10.1007/s12665-021-09574-0

FAO. (2005). *Land cover classification system - classification concepts and user manual* (Inf. Téc.). Food and Agriculture Organization of the United Nations.

Giraldo, M., Ramírez, J., and Galán, A. (2013). *Amazonia posible y sostenible* (Naciones Unidas, Ed.). Bogotá: Naciones Unidas.

Instituto de Ingeniería del Agua y Medio Ambiente (IIAMA). (2021). *Modelo hidrológico tetis: Manual técnico* (Inf. Téc.). Valencia: Universidad Politécnica de Valencia. Online: https://www.iiama.upv.es

Instituto Nacional de Investigaciones Agropecuarias (INIAP). (2018). *Agroforestería sostenible en la amazonía ecuatoriana, no 2. fragilidad de los suelos en la amazonía ecuatoriana y potenciales alternativas agroforestales para el manejo sostenible* (Inf. Téc.). INIAP.

MAATE. (2023). *Plan nacional de adaptación al cambio climático del ecuador (2022-2027)* (Inf. Téc.). Ministerio del Ambiente, Agua y Transición Ecológica del Ecuador.

Mintegui Aguirre, J. , and Robredo Sánchez, J. C. (1994). Caracterización de las cuencas hidrográficas, objeto de restauración higrológico-forestal, mediante modelos hidrológicos. *Ingeniería del Agua*, *1*. Online: https://doi.org/10.4995/ia.1994.2637

Mintegui Aguirre, J. , and Robredo Sánchez, J. C. (2008). *Estrategias para el control de los fenómenos torrenciales y la ordenación sustentable de las aguas, suelos y bosques de las cuencas de montaña.* (Documento técnico/Libro)

Montaño, D. (2021). *Nuevo estudio: en los últimos 26 años ecuador ha perdido más de 2 millones de hectáreas de bosque.* (Reporte de prensa/Artículo)

Moreno Farfán, R. A. (2022). Restauración geomorfológica sobre depósitos de relaves: caso de estudio aplicado a la concesión minera río blanco, ecuador. *La Granja: Revista de Ciencias de la Vida*, *37*. Online: https://doi.org/10.17163/lgr.n37.2023.10

Nobre, C. A., Sampaio, G., Borma, L. S., Castilla-Rubio, J. C., Silva, J. S., and Cardoso, M. (2016). Land-use and climate change risks in the amazon and the need of a novel sustainable development paradigm. *Proceedings of the National Academy of Sciences*, *113*, 10759–10768. Online: https://doi.org/10.1073/pnas.1605516113

©2026, Universidad Politécnica Salesiana, Ecuador.

Pascual, J. (2002). *Cambios del suelo y régimen hídrico en la rambla de poyo y el barranc de carraixet.* (Tesis/Informe de investigación)

Paz, A. (2024). *Ecuador perdió poco más de un millón de hectáreas de formación boscosas en 38 años.* Online: https://n9.cl/nuqhvb

Prats, A., Torrent, J., López, M., and del Campo García, A. (2011). Influencia de la vegetación en el ciclo hidrológico, factores escorrentía e infiltración. *Cuadernos de la Sociedad Española de Ciencias Forestales*(32), 137–143.

Rodríguez-Lloveras, X., et al. (2015). Hydrological response to land-use changes. *Hydrological Processes*, *29*(7), 1625–1637. Online: https://doi.org/10.1002/hyp.10215

Siswanto, S. Y., and Francés, F. (2019). How land use/land cover changes can affect water, flooding and sedimentation in a tropical watershed: a case study using distributed modeling in the upper citarum watershed, indonesia. *Environmental Earth Sciences*, *78*, 550. Online: https://doi.org/10.1007/s12665-019-8561-0

Suquilanda, M. (2008). El deterioro de los suelos en el ecuador y la producción agrícola. En *Memorias del xi congreso ecuatoriano de la ciencia del suelo* (p. 12). Quito, Ecuador: Sociedad Ecuatoriana de la Ciencia del Suelo. Online: https://n9.cl/ay5i8o

Tejada Espinoza, H. (2016). *Caracterización del régimen de crecidas mediante la implementación del modelo hidrológico tetis en la cuenca del barranco del carraixet - valencia.* (Trabajo de investigación / Tesis)

Terán, C. (2017). *Curso virtual de modelamiento hidrológico distribuido con tetis v. 8.3.1.*

Vásconez, M., and Torres, L. (2018). Minería en el ecuador: sostenibilidad y licitud. *Revista Estudio Desarrollo Social: Cuba y América Latina*, *6*, 83–103. Online: https://n9.cl/g5fjq

Winkler, K., Fuchs, R., Rounsevell, M., and Herold, M. (2021). Global land use changes are four times greater than previously estimated. *Nature Communications*, *12*, 2501. Online: https://doi.org/10.1038/s41467-021-22702-2

©2026, Universidad Politécnica Salesiana, Ecuador.

La Granja: Revista de Ciencias de la Vida
pISSN:1390-3799; eISSN:1390-8596
https://doi.org/10.17163/lgr.n44.2026.05

Scientific paper/ Artículo científico

Biotechnology

Freeze-dried extract of *Ilex guayusa*: a potential ingredient for energy drinks

Extracto liofilizado de *Ilex guayusa*: potencial ingrediente para bebidas energizantes

Laura Scalvenzi*[1], Sting Luna Fox[2] and Matteo Radice[1]

[1]*Universidad Estatal Amazónica. Departamento de Matemáticas y Ciencias Físicas. Puyo, Ecuador. [https://ror.org/029ss0s83]*
[2]*Instituto de Investigaciones en Ciencia y Tecnología de Materiales. Consejo Nacional de Investigaciones Científicas y Técnicas. Universidad Nacional de Mar del Plata. Mar del Plata, Argentina.[https://ror.org/055eqsb67]*

*Corresponding author: lscalvenzi@uea.edu.ec

Article received on February 6th, 2025. Accepted, after review, on July 10th, 2025. Published on September 1st, 2026.

Abstract

The objective of this study is to produce and analyze a freeze-dried extract of *Ilex guayusa*, with a high caffeine concentration potentially used as ingredient in energy drinks. The caffeine extraction from dried leaves was done by ultrasounds, using water as solvent. The parameters considered were time, citric acid concentration, ultrasonic amplitude, solid/liquid ratio. Significant factors were optimized using a Box-Behnken response surface design. Physicochemical parameters and heavy metals were performed according to (Servicio Ecuatoriano de Normalización (INEN), 2013). The shelf life was determined by accelerated temperature tests. The results showed that time, citric acid concentration and ultrasonic amplitude had significant effects on caffeine extraction, while the solid-liquid ratio was not significant. The optimum conditions for caffeine extraction were a time of 26.94 minutes, a citric acid concentration of 2.72 %, an ultrasonic amplitude of 68.29 % and caffeine concentration of 3.36 %. The physicochemical parameters of the freeze-dried product were: moisture of 1.2±0.1 %, total ash of 11.87±0.12 %, pH of 5.1±0.2, hot solubility of 17±1 s and cold solubility of 1.8±0.2 minutes. The levels of heavy metals found were zinc (19.16±0.04 mg/kg), copper (12.35±0.23 mg/kg) and tin (8.64±0.17 mg/kg). The shelf life of the freeze-dried extract at 20 °C was 3.5 months. This paper provides valuable information for developing a freeze-dried product rich in caffeine.

Keywords: Citric acid, caffeine, aqueous extract, ultrasound extraction, optimization.

©2026, Universidad Politécnica Salesiana, Ecuador.

Resumen

El objetivo de este estudio es producir y analizar un extracto liofilizado de *Ilex guayusa*, con elevada concentración de cafeína y con potencial de uso como ingrediente de bebidas energizantes. La extracción de cafeína desde hojas secas se realizó mediante ultrasonido en medio acuoso. Los parámetros considerados fueron: tiempo, concentración de ácido cítrico, amplitud ultrasónica, relación sólido-líquido. Los factores significativos se optimizaron mediante un diseño de superficie de respuesta Box-Behnken. Se evaluaron los parámetros fisicoquímicos y los metales pesados según la norma (Servicio Ecuatoriano de Normalización (INEN), 2013). La vida útil se determinó mediante pruebas aceleradas de temperatura. Los resultados mostraron que el tiempo, la concentración de ácido cítrico y la amplitud ultrasónica tuvieron efectos significativos sobre la extracción de cafeína, mientras que la relación sólido-líquido no fue significativa. Las condiciones óptimas para la extracción de cafeína fueron en un tiempo de 26.94 min, una concentración de ácido cítrico del 2.72 %, una amplitud ultrasónica de 68.29 % y una concentración de cafeína de 3.36 %. Los parámetros fisicoquímicos del liofilizado fueron: humedad (1.2±0.1 %), cenizas totales (11.87±0.12 %), pH (5.1±0.2), solubilidad en caliente (17±1 s) y solubilidad en frío (1.8±0.2 minutos). Los niveles de metales pesados fueron: zinc (19.16±0.04 mg/kg), cobre (12.35±0.23 mg/kg) y estaño (8.64±0.17 mg/kg). La vida útil del producto liofilizado a 20 °C fue de 3.5 meses. El presente estudio proporciona información valiosa para el desarrollo de un producto liofilizado rico en cafeína.

Palabras clave: Ácido cítrico, cafeína, extracto acuoso, extracción con ultrasonido, optimización.

Suggested citation: Scalvenzi, L., Luna, S. and Radice, M. (2026). Freeze-dried extract of *Ilex guayusa*: a potential ingredient for energy drinks. La Granja: Revista de Ciencias de la Vida. Vol. 44(2):78-96. https://doi.org/10.17163/lgr.n44.2026.05.

Orcid IDs:

Laura Scalvenzi: https://orcid.org/0000-0001-6015-9871
Sting Luna Fox: https://orcid.org/0000-0001-6058-7024
Matteo Radice: https://orcid.org/0000-0002-4771-8912

©2026, Universidad Politécnica Salesiana, Ecuador.

1 Introduction

Ilex guayusa Loes. is a plant with great cultural and medicinal importance in the Amazonian regions of Ecuador, Peru, Colombia, and Bolivia, where it grows at altitudes ranging from 200 to 2000 meters above sea level. This species, which can reach heights of up to 30 meters, has been used for centuries by Indigenous peoples due to its various medicinal properties, including antipyretic, diuretic, and analgesic uses, as well as applications in the treatment of arthritis and the improvement of fertility (Meneses et al., 2024). However, the most popular use of *I. guayusa* is its stimulant content, mainly derived from its high concentration of caffeine, which exceeds 3 % in the leaves (Negrin et al., 2019).

The growing global demand for natural products with functional properties has driven interest in *I. guayusa*, whose leaves not only contain caffeine but also a variety of bioactive compounds, such as antioxidants, anti-inflammatory, and antibacterial compounds (Cakmak et al., 2023).
Recent research has identified the presence of theobromine, theophylline, and chlorogenic acids, which provide additional health benefits beyond the stimulant action of caffeine (Chianese et al., 2019; Cadena-Carrera et al., 2019).

Among the phenolic compounds detected in *I. guayusa* leaf extracts, 14 compounds have been identified, including chlorogenic acid derivatives and flavonoids such as quercetin, which reinforces its potential as a functional ingredient in the formulation of new products (García-Ruiz et al., 2017).

Caffeine extraction has traditionally been carried out through several methods, including extraction with organic solvents, maceration extraction, and Soxhlet extraction. Although these methods are effective, many have significant disadvantages, such as the use of toxic solvents, long processing times, and high temperatures that can degrade bioactive compounds (Ivanović et al., 2020; Lezoul et al., 2020). In recent years, considerable emphasis has been placed on developing more efficient and environmentally friendly extraction techniques. Ultrasound-assisted extraction (UAE) has gained popularity due to its ability to improve extraction efficiency through acoustic cavitation, a process that generates micro-bubbles in the liquid medium, facilitating the rupture of cell walls and the release of bioactive compounds such as caffeine (Kumar et al., 2020).

UAE offers several advantages over conventional techniques, including shorter extraction times, lower temperatures, and the possibility of using safer solvents such as water, making it a sustainable option for the food and pharmaceutical industries (Carreira-Casais et al., 2021). In addition, the combination of citric acid as an acidifying agent further enhances the extraction of alkaloids, since these compounds in acidic media release more easily (Yang et al., 2024). This makes UAE an ideal technique to maximize the extraction of caffeine from *I. guayusa* leaves.

Likewise, the growing demand for natural and functional products has highlighted the importance of developing healthy alternatives to commercial energy drinks, which often contain synthetic additives. A lyophilized product based on *I. guayusa* would not only take advantage of the bioactive properties of the plant but would also respond to current market demands for natural energy products that offer additional health benefits, such as antioxidants and anti-inflammatory compounds. *I. guayusa*, due to its caffeine content and other beneficial polyphenolic compounds, represents a potential option for creating an innovative product that can be reconstituted as an energy drink. The objective of the present study is to formulate and evaluate the shelf life of a lyophilized *I. guayusa* intended for the preparation of an energy drink.

2 Materials and Methods

2.1 Raw material and sample preparation

I. guayusa leaves were purchased dried at "Los plátanos" market in the city of Puyo, Ecuador, located at coordinates 1.4837° S and 78.0026° W (Bromatology Laboratory of Universidad Estatal Amazónica, km 2 ½ vía Tena, canton and province of Pastaza). The leaves were ground in a mill (KitchenAid brand, model BCG111OB) and sieved until a particle diameter smaller than 0.5 mm was obtained. Citric acid (purity >99 %) of food grade, used to favor caffeine extraction, was purchased from the chemi-

©2026, Universidad Politécnica Salesiana, Ecuador.

cal store "QUIMICOSAS" located in the city of Quito, Ecuador.

2.2 Ultrasound-assisted caffeine extraction

A solid–liquid extraction was carried out using a thermostatic ultrasonic bath (Wisd.23 brand, model WUC-DO6H). The extractions were performed according to the conditions established for each experiment. Samples of pulverized *I. guayusa* were weighed in 200 mL flasks and 100 mL of a citric acid solution (m/v) dissolved in water were added. The flasks were placed in the equipment previously calibrated at a constant temperature of 50 °C. The extracts obtained were filtered using Whatman No. 4 paper. The determination of caffeine content was performed immediately.

2.3 Spectrophotometric determination of caffeine

Caffeine determination was performed by spectrometry, according to the methodology employed by Luna-Fox et al. (2024). 1 mL of NaOH (0.1 M) was added to 10 mL of guayusa aqueous extract to increase the pH of the solution. Caffeine was extracted in two fractions of 15 mL of chloroform each. The obtained extracts were combined and then evaporated in a water bath. The resulting caffeine was dissolved in 50 mL of hot water (at a temperature between 60 and 90 °C) and allowed to cool. Subsequently, the solution was transferred to a 100 mL flask, adjusting the final volume with distilled water. 5 mL of this solution were placed in a 25 mL volumetric flask and 1 mL of HCl (0.01 M) was added; it was then completed with distilled water. Finally, the absorbance of the samples was measured at 275 nm in a UV–vis spectrophotometer (Perkin Elmer brand, model Lambda 20) and the concentration was determined using the calibration curve obtained from nine concentrations (1, 2, 3, 5, 10, 12, 16, 20 and 25 mg/mL; $R^2 = 0.9991$), according to equation (1). The results were expressed as a percentage on a dry matter basis.

$$A = 0.006C + 0.0011 \quad (1)$$

Where C: caffeine concentration in the sample (mg/mL) and A: absorbance of the sample.

2.4 Experimental design

The experiment was carried out in two stages. In the initial phase, a two-level factorial design with four factors (Table 1) was used, comprising 36 experiments: 16 trials with two replicates each and four repetitions at the central point to evaluate the curvature of the model. The influence of extraction time, citric acid concentration, ultrasonic amplitude, and the solid/liquid ratio on the caffeine content in *I. guayusa* leaves was analyzed. To identify significant and non-significant variables, a standardized effects diagram was employed, while the selection of relevant variables was consolidated through the Pareto diagram and the Bonferroni limit (Anderson and Whitcomb, 2016).

In the second phase, the significant variables were analyzed to determine the optimal levels of the studied variables to optimize caffeine extraction. For this purpose, a Box–Behnken design (Response Surface Methodology – RSM) was used, implemented through the software Design Expert version 13.0.5.0 (trial version, Stat-Ease Inc., Minneapolis, MN, USA). The experimental results were fitted using the following second-order polynomial model:

$$y = \beta_0 + \sum_{i=1}^{n} \beta_{ii} x_i + \sum_{i=1}^{n} \beta_{ii} x_i^2 + \sum_{i=1}^{n-1} \sum_{j=i+1}^{n} \beta_{ij} x_i x_j \quad (2)$$

Where y indicates the estimated response, while β_0, β_{ii} and β_{ij} represent the regression coefficients associated with the mean, linear, and quadratic terms, respectively. These were determined from the experimental results using the least squares method. The independent variables x_i and x_j were coded within an interval from -1 to 1.

©2026, Universidad Politécnica Salesiana, Ecuador.

Table 1. Levels of the studied variables.

Study variable		Levels		
	Code	Low -1	Central 0	High 1
Time (min)	A	15	22.5	30
Citric acid (%)	B	0	1.5	3
Ultrasonic amplitude (%)	C	30	50	70
Solid-liquid relationship (m/v)	D	5	10	15

2.5 Model validation

To corroborate the model, the values of the adjusted R^2 and predicted R^2 coefficients were examined. The validity of each experimental series, along with that of the model, was verified through an analysis of variance (ANOVA) (Dinardo et al., 2019). The optimization of caffeine extraction from dried *I. guayusa* leaves was performed considering extraction time, citric acid concentration, and ultrasonic amplitude as independent factors. The ideal extraction conditions were established using the predictive equation of the response surface methodology.

2.6 Preparation of the lyophilized product

The lyophilized product was obtained from the aqueous extract produced under the optimal extraction conditions, which was processed in a lyophilizer (SCANVAC brand, model COOLSAFE). The operating conditions were condenser temperature of $-90\,^{\circ}\mathrm{C}$, pressure of 0.105 Torr, and a processing time of 7 days.

2.7 Determination of physicochemical parameters and heavy metals in the lyophilized extract

Moisture, pH, solubility in hot and cold water, total ash content, and heavy metals (lead, cadmium, zinc, copper, arsenic, and tin) were analyzed according to the procedures established by the Ecuadorian technical standard (NTE) INEN 1122:2013 corresponding to freeze-dried coffee. The analyses were carried out using an atomic absorption spectrophotometer (Perkin Elmer, Model A Analyst 800, dimensions 1524.00 × 1016.00 × 812.80 mm, automatic sampler AS800, weight 136.08 kg). The results of this study were compared with the permissible limit proposed by NTE INEN 1122:2013 for soluble coffee, since it is the product that most closely resembles the one obtained in this study. Furthermore, there is currently no INEN standard for *I. guayusa*. Table 2 shows the standard used for each analysis.

2.8 Determination of shelf life

The shelf life of the lyophilized extract was determined through accelerated temperature tests considering moisture as the measurement parameter. For this purpose, 1 g of lyophilized extract was weighed in triplicate in glass containers with screw caps and placed in an oven (MEMMERT brand, model SFE700) at 30, 40, and 50 °C. The moisture content was evaluated at 0, 7, 14, 21, and 28 days. The data were fitted to the differential equation (3) proposed by Herrera et al. (2022).

$$\frac{dH}{dt} = kH^n \tag{3}$$

Where H is the moisture content of the freeze-dried extract, k represents the reaction kinetic constant, t indicates time, and n indicates the reaction order.

The experimental results in this study followed a first-order reaction. Therefore, by integrating equation (3) from a moisture content of H_0 to H, and from an initial time of 0 to t, equation (4) was obtained, which allowed the shelf life of the freeze-dried extract to be determined.

$$\ln(H) = \ln(H_0) + kt \tag{4}$$

The reaction kinetic constant (k) was determined using the linearized Arrhenius equation (5) by plotting $\ln(k)$ against the inverse of the temperature ($1/T$).

$$\ln(k) = \ln(k_0) - \frac{E_a}{RT} \tag{5}$$

©2026, Universidad Politécnica Salesiana, Ecuador.

Where k_0 is the pre-exponential factor, E_a represents the activation energy (kJ/mol), R is the universal gas constant (8.314 kJ/molK) and T is the absolute temperature (K). The shelf life was estimated at a temperature of 20 °C. The data were processed using Origin Pro 2022 software (OriginLab, Northampton, MA, USA).

Table 2. Physicochemical and heavy metal analyses according to NTE INEN 1122:2013

Analysis	Test method
H (%)	NTE INEN-ISO 3726
CT (%)	NTE INEN 1117
pH	NTE INEN 389
SC (s)	Cup test
SF (min)	Cup test
Pb (mg/kg)	Atomic absorption spectrophotometry
Cd (mg/kg)	
Zn (mg/kg)	
Cu (mg/kg)	
As (mg/kg)	
Sn (mg/kg)	

H: moisture, CT: total ash, SC: solubility in hot water, SF: solubility in cold water, Pb: lead, Cd: cadmium, Zn: zinc, Cu: copper, As: arsenic, Sn: tin.

3 Results and Discussion

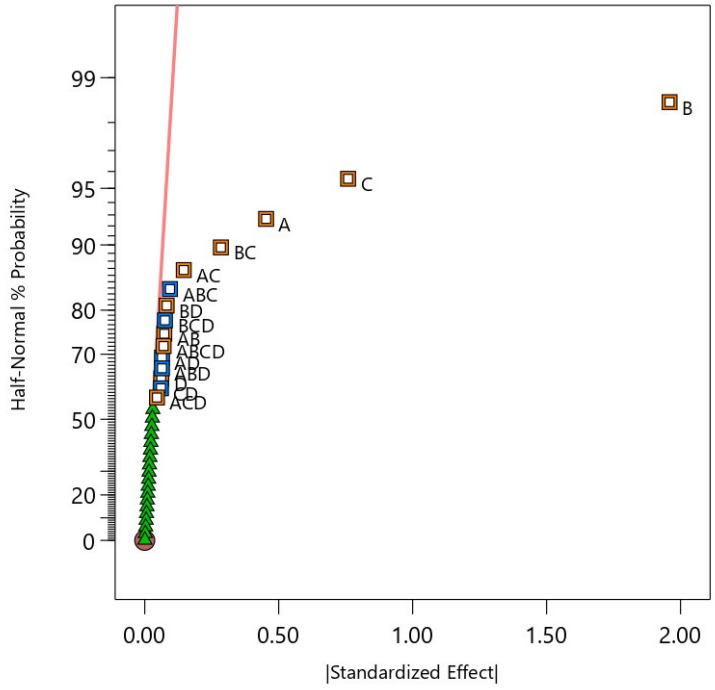
3.1 Effect of the study factors on caffeine extraction

The estimation of standardized effects, both positive and negative, in the UAE of caffeine is shown in Figure 1A, where the significant variables correspond to the highest values of the standardized effects (≥ 0.5) according to what was mentioned by Held et al. (2023). On the other hand, the non-significant effects (< 0.5) followed a normal distribution with a mean of zero and constant variation. This indicates that when plotting the effects on a normal probability plot, the non-significant effects are located on a straight line, while the active effects deviate from this line of normality.

The Pareto diagram, together with the Bonferroni limit, reinforced the selection of significant factors. As indicated in Figure 1B, extraction time (A), citric acid concentration (B), and ultrasonic amplitude (C) were located above the Bonferroni limit, indicating that they were significant variables, whereas the solid–liquid ratio was located below this limit, showing that it did not have statistical influence. Likewise, according to the results shown in Table 3, the significant variables ($p < 0.05$) and non-significant variables ($p > 0.05$) are confirmed. The interactions between the studied variables (A, B, C, and D) were also not significant. The factorial model presented a good fit, supported by a coefficient of determination (R^2) equal to 0.9934. In addition, the difference between the adjusted R^2 (0.9881) and the predicted R^2 (0.9757) was less than 0.2, which is considered adequate according to Anderson and Whitcomb (2016) and Arteaga-Crespo et al. (2019).

©2026, Universidad Politécnica Salesiana, Ecuador.

(A)



(B)

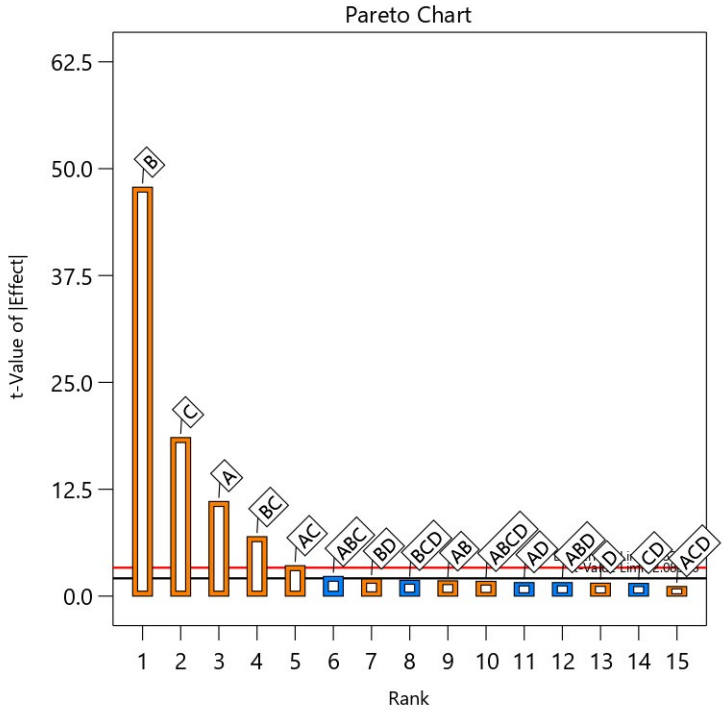


Figure 1. Positive (orange) and negative (blue) effects on caffeine extraction. Half-normal distribution plot (A), Pareto diagram (B).

©2026, Universidad Politécnica Salesiana, Ecuador.

Previous studies have highlighted the positive influence of extraction time and ultrasonic amplitude on caffeine extraction due to their effect on cell rupture and mass transfer. Hassan and Yaqoobi (2023) observed that a longer extraction time and higher ultrasonic amplitude significantly improved the yield in the UAE of caffeine from coffee beans, since these factors facilitate the release of this compound by increasing acoustic cavitation. Similarly, Serna-Jiménez et al. (2023) reported a proportional relationship between extraction time and caffeine recovery in coffee pulp, due to a longer contact between the solvent and the plant material, a factor that optimizes the solubilization of this alkaloid.

The significant effect of citric acid on caffeine extraction can be explained by its ability to acidify the medium, optimizing the solubility and release of caffeine. In acidic media, the interaction of the solvent with the plant material is strengthened, facilitating extraction. Yang et al. (2024) supported this observation by demonstrating that a eutectic solvent composed of polypropylene glycol, polyethylene glycol, and citric acid showed remarkable efficiency in extracting caffeine from tea residues through microwave irradiation, because the acidic environment favors its solubility and extraction.

The solid/liquid ratio factor did not show a statistical influence on caffeine extraction; this can be explained because when this factor increases, the amount of solvent used was not able to adequately cover all the plant material, limiting mass transfer and reducing the efficiency of the process. This suggests that, beyond a certain limit, the available solvent becomes insufficient to effectively extract caffeine. Similar results were reported by Abreu-Naranjo et al. (2018), who found that the solid/liquid ratio also had no significant effect on the extraction of bioactive compounds from the bark of *Maytenus macrocarpa*, which reinforces the idea that this factor may lose relevance when the proportion of solvent and plant material is not optimized.

Table 3. ANOVA for the effect of the study factors on caffeine extraction.

Caffeine	**Sum of squares**	**df**	**Mean square**	**F value**	**P value**	
Model	38.33	15	2.56	19.07	< 0.0001	Significant
A–Time	1.20	1	1.20	8.92	0.0076	
B–Citric acid	30.56	1	30.56	228.07	< 0.0001	
C–Amplitude	3.74	1	3.74	27.91	< 0.0001	
D–S/L ratio	0.0004	1	0.0004	0.0028	0.9582	
AB	0.0025	1	0.0025	0.0189	0.8921	
AC	0.3026	1	0.3026	2.26	0.1493	
AD	0.0007	1	0.0007	0.0052	0.9435	
BC	0.3970	1	0.3970	2.96	0.1014	
BD	0.0055	1	0.0055	0.0412	0.8413	
CD	0.0003	1	0.0003	0.0019	0.9656	
ABC	0.0118	1	0.0118	0.0881	0.7699	
ABD	0.0007	1	0.0007	0.0052	0.9435	
ACD	0.0006	1	0.0006	0.0047	0.9459	
BCD	0.0033	1	0.0033	0.0244	0.8776	
ABCD	0.0019	1	0.0019	0.0141	0.9068	
Residual	2.55	19	0.1340			
Lack of fit	0.0042	1	0.0022	1.45	0.895	Not significant
Pure error	0.0170	18	0.0009			

©2026, Universidad Politécnica Salesiana, Ecuador.

3.2 Optimization of the extraction process

An optimization design with 17 experiments was used to determine the optimal levels of extraction time, citric acid concentration, and ultrasonic amplitude, which were the significant variables. The objective of the optimization of the extraction process was to determine the best combination of these three variables to maximize caffeine extraction. Four mathematical models (Table 4) generated by the Design-Expert software were analyzed, where the quadratic model presented the best results, with an R^2 value equal to 0.9895. This value shows that 98.95 % of the total variation in caffeine extraction was determined by the studied variables.

Table 4. Mathematical models generated by the Design-Expert software

Model	p-value	Lack of fit	Adjusted R^2	Predicted R^2	
Linear	0.0014	0.0033	0.6153	0.4103	
2FI	0.5796	0.0023	0.5855	-0.0627	
Quadratic	**$<$ 0.0001**	**0.3733**	**0.9761**	**0.9072**	**Suggested**
Cubic	0.3733	0.0087	0.9793	-0.1258	

Table 5. Caffeine concentration obtained experimentally

Caffeine (%)	Time (min)	Citric acid (%)	Amplitude (%)
3.24	22.50	3.00	70
3.08	30.00	1.50	70
2.68	15.00	1.50	70
2.64	30.00	3.00	50
2.61	22.50	1.50	50
2.50	22.50	1.50	50
2.50	22.50	1.50	50
2.45	22.50	1.50	50
2.36	22.50	1.50	50
2.22	15.00	3.00	50
2.15	30.00	1.50	30
1.98	15.00	1.50	30
1.88	22.50	3.00	30
1.60	22.50	0.00	70
1.37	22.50	0.00	30
1.22	30.00	0.00	50
0.98	15.00	0.00	50

©2026, Universidad Politécnica Salesiana, Ecuador.

The quadratic model in terms of the study variables was the following:

$$\begin{aligned}\textbf{Caffeine} &= 0.66 + 0.10A + 0.62B - 0.03C \\ &+ 0.40 \times 10^{-2}AB + 3.83 \times 10^{-4}AC \\ &+ 9.42 \times 10^{-3}BC - 2.39 \times 10^{-3}A^2 \\ &- 2.60B^2 + 3.08 \times 10^{-4}C^2 \end{aligned} \quad (6)$$

Where A, B, and C represent extraction time, citric acid concentration, and ultrasonic amplitude, respectively. The experimental results of caffeine content are shown in Table 5, and those estimated by the quadratic model were compared in Figure 2. The distribution of points validated the model's ability to cover the entire range of experiments analyzed. This pattern confirms the suitability of the model to cover the entire data interval, suggesting that it can be successfully applied.

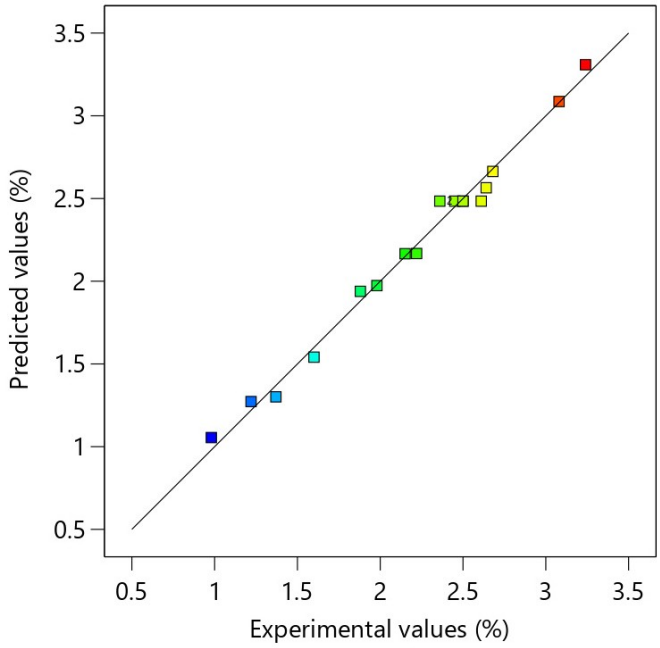


Figure 2. Experimental vs predicted caffeine results.

The ideal extraction conditions, which resulted in the maximum caffeine content (3.36 %), were the following: extraction time of 26.94 minutes, citric acid at 2.72 %, and ultrasonic amplitude of 68.29 %. Under these experimental conditions, the obtained caffeine content was 3.22, which coincided with that predicted by the quadratic model.

The statistical significance of the regression equation corresponding to the quadratic model of the response surface methodology was evaluated by the F test and ANOVA, whose results are presented in Table 6.

The result of Fisher's F test was 75.53, with a p-value lower than 0.0001, which demonstrates that the model is highly significant. In addition, the coefficient of determination (R^2) was 0.9895, reflecting a high agreement between the experimental values and those predicted by the model. The adjusted R^2 reached a value of 0.9761, indicating that the quadratic model was able to predict 97.61 % of the variation in caffeine extraction. On the other hand, the lack of fit was not statistically significant, with an F value of 1.37 and a p-value of 0.3733. These results indicate that the lack of fit did not have a significant impact on the results obtained. The graphical representations of the quadratic equation generated by the Design-Expert software are shown through

©2026, Universidad Politécnica Salesiana, Ecuador.

a 3D response surface (Figure 3A) and 2D contour plots (Figure 3B). The optimal levels of the investigated variables were determined from the analysis of these graphs.

Table 6. ANOVA for the quadratic model of the RSM.

Caffeine	Sum of squares	df	Mean square	F value	P value	
Model	6.30	9	0.7001	73.53	< 0.0001	Significant
A-Time	0.1891	1	0.1891	19.86	0.0029	
B-Citric acid	2.89	1	2.89	303.76	< 0.0001	
C-Amplitude	1.30	1	1.30	136.13	< 0.0001	
AB	0.0081	1	0.0081	0.8508	0.3870	
AC	0.0132	1	0.0132	1.39	0.2771	
BC	0.3192	1	0.3192	33.53	0.0007	
A^2	0.0762	1	0.0762	8.00	0.0255	
B^2	1.44	1	1.44	151.09	< 0.0001	
C^2	0.0637	1	0.0637	6.69	0.0361	
Residual	0.0666	7	0.0095			
Lack of fit	0.0337	3	0.0112	1.37	0.3733	Not significant
Pure error	0.0329	4	0.0082			

$R^2 = 0.9895$; Adjusted $R^2 = 0.9761$; Predicted $R^2 = 0.9071$

The caffeine content present in dried *I. guayusa* leaves has been the subject of several studies, with results showing variability in the concentration of this compound. In a recent study by Luna-Fox et al. (2024), caffeine levels ranging between 0.24 % and 1.52 % were reported in aqueous extracts obtained by the ultrasound-assisted extraction technique. However, Cadena-Carrera et al. (2022) found a higher yield ($2.27 \pm 0.05\,\%$) using ethanol as a solvent and the supercritical fluid extraction technique. This difference in the obtained values can be due to several factors, such as the type of extraction technique, the solvent used, the particle size of the plant material, and environmental conditions. Previous research has indicated that variables such as climatic conditions and soil characteristics, as observed in the studies of Repajić et al. (2021) and Mazumder et al. (2020), also play a crucial role in the concentration of bioactive compounds, which demonstrates the complexity of the factors that affect the extraction of these compounds.

©2026, Universidad Politécnica Salesiana, Ecuador.

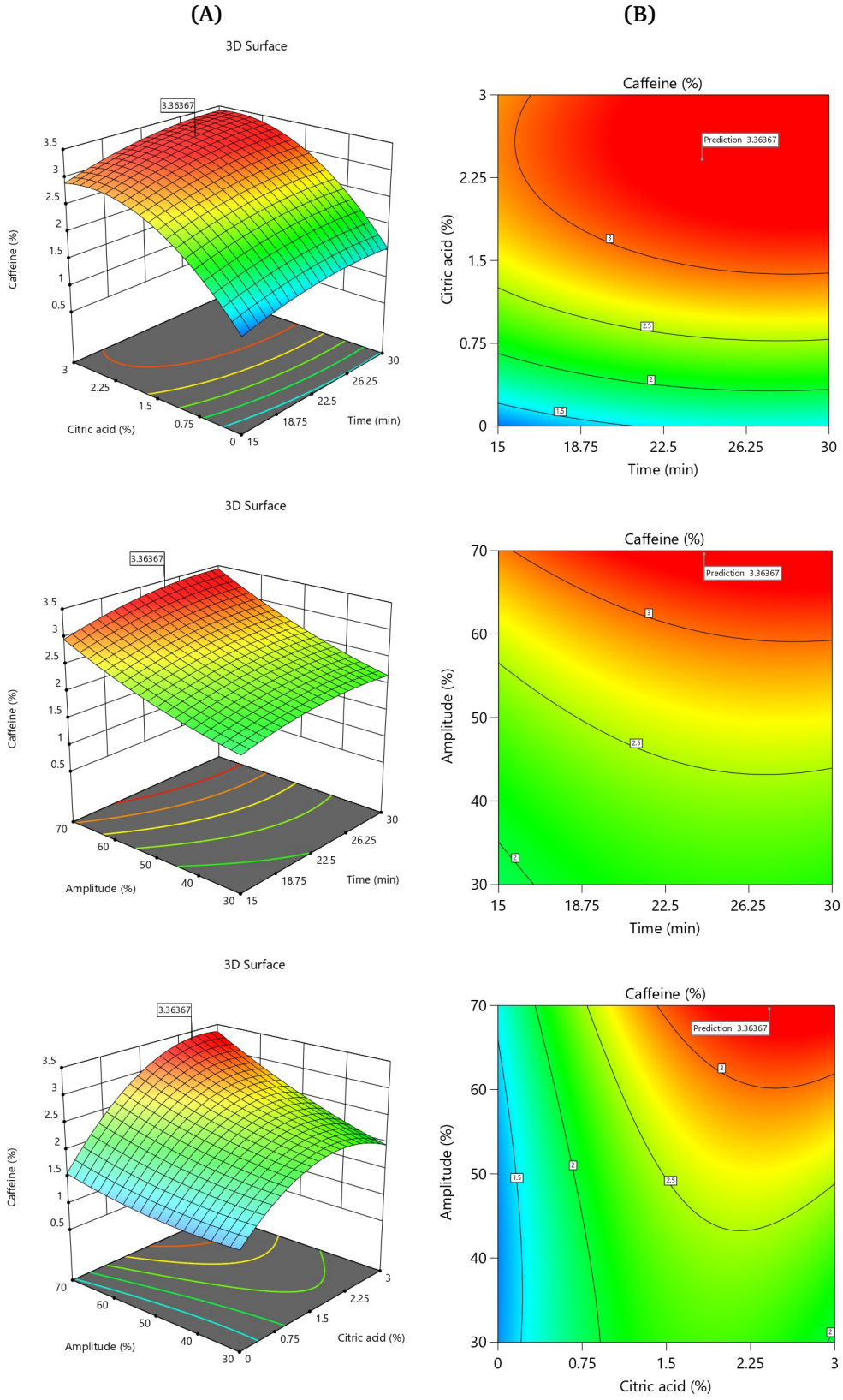


Figure 3. Optimal conditions for caffeine extraction. Response surface plots (A), contour plots (B).

©2026, Universidad Politécnica Salesiana, Ecuador.

3.3 Physicochemical parameters of the lyophilized extract

The lyophilized product was prepared from the aqueous extract obtained under the optimal extraction conditions defined by the quadratic model of the RSM. The lyophilized extract was processed to ensure that it complied with the specifications established in the NTE INEN 1122:2013 standard for freeze-dried coffee, which regulates key parameters such as pH, moisture, total ash content, and solubility in hot and cold water.

In this study, the results obtained for each of these parameters were adjusted to the specifications of the NTE INEN 1122:2013 standard (Table 7). The pH of the lyophilized extract was 5.1 ± 0.2, which is within the permitted range. Moisture was $1.2 \pm 0.1\,\%$, well below the maximum limit of 3.5 %, indicating a good lyophilization process that ensures low water activity and greater product stability. The total ash content was $11.87 \pm 0.12\,\%$, reflecting proper extract quality without excessive presence of mineral impurities. Regarding solubility, the lyophilized extract showed a good dissolution capacity, with a solubility time in hot water of 17 ± 1.0 s and in cold water of 1.8 ± 0.2 min, values that are below the limits established by the standard. These results reflect the high quality of the lyophilized extract obtained under the optimal extraction conditions. This regulatory compliance is an important indicator of the suitability of the extraction and lyophilization process and suggests that the produced lyophilized extract has characteristics that make it suitable for commercialization and consumption, ensuring quality and safety standards for the final consumer.

Table 7. Acceptable physicochemical parameters according to NTE INEN 1122:2013.

Analysis	Lyophilized extract of *I. guayusa*	Freeze-dried coffee	
		Minimum	Maximum
H (%)	1.2±0.1	-	3.5
CT (%)	11.87±0.12	-	14
pH	5.1±0.2	4.7	5.5
SC (s)	17±1	-	30
SF (min)	1.8±0.2	-	3

H: moisture, CT: total ash, SC: solubility in hot water, SF: solubility in cold water.

3.4 Heavy metal content in the lyophilized extract

The NTE INEN 1122:2013 standard establishes specific limits for the presence of heavy metals in freeze-dried coffee to guarantee the safety and quality of the product. These values were used as a reference to evaluate the heavy metal content in the lyophilized extract of *I. guayusa* in this study.

The results obtained showed that the heavy metal content in the lyophilized extract strictly complied with the limits established by the standard (Table 8). In particular, the levels of zinc, copper, and tin were 19.16 ± 0.04 mg/kg, 12.35 ± 0.23 mg/kg, and 8.64 ± 0.17 mg/kg, respectively, all below the maximum permitted limit. In addition, the presence of lead, cadmium, and arsenic was not detected, which highlights the quality and safety of the product.

©2026, Universidad Politécnica Salesiana, Ecuador.

Table 8. Maximum acceptable values of heavy metals according to NTE INEN 1122:2013

Metal analyzed	Lyophilized extract of *I. guayusa* (mg/kg)	Freeze-dried coffee (mg/kg)
Pb	ND	1
Cd	ND	0.1
Zn	19.16±0.04	50
Cu	12.35±0.23	20
As	ND	0.5
Sn	8.64±0.17	20

Pb: lead, Cd: cadmium, Zn: zinc, Cu: copper, As: arsenic, Sn: tin, ND: not detected.

Different studies have indicated that the presence of these metals may have toxic and cumulative effects in the human body. Lead, for example, is a neurotoxin that can affect the central nervous system, causing cognitive and behavioral disorders, especially in children (Sobin et al., 2023). Cadmium accumulates mainly in the kidneys and can cause renal damage, in addition to being associated with a higher risk of cancer in the lungs and other organs (Howard et al., 2023). Regarding arsenic, prolonged exposure may cause problems in the skin and respiratory system and increase the risk of developing cancer (Chappells and Dummer, 2024). On the other hand, Yan et al. (2023) have indicated that zinc, although essential in small amounts for health, at elevated levels may interfere with the absorption of other minerals and cause adverse effects such as nausea, vomiting, and liver dysfunction. Copper, in turn, is vital for biological functions, but at high concentrations it may damage the liver and nervous system (Min et al., 2024). Tin, although less studied, at high concentrations may cause gastrointestinal discomfort and affect kidney function (Liu et al., 2022). In this study, the absence of lead, cadmium, and arsenic, and the low concentration of zinc, copper, and tin in the lyophilized extract of *I. guayusa* highlight the safety and quality of the product, minimizing any risk to consumer health.

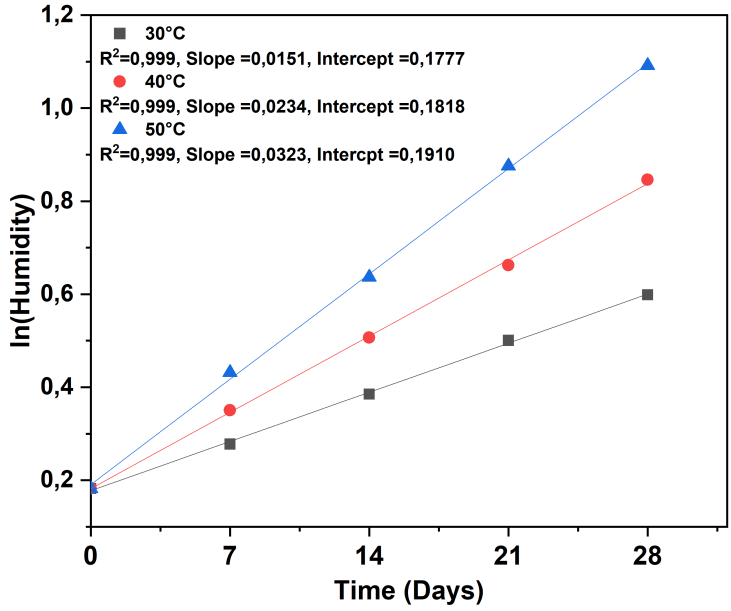


Figure 4. Relationship between ln (moisture) as a function of storage time (days) of the lyophilized extract of *I. guayusa* at 30, 40 and 50 °C.

©2026, Universidad Politécnica Salesiana, Ecuador.

3.5 Determination of shelf life

The relationship between the moisture content of the lyophilized extract and time was calculated by plotting $\ln(\text{moisture})$ as a function of time, according to Equation 4 (Figure 4). The results showed behavior consistent with a first-order reaction, which was confirmed by a coefficient of determination (R^2) of 0.999 for the curves obtained at 30, 40, and 50 °C (Table 9). The kinetic reaction constant (k) was represented by the slope of the line in each case.

Table 9. k values for storage temperatures.

Temperature (°C)	R^2	k	Intercept
30	0.999	0.0151	0.1777
40	0.999	0.0234	0.1818
50	0.999	0.0323	0.1910

K: kinetic reaction constant

Temperature had a strong influence on the kinetic reaction constant, reflected in a proportional increase in its value as temperature increased. This behavior can be explained by the increase in the kinetic energy of the reacting molecules, which favors a greater number of effective collisions, overcoming the energy barrier of the chemical process (Karal et al., 2024).

This trend is consistent with the Arrhenius equation, which states that the reaction constant depends exponentially on temperature. Similar results were reported by Isuiza et al. (2018), who documented a proportional increase in the reaction constant as temperature increased in similar kinetic processes. These authors concluded that this phenomenon was attributable to the decrease in activation energy and the enhancement of the molecular dynamics of the system.

The linearized Arrhenius equation was used to calculate the activation energy (E_a) and the kinetic reaction constant at a temperature of 20 °C to estimate the shelf life of the lyophilized extract. In Figure 5, the relationship between $\ln(k)$ and the inverse of absolute temperature is presented, where the data showed a good fit, with an R^2 of 0.995.

The shelf life at 20°C was calculated using Equation 4, taking moisture as the critical parameter according to the NTE INEN 1122:2013 standard for freeze-dried coffee, which establishes a maximum moisture limit of 3.5 %. The estimated shelf life is detailed in Table 10.

Table 10. Activation energy, kinetic reaction constant at 20 °C, and shelf life of the lyophilized extract.

Ea (kJ/mol)	k_0	k_{20}	H_0 (%)	$H_{\text{máx}}$ (%)	$t_{20\,^\circ\text{C}}$ (days)	$t_{20\,^\circ\text{C}}$ (months)	First-order equation used
30.097	3 361.02	0.0101	1.2	3.5	106	3.5	$\ln(H) = \ln(H_0) + kt$

E_a: activation energy, k_0: pre-exponential factor, $k_{20\,^\circ\text{C}}$: kinetic reaction constant at 20 °C, H_0: initial moisture of the lyophilized extract, $H_{\text{máx}}$: maximum acceptable moisture, $t_{20\,^\circ\text{C}}$: shelf life of the lyophilized extract.

©2026, Universidad Politécnica Salesiana, Ecuador.

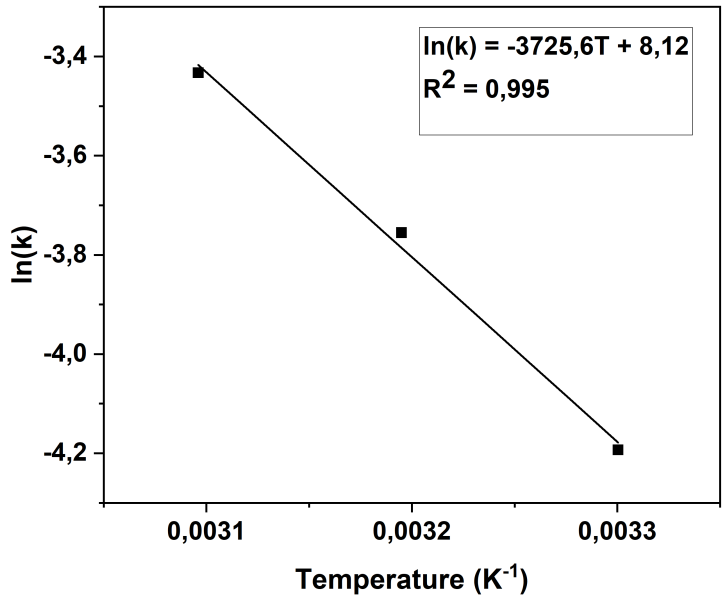


Figure 5. Relationship between the kinetic reaction constant (k) and the inverse of absolute temperature.

Currently, no previous studies have been identified that determine the activation energy and shelf life of a lyophilized product derived from aqueous extracts of dried *I. guayusa* leaves. However, studies conducted on other lyophilized products provide a reference framework to compare the obtained results. Isuiza et al. (2018) and López-Quiroga et al. (2019) reported activation energy values ranging between 18.3 and 31.35 kJ/mol, a range within which the activation energy determined for the *I. guayusa* lyophilized product in this study falls. This result indicates an energetic behavior comparable with other lyophilized products of plant origin.

Regarding shelf life, the 106 days estimated for the lyophilized extract of *I. guayusa* are similar to those reported by González-Pérez et al. (2024) for a product made from apple (105 days). This finding positions the lyophilized extract of *I. guayusa* as a competitive product in terms of storage stability. Setiawan et al. (2022) determined a shorter shelf life (59 days) for a coconut-based lyophilized beverage, which highlights the variability in preservation times among lyophilized products and reveals the influence of factors such as chemical composition, processing methods, and packaging materials.

The results of this research provide a starting point for future studies aimed at optimizing the stability of *I. guayusa* lyophilized products and extending their storage time. In addition, this study contributes to filling a gap in the literature by establishing key parameters for the development of innovative products based on *I. guayusa*.

4 Conclusions

Citric acid concentration was the factor that most influenced caffeine extraction from dried *I. guayusa* leaves, followed by ultrasonic amplitude and extraction time. The solid–liquid ratio did not show a significant effect.

A lyophilized product was prepared from the aqueous extract of *I. guayusa* obtained under the optimal extraction conditions. The final product complied with the physicochemical parameters and heavy metal limits established in the NTE INEN 1122:2013 standard.

The results of this research provide valuable information for the development of a lyophilized product rich in natural caffeine, positioning it as a potential alternative to products that use synthetic caffeine. It is necessary to study the long-term stability of the product under different storage conditions to assess its commercial viability.

©2026, Universidad Politécnica Salesiana, Ecuador.

Declaration on the use of Artificial Intelligence

The authors DECLARE that, during the preparation of the article entitled "Freeze-dried extract of *Ilex guayusa*: a potential ingredient for energy drinks", no generative artificial intelligence tools or automated assistance systems were used for the writing, analysis, data interpretation, content generation, translation, or editing of the manuscript.

The authors assume full responsibility for the content, originality, integrity, and final version of the article.

Author Contributions

L.S.: Conceptualization, investigation, writing – original draft, writing – review and editing. **S.L.F.:** Formal analysis, writing – original draft. **M.R.:** Methodology, project administration, writing – original draft, writing – review and editing.

References

Abreu-Naranjo, R., Arteaga-Crespo, Y., Bravo-Sanchez, L. R., Pérez-Quintana, M. L., and García-Quintana, Y. (2018). Response surface methodology for optimisation of total polyphenol content and antioxidant activity of extracts from Maytenus macrocarpa bark by means of ultrasound-assisted extraction. *Wood Science And Technology*, *52*(5), 1359–1376. Online: https://doi.org/10.1007/s00226-018-1034-x

Anderson, M. J., and Whitcomb, P. J. (2016). *RSM simplified*. Productivity Press eBooks. Online: https://doi.org/10.1201/9781315382326

Arteaga-Crespo, Y., Radice, M., Bravo-Sanchez, L. R., García-Quintana, Y., and Scalvenzi, L. (2019). Optimisation of ultrasound-assisted extraction of phenolic antioxidants from Ilex guayusa Loes. leaves using response surface methodology. *Heliyon*, *6*(1), e03043. Online: https://doi.org/10.1016/j.heliyon.2019.e03043

Cadena-Carrera, S., Tramontin, D. P., Cruz, A. B., Cruz, R. C. B., Müller, J. M., and Hense, H. (2019). Biological activity of extracts from guayusa leaves (Ilex guayusa Loes.) obtained by supercritical CO2 and ethanol as cosolvent. *The Journal of Supercritical Fluids*, *152*, 104543. Online: https://doi.org/10.1016/j.supflu.2019.104543

Cadena-Carrera, S., Tramontin, D. P., Jacques, R., Scapin, E., Müller, J. M., and Hense, H. (2022). Green-based methods to obtain bioactive compounds from Ilex guayusa Loes. using polar solvent. *Natural Product Research*, *37*(18), 3103–3108. Online: https://doi.org/10.1080/14786419.2022.2140802

Cakmak, H., Ilyasoglu-Buyukkestelli, H., Sogut, E., Ozyurt, V. H., Gumus-Bonacina, C. E., and Simsek, S. (2023). A review on recent advances of plant mucilages and their applications in food industry: Extraction, functional properties and health benefits. *Food Hydrocolloids for Health*, *3*, 100131. Online: https://doi.org/10.1016/j.fhfh.2023.100131

Carreira-Casais, A., Otero, P., Garcia-Perez, P., Garcia-Oliveira, P., Pereira, A. G., Carpena, M., ... Prieto, M. A. (2021). Benefits and drawbacks of ultrasound-assisted extraction for the recovery of bioactive compounds from marine algae. *International Journal Of Environmental Research And Public Health*, *18*(17), 9153. Online: https://doi.org/10.3390/ijerph18179153

Chappells, H., and Dummer, T. (2024). Situating people and place in cancer prevention: Arsenic in drinking water in global to local context. En *Global perspectives on health geography* (pp. 243–267). Springer. Online: https://doi.org/10.1007/978-3-031-66413-7_10

Chianese, G., Golin-Pacheco, S., Taglialatela-Scafati, O., Collado, J., Munoz, E., Appendino, G., and Pollastro, F. (2019). Bioactive triterpenoids from the caffeine-rich plants guayusa and maté. *Food Research International*, *115*, 504–510. Online: https://doi.org/10.1016/j.foodres.2018.10.005

Dinardo, A., Brar, H. S., Subramanian, J., and Singh, A. (2019). Optimization of microwave-assisted extraction parameters and characterization of phenolic compounds in yellow european plums. *Canadian Journal of Chemical Engineering*, *97*, 256–267. Online: https://doi.org/10.1002/cjce.23237

García-Ruiz, A., Baenas, N., Benítez-González, A. M., Stinco, C. M., Meléndez-Martínez, A. J., Moreno, D. A., and Ruales, J. (2017). Guayusa

©2026, Universidad Politécnica Salesiana, Ecuador.

(Ilex guayusa L.) new tea: phenolic and carotenoid composition and antioxidant capacity. *Journal Of The Science Of Food And Agriculture*, *97*(12), 3929–3936. Online: https://doi.org/10.1002/jsfa.8255

González-Pérez, J. E., Jiménez-González, O., Romo-Hernández, A., Lóp-Malo, A., and Ramírez-Corona, N. (2024). Time-to-failure approach for estimating the shelf life of freeze-dried carotenoid-enriched apples: Forecasting the deterioration of quality properties for different packaging types and storage conditions. *ACS Agricultural Science & Technology*, *4*(11), 1241–1249. Online: https://doi.org/10.1021/acsagscitech.4c00465

Hassan, S., and Yaqoobi, A. A. (2023). Assessment of ultrasound-assisted extraction of caffeine and its bioactivity. *Journal Of Ecological Engineering*, *24*(3), 126–133. Online: https://doi.org/10.12911/22998993/157540

Held, S., Hildenbrand, A., Herdt, A., and Wachtmeister, G. (2023). Multiobjective metamodel-based design optimization—a review and classification approach using the example of engine development. *SAE Technical Papers*. Online: https://doi.org/10.4271/2023-01-5026

Herrera, D. C. V., Mallea, C. L. B., Del Rosario Crisosto Fuster, A., and Marin, C. A. H. (2022). Estabilidad de bebida funcional de suero deslactosado con Passiflora mollissima en condiciones termales: Un estudio de vida útil. *Revista de Ingeniería (UPT)*. Online: https://revistas.upt.edu.pe/ojs/index.php/ingenieria/article/view/648

Howard, J. A., Kuznietsova, H., Dziubenko, N., Aigle, A., Natuzzi, M., Thomas, E., … Tillement, O. (2023). Combating lead and cadmium exposure with an orally administered chitosan-based chelating polymer. *Scientific Reports*, *13*(1). Online: https://doi.org/10.1038/s41598-023-28968-4

Isuiza, G. G. P., Perez, J. F. L., Sánchez, I. C., Olano, J. C., Valerio, W. F. S., and Delgado, L. F. V. (2018). Vida en anaquel de galletas saladas utilizando pruebas aceleradas. *Anales Científicos*, *79*(1), 218. Online: https://doi.org/10.21704/ac.v79i1.1166

Ivanović, M., Razboršek, M. I., and Kolar, M. (2020). Innovative extraction techniques using deep eutectic solvents and analytical methods for the isolation and characterization of natural bioactive compounds from plant material. *Plants*, *9*(11), 1428. Online: https://doi.org/10.3390/plants9111428

Karal, M. A. S., Billah, M. M., and Ahamed, M. K. (2024). Determination of pore edge tension from the kinetics of rupture of giant unilamellar vesicles using the arrhenius equation: effects of sugar concentration, surface charge and cholesterol. *Physical Chemistry Chemical Physics*, *26*(7), 6107–6117. Online: https://doi.org/10.1039/d3cp04451c

Kumar, K., Srivastav, S., and Sharanagat, V. S. (2020). Ultrasound assisted extraction (UAE) of bioactive compounds from fruit and vegetable processing by-products: A review. *Ultrasonics Sonochemistry*, *70*, 105325. Online: https://doi.org/10.1016/j.ultsonch.2020.105325

Lezoul, N. E. H., Belkadi, M., Habibi, F., and Guillén, F. (2020). Extraction processes with several solvents on total bioactive compounds in different organs of three medicinal plants. *Molecules*, *25*(20), 4672. Online: https://doi.org/10.3390/molecules25204672

Liu, Y., Wang, S., Niu, X., Yin, M., He, Z., Hou, J., … Luo, Y. (2022). Vertical distribution and health risk assessment of heavy metals in soils around tin ore areas in yunnan, china. *International Journal Of Environmental & Analytical Chemistry*, 1–14. Online: https://doi.org/10.1080/03067319.2022.2128794

López-Quiroga, E., Prosapio, V., Fryer, P. J., Norton, I. T., and Bakalis, S. (2019). Model discrimination for drying and rehydration kinetics of freeze-dried tomatoes. *Journal Of Food Process Engineering*, *43*(5). Online: https://doi.org/10.1111/jfpe.13192

Luna-Fox, S., Uvidia-Armijo, J. H., and Rivera-Barreto, J. (2024). Kinetic study of solid-liquid extraction of caffeine in Ilex guayusa Loes. *Revista de la Facultad de Agronomía (LUZ)*, *41*(3), e244128. Online: https://doi.org/10.47280/RevFacAgron(LUZ).v41.n3.08

Mazumder, K., Nabila, A., Aktar, A., and Farahnaky, A. (2020). Bioactive variability and in vitro and in vivo antioxidant activity of unprocessed and processed flour of nine cultivars of aus-

©2026, Universidad Politécnica Salesiana, Ecuador.

tralian lupin species: A comprehensive substantiation. *Antioxidants*, *9*(4), 282. Online: https://doi.org/10.3390/antiox9040282

Meneses, M. Á., Guzmán, J., Cabrera, J., Magallanes, J., Valarezo, E., and Guamán-Balcázar, M. D. C. (2024). Green processing of Ilex guayusa: Antioxidant concentration and caffeine reduction using encapsulation by supercritical antisolvent process. *Molecules*, *29*(22), 5309. Online: https://doi.org/10.3390/molecules29225309

Min, J., Sarlus, H., and Harris, R. A. (2024). Copper toxicity and deficiency: the vicious cycle at the core of protein aggregation in ALS. *Frontiers In Molecular Neuroscience*, *17*. Online: https://doi.org/10.3389/fnmol.2024.1408159

Negrin, A., Long, C., Motley, T. J., and Kennelly, E. J. (2019). LC-MS metabolomics and chemotaxonomy of caffeine-containing holly (Ilex) species and related taxa in the Aquifoliaceae. *Journal Of Agricultural And Food Chemistry*, *67*(19), 5687–5699. Online: https://doi.org/10.1021/acs.jafc.8b07168

Repajić, M., Cegledi, E., Zorić, Z., Pedisić, S., Garofulić, I. E., Radman, S., … Dragović-Uzelac, V. (2021). Bioactive compounds in wild nettle (Urtica dioica L.) leaves and stalks: Polyphenols and pigments upon seasonal and habitat variations. *Foods*, *10*(1), 190. Online: https://doi.org/10.3390/foods10010190

Serna-Jiménez, J., Torres-Valenzuela, L., Villarreal, A. S., Roldan, C., Martín, M., Siles, J., and Chica, A. (2023). Advanced extraction of caffeine and polyphenols from coffee pulp: Comparison of conventional and ultrasound-assisted methods. *LWT*, *177*, 114571. Online: https://doi.org/10.1016/j.lwt.2023.114571

Servicio Ecuatoriano de Normalización (INEN). (2013). *NTE INEN 1122:2013 – requisitos del café soluble* (Inf. Téc.). Servicio Ecuatoriano de Normalización. Online: https://www.bing.com/search?q=NTE+INEN+1122%3A2013

Setiawan, B., Azra, J. M., Nasution, Z., Sulaeman, A., and Estuningsih, S. (2022). Development of freeze-dried coconut drink and its nutrient content, sensory profile, and shelf life. *Journal Of Culinary Science & Technology*, *22*(4), 787–803. Online: https://doi.org/10.1080/15428052.2022.2079578

Sobin, C., Gutiérrez-Vega, M., Flores-Montoya, G., Del Rio, M., Alvarez, J. M., Obeng, A., … Hettiarachchi, G. (2023). Improving equitability and inclusion for testing and detection of lead poisoning in US children. *Milbank Quarterly*, *101*(1), 48–73. Online: https://doi.org/10.1111/1468-0009.12596

Yan, H., Li, S., Zhong, J., and Li, B. (2023). An electrochemical perspective of aqueous zinc metal anode. *Nano-Micro Letters*, *16*(1). Online: https://doi.org/10.1007/s40820-023-01227-x

Yang, Y., Guan, M., Fang, M., Gu, Y., Yi, L., and Ren, D. (2024). Simultaneous extraction and selective separation of catechins, caffeine and theanine from waste tea residue facilitated by citric acid-based deep eutectic solvent. *Separation And Purification Technology*, 130918. Online: https://doi.org/10.1016/j.seppur.2024.130918

©2026, Universidad Politécnica Salesiana, Ecuador.

La Granja: Revista de Ciencias de la Vida
pISSN:1390-3799; eISSN:1390-8596
https://doi.org/10.17163/lgr.n44.2026.06

Artículo científico / Scientific paper

BIOTECHNOLOGY

Antimicrobial potential of *Vaccinium floribundum* extract fluid against *Staphylococcus saprophyticus* causing urinary tract infections

Potencial antimicrobiano del extracto fluido de *Vaccinium floribundum* frente a *Staphylococcus saprophyticus* causante de infecciones de vías urinarias

Johana Meneses*, Stephanie Moncayo, María E. Maldonado and Ramiro Acurio

Universidad Politécnica Salesiana, Ecuador. [https://ror.org/00f11af73]

*Corresponding author: jmeneses@ups.edu.ec

Article received on October 26th, 2024. Accepted, after review, on November 6th, 2025. Published on September 1st, 2026.

Abstract

Vaccinium floribundum, belonging to the Ericaceae family, was evaluated for its antimicrobial, antioxidant, anti- inflammatory, and anticancer properties due to its high anthocyanin content. The objective of this study was to determine the content of anthocyanins present in the fluid extract of *V. floribundum*, as well as to evaluate its antimicrobial activity in the prevention of UTIs, establishing the minimum inhibitory concentration (MIC) against *Staphylococcus saprophyticus* ATCC 15305, a causative agent of urinary tract infections. The study was conducted at the Life Sciences Laboratories of the Salesian Polytechnic University, beginning with the preparation of 20 % and 50 % ethanolic extracts from fruits harvested in the Province of Cotopaxi, Sigchos Canton; the assays were performed *in vitro*. The concentration of total phenols was quantified using the Folin-Ciocalteu method, yielding 537.26 mg AG/100 mL for the 20 % extract and 621.04 mg AG/100 mL for the 50 % extract. In the quantification of total anthocyanins, 11.6391 mg/L was obtained for the 20 % extract and 43.63 mg/L for the 50 % extract, respectively. Subsequently, the minimum inhibitory concentration (MIC) and the percentage of inhibition were evaluated for the extracts against *S. saprophyticus*; the MIC was 390.63 μg/mL for both extracts, with 88.42 % inhibition for the 20 % extract and 88.44 % for the 50 % extract. Using thin-layer chromatography (TLC), the retention factors (R_f) were 0.42 (cyanidin 3-*O*-glucoside), 0.62 (malvidin), and 0.86 (cyanidin). In conclusion, the 20 % and 50 % ethanolic extracts of *V. floribundum* exhibit antimicrobial activity against *S. saprophyticus*.

Keywords: Microbial control, Mortiño, *Vaccinium floribundum*, ethanolic extracts, anthocyanins.

©2026, Universidad Politécnica Salesiana, Ecuador.

Resumen

Se evaluó *Vaccinium floribundum*, de la familia Ericaceae, por sus propiedades antimicrobianas, antioxidantes, antiinflamatorias y anticancerígenas, debido a su alto contenido de antocianinas. El objetivo de este estudio es determinar la cantidad de antocianinas presentes en el extracto fluido de *V. floribundum*, así como evaluar la actividad antimicrobiana en la prevención de infecciones del tracto urinario (IVU), estableciendo la concentración mínima inhibitoria (MIC) frente a *Staphylococcus saprophyticus* ATCC 15305, causante de infecciones urinarias. El estudio se realizó en los Laboratorios de Ciencias de la Vida de la Universidad Politécnica Salesiana, iniciando con la obtención de extractos etanólicos al 20 y 50 % a partir de frutos recolectados en la provincia de Cotopaxi, cantón Sigchos; los ensayos fueron aplicados a nivel *in vitro*. Se cuantificó la concentración de fenoles totales por el método de Folin-Ciocalteu, obteniendo 537.26 mg AG/100 mL de extracto al 20 % y 621.04 mg AG/100 mL al 50 %. En la cuantificación de antocianinas totales se obtuvieron 11.6391 mg/L de extracto al 20 % y 43.63 mg/L al 50 %, respectivamente. Posteriormente, se evaluó la concentración mínima inhibitoria (MIC) y el porcentaje de inhibición de los extractos frente a *S. saprophyticus*; la MIC fue de 390.63 μg/mL para ambos extractos, con un 88.42 % de inhibición para el extracto al 20 % y un 88.44 % para el extracto al 50 %. Mediante cromatografía en capa fina (TLC), los factores de retención (R_f) fueron: 0.42 (cianidina 3-*O*-glucósido), 0.62 (malvidina) y 0.86 (cianidina). En conclusión, los extractos etanólicos de *V. floribundum* al 20 y 50 % presentan actividad antimicrobiana frente a *S. saprophyticus*.

Palabras clave: Control microbiano, Mortiño, *Vaccinium floribundum*, extractos etanólicos, antocianinas.

Suggested citation: Meneses, J., Moncayo, S., Maldonado, M. E. and Acurio, R. (2026). Antimicrobial potential of *Vaccinium floribundum* extract fluid against *Staphylococcus saprophyticus* causing urinary tract infections. La Granja: Revista de Ciencias de la Vida. Vol. 44(2):97-113. https://doi.org/10.17163/lgr.n44.2026.06.

Orcid IDs:

Johana Gabriela Meneses Morillo: https://orcid.org/0000-0001-9920-959X
Stephanie Abigail Moncayo Picerno: https://orcid.org/0000-0003-1614-0676
María Elena Maldonado Rodríguez: https://orcid.org/0000-0003-3658-5445
Ramiro Daniel Acurio Vásconez: https://orcid.org/0000-0002-2305-4349

©2026, Universidad Politécnica Salesiana, Ecuador.

1 Introduction

Vaccinium floribundum, known as mortiño in Ecuador, is a wild shrub belonging to the Ericaceae family and the genus *Vaccinium*. It grows at altitudes ranging from 3400 to 3800 meters above sea level in the Andean region. It is a perennial species whose ecosystem is considered sensitive; therefore, there is no propagation method that ensures plant uniformity. *Vaccinium floribundum* contains a variety of phenolic compounds and high concentrations of anthocyanins in the form of pigments in berries, leaves, flowers, and fruits. These compounds possess a sugar moiety at position 3 and an aglycone (Pérez et al., 2020; Llerena et al., 2004).

Recent studies have shown that the active substances in mortiño fruits—fructose and proanthocyanidins—act by preventing the adhesion of bacteria, such as *Escherichia coli*, to the uroepithelium in women, although not in patients with neurogenic bladder. Therefore, the use of this plant species is recommended as a preventive measure in cases of urological pathologies (De León et al., 2009).

Within Urinary Tract Infections (UTIs), Urinary Tract Infection (UTI) is classified as occurring in 1–3 % of school-aged adolescents and increases with the onset of sexual activity, being very common in women between 20 and 50 years of age. According to statistics from the Ministry of Public Health of Ecuador (MSP), 4 out of 10 inhabitants reported urinary tract infections during 2009 (Ministerio de Salud Pública, 2013). In 2019, the National Institute of Statistics and Census (INEC) reported 9,916 cases of genitourinary infections in females aged 18 to 29, of which 9.0 % occurred in the Highlands and 7.2 % in the Coastal region (Instituto Nacional de Estadística y Censos, 2019; Rengifo, 2013; Palacio Rojas et al., 2018).

Focusing on the genus *Vaccinium* and its bactericidal activity in the prevention of urinary tract infections, *Vaccinium floribundum* is known to be associated with the presence of flavonol glycosides and polyphenols (proanthocyanidins, anthocyanins, and flavan-3-ols) (Baenas et al., 2020). Its bactericidal activity can be assessed through the Minimum Inhibitory Concentration (MIC), which consists of a serial dilution technique in a sterile plate containing defined concentrations of an extract against various microorganisms. The lowest microbial growth allows determination of the corresponding inhibition percentage. To apply this technique, it is important to use chemically stable dyes, among which 2,3,5-triphenyltetrazolium chloride (TTC) at 1 % stands out, forming formazan salts that enable detection of microbial colonies at a wavelength of 450 nm, evidenced by a color change from colorless to reddish (Hemeg et al., 2020; Condalab, 2019).

It is necessary to quantify the total phenolic content of *Vaccinium floribundum* samples. Therefore, fluid extracts of mortiño prepared with 20 % and 50 % ethanol are quantified colorimetrically using the Folin–Ciocalteu (F–C) reagent with gallic acid as a standard in a plate. The F–C reagent is characterized by forming phosphomolybdic–phosphotungstic complexes due to the formation of chromogenic oxides under basic pH conditions, resulting in a blue coloration, at which point a chemical reduction occurs. Measurement performed with a UV–visible spectrophotometer determines the absorbance of the blue compounds (phenols), which is directly proportional to their concentration (Cortez et al., 2018). Subsequently, the concentration of monomeric anthocyanins is determined considering the maximum wavelength of the samples, in this case at 520 and 700 nm using the differential pH method (Zapata et al., 2014).

To separate the chemical fractions of crude mortiño extracts, thin-layer chromatography (TLC) was employed, considering the retention factor (R_f) as a fundamental parameter to identify the type of bioactive compounds separated. In this case, these include glycosylated derivatives of anthocyanins, such as pelargonidin, cyanidin, delphinidin, peonidin, petunidin, and malvidin (Zapata et al., 2014). The TLC technique involves a stationary phase (silica gel plate 10×10 cm, factor 254 nm) and a mobile phase composed of solvents of medium polarity in various proportions. These mortiño extracts were compared with a cyanidin-3-*O*-glucoside standard with an R_f value of 0.44 (Santacruz, 2017).

The fluid extracts were obtained through drying and extraction by maceration, a process consisting of leaving the solvent in contact with the plant material for several days under moisture conditions at

©2026, Universidad Politécnica Salesiana, Ecuador.

a temperature suitable for the bioactive compounds to be extracted (Urquizo, 2016). The solvents used for each assay were ethanol at concentrations of 20 % and 50 %.

The main objective of this research project is to determine the concentration of phenolic compounds present in the fluid extract of *Vaccinium floribundum* and to evaluate its antimicrobial activity *in vitro*. Additionally, it aims to identify the secondary metabolites present in *Vaccinium floribundum* with antimicrobial potential relevant to the control of pathogens causing urinary tract infections, and to determine the minimum inhibitory concentration (MIC) of cyanidin from *Vaccinium floribundum* against *Staphylococcus saprophyticus*.

2 Materials and Methods

2.1 Obtaining ethanolic extracts

The fruits of *Vaccinium floribundum* were collected in the Sigchos Canton, Cotopaxi province, at 3023 meters above sea level, with coordinates S 00°4242.6 – W 078°5322.1. The classified and cleaned fruits were placed on aluminum trays and dried at 40 °C in an oven for 6 days. The dried material was ground, and 100 g were placed into a 250 mL Erlenmeyer flask, hydrated with 200 mL of ethanol at 20 % and 50 %, respectively. The mixture was stirred for 24 hours, then filtered and concentrated using a rotary evaporator until a final volume of 100 mL was obtained. Finally, the extracts were stored in amber containers for subsequent analyses (Narváez, 2016).

2.2 Determination of total phenolic content

The Folin–Ciocalteu colorimetric method was employed. Starting from a stock solution of gallic acid at a concentration of 2000 ppm, solutions at six different concentrations (100, 150, 200, 250, 300, 350, and 400 ppm) were prepared. From each solution, 0.5 mL were taken, to which 3.95 mL of distilled water and 0.25 mL of Folin-Ciocalteu reagent were added. The mixture was allowed to stand for 2 minutes, after which 0.75 mL of 20 % (w/v) sodium carbonate was added. The absorbance was measured at a wavelength of 765 nm after 2 hours of incubation in complete darkness. Using the obtained data, the calibration curve was constructed.

Subsequently, the samples were prepared by taking 0.5 mL of each ethanolic extract of *Vaccinium floribundum* at 20 % and 50 %, and the same procedure as for the calibration standards was followed. To quantify the concentration of total phenols in the extracts (mg GA/100 mL of extract), the following Equation 1 was used (Varela and Musuña, 2020):

$$\text{Abs} = mx + b \tag{1}$$

Where: x is the value of total polyphenols expressed as gallic acid equivalents (mg/mL); Abs is the absorbance at 765 nm; m is the slope of the line; and b is the intercept with the y-axis (Urbano, 2016).

2.3 Quantification of anthocyanins

The differential pH method (Giusti and Wrolstad, 2001) was applied. pH 1 and pH 4.5 buffers were prepared; their detailed composition is described in Table 1.

A volume of 2.5 mL of each ethanolic extract of mortiño at 20 % and 50 % was measured in triplicate and brought to a final volume of 5 mL, followed by sonication for 30 minutes. The extracts were filtered into Falcon tubes, protected from light with aluminum foil, and the pH was adjusted to 2.3 using 2 M HCl. The samples were then left to stand in darkness for 4 hours, with sonication for 5 minutes every 2 hours. After this period, the tubes were centrifuged at 3500 rpm for 30 minutes.

Table 1. Preparation of the buffers used

Buffer	Composition / Reagents
Buffer pH 1	0.076 g of potassium chloride in 40 mL of distilled water.
Buffer pH 4.5	2.27 g of sodium acetate in 40 mL of distilled water.

©2026, Universidad Politécnica Salesiana, Ecuador.

Subsequently, 0.5 mL of the supernatant from each Falcon tube was taken and diluted to 5 mL with each of the prepared buffers (pH 1 and pH 4.5) and left to stand for 45 minutes. Then, 100 μL were added into a 96-well microplate to measure absorbance at 510 and 700 nm. Finally, by applying Equations 2 and 3, the anthocyanin concentration present in each ethanolic extract of *Vaccinium floribundum* was determined (Giusti and Wrolstad, 2001; Kayima, 2012).

$$\Delta A = (A_{\lambda max} - A_{700})_{pH1.0} - (A_{\lambda max} - A_{700})_{pH4.5} \quad (2)$$

$$AT\left(\frac{\text{mg}}{\text{L}}\right) = \frac{\Delta A \times PM \times FD \times 1000}{\varepsilon \times 1} \quad (3)$$

Where: ΔA is the absorbance variation; $A_{\lambda \text{max}}$ is the absorbance at the maximum wavelength; A_T corresponds to total anthocyanins (mg/L); F_D is the dilution factor; PM is the molecular weight of cyanidin-3-glucoside (449.2 g/mol); 1000 is the conversion factor from grams to milligrams; and ε is the molar absorptivity coefficient of cyanidin-3-glucoside (26,900) (Giusti and Wrolstad, 2001).

2.4 Determination of the Minimum Inhibitory Concentration (MIC)

Certified ATCC 15305 Microbiologics strains of *Staphylococcus saprophyticus*, in KWIK-STIK presentation, were reactivated by swabbing and from cryobank beads in both solid and liquid Tryptic Soy media (TSA/TSB). They were incubated for 24 hours at 37 °C at a pH of 7.3 ± 0.2.

An overnight culture was obtained by inoculating in Müller–Hinton broth for 24 hours at 37 °C. After this period, the tubes were centrifuged at 3500 rpm for 30 minutes, the supernatant was discarded, and 5 mL of sterile 0.9 % physiological solution was added, followed by vortexing for 3 minutes. By adding small amounts of physiological solution, the suspension was adjusted to 0.5 on the McFarland scale, and the absorbance was measured at 625 nm within the range of 0.08–0.2 to achieve a concentration of 10^8 CFU/mL. The solutions of the commercial and natural antibiotics to be tested were prepared; additionally, the extracts were diluted 1:10 to a final volume of 10 mL (Guzmán, 2018; Veloz, 2018). Subsequently, with all materials and the working area completely sterile, inoculation in the microplate was carried out (León et al., 2011), as detailed in Table 2.

Table 2. Layout of the contents of each well on the microplate for determining the MIC

Treatment	Location	Contents
Blank	Column A12-H12	200 μL MC
Negative control (C_E)	Column A11-H11	200 μL MC
Positive control (C_C)	Rows H9-H1	150 μL MC + 50 μL inoculum
Ethanolic extract samples	Rows A9-B9-C9	150 μL MC + 50 μL Ext + 50 μL inoculum
	Rows A8-A1/B8-B1/C8-C1	150 μL MC + 50 μL inoculum. Serial dilution
Positive control (antibiotic)	Rows D9-E9	150 μL MC + 50 μL Antb + 50 μL inoculum
	Rows D8-D1/E8-E1	150 μL MC + 50 μL inoculum. Serial dilution
Positive control (natural)	Rows F9-G9	150 μL MC + 50 μL thymol solution + 50 μL inoculum
	Rows F8-F1/G8-G1	150 μL MC + 50 μL inoculum. Serial dilution

Note. MC: culture medium; Ext: extract; Antb: antibiotic. The remaining 50 μL of each dilution is discarded.
Source. (León et al., 2011).

©2026, Universidad Politécnica Salesiana, Ecuador.

The microplate was incubated for 24 hours at 35 °C with agitation. After the incubation period, 30 μL of 1 % 2,3,5-triphenyltetrazolium chloride (TTC) was added to each of the 96 wells of the microplate and incubated at 37 °C for 40 minutes. Finally, absorbance was measured at 450 nm using a microplate reader.

To determine the Minimum Inhibitory Concentration (MIC), the following equation was applied (Equation 4):

$$\%\text{Inhibition} = 100 - \left(\frac{A \times 100}{B}\right) \tag{4}$$

Where: A is the average absorbance of the three replicates, and B is the absorbance of the positive control (Rosales, 2018).

2.5 Separation of compounds by Thin-Layer Chromatography (TLC)

Prior to the separation of components using Thin-Layer Chromatography (TLC), the ethanolic extracts of mortiño at 20 % and 50 % were concentrated using a rotary evaporator for 2 hours. Subsequently, using a reflux system, they were acidified with 10 mL of 2 M HCl for one hour and then filtered and transferred into amber flasks.

The mobile phase used was a mixture of ethyl acetate, formic acid, acetic acid, and water in the proportion (10:1.1:1.1:2.6), which was also used to condition the chromatographic chamber for 30 minutes (Poole, 2015).

The cyanidin-3-glucoside chloride standard was prepared by dissolving 2 mg of the standard in 1 mL of HPLC-grade methanol (Narváez, 2016).

On a silica gel HPTLC glass plate (Factor 254, size 10×10 cm), a line was drawn 1 cm from the edge of the plate (Corzo, 2019; Pássaro Carvalho et al., 2016). Using a TLC applicator, 7 μL of the cyanidin-3-glucoside chloride standard and 10 μL of the ethanolic mortiño extracts at 20 % and 50 % were applied. The plate was placed in the previously saturated chromatographic chamber for component elution for 1 hour and 15 minutes. The plate was then removed from the chamber, and the solvent was dried using a cold air dryer. The spots generated during the run were observed using a UV visualizer at 254 and 365 nm. Subsequently, the retention factors (R_f) of the standard and the ethanolic mortiño extracts were calculated using Equation 5 (Pássaro Carvalho et al., 2016):

$$R_f = \frac{\text{dist.run by the compound}}{\text{dist.run by the solvent}} \tag{5}$$

2.6 Statistical analysis

Within the experimental design, two concentrations of ethanolic extract of *Vaccinium floribundum* (20 % and 50 %) were evaluated, with three replicates for each concentration. For both the determination of total phenols and the quantification of anthocyanins, data processing was performed using analysis of variance (ANOVA) to establish significant differences with parametric variables. For the functional analysis of the study factors, Tukey's significance test at 0.05 % and the independent samples t-test were applied using the INFOSTAT software.

3 Results and Discussion

3.1 Quantification of total phenols

The calibration curve was constructed using seven concentrations of gallic acid, with a linear regression coefficient (R^2) of 0.9975 (Figure 1).

Based on the absorbance readings at 765 nm from each replicate of the ethanolic extract samples of *Vaccinium floribundum* at concentrations of 20 and 50 %, and using the linear equation, the total phenolic compound concentrations were calculated, expressed as mg of gallic/100 mL of extract. Values of 537.2624 were obtained for the 20 % ethanolic extract and 621.0393 for the 50 % extract.

©2026, Universidad Politécnica Salesiana, Ecuador.

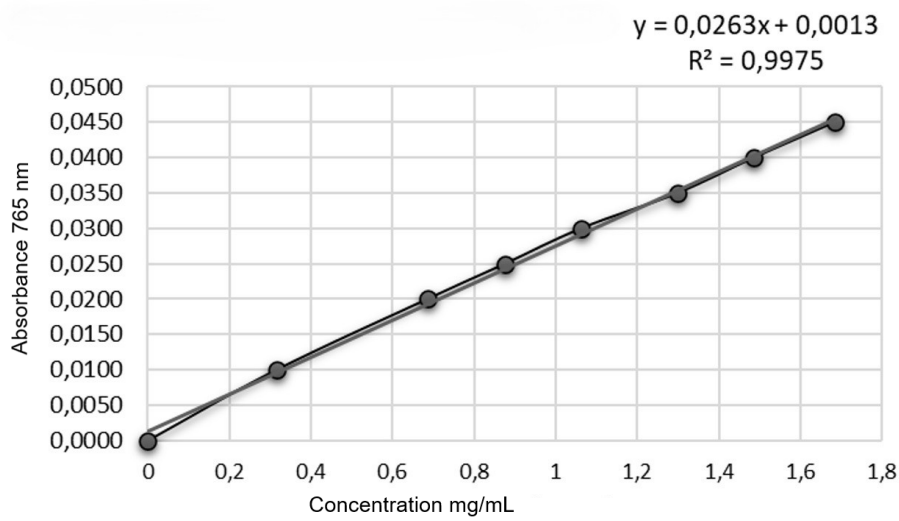


Figure 1. Calibration curve for gallic acid (mg/mL)

Figure 2 shows the total phenolic content in the *Vaccinium floribundum* samples at 20 % and 50 % ethanol.

Based on parametric statistical tests, a significant difference can be identified between the phenolic compound content of the 20 % ethanolic extract and the 50 % ethanolic extract of *Vaccinium floribundum*, with a p-value < 0.0001. Therefore, it can be stated that the 50 % ethanolic extract has a higher content of phenolic compounds than the 20 % ethanolic extract, as evidenced in the bar graph shown in Figure 2.

The phenolic compound content of both the 20 % and 50 % ethanolic extracts of *Vaccinium floribundum* can be corroborated with the results reported by Aaby et al. (2013) in their study on blueberries, which reported 564 mg GA/100 g dry fruit of total phenolic content. Grace et al. (2015) analyzed several species of the genus *Vaccinium*, including *Vaccinium uliginosum* (bog bilberry), in which 504.5 mg GA/100 g of fruit was found. Meanwhile, Llivisaca et al. (2018) reported a content of 146.10 mg GA/100 g fruit in samples collected in Pichincha province and 107.37 mg GA/100 g fruit in samples from Chimborazo province. They also mention that the total polyphenol content in the leaves of *Vaccinium floribundum* is significantly higher than that present in the fruit (Espinosa et al., 2016).

3.2 Quantification of anthocyanins

By applying Equations 2 and 3, different anthocyanin concentrations expressed in mg/L were obtained, as detailed in Table 3.

Table 3. Quantification of total anthocyanins in *Vaccinium floribundum* extracts at concentrations of 20 % and 50 %

Samples	Absorbance Reading by Differential pH				Anthocyanin Concentration		
Ethanolic extract	pH 1		pH 4,5		Average Abs	mg/L	mg/mL
E20	0.1447	0.0383	0.1447	0.0393	0.0697	11.6391	0.0116
E50	0.4203	0.0413	0.1630	0.0437	0.2613	43.6342	0.0436

Note. The concentrations correspond to results obtained from Equation 3 and are expressed in mg/L. Abs Prom: average absorbance.

©2026, Universidad Politécnica Salesiana, Ecuador.

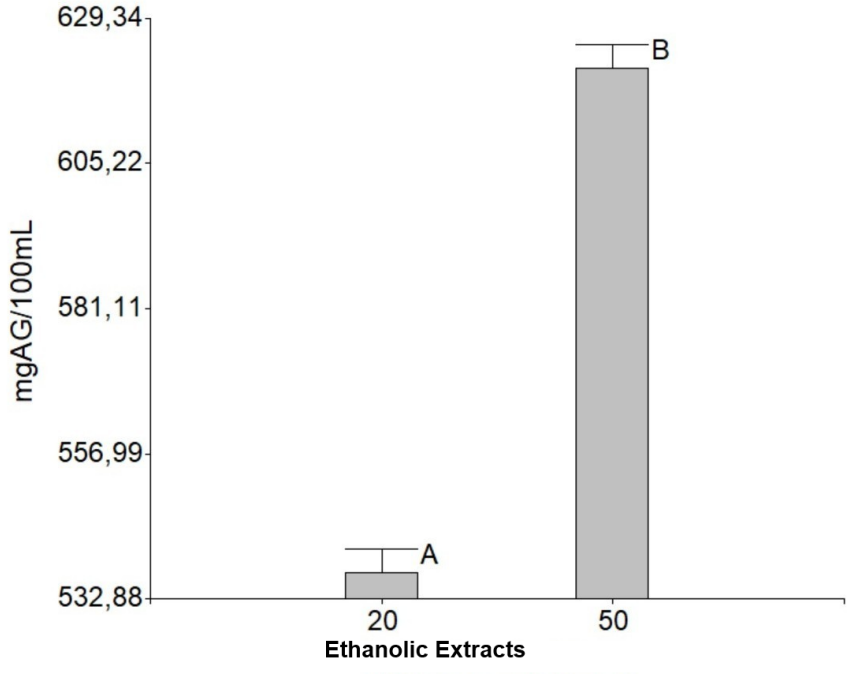


Figure 2. Comparison between 20 % and 50 % extracts in terms of total phenolic content.

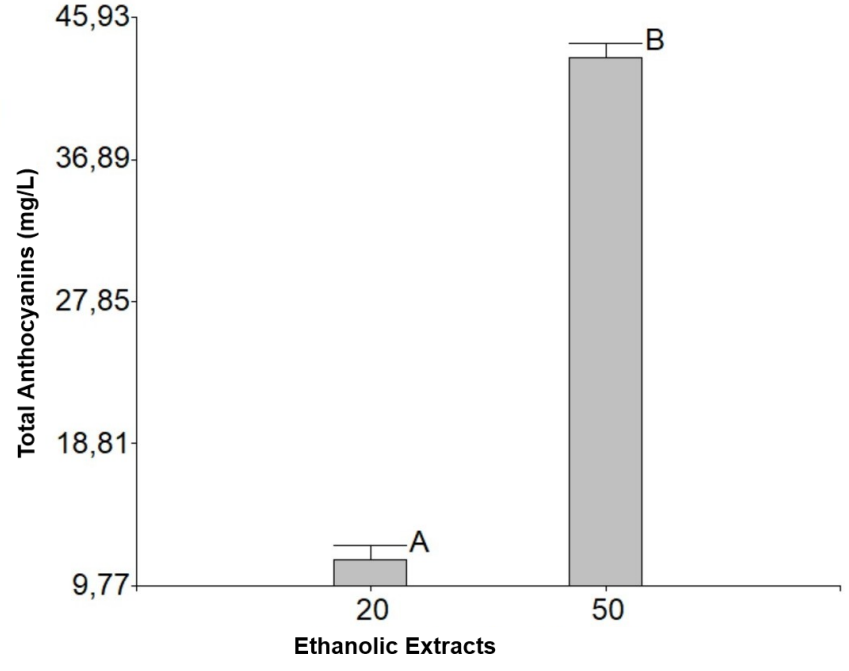


Figure 3. Comparison between 20 % and 50 % extracts in terms of total anthocyanin content.

©2026, Universidad Politécnica Salesiana, Ecuador.

Figure 3 shows the total anthocyanin content in *Vaccinium floribundum* samples at 20 % and 50 % ethanol. From the values obtained using the differential pH method, the anthocyanin concentration in the 20 % ethanolic extract was 11.6391 mg/L (Table 3), which is considered similar to that reported in *Vaccinium myrtillus* (blueberry) (Medina, 2016). In contrast, the 50 % ethanolic extract showed a significant difference ($p < 0.05$) and a concentration of 43.63 mg/L (Figure 3). This extract presented a higher number of anthocyanins obtained from mortiño, while also providing a good yield.

This may be explained by the fact that extraction processes are related to the maturity stage of the berry during harvest, which may change color due to the influence of temperature, oxygen, and light. High temperatures increase acid breakdown, while acidity is related to the pH found in mortiño (Guerrero, 2019). On the other hand, Pérez et al. (2020) worked with *Vaccinium floribundum* and, regarding anthocyanin quantification, obtained satisfactory results using 60 % ethanol at 40 °C, with a result of 332.63 mg C3G 100 g^{-1} FW. Meanwhile, in the case of anthocyanin extraction from cranberry pomace (*Vaccinium macrocarpon*) using 75 % ethanol, greater extraction efficiency and selectivity were achieved (Constantine and Istrati, 2022).

Finally, species such as *Ficus carica* L., *Syzygium cumini* L., *Lonicera cerulea* L., and *Purple Majesty* potato, when subjected to extraction with ethanol at 100 %, 79.6 %, 79.6 %, and 70 %, respectively, yielded different cyanidin glycosides: 4.32 mg C3R/g fig peel DW; 60.5 mg C3GE/g fruit DW; 22.45 mg C3GE/g berries DW; and 364.3 mg C3G/kg potato FW (Tena and Azuero, 2022). The results obtained in this study are similar to those reported by other authors in different plant species.

3.3 Determination of the Minimum Inhibitory Concentration (MIC)

As shown in Table 4, which corresponds to the antimicrobial activity of the 20 % ethanolic extract of *Vaccinium floribundum* against the bacterium *Staphylococcus saprophyticus*, the minimum inhibitory concentration obtained was 390.6 μg/mL, and the percentage of inhibition was 88.42 %. Meanwhile, Figure 5 illustrates the behavior of the 20 % ethanolic extract against the microorganism *S. saprophyticus*, confirming that higher extract concentrations result in greater inhibition of the microorganism (Varela and Musuña, 2020).

Figure 4 shows the microplate stained red with 1 % TTC dye; this coloration indicates the presence of *Staphylococcus saprophyticus*, while the wells that do not show coloration correspond to those in which microbial growth is being inhibited.

To calculate the percentage of inhibition relative to the concentration of each of the ethanolic extracts of *Vaccinium floribundum*, the equation proposed by Owen et al. (2014) was applied.

Table 5 details the value obtained for the minimum inhibitory concentration and the percentage of inhibition of the 50 % ethanolic extract of *Vaccinium floribundum* against *Staphylococcus saprophyticus*, being 390.6 μg/mL and 88.44 %, respectively.

Figure 5 shows the microplate stained red with 1 % TTC dye; this coloration indicates the presence of *Staphylococcus saprophyticus*, while the wells that do not show coloration correspond to those in which microbial growth is being inhibited.

In Table 6, by comparing the data obtained for the minimum inhibitory concentration and the percentage of inhibition of the ethanolic extracts of *Vaccinium floribundum* at 20 % and 50 % against *Staphylococcus saprophyticus*, it is evident that the 50 % ethanolic extract shows a higher percentage of inhibition compared to the 20 % ethanolic extract.

In the case of the commercial antibiotic nitrofurantoin, the percentage of inhibition and minimum inhibitory concentration were 87.7 % and 0.78 μg/mL, respectively. The obtained value was superior to that of the natural agent tested. This is since uropathogens, in large numbers, are susceptible to this drug because their nitroreductase enzymes possess highly reactive electrophilic intermediates that non-specifically attack proteins in the bacterial ribosome, causing complete inhibition and resulting in high inhibition percentages (Komp et al., 2014). Additionally, it is necessary to mention that the MIC achieved in the experiments is close to the theoretical values reported in studies with nitrofurantoin, which indicate ≤ 16 μg/mL within the sensitivity range (IDEXX, 2022).

©2026, Universidad Politécnica Salesiana, Ecuador.

Table 4. Antimicrobial activity of the 20 % ethanolic extract of *Vaccinium floribundum* against *Staphylococcus saprophyticus*

Extract concentration (μg/mL)	Growth Control Abs. (C_c)	Average Abs. at 450 nm	% Inhibition
390.6*	1.229	0.142	88.419**
781.3	1.206	0.135	88.778
1562.5	1.579	0.170	89.234
3125.0	1.462	0.149	89.831
6250.0	1.628	0.164	89.947
12 500.0	1.452	0.138	90.519
25 000.0	1.644	0.143	91.322
50 000.0	1.652	0.143	91.344
100 000.0	1.326	0.112	91.554

Note. The asterisks represent: * Minimum Inhibitory Concentration and ** Percentage of inhibition. Abs.: Absorbance.

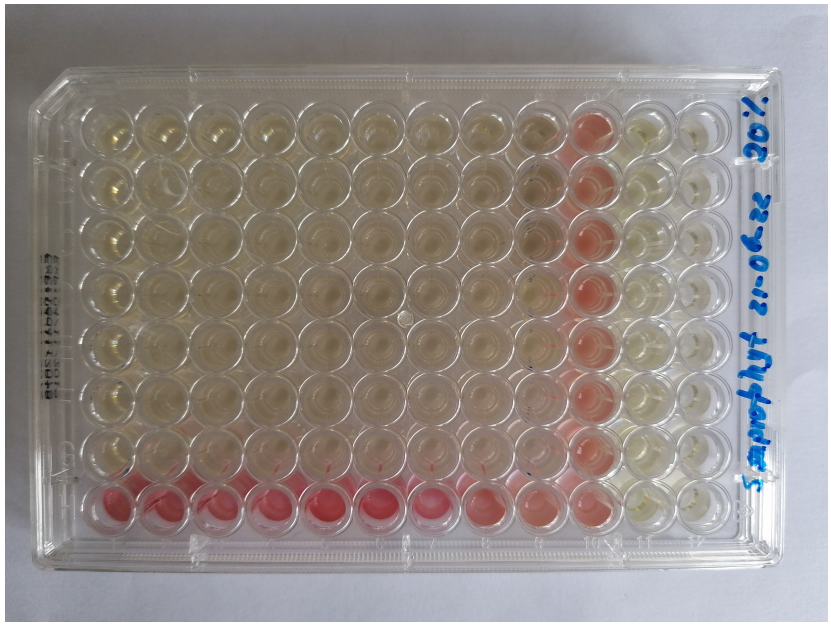


Figure 4. Microplate of *Staphylococcus saprophyticus* with 20 % ethanolic extract stained with 1 % TTC and incubated for 24 hours.

©2026, Universidad Politécnica Salesiana, Ecuador.

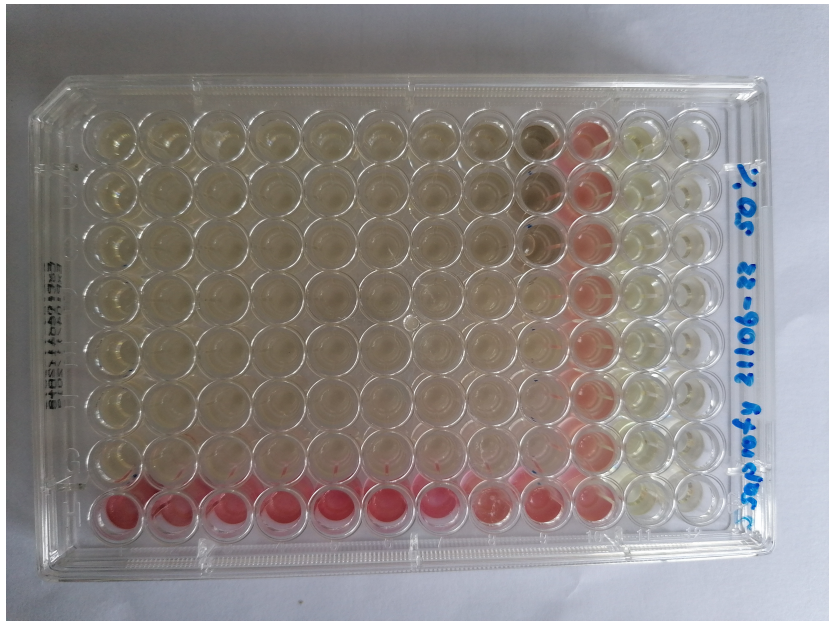


Figure 5. Microplate of *Staphylococcus saprophyticus* with 50 % ethanolic extract stained with 1 % TTC and incubated for 24 hours.

Table 5. Antimicrobial activity of the 50 % ethanolic extract of Vaccinium floribundum against *Staphylococcus saprophyticus*

Extract concentration (μg/mL)	**Growth Control Abs. (C_c)**	**Average Abs. at 450 nm**	**% Inhibition**
390.6*	1.206	0.143	88.439**
781.3	1.229	0.137	88.816
1 562.5	1.579	0.153	88.913
3 125.0	1.462	0.153	88.921
6 250.0	1.628	0.123	88.969
12 500.0	1.452	0.133	89.116
25 000.0	1.644	0.145	89.220
50 000.0	1.652	0.116	89.397
100 000.0	1.326	0.117	89.432

Note. The asterisks represent: * Minimum Inhibitory Concentration and ** Percentage of inhibition. Abs.: Absorbance.

©2026, Universidad Politécnica Salesiana, Ecuador.

Table 6. Percentage of inhibition and MIC of the ethanolic extracts of *Vaccinium floribundum* and established controls against *Staphylococcus saprophyticus*

Microorganism	Extract 20 %		Extract 50 %		Thymol		Nitrofurantoin	
	MIC (μg/mL)	% Inh.	MIC (μg/mL)	% Inh.	MIC (μg/mL)	% Inh.	MIC (μg/mL)	% Inh.
S. saprophyticus	390.63	88.42	390.63	88.44	3.91	87.42	0.78	87.73

Note. % Inh: Percentage of inhibition; MIC: Minimum Inhibitory Concentration.

The best result against *S. saprophyticus* was obtained with the 50 % ethanolic extract of *Vaccinium floribundum*, with a MIC of 390.63 μg/mL and an inhibition percentage of 88.44 %. According to Varela and Musuña (2020), who worked with granules of *Vaccinium floribundum* at 150 mg, 200 mg, and 250 mg against the same microorganism, the inhibition percentages were 50.48 %, 91.17 %, and 86.56 %, respectively, data that corroborate the inhibition percentage obtained in this study.

3.4 Separation of compounds by thin-layer chromatography (TLC)

The chromatographic plates obtained after one hour and 15 minutes of development were as follows:

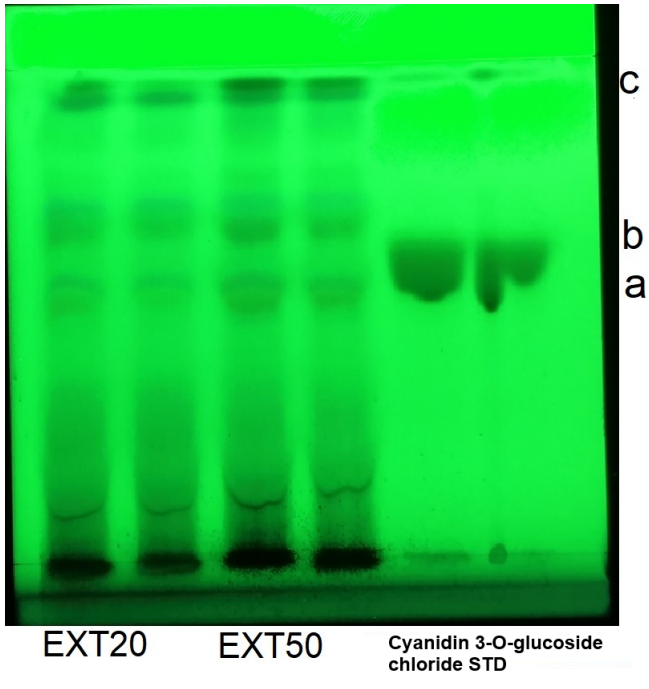


Figure 6. HPTLC plate factor 254 nm 10×10 cm showing separated components of the ethanolic extracts at 20 % (EXT 20) and 50 % (EXT 50) of *Vaccinium floribundum*, respectively. Plate reading wavelength: 254 nm.

©2026, Universidad Politécnica Salesiana, Ecuador.

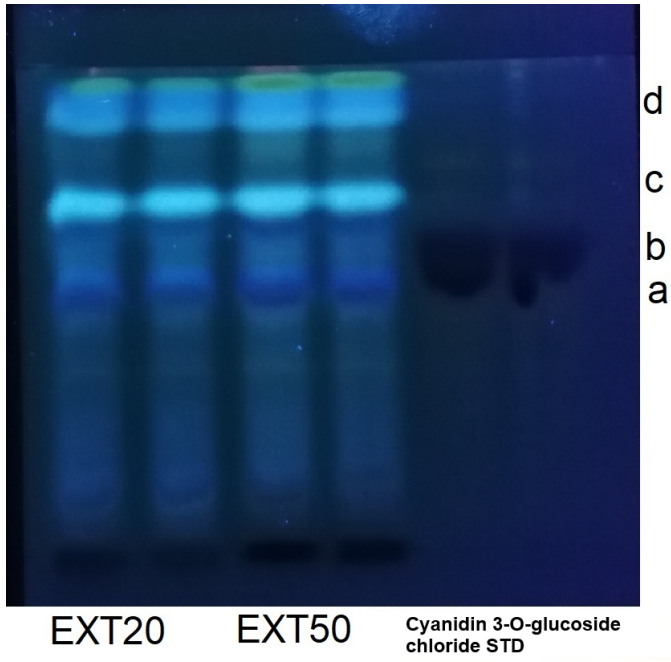


Figure 7. HPTLC plate 254 nm 10×10 cm showing separated components of the ethanolic extracts at 20 % (EXT 20) and 50 % (EXT 50) of *Vaccinium floribundum*, respectively. Plate reading wavelength: 365 nm.

Once the process was completed, the retention factors were determined by relating the distance traveled by the compound to the distance traveled by the solvent (Figure 6). The results are reported in Table 7.

Regarding the results obtained, retention factors may vary due to the different maximum wavelengths at which the compounds are identified. In the case of anthocyanins and anthocyanidins—cyanidin 3-galactoside, cyanidin 3-arabinoside, and malvidin reported in Table 8—these present values similar to those described in studies on the genus *Vaccinium* (blueberries) using methanolic extracts and hydrolyzed compounds (Filip et al., 2012).

According to the results in Table 8, the compounds were identified as cyanidin 3-galactoside, cyanidin 3-arabinoside, malvidin, and cyanidin in the species *Vaccinium floribundum* (mortiño), as also reported by Taco (2017).

Meanwhile, the cyanidin 3-*O*-glucoside standard dissolved in methanol (2 mg/1 mL) presented a retention factor of 0.42, similar to values reported by Narváez (2016) for the species *Vaccinium floribundum* (mortiño).

Other relevant bioactive compounds not detected on the HPTLC plate were delphinidin and pelargonidin, which are found at wavelengths between 520–546 nm, and their respective monoglucosides can be distinguished within a range of 10 to 15 nm from these wavelengths. Additional factors that may affect anthocyanin identification include the nature of the solvent and pH; therefore, acidification of the extracts with HCl is important, as it induces a systematic shift toward higher wavelengths compared to aqueous extracts (Filip et al., 2012). It is also worth noting that the solubility of anthocyanins in alcohol increases when stable hydrochloric acid is added (Eng et al., 2017).

©2026, Universidad Politécnica Salesiana, Ecuador.

Table 7. Identification of anthocyanins and anthocyanidins present in the 20 % and 50 % ethanolic extracts of *Vaccinium floribundum* at a maximum wavelength of 254 nm (see Figure 6)

Fraction	Compound	$\lambda_{máx}$ nm	Rf (Retention factor)
A	Cyanidin 3-O-glucoside	254	0.42
B	Malvidin	254	0.62
C	Cyanidin	254	0.86

Table 8. Identification of anthocyanins and anthocyanidins present in the 20 % and 50 % ethanolic extracts of *Vaccinium floribundum* at a maximum wavelength of 365 nm (see Figure 7)

Fraction	Compound	$\lambda_{máx}$ nm	Rf (Retention factor)
A	Cyanidin 3-galactoside	365	0.39
B	Cyanidin 3-arabinoside	365	0.51
C	Malvidin	365	0.67
D	Cyanidin	365	0.86

4 Conclusions

The 50 % ethanolic extract of *Vaccinium floribundum* showed better results in the quantification of phenolic compounds and total monomeric anthocyanins, yielding 621.04 mg GA/mL of extract and 43.63 mg/L, respectively.

It was possible to separate and identify, through thin-layer chromatography (TLC), anthocyanin bioactive compounds in the 20 % and 50 % ethanolic extracts of *Vaccinium floribundum*, which were: cyanidin 3-arabinoside (R_f 0.51), cyanidin 3-galactoside (R_f 0.39), malvidin (R_f 0.67), and cyanidin (R_f 0.86).

In this study, it was validated that the ethanolic extracts of *V. floribundum* at 20 % and 50 % exhibit antimicrobial activity aimed at inhibiting *Staphylococcus* spp., a pathogen associated with urinary tract diseases.

It is recommended to continue studies using effective, sensitive, and reproducible analytical techniques such as HPLC (High-Performance Liquid Chromatography) for each identified chemical component.

Acknowledgments

We thank the Universidad Politécnica Salesiana, the Life Sciences Laboratories, Mr. Luis Eduardo Grandes, owner of Hacienda San José in Cotopaxi – Sigchos Canton, and the BIOARN Research Group.

Declaration on the use of artificial intelligence

The authors DECLARE that, during the preparation of the article entitled "Antimicrobial potential of *(Vaccinium floribundum)* extract fluid against *Staphylococcus saprophyticus* causing urinary tract infections", no generative artificial intelligence tools or automated assistance systems were used for the writing, analysis, data interpretation, content generation, translation, or editing of the manuscript.

The authors assume full responsibility for the content, originality, integrity, and final version of the article.

©2026, Universidad Politécnica Salesiana, Ecuador.

Author's contribution

J.G.M.M.: Conceptualization, investigation, methodology, supervision, writing – original draft, writing – review and editing. **S.A.M.P.:** Investigation, methodology. **M.E.M.R.:** Funding acquisition, resources. **R.D.A.V.:** Data curation.

References

Aaby, K., Grimmer, S., and Holtung, L. (2013). Extraction of phenolic compounds from bilberry (Vaccinium myrtillus L.) press residue: Effects on phenolic composition and cell proliferation. *LWT - Food Science and Technology*, *54*(1), 257–264.

Baenas, N., Ruales, J., Moreno, D. A., Barrio, D. A., Stinco, C. M., Martínez-Cifuentes, G., … García-Ruiz, A. (2020). Characterization of Andean blueberry in bioactive compounds, evaluation of biological properties, and in vitro bioaccessibility. *Foods*, *9*(10), 1483. Online: https://doi.org/10.3390/foods9101483

Condalab. (2019). *Condalab Online.* Online: http://www.condalab.com (Accedido: 23 de agosto de 2022)

Constantine, O., and Istrati, D. (2022). Técnicas de extracción, cuantificación y caracterización de compuestos de antocianina en diversas matrices alimentarias: una revisión. *Review Horticultura*, 1–18. (16 de noviembre)

Cortez, J., Faicán, M., Pirovani, M., and Piagentini, A. (2018). Determinación de polifenoles en frutas con vitamina C incorporada: Metodología para mejorar la especificidad del ensayo de Folin-Ciocalteu. *Revista Iberoamericana de Tecnología Postcosecha*, *19*(2), 813–818.

Corzo, A. (2019). Cromatografía. En *Técnicas de análisis en química orgánica* (pp. 9–14). Santiago del Estero, Argentina: Universidad Nacional de Santiago del Estero - UNSE. Facultad de Ciencias Forestales.

De Léón, J., Ovadía, R., Vásquez, L., and Fainsod, T. (2009). El arándano y su aplicación en urología. *Revista Mexicana de Urología*, *69*(3), 104–107. (Mayo)

Eng, H., Azlan, A., Teng, S., and Meng, S. (2017). Anthocyanidins and anthocyanins: colored pigments as food, pharmaceutical ingredients, and the potential health benefits. *Food & Nutrition Research*, *61*(1), 1–21.

Espinosa, W., Garzón, L., and Medina, O. (2016). Validación de una metodología analítica para la cuantificación de polifenoles totales, en procesos de extracción asistida por microondas sobre frutos de la especie colombiana Vaccinium meridionale. *Revista Colombiana de Ciencias Químico - Farmacéuticas*, *45*(1), 109–126.

Filip, M., Vlassa, M., Copaciu, F., and Coman, V. (2012). Identification of Anthocyanins and Anthocyanidins from Berry Fruits by Chromatographic and Spectroscopic Techniques to Establish the Juice Authenticity from Market. *Journal of Planar Chromatography*, *25*(6), 534–541.

Giusti, M. M., and Wrolstad, R. (2001). Characterization and Measurement of Anthocyanins by UV-Visible Spectroscopy. En *Current protocols in food analytical chemistry.* Current Protocols.

Grace, M., Esposito, D., Dunlap, K., and Lila, M. A. (2015). Comparative Analysis of Phenolic Content and Profile, Antioxidant Capacity and Anti-inflammatory Bioactivity in Wild Alaskan and Commercial Vaccinium Berries. *HHS Author Manuscripts*, *62*(18), 4007–4017. (7 de mayo)

Guerrero, A. (2019). *Caracterización de compuestos bioactivos: Físicos y químicos del fruto (Vaccinium floribundum Kunth) en la Sierra del Ecuador para uso Agroindustrial* (Tesis Doctoral no publicada). Universidad de las Américas, Quito, Ecuador. (Repositorio Institucional)

Guzmán, D. (2018). *Análisis químico del antibiótico producido por Bacillus megaterium aislado de muestras de suelo, mediante cromatografía y técnicas espectroscópicas* (Tesis Doctoral no publicada). Universidad Politécnica Salesiana, Quito, Ecuador. (Repositorio Institucional)

Hemeg, H. A., Moussa, I. M., Ibrahim, S., Dawoud, T. M., Alhaji, J. H., Mubarak, A. S., … Marouf, S. A. (2020). Antimicrobial effect of different herbal plant extracts against different microbial population. *Saudi Journal of Biological Sciences*, *27*(12), 3221–3227. Online: https://doi.org/10.1016/j.sjbs.2020.08.015

©2026, Universidad Politécnica Salesiana, Ecuador.

IDEXX. (2022). *Guía microbiológica.* Online: https://n9.cl/rsq75r

Instituto Nacional de Estadística y Censos. (2019). *Boletín técnico ECEH 2019* (Inf. Téc.). INEC. Online: https://n9.cl/27oan1 (Accedido: 4 de junio de 2022)

Kayima, F. (2012). *Solvent systems for separation of novel anthocyanin aglycones with methylated A - rings from noruega* (Tesis Doctoral no publicada). Noruega.

Komp, P., Klockars, O., Malmberg, C., and Cars, O. (2014). Pharmacodynamic studies of nitrofurantoin against common uropathogens. *Journal of Antimicrobial Chemotherapy*, *15*(12), 1076–1082.

León, J., Aponte, J. J., Rojas, R., Cuadra, D. L., Ayala, N., Tomás, G., and Guerrero, M. (2011). Estudio de actinomicetos marinos aislados de la costa central del Perú y su actividad antibacteriana frente a Staphylococcus aureus meticilina resistentes y Enterococcus faecalis vancomicina resistentes. *Revista Peruana de Medicina Experimental y Salud Pública*, *28*(2), 237–246. Online: https://n9.cl/ar6j98

Llerena, W., Samaniego, I., Ramos, M., and Brito, B. (2004). Caracterización fisicoquímica y funcional de seis frutas tropicales y andinas ecuatorianas. *Revista de Alimentos Ciencia e Ingeniería*, *22*(2), 13–22.

Llivisaca, S., Manzano, P., Ruales, J., Flores, J., Mendoza, J., Peralta, E., and Cevallos-Cevallos, J. M. (2018). Chemical, antimicrobial, and molecular characterization of mortiño (Vaccinium floribundum Kunth) fruits and leaves. *Food Science & Nutrition*, *6*(4), 934–942. Online: https://doi.org/10.1002/fsn3.638

Medina, L. (2016). *Laboratorio de farmacognosia y farmacobotanica de la Facultad de Farmacia y Bioquímica* (Tesis Doctoral no publicada). Universidad Nacional de Trujillo, Trujillo, Perú. (Repositorio Institucional)

Ministerio de Salud Pública. (2013). *Infección de vías urinarias en el embarazo, guía de práctica clínica* (Inf. Téc.). Quito, Ecuador: MSP.

Narváez, G. (2016). *Estabilización de las antiocianinas presentes en el fruto de mortiño (Vaccinium floribundum Kunth) mediante el método de copigmentación intermolecular para la obtención de pigmentos antociánicos de aplicación en la industria farmacéutica y cosmética* (Tesis Doctoral no publicada). Universidad Central del Ecuador, Quito, Ecuador.

Owen, S. C., Doak, A. K., Ganesh, A. N., Nedyalkova, L., McLaughlin, C. K., Shoichet, B. K., and Shoichet, M. S. (2014). Colloidal drug formulations can explain "bell-shaped" concentration–response curves. *ACS Chemical Biology*, *9*(3), 777–784. Online: https://doi.org/10.1021/cb4007584

Palacio Rojas, M., Mejía Fernández, E., Alcivar Banguera, R., Maldonado Reinozo, N., Medina Apolo, M., Bermeo Ortega, J., … ya Muñoz González, J. (2018). Caracterización clínico-demográfica y resistencia bacteriana de las infecciones del tracto urinario en el Hospital Básico de Paute, Azuay - Ecuador. *AVFT – Archivos Venezolanos de Farmacología y Terapéutica*, *37*(2), 62–67. Online: https://n9.cl/cxgx2vy

Poole, C. (2015). *Instrumental thin-layer chromatography* (1ra ed.). Detroit, USA: Elsevier.

Pássaro Carvalho, C. P., Rivera Narváez, C. M., Román Páez, M. A., Cardona Bermúdez, L. M., Muñoz Echeverri, L. M., Gómez, D. D., … Rojas Bedoya, L. C. (2016). *Guía sobre principios básicos de cromatografía y sus aplicaciones*. Servicio Nacional de Aprendizaje SENA. Online: https://hdl.handle.net/11404/4694

Pérez, B., Endara, A., Garrido, J., and Ramírez, L. (2020). Extraction of anthocyanins from Mortiño (Vaccinium floribundum) and determination of their antioxidant capacity. *Revista Facultad Nacional de Agronomía*, *1*(74), 9453–9460.

Rengifo, D. E. (2013). *Prevalencia de las Infecciones Genitourinarias en mujeres de 14 a 49 años de edad, en el Hospital Delfina Torres y Área 1 de la Provincia de Esmeraldas , de enero a agosto de 2013 y evaluación de su manejo clínico terapéutico* (Tesis Doctoral no publicada). Esmeraldas, Ecuador.

Rosales, R. (2018). *Determinación de la capacidad antimicrobiana de extractos de hongos endófitos de la Colección de Endófitos Quito- Católica (CEQCA) sobre cepas multirresistentes de de staphylococcus aureus* (Tesis Doctoral no publicada). Pontificia Universidad Católica del Ecuador, Quito, Ecuador.

©2026, Universidad Politécnica Salesiana, Ecuador.

Santacruz, C. (2017). *Uso de pigmentos naturales de mortiño (Vaccinium floribundum) como sensibilizadores en celdas solares DSSC* (Tesis Doctoral no publicada). Universidad Politécnica Nacional, Quito, Ecuador.

Taco, M. (2017). *Uso de pigmentos naturales de mortiño (Vaccinium floribundum) como sensibilizadores en celdas solares DSSC* (Tesis Doctoral no publicada). Escuela Politécnica Nacional, Quito, Ecuador.

Tena, N., and Azuero, A. (2022). Análisis Actualizado de los Métodos de Extracción de Antocianinas: Principios de las Técnicas, Optimización, Avances Técnicos y Aplicación Industrial. *Antioxidants*, *11*(2), 286.

Urbano, C. (2016). *Validación del método analítico para la cuantificación de polifenoles totales en productos elaborados con té verde por método colorimétrico Folin Ciocalteu* (Tesis Doctoral no publicada). Universidad ICESI, Cali, Colombia.

Urquizo, L. (2016). *Influencia de los solventes y los métodos de extracción en la determinación de la actividad antioxidante de la especie "Disterigma alaternoides (Kunth) Nied." planta nativa del Ecuador* (Tesis Doctoral no publicada). Universidad Central del Ecuador, Quito, Ecuador.

Varela, S., and Musuña, A. (2020). *Evaluación de la eficacia antimicrobiana in vitro de cápsulas de extracto fluido de Vaccinium floribundum kunth (mortiño); en infecciones agudas del tracto urinario* (Tesis Doctoral no publicada). Universidad Politécnica Salesiana, Quito, Ecuador.

Veloz, T. (2018). *Evaluación de la composición química y actividad biological del aceite esencial proveniente de las hojas de Piper barbatum Kunth (cordoncillo)* (Tesis Doctoral no publicada). Universidad Politécnica Salesiana, Quito, Ecuador.

Zapata, L. M., Heredia, A. M., Quinteros, C. F., Malleret, A. D., Clemente, G., and Cárcel, J. A. (2014). Optimización de la extracción de antocianinas de arándanos. *Ciencia, Docencia y Tecnología*, *25*(49), 166–192. Online: https://n9.cl/707evp

©2026, Universidad Politécnica Salesiana, Ecuador.

La Granja: Revista de Ciencias de la Vida
pISSN:1390-3799; eISSN:1390-8596
https://doi.org/10.17163/lgr.n44.2026.07

Artículo científico / Scientific paper

Agricultural Sciences

Application of a response surface Model for solar and indirect drying of muscat of alexandria grapes (*Vitis vinífera*)

Aplicación de un Modelo de superficie de respuesta en el secado al sol y solar indirecto de uvas variedad moscatel de alejandria (*Vitis vinífera*)

David Vivanco Pezantes*[1], Haydee Rodriguez Navarro[2], Raúl Siche Jara[3] and David Callirgos Romero[4]

[1]*Universidad Nacional del Callao. Facultad de Ingeniería Pesquera y de Alimentos. Escuela Profesional de Ingeniería de Alimentos. Departamento Académico de Ingeniería de Alimentos.Lima-Perú. [https://ror.org/01d03q474]*
[2]*Universidad Nacional de Educación Enrique Guzmán y Valle; Escuela Profesional de Industria Alimentaria y Nutrición. Lima-Perú.[https://ror.org/0431avj27]*
[3]*Universidad Nacional de Trujillo (UNT) - Escuela de Ingeniería Agroindustrial, Facultad de Ciencias Agropecuarias. La Libertad, Perú.[https://ror.org/001b4cb05]*
[4]*Universidade Federal de Pelotas (UFPel) - Departamento de Ciência e Tecnologia de Alimentos, Faculdade de Agronomia Eliseu Maciel. Pelotas, Brasil.[https://ror.org/05msy9z54]*

*Corresponding author: dvivancop@unac.edu.pe

Article received on October 19th, 2023. Accepted, after review, on October 30th, 2024. Published on September 1st, 2026.

Abstract

By applying the response surface methodology, we optimized the sun and indirect solar drying of *Muscat of Alexandria* grapes. Initial moisture was measured and then the grapes were pretreated by thermochemical treatment with sodium hydroxide. Employing a centralized planning of rotating compounds, the pretreatment conditions were established, considering: temperatures, concentrations and times between 55–95 °C, 0.5–3.0 % and 2–30 seconds, respectively. For each drying process, drying times were determined, considering the final moisture content of 20 % on a wet basis, as well as the overall acceptance of the product. Using quadratic order polynomial equations, response surfaces were generated to obtain a shorter drying time and a maximum value of product acceptability, obtaining high values of coefficient of determination ($R^2 > 0.97$) and significant interactions of the independent variables ($p < 0.001$). Solar and indirect drying were optimized at 80 °C, 1.75 % and 16 s, for the temperature and concentration of the sodium hydroxide solution and immersion time, to obtain drying times of 75 h and 50 h, respectively, with a high degree of overall product acceptability and a score above 8 points on the established hedonic scale. Effective water diffusivity values of $8.57 \cdot 10^{-11}$ and $1.90 \cdot 10^{-10}$ m^2/s were obtained for the sun-drying and indirect solar drying process, respectively. Under optimal conditions, the mathematical model of Midilli et al. (2002) best simulates the variation of moisture versus drying time of *Muscat of Alexandria* grapes.

Keywords: Optimization, Grape drying, Mathematical modeling, Diffusivity, Response surface methodology.

©2026, Universidad Politécnica Salesiana, Ecuador.

Resumen

Al aplicar la metodología de superficie de respuesta, se optimizó el secado al sol y solar indirecto de uvas *Moscatel de Alejandría*. Se midió la humedad inicial y a continuación se pretrataron las uvas mediante tratamiento termoquímico con bajas concentraciones de hidróxido sódico, temperatura y tiempo de inmersión. Las condiciones se establecieron mediante un diseño experimental de compuesto central rotacional, considerando: temperaturas, concentraciones y tiempos entre 55–95 °C, 0.5–3.0 % y 2–30 segundos, respectivamente. Para cada proceso se determinaron los tiempos de secado, considerando el contenido de humedad final del 20 % en base húmeda, así como la aceptación global del producto. Empleando ecuaciones polinómicas de orden cuadrático, se generaron superficies de respuesta para obtener un menor tiempo de secado y un valor máximo de aceptabilidad del producto, obteniéndose altos valores de coeficiente de determinación ($R^2 > 0.97$) e interacciones significantes de las variables independientes ($p < 0.001$). El secado al sol y solar indirecto optimizó el pretratamiento a 80 °C, 1.75 % y 16 s, para la temperatura y concentración de la solución de hidróxido de sodio y tiempo de inmersión, para obtener tiempos de secado de 75 h y 50 h, respectivamente, con un alto grado de aceptabilidad global del producto y una puntuación superior a 8 puntos en la escala hedónica establecida. Se obtuvieron valores de difusividad efectiva del agua de $8.57 \cdot 10^{-11}$ y $1.90 \cdot 10^{-10}$ m^2/s para el proceso de secado al sol y secado solar indirecto, respectivamente. En condiciones óptimas, el modelo matemático de Midilli et al. (2002) es el que mejor simula la variación de la humedad frente al tiempo de secado de la uva *Moscatel de Alejandría*.

Palabras clave: Optimización, Secado de uva, Modelación matemática, Difusividad, Metodología de superficie de respuesta.

Suggested citation: Vivanco, D., Rodriguez, H., Siche, R. and Callirgos, D. (2026). Application of a response surface Model for solar and indirect drying of muscat of alexandria grapes (*Vitis vinífera*). La Granja: Revista de Ciencias de la Vida. Vol. 44(2):114-135. https://doi.org/10.17163/lgr.n44.2026.07.

Orcid IDs:

David Vivanco Pezantes: https://orcid.org/0000-0002-9474-0290
Haydee Rodriguez Navarro: https://orcid.org/0000-0001-7346-4496
Raúl Siche Jara: https://orcid.org/0000-0003-3500-4928
David Callirgos Romero: https://orcid.org/0009-0004-7428-4154

©2026, Universidad Politécnica Salesiana, Ecuador.

1 Introduction

Grapes in their fresh state and immediately after harvest have a high moisture content (Gopinath et al., 2022), so their water activity and sugar content make them highly susceptible to microbial spoilage during storage, even under low-temperature refrigeration conditions. Therefore, after harvest, they must be consumed or processed into different products through methods such as drying (Adiletta et al., 2016).

Raisins are an edible product with high nutritional and energy value; in Peru, they are produced using traditional methods through direct sun-drying. This activity takes place in areas with high solar radiation and generally occurs between January and April. In Latin America, Argentina is the country that produces raisins on a large scale, and globally, the leading producers are China and the United States (FAO, 2020).

The industry has developed artificial drying methods, and there are currently a variety of industrial dryers available for agribusiness. Solar energy is the predominant renewable energy source, compared to wind energy and biomass, due to its constant availability (Gunasekaran et al., 2021; Kumar et al., 2021). Sun drying is one of the oldest forms of preservation and perhaps the cheapest and most common method of preserving agricultural products practiced in most tropical countries. However, this technique has disadvantages: it is weather-dependent, requires a long drying time, leads to dust formation, microbial growth, contamination, insect infestation, spoilage, high labor costs, and variable quality, among others (Djebli et al., 2020; Naigam et al., 2021).

On the other hand, the use of indirect solar drying equipment is a good alternative from both an economic and environmental standpoint. Solar drying involves converting solar energy into thermal energy, which is then used to remove moisture from the product (Shalaby and Bek, 2014); through natural convection, air flows inside the dryer (Gopinath et al., 2022). Therefore, the use of solar energy and hot air in convective dryers is a potential alternative for application in tropical and subtropical countries (Vigneshkumar et al., 2021) and also because it is faster, economically viable, hygienic, and more efficient than sun drying, providing dried products with better color and surface texture (Castillo-Téllez et al., 2017; Singh et al., 2012).

Currently, there are numerous research studies on agro-industrial products that were processed using conventional drying methods (sun and air) and modern drying techniques, such as direct sun drying, solar dryers, hot-air convection dryers, hot-air convection dryers assisted by different types of energy, microwaves, infrared, and a combination of these, the use of the ice sublimation process or freeze-drying, heating and air or vacuum drying, and other combined hybrid drying techniques (Atak et al., 2022; Javed et al., 2023), where attempts have been made to apply pretreatments in various forms prior to drying and to observe several parameters, including, primarily, product quality and overall acceptance, drying times, effects on rehydration characteristics, and nutritional quality in the final product (Pragati and Preeti, 2012).

However, there is interest in optimizing drying processes using response surface methodologies, a technique in which a set of variables is examined simultaneously through experimental design, allowing for the identification of variable interactions and the optimal conditions for a maximum or minimum value or a specific area of the generated surface (Bitaraf et al., 2012; Chopra et al., 2011; Myers et al., 2016; Ramos et al., 2015).

A review of the prior literature revealed no research on the optimization of the drying process for Muscat of Alexandria grapes. Therefore, the objectives of this study are to investigate the effect of sodium hydroxide concentration pretreatment, temperature, and immersion time on drying time under direct sunlight and solar drying using an extended-surface collector; to evaluate the quality of the raisins in terms of overall product acceptance; to estimate the constants of the drying curve equations; and to evaluate the water diffusivity under optimal drying conditions.

2 Materials and methods

2.1 Raw Material

The freshly harvested fresh grapes come from the Ica Valley in Peru and were purchased at the fruit

©2026, Universidad Politécnica Salesiana, Ecuador.

market in the city of Chincha Alta. The grapes were washed, then dried and measured with a Vernier caliper. For the physicochemical characterization of the raw material, preliminary determinations were made of pH, Brix degrees (°Brix), refractive index (–), water content (%), and water activity (a_w).

2.2 Grape Pretreatment

Before drying, the selected samples underwent a chemical-thermal treatment, considering temperature, concentration, and immersion time; they were then washed with plenty of cold water at 20 °C and drained, with surface moisture removed using paper towels.

Table 1 shows the coding of the operational variables (temperature, concentration, and immersion time), investigated at five levels each, and the effects on the response variable, drying time, and overall acceptance.

Table 1. Coding of the operational variables for drying the Muscat of Alexandria grape variety (*Vitis vinifera*).

Variables	**Code**	-1.68	-1	0	$+1$	$+1.68$
Temperature (°C)	x_1	55	63	75	87	95
Concentration (%)	x_2	0.5	1	1.75	2.5	3.0
Immersion time (s)	x_3	2	7.7	16	24.3	30

A rotational central composite design (RCCD) was used, consisting of a full factorial design 2^3, 06 axial points (levels ± 1.68), and 06 central points (level 0), totaling 20 trials, conducted in duplicate and randomly, to determine the optimal process conditions. The design with coded and actual levels and the results are shown in Table 4.

2.3 Drying System

A stainless-steel solar dryer (Figure 1) built specifically for this research project was used. The dryer is a commercial-scale prototype. The total dimensions of the dryer are: $2276 \times 2558 \times 806$ mm (height $\times$ length $\times$ width), constructed from 1.5 mm thick 304 stainless steel sheets and structural supports made of 2-inch square profiles. The dimensions of the solar collector with an expanded surface area were: $173 \times 806 \times 2000$ mm, with a 3-mm-thick transparent glass cover, at a $15°$ angle of inclination relative to the horizontal plane and oriented toward the north. The dimensions of a single fin were $1.5 \times 25 \times 2000$ mm, and there were 27 fins on the collector surface. The approximate weight of the equipment was 350 kg. The drying equipment was installed in the open-air courtyard of the Navarro winery in Chincha Alta, at $13°25.3'$ S latitude and $76°7'57''$ W longitude. The experimental module was equipped with thermometers to measure the air temperatures at the solar collector's inlet and outlet, the drying air temperatures along the length of the dryer, and the drying air velocity.

Following the chemical-thermal treatments, the grape drying process was carried out by placing samples with an average weight of 101.27 ± 4.58 g on their respective sample holders in direct sunlight and in the indirect solar dryer. In the latter, the chimney effect combined with the heating of the air in the solar collector contributed to the movement of the drying air and its flow through the drying chamber until it exited the dryer. During the test period, the average ambient air temperature and the temperature of the air entering the drying chamber were 27 and 40 °C, respectively, with an average solar radiation value of 300 W/m^2.

©2026, Universidad Politécnica Salesiana, Ecuador.

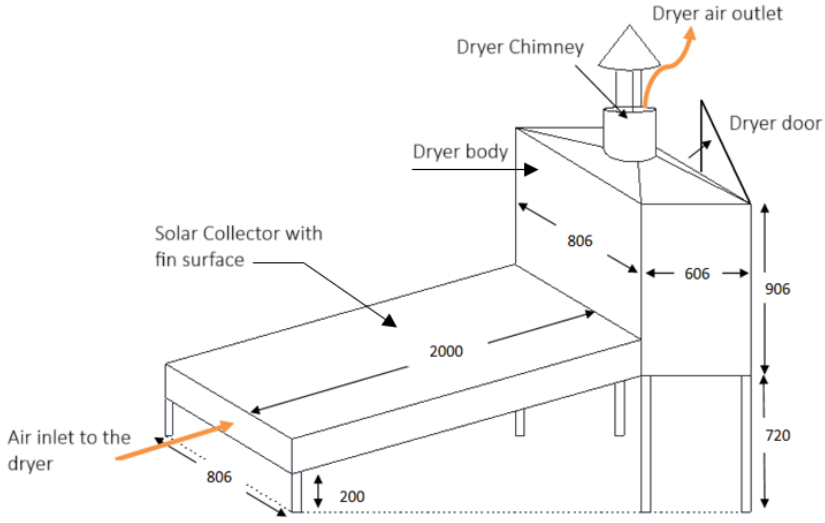


Figure 1. Schematic of the commercial-scale solar dryer.

2.4 Moisture Ratio

The dimensionless moisture module during sun-drying and indirect solar drying (Kusuma et al., 2023) is presented in Equation 1:

$$MR = \frac{X(t) - X_e}{X_o - X_e} \tag{1}$$

Where: $X(t)$ is the average moisture content at time t, X_0 is the initial average moisture content, and X_e is the average moisture content at equilibrium.

2.5 Effective water diffusivity (D_{eff})

In the general form of the diffusion equation in spherical coordinates without considering mass generation, the expression is represented as Equation 2:

$$\frac{1}{r^2}\frac{\partial}{\partial r}\left(r^2\frac{\partial X}{\partial r}\right) + \frac{1}{r^2 sin\theta}\frac{\partial}{\partial \theta}\left(sin\theta\frac{\partial X}{\partial \theta}\right) + \frac{1}{r^2 sin^2\theta}\frac{\partial^2 X}{\partial \phi^2} = \frac{1}{D}\frac{\partial X}{\partial t} \tag{2}$$

Likewise, considering that diffusion occurs only along the radial axis, the simplified equation for water mass diffusion through the grape cross-section in spherical coordinates is given by Equation 3:

$$\frac{\partial X(r,t)}{\partial t} = \frac{1}{r^2}\frac{\partial}{\partial r}\left(r^2 D\frac{\partial X}{\partial r}\right) \tag{3}$$

For the initial and boundary conditions at the surface ($r = R$) and at the center of the grape berry ($r = 0$), they are (Equations 4 and 5):

$$X(t = 0.0 \leq r < R) = X_0 \tag{4}$$

$$X(t = 0.0 \leq r < R) = X_0 \tag{5}$$

It is assumed that the initial moisture distribution is uniform within the sphere, that the surface moisture is equal to the equilibrium moisture content, and that radial diffusion is symmetric.

Considering that the entire drying process occurs during a period of decreasing drying rate and that the liquid diffusivity is the dominant factor in the entire process—*i.e.*, the drying process is entirely controlled by the internal resistance to mass transfer—, Fick's second law of diffusion can be used to describe the drying process (Doymaz, 2007; Saravacos and Maroulis, 2001; Srikiatden and Roberts, 2006).

Equation 3 can be solved analytically by assuming a constant radius (shrinkage is not considered) and a constant diffusivity coefficient during the drying process, which yields Fick's law for diffusion in spherical geometries (Equation 6):

$$MR = \frac{X(t) - X_e}{X_o - X_e} = \frac{6}{\pi^2}\sum_{n=0}^{\infty}\frac{1}{n^2}\exp\left[\frac{-n^2\pi^2 \cdot D \cdot t}{R^2}\right] \tag{6}$$

©2026, Universidad Politécnica Salesiana, Ecuador.

And for long drying times, Equation 6 can be simplified and expressed (Crank, 1975; Di Matteo et al., 2000; Doymaz, 2004; Rizvi, 1986) as shown in Equation 7:

$$MR = \frac{X(t) - X_e}{X_o - X_e} = \frac{6}{\pi^2} \exp\left(\frac{-\pi^2 \cdot D_{\text{eff}} \cdot t}{R^2}\right) \quad (7)$$

Taking the logarithm of both sides Ecuation 8:

$$\text{Ln}(MR) = \text{Ln}\left(\frac{6}{\pi^2}\right) - \left(\frac{\pi^2 D_{\text{eff}} .t}{R^2}\right) \quad (8)$$

Where R (m) is the average radius of the grape and D_{eff} is the effective moisture diffusivity (m^2/s), which is determined from the slope of the graph of $\ln(\text{MR})$ versus drying time (t).

2.6 Response Surface Methodology

This methodology comprises a set of mathematical techniques used to optimize the drying process, where the response variables were drying time and overall product acceptance, which were influenced by the quantitative factors: temperature (°C): x_1, concentration (%): x_2, and immersion time (s): x_3.

According to the proposed experimental design, the response surface methodology technique approximates a second-order polynomial mathematical relationship, as shown in Equation 9:

$$y = \beta_o + \sum_{i=1}^{k} \beta_i x_i + \sum_{i=1}^{k} \beta_{ii} x_i^2 \sum_{i<1} \sum \beta_{ij} x_i x_j + \varepsilon \quad (9)$$

2.7 Mathematical Simulation of the Drying Curve

Six mathematical models (Table 2) were used to simulate the drying curve under optimal conditions, namely: Henderson-Pabis, modified Henderson-Pabis, Page, modified Page, Newton, and Midilli et al. (2002) (Bombana et al., 2023; Kusuma et al., 2023; Subbian et al., 2021).

Table 2. Mathematical models for simulating the drying curve.

Model	Equation	
Henderson-Pabis	$MR = a \,.\, \exp(-k.t)$	(10)
Modified Henderson-Pabis	$MR = a \,.\, \exp(-k.t) + b \,.\, \exp(-g.t) + c \,.\, \exp(-h.t)$	(11)
Page	$MR = \exp(-k.t^n)$	(12)
Modified Page	$MR = [\exp(-k.t)]^n$	(13)
Newton	$MR = a \, \exp(-k.t)$	(14)
Midilli *et al.*	$MR = a \,.\, \exp(-k.t^n) + b.t$	(15)

2.8 Statistical Analysis

The Statistica v. 7.0 software was used to analyze the effects of the independent variables on drying time and overall product acceptance. The coefficient of determination R^2 was also determined, indicating the degree of fit of the quadratic polynomial to the response surface. The fit of the constants of the proposed nonlinear mathematical models to simulate the drying curve was determined using the SOLVER software package (Microsoft Corporation MS-Excel®), which employs the generalized reduced gradient method with a convergence level of 10^{-5}.

For the proposed models, the quality of fit of the equation to the experimental data was evaluated by calculating the coefficient of determination (R^2), the sum of squared errors (SSE), the root mean square error (RMSE), the mean relative percentage error (EMR), and the reduced chi-square (χ^2) (Equations 16, 17, 18, 19, and 20, respectively).

$$R^2 = 1 - \frac{\sum_{i=1}^{N} (MR_{\text{exp}_i} - MR_{\text{mod}_i})^2}{\sum_{i=1}^{N} \left(\overline{MR}_{\text{exp}_i} - MR_{\text{mod}_i}\right)^2} \quad (16)$$

$$SSE = \frac{1}{N} \sum_{i=1}^{N} (MR_{\text{exp}_i} - MR_{\text{mod}_i})^2 \quad (17)$$

$$RMSE = \left[\frac{1}{N} \sum_{i=1}^{N} (MR_{\text{exp}_i} - MR_{\text{mod}_i})^2\right]^{1/2} \quad (18)$$

©2026, Universidad Politécnica Salesiana, Ecuador.

$$EMR(\%) = \frac{100}{n}\sum_{i=1}^{n}\frac{\left|MR_{\exp_i} - MR_{\mathrm{mod}_i}\right|}{MR_{\exp_i}} \quad (19)$$

$$\chi^2 = \frac{1}{N-n}\sum_{i=1}^{N}(MR_{\exp_i} - MR_{\mathrm{mod}_i})^2 \quad (20)$$

3 Results and Discussion

3.1 Physicochemical Characterization

The results of the grapes' physicochemical properties are shown in Table 3, presenting the mean values and corresponding standard deviation. The pH value ranges from 4.00 to 3.26, classifying it as a sweet-and-sour product. Meanwhile, the water content ranges from 79.24 % to 80.76 %, falling within the typical range found in all grape varieties, which ranges from 70 % to 80 % (Srivastava et al., 2021), and the water activity value fluctuated between 0.9627 and 0.9671.

Meanwhile, the concentration of soluble solids in the form of sucrose found in the berry ranged from 17.21 to 23.35 Brix degrees, a characteristic value of this type of berry product in its ripe state. Similar values of 22.4, 22, and 21.4 °Brix and 3.63, 3.20, and 3.44 for pH have been reported for Muscat of Alexandria grape varieties of fruits considered ripe and suitable for making grapes or wine (Corona et al., 2020; Harutyunyan et al., 2022; Pedrosa-López et al., 2022).

Table 3. Physicochemical variables of the Muscat of Alexandria grape variety (*Vitis vinifera*)

Physicochemical variable	Mean ± standard deviation
Hydrogen ion concentration (pH)	3.63 ± 0.37
Brix degrees (°Bx)	20.28 ± 0.36
Refractive index (–)	1.364 ± 0.005
Water content (%)	80.00 ± 0.76
Water activity (a_w)	0.9649 ± 0.0022

3.2 Influence of independent variables on drying time under direct and indirect sunlight

Figure 2 (a and b) shows the Pareto chart for analyzing the effect of the independent variables: T (°C), C (%), and t (s), combined on the response variable of drying time, using sun drying and the indirect solar dryer to produce Muscat of Alexandria grapes (Table 4). A strong influence of solution temperature (°C), immersion time (s), and concentration (%) is observed. The linear interaction of concentration with immersion time is not influential in either process; concentration is not influential for sun drying. However, in indirect solar drying, the interactions between temperature-concentration and temperature-immersion time were included in the regression model. Although they did not show a significant influence on the response variable, their inclusion allows for greater precision in surface area modeling.

3.3 Influence of independent variables on the overall acceptance of fruit berries: sun-drying and indirect solar drying

Table 4 presents the global acceptance values. Furthermore, the estimated effects of the independent variables on the global acceptance of the Muscat of Alexandria grape variety are presented in Figures 2 (a, b) and 3 (a, b).

It is observed that the three variables—temperature, concentration, and immersion time—in their linear and quadratic forms have effects on the dependent variables of drying time and overall acceptance, except concentration in its quadratic function (Q) in sun-drying; likewise, the linear interaction of temperature and concentration (1L × 2L) and temperature and immersion time (1L × 3L) in the evaluation of drying time and overall acceptance is considered less important in indirect solar drying. However, to ensure that the

©2026, Universidad Politécnica Salesiana, Ecuador.

mathematical model did not lose accuracy in the coefficient of determination (R^2), all interactions were considered to obtain the regression coefficients of the response surface.

Table 4. Central rotational composite design with coded and actual values and response variables.

Treatment	Coded variables			Actual variables			Sun-drying		Indirect solar drying	
	x_1	x_2	x_3	T (°C)	C (%)	t (s)	Drying time (h)	Overall acceptance	Drying time (h)	Overall acceptance
1	-1	-1	-1	63	1	7.7	112	6	110	3
2	1	-1	-1	87	1	7.7	90	7	64	6
3	-1	1	-1	63	2.5	7.7	122,5	6.5	72	8
4	1	1	-1	87	2.5	7.7	63	7	60	9
5	-1	-1	1	63	1	24.3	66.5	7	64	3
6	1	-1	1	87	1	24.3	72	8	51	6
7	-1	1	1	63	2.5	24.3	149	6	92	5
8	1	1	1	87	2.5	24.3	82.5	7	60	8
9	-1.68	0	0	55	1.75	16	142.5	6	112	6
10	1.68	0	0	95	1.75	16	79.5	7	45	7
11	0	-1.68	0	75	0.5	16	84.5	8	80	4
12	0	1.68	0	75	3	16	81.5	6	75	7
13	0	0	-1.68	75	1.75	2	171	6.5	107	4
14	0	0	1.68	75	1.75	30	82.5	9	60	8
15	0	0	0	75	1.75	16	77.5	8.5	68	9
16	0	0	0	75	1.75	16	73	8	65	8
17	0	0	0	75	1.75	16	75	8.5	58	9
18	0	0	0	75	1.75	16	79.5	8	64	9
19	0	0	0	75	1.75	16	74	8.5	68	8
20	0	0	0	75	1.75	16	76	8	63	8

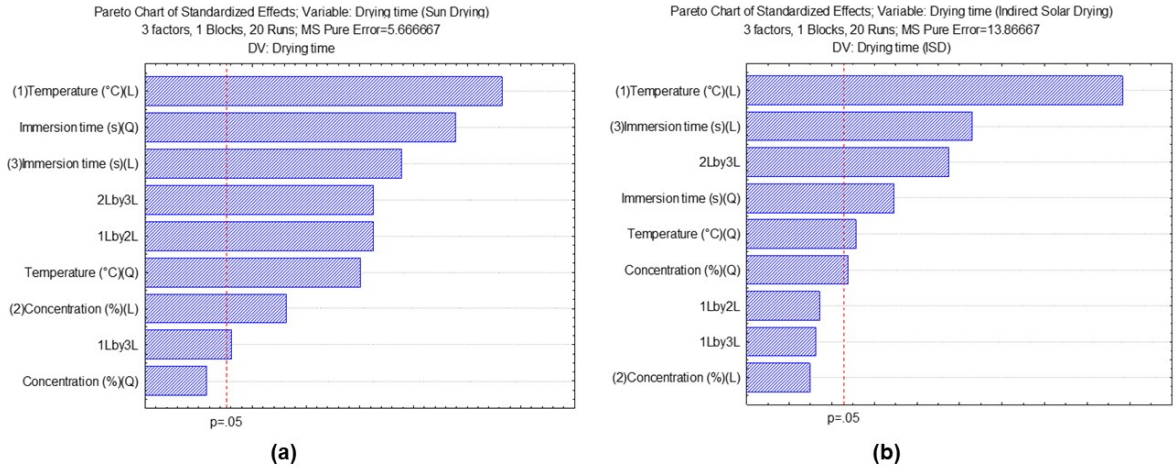


Figure 2. Effect of independent variables on the drying time of the Muscat of Alexandria grape variety (a) sun drying (b) indirect sun drying.

©2026, Universidad Politécnica Salesiana, Ecuador.

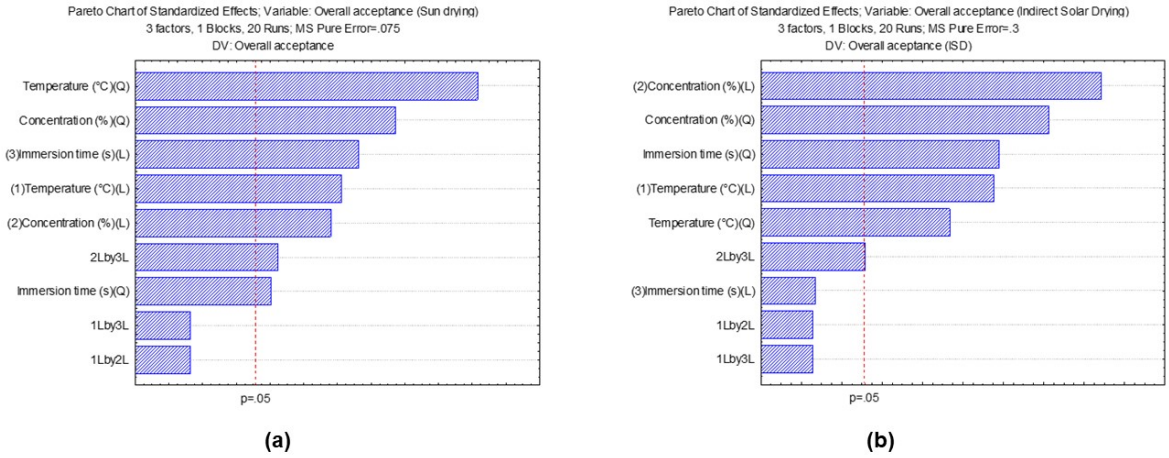


Figure 3. Effect of independent variables on the overall acceptance of the Muscat of Alexandria fruit berry (a) sun-dried (b) indirectly sun-dried.

3.4 Analysis of variance in the estimation of drying time and overall product acceptance for sun-drying and indirect solar drying

Upon analyzing the significance of the constants in the regression equations (Table 5), it was observed that the calculated F-value (F_c) exceeded the critical value from the F-table $F_{0.95;9;10} = 3.02$ for a 95 % confidence level. Since in all cases $F_c > F_t$, both for the prediction of drying time and for the overall acceptance of the berry, it is concluded that the regression models are statistically significant. The regression constants for estimating drying time and overall acceptance of the berries are presented in Tables 6 and 7, respectively, for both sun drying and indirect drying.

3.5 Response surface in the estimation of drying time and overall product acceptance in sun-drying

During the drying process, the waxy layer on the grape skin hinders the removal of water *in situ* and extends the drying time. For this reason, chemical pretreatments have been proposed that cause the dissolution of this layer, along with the formation of microcracks on its surface, thereby controlling the rate of water loss and reducing the time required to achieve the correct level of dehydration (Corona et al., 2020; Patidar et al., 2021).

Figure 4 shows the response surface of drying time (h) (a) and contour (b) versus Temperature (°C) and immersion time. For immersion times in the range of 16 to 20 seconds and solution temperatures in the range of 80 to 90 °C and solution concentrations ranging from 1 % to 1.5 %, drying times of less than 80 hours were achieved, equivalent to less than 11 days of direct sun drying, thereby reducing the processing time compared to the results reported by Corona et al. (2020), who applied a chemical pretreatment to Muscat of Alexandria grapes by immersing them in a sodium hydroxide solution (45 g/L) for 185 seconds at a temperature of 25 °C, resulting in a drying time of 13 days under these conditions. This is due to the phenomenon of dehydration, which is explained by mass transfer, influenced by water and sugar content, as well as by the homogeneity of the berries to be dried in terms of size, weight, and density.

The drying rate of berries is directly proportional to the dehydration temperature: at higher temperatures, the mass transfer rate increases and the processing time decreases. For example, in the 'Zicui' cultivar, the most efficient dehydration occurred at 50 °C; in contrast, the time required to complete the process extended to 11 days at 40 °C and up to 20 days when processed at 30 °C (Chen et al., 2022).

©2026, Universidad Politécnica Salesiana, Ecuador.

Figure 5 shows the response surface (a) and contour (b) of Overall Acceptance versus Temperature (°C) and solution concentration (%), while keeping the immersion time constant at 16 seconds.

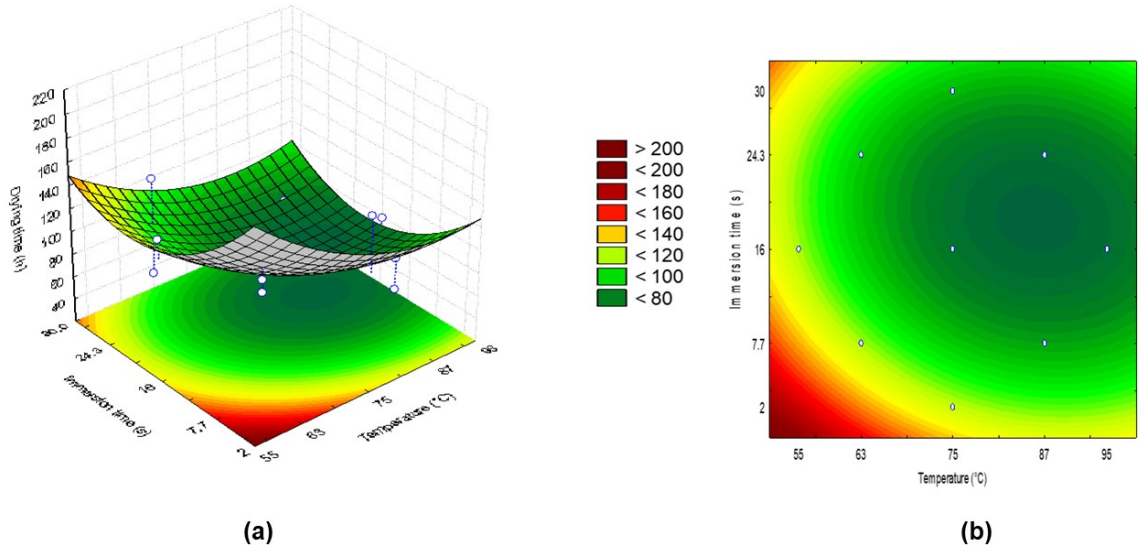


Figure 4. Response surface of drying time (h) (a) and contour (b) for the Muscat of Alexandria grape variety versus temperature (°C)and immersion time (s).

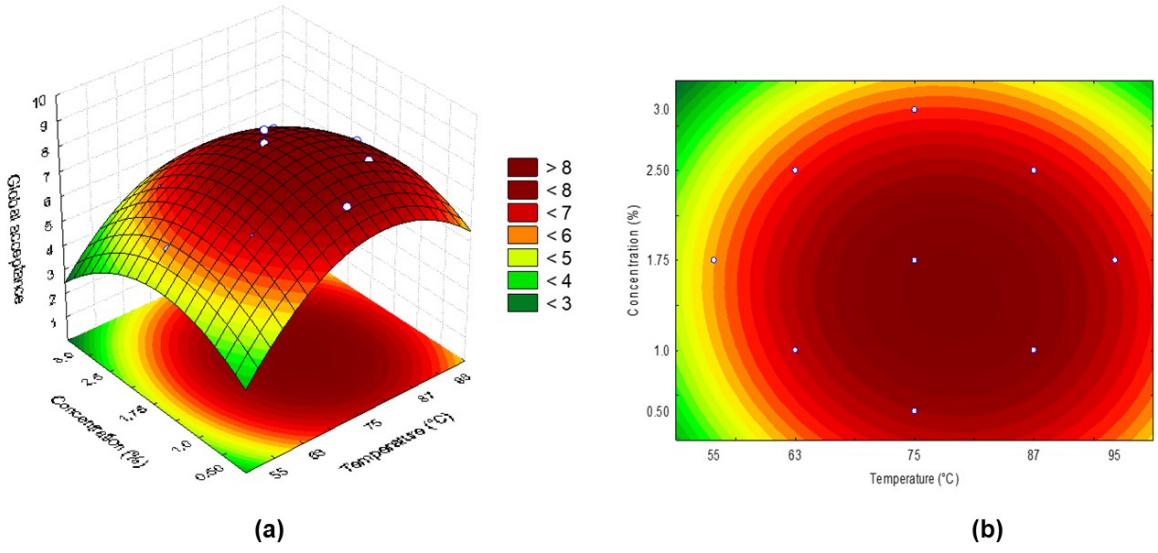


Figure 5. Response surface (a) and contour (b) of the overall acceptance of Alexandria Muscat berries versus Temperature (°C)and solution concentration (%).

©2026, Universidad Politécnica Salesiana, Ecuador.

Table 5. Analysis of variance for drying time and overall acceptance of the Muscat of Alexandria grape variety in sun-drying and indirect sun-drying.

		Drying time					Overall acceptance				
Process		SS	DF	MS	F_c	F_t	SS	DF	MS	F_c	F_t
Sun-dried	Regression	14 250.11	9	1 583.34	5.10	3.02	15.99	9	1.776	8.27	3.20
	Residual error	3 105.59	10	310.56			2.15	10	0.215		
	Misalignment	3 077.26	5	615.45	108.62		1.77	5	0.335	4.73	
	Pure error	28.33	5	5.67			0.38	5	0.075		
Indirect solar drying	Regression	5 755.14	9	639.46	5.62	3.02	62.06	9	6.896	4.40	3.02
	Residual error	1 138.66	10	113.87			15.69	10	1.569		
	Adjustment error	1 069.32	5	213.87	15.42		14.19	5	2.838	9.46	
	Pure error	69.33	5	13.87			1.50	5	0.30		

Note: SS: sum of squares; DF: degrees of freedom; SM: standard mean; F_c and F_t: calculated and table F-values, respectively.

Table 6. Estimated effects and regression coefficients of the independent variables on the response variable of sun-drying time and overall acceptance of the Muscat of Alexandria raisin

	Drying time (h) ($R^2 = 0.82062$)				**Overall acceptance** ($R^2 = 0.88033$)			
Coded parameter	Estimated effect	P- value	Regression coefficient	P-value	Estimated effect	P-value	Regression coefficient	P-value
k_0	76.3072	0.000000	76.3072	0.000000	8.256595	0.000000	8.256595	0.000000
x_1	-36.4007	0.000001	-18.2003	0.000001	0.75926	0.003705	0.379632	0.003705
x_2	18.9122	0.000023	9.4561	0.000023	-1.32369	0.000260	-0.661845	0.000260
x_3	10.4743	0.000458	5.2372	0.000458	-0.71236	0.004866	-0.356180	0.004866
x_1^2	-0.9291	0.492746	-0.4646	0.492746	-0.96938	0.001115	-0.484690	0.001115
x_2^2	-24.3580	0.000008	-12.1790	0.000008	0.83548	0.002441	0.417742	0.002441
x_3^2	30.0729	0.000002	15.0346	0.000002	-0.43729	0.029070	-0.218959	0.029070
$x_1 \cdot x_2$	-27.3750	0.000016	-13.6875	0.000016	-0.12500	0.547054	-0.0625000	0.547054
$x_1 \cdot x_3$	5.1250	0.028597	2.5625	0.028597	0.12500	0.547054	0.0625000	0.547054
$x_2 \cdot x_3$	27.3750	0.000016	13.6875	0.000016	-0.62500	0.023271	-0.3125000	0.023271

Note: $x_1 = \dfrac{T - 75}{12}$; $x_2 = \dfrac{C - 1.75}{0.75}$ and $x_3 = \dfrac{t - 16}{8.30}$, where: T: temperature, C: concentration and t: immersion time.

©2026, Universidad Politécnica Salesiana, Ecuador.

Table 7. Estimated effects and regression coefficients of the independent variables on the response variables of indirect solar drying time and overall acceptance of Muscat of Alexandria raisins

	Drying time (h) ($R^2 = 0.82062$)				**Overall acceptance** ($R^2 = 0.88033$)			
Coded parameter	Estimated effect	P- value	Regression coefficient	P-value	Estimated effect	P-value	Regression coefficient	P-value
k_0	64.6401	0.000000	64.6401	0.000000	8.49475	0.000000	8.49475	0.000000
x_1	-31.5959	0.000019	-15.7980	0.000019	1.71201	0.002192	0.85600	0.002192
x_2	6.1494	0.025972	3.0747	0.025972	-1.35061	0.005468	-0.67530	0.005468
x_3	-1.9641	0.374713	-0.9821	0.374713	2.49765	0.000387	1.24883	0.000387
x_1^2	5.4407	0.039418	2.7204	0.039418	-2.05923	0.000845	-1.02961	0.000845
x_2^2	-17.2901	0.000355	-8.6451	0.000355	0.39869	0.236591	0.19934	0.236591
x_3^2	9.6924	0.004350	4.8462	0.004350	-1.70492	0.001992	-0.85246	0.001992
$x_1 \cdot x_2$	3.7500	0.213701	1.8750	0.213701	-0.50000	0.253170	-0.25000	0.253170
$x_1 \cdot x_3$	3.2500	0.271944	1.6250	0.271944	0.50000	0.253170	0.25000	0.253170
$x_2 \cdot x_3$	19.7500	0.000666	9.8750	0.000666	-1.00000	0.049313	-0.50000	0.049313

Note: $x_1 = \dfrac{T - 75}{12}$; $x_2 = \dfrac{C - 1.75}{0.75}$ and $x_3 = \dfrac{t - 16}{8.30}$, where: T: temperature, C: concentration and t: immersion time.

As the values of the independent variables increase, they generate a curve with a maximum inflection point for Overall Acceptance (> 8) of the berries at 20 % moisture content on a wet basis. It is observed that the highest values of Overall Acceptance occur in the temperature range of 80–85 °C for the NaOH solution at concentrations between 1 % and 1.5 %. It is recommended to use low concentrations of the solution so that it can be easily removed with plenty of cold water after the chemical-thermal treatment.

According to Patidar et al. (2021), many desirable changes in the physical, chemical, and biochemical properties occur during dehydration due to the pretreatment and drying conditions. Thus, the carbohydrates and organic compounds from the fresh grapes are retained in a concentrated form in the grapes, improving their acceptability to consumers. Furthermore, NaOH not only improves drying characteristics but also enhances the color attributes of the grapes (Vázquez et al., 2000).

In addition to producing high-quality raisins, unfortunately there are some environmental and health concerns related to the use of chemicals for the pretreatment of grapes. On the environmental aspect, wastewater containing organic, saline, and highly corrosive solids is generated; and in terms of food safety, these chemicals remain in the dried product, which can cause food safety issues (Adiletta et al., 2016; Deng et al., 2019; Wang et al., 2017). The low concentration of NaOH (1–1.5 %) used in this study accelerates the drying process while reducing the likelihood of producing raisins with a negative environmental impact and unsafe food, as these two factors intensify at higher NaOH concentrations.

Based on the analysis, Table 8 presents the independent variables or processing parameters for direct sun drying to minimize and maximize drying time and overall product acceptance, respectively.

Table 8. Direct sun-drying processing parameters for the Muscat of Alexandria grape variety

Independent variable	**Process parameters**	**Drying time (h)**	**Overall acceptance (–)**
Temperature (°C)	80–85	Approximately ≤ 80 h	Approximately > 8
Concentration (%)	1–1.5		
Immersion time (s)	16–20		

©2026, Universidad Politécnica Salesiana, Ecuador.

3.6 Response surface for estimating drying time and overall product acceptance in indirect solar drying

Figure 6 shows the response surface (a) and contour surface (b) of the drying time of Muscat of Alexandria grapes versus temperature (°C) and immersion time (s). It is stated that, for immersion times of 16 to 20 seconds, a solution temperature of 80 to 90 °C, and a solution concentration of 1 % to 2 %, using the indirect solar dryer, drying times of less than 60 hours are achieved, equivalent to less than 6 to 7 days of drying.

The shortest drying time was obtained with indirect solar drying compared to sun drying; this is because the former uses a solar collector consisting of a transparent glass surface and a black absorber, where solar energy is collected to heat the fresh air entering the drying chamber, where the grapes are heated by indirect heat absorption. Furthermore, due to the pressure difference generated by the chimney, natural air circulation is achieved, which accelerates the evaporation of moisture present in the grapes (EL-Mesery et al., 2022).

Another factor to consider is that indirect solar drying was performed with an average solar radiation of 300 W/m^2. Leon Dharmadurai et al. (2022), using reflectors, achieved a maximum solar radiation of 1079.8 W/m^2 and a drying time of 5 days for seedless green grapes and concluded that the reduction in drying time is positively influenced by the indirect solar drying method and the natural convection of hot air within the drying chamber.

Figure 7 shows the response surface (a) and contour plot (b) of the overall acceptability score of Alexandria Muscat grapes versus temperature (°C) and immersion time (s). Global acceptability values for the product greater than 8 are achieved provided that the solution concentration is maintained at 1 % and temperatures between 75–90 °C and immersion times of 16–25 seconds are used.

The curves show an inflection point, with maximum acceptance levels for the grapes occurring at concentrations of 1 % and 1.5 %, respectively, and the highest acceptance levels corresponding to approximately 16 seconds. The parameters of the indirect solar drying process are presented in Table 9.

Unlike sun drying, the indirect solar drying process reduces drying time by 20 hours, yielding grapes with a high overall acceptance rate. Likewise, the optimal conditions are found near the central points of the experimental design, where the overall acceptance values were the highest. Therefore, for analyzing the drying curve and kinetics, the experimental data obtained were: $T = 80$ °C, $C = 1.5\,\%$, and $t = 16$ s.

Figures 8 (a and b) present the simulations, using the regression equations for the drying time of grapes in the sun (Table 6) and the overall acceptance of the product in the indirect solar drying process (Table 7), showing the curves of the minimum and maximum values, respectively.

3.7 Drying curve and kinetics

3.7.1 Drying curve

Figure 9 shows the behavior of the evolution of dry-matter moisture content as a function of drying time, both for the sun-drying of the Moscatel of Alejandría grape variety and for the use of the indirect solar dryer. In the direct sun-drying curve, the moisture content of the grapes decreases gradually until reaching a final moisture content of 20 % on a wet basis, which corresponds to approximately 0.25 kg/kg on a dry basis, with an average drying time of 75 hours. Meanwhile, the grapes dried in the indirect solar dryer exhibited two drying phases: a pronounced initial phase after 24 hours of drying, followed by a gradual decline to the indicated final moisture content, with an average drying time of 50 hours.

©2026, Universidad Politécnica Salesiana, Ecuador.

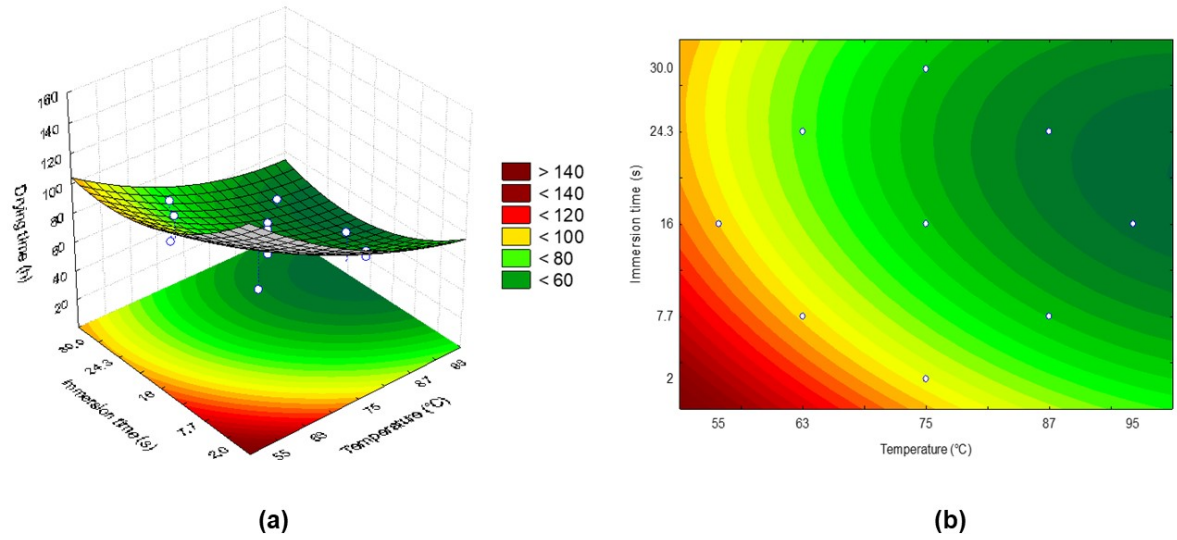


Figure 6. Response surface of drying time (h) (a) and contour (b) versus Temperature (°C) and immersion time (s) using an indirect solar dryer for drying the Muscat of Alexandria grape variety.

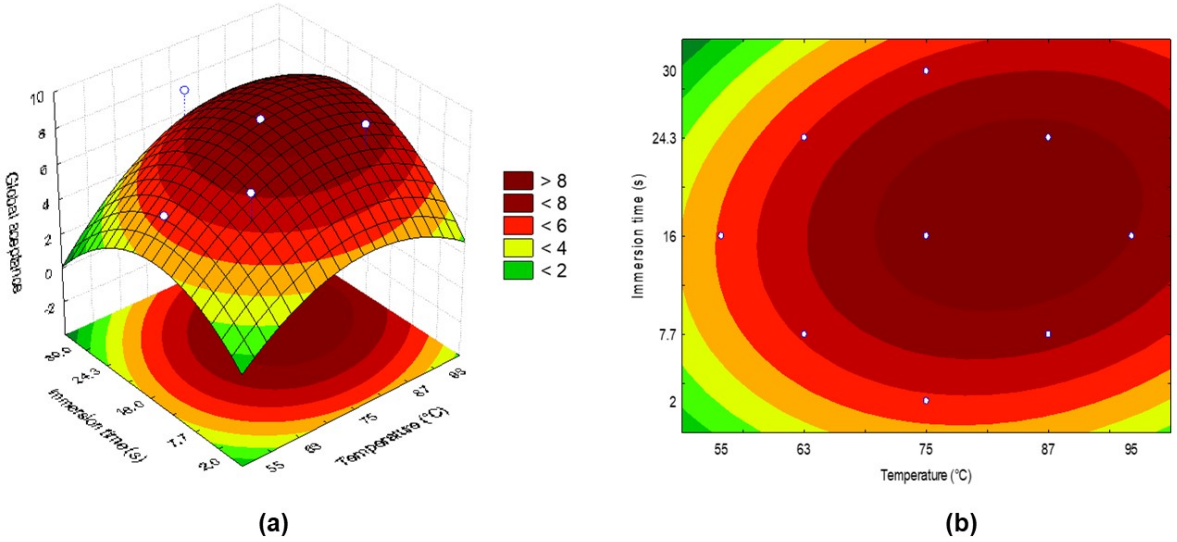


Figure 7. Response surface of global acceptance (a) and contour (b) for the Muscat of Alexandria grape variety versus temperature (°C) and immersion time (s) for drying using an indirect solar dryer.

Table 9. Processing parameters for indirect solar drying of the Muscat of Alexandria grape variety

Independent variable	Process parameters	Drying time (h)	Overall acceptance (–)
Temperature (°C)	80–85	Approximately ≤ 60 h	Approximately > 8
Concentration (%)	1–2.5		
Immersion time (s)	16–20		

©2026, Universidad Politécnica Salesiana, Ecuador.

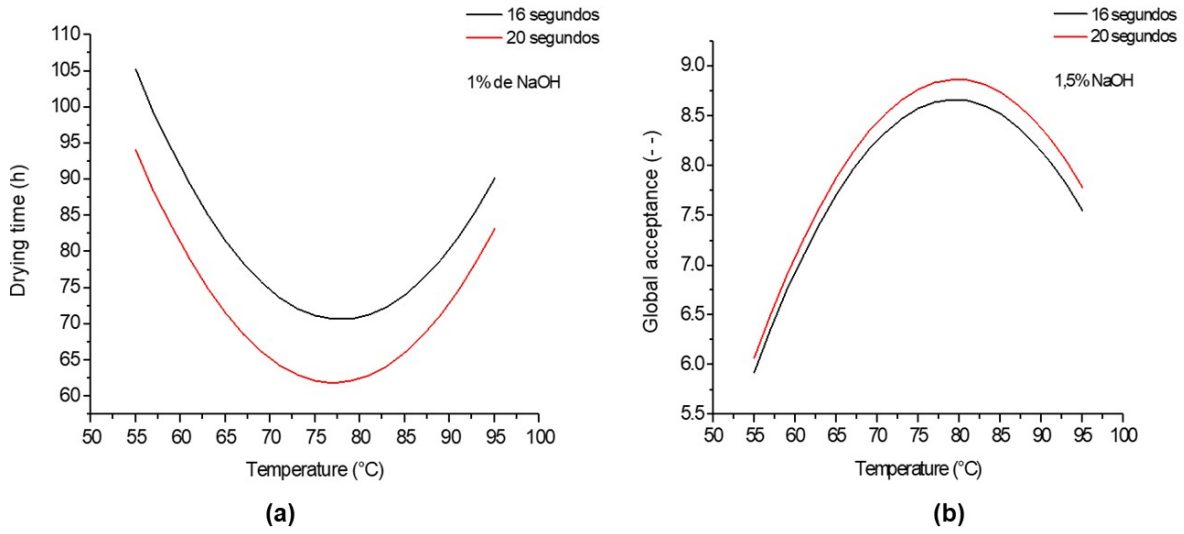


Figure 8. (a) Simulation of grape drying time versus temperature during sun drying (b) Simulation of overall raisin acceptance versus temperature during indirect solar drying

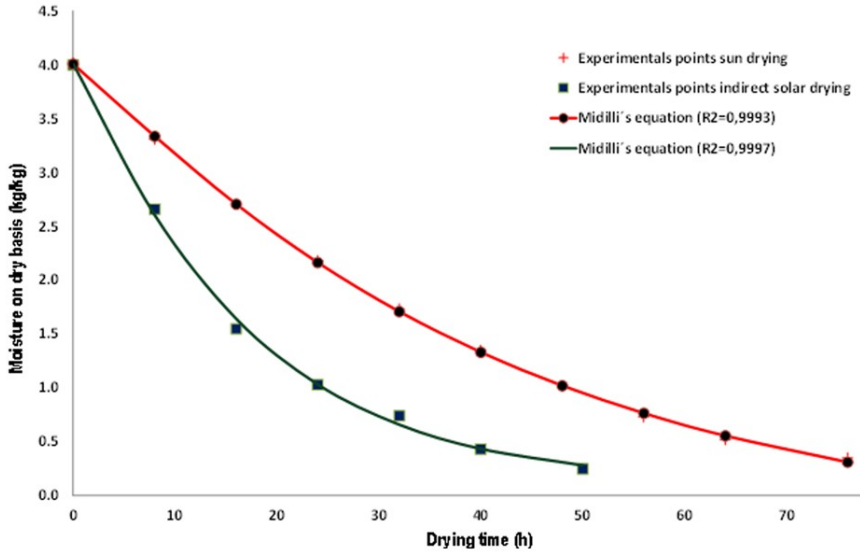


Figure 9. Evolution of moisture content versus drying time and mathematical modeling of the drying curve for the Muscat of Alexandria grape variety

Generally, the drying process consists of three consecutive phases: the initial phase, where the drying rate increases due to the temperature rise of the product and the consequent increase in vapor pressure; a second phase, where the drying rate is constant; and a final phase, characterized by a significantly reduced drying rate (Barbosa de Lima et al., 2016). These phases were observed in the drying of Muscat of Alexandria grapes pretreated with a NaOH solution (80 g/L) at a temperature of 25 °C for an immersion time of 360 seconds, where convective drying was carried out at a temperature of 30 °C for 13 days (Corona et al., 2016).

The first phase of the curve, corresponding to indirect solar drying, is due to microstructural chan-

©2026, Universidad Politécnica Salesiana, Ecuador.

ges in the epicuticular wax layer covering the grape cuticle, caused by pretreatment with NaOH; among these changes, the formation of cracks in the skin and the general softening of the tissue stand out, improving skin permeability and moisture diffusion (Lara et al., 2014). In phase two, the cracks gradually close as the grape shrinks and sugar from the pulp migrates toward the skin, where it acts as a barrier to water diffusion; this retarding effect can be overcome by increasing the drying temperature above 40 °C (Azzouz et al., 2002; Giordano et al., 2009; Toğrul, 2010). Meanwhile, the curve shown for sun drying exhibits almost a linear behavior, influenced only by the type of process. Thus, the solar dryer and the chemical-thermal treatment used in the research project reduced traditional drying time by 33 %, whereas Serratosa et al. (2008) achieved a 25 % reduction during chamber drying at 50 °C of Pedro Ximénez grapes pretreated in an alkaline medium.

The same figure shows the fit of the experimental data for moisture content versus drying time, using the equation by Midilli et al. (2002) to model the drying curve. For model selection, the following values were considered: the coefficient of determination (R^2), and error metrics including the sum of squared errors (SSE)—which served as the cell for the Solver—the root mean square error (RMSE), the mean relative percentage error (ERM), and the reduced chi-square value (χ^2) (Mehta, 2023).

It can be stated that the model by Midilli et al. (2002) best simulates the distribution of the experimental data for the drying curve of the Muscat of Alexandria grape variety, as it presented the highest values of the coefficient of determination and the lowest values of the calculated relative errors. The results are presented in Tables 10 and 11. Martín-Gómez et al. (2019) modeled the drying of whole Tempranillo grapes in a chamber at 50 °C with a relative humidity of 20 %. To do so, they evaluated the Newton, Henderson-Pabis, logarithmic, Wang and Singh, diffusion approximation, and Midilli et al. (2002) models, with the latter being selected based on the values of R^2, SSE, RMSE, EMR (%), and χ^2.

The mathematical model proposed by Midilli et al. (2002) is a suitable model for representing the drying behavior of grapes and tomatoes (Doymaz, 2004; Midilli et al., 2002; Yaldiz et al., 2001).

3.7.2 Drying kinetics

When plotting the drying rate of the Muscat of Alexandria grape variety against the average absolute humidity and drying time, as shown in Figure 10 (a and b), respectively, it is observed that the highest values of the drying kinetics correspond to the first 10 hours of drying at 0.18 and 0.08 $\mathrm{kg/(kg{\cdot}h)}$, which correspond to dR/dt slopes of 0.250 and 0.253 for sun drying and indirect solar drying, respectively. Only the period of decreasing drying rate with a linear fit is observed in both processes.

3.7.3 Value of the effective water diffusivity

Using Equation 8, the slopes of $\ln(\mathrm{MR})$ versus time were determined to calculate the effective water diffusivity ($\mathrm{m^2/s}$). For the diffusivity calculation, the average grape radius of 0.009693 m was used. The values of the effective water diffusivity for the Alexandria Muscat grape were 8.57×10^{-11} and 1.90×10^{-10} $\mathrm{m^2/s}$ for sun-drying and indirect solar drying, respectively. The calculated values of effective water diffusivity fall within the desired range for food material drying, 10^{-12} and 10^{-8} $\mathrm{m^2/s}$ (Zhao et al., 2019). It was observed that the water diffusivity of the grapes was 2.2 times higher in the indirect solar dryer than in direct sun drying.

In general, pretreated grapes exhibit higher water diffusivity; in the case of whole, punctured grapes dried at 50 °C, an effective diffusivity value of 7.31×10^{-11} $\mathrm{m^2/s}$, and in whole, untreated grapes dried at the same temperature, their diffusivity reached 3.22×10^{-11} $\mathrm{m^2/s}$ (Martín-Gómez et al., 2019).

However, the calculated coefficient of determination values were 0.6933 and 0.7647 for the diffusive model of sun-drying and indirect solar drying, as shown in Fig. 11 a and b, indicating a poor fit to the experimental data—a common issue in agro-industrial products due to shrinkage and transient moisture gradients that occur within the product during drying (Doymaz, 2007).

©2026, Universidad Politécnica Salesiana, Ecuador.

Table 10. Fitting parameters of the mathematical models for the drying curve of the Muscat of Alexandria.

Models	**Parameters**		R^2	**SSE**	**RMSE**	**EMR (%)**	χ^2
Henderson y Pabis	a	1.0291	0.99366	0.0091	0.0952	4.168	0.0113
	k	0.0290					
Henderson-Pabis Modificado	a	0.3716	0.99367	0.0091	0.0952	4.803	0.0226
	k	0.0290					
	b	0.2859					
	g	0.0290					
	c	0.3716					
	h	0.0290					
Page	k	0.0154	0.99890	0.0016	0.0398	1.212	0.00198
	n	1.1671					
Page Modificado	k	0.0218	0.99190	0.0112	0.1060	6.503	0.01404
	n	1.2897					
Newton	k	0.0281	0.99190	0.0112	0.1060	7.219	0.01248
	a	0.9972					
Midilli *et al.*	k	0.0182	0.99928	0.0006	0.0242	0.096	0.00098
	n	1.0938					
	b	-0.00068					

Table 11. Fitting parameters of the mathematical models for the drying curve of the Muscat of Alexandria grape variety using an indirect solar dryer.

Models	**Parameters**		R^2	**SSE**	**RMSE**	**EMR (%)**	χ^2
Henderson and Pabis	a	1.0060	0.99797	0.0032	0.0567	0.048	0.00451
	k	0.0564					
Modified Henderson-Pabis	a	0.0765	0.99796	0.0032	0.0568	0.352	0.02259
	k	0.0646					
	b	0.8537					
	g	0.0552					
	c	0.0765					
	h	0.0646					
Page	k	0.0519	0.99806	0.0031	0.0556	1.193	0.00433
	n	1.0256					
Modified Page	k	0.2369	0.99792	0.0033	0.0576	0.265	0.00464
	n	0.2369					
Newton	k	0.0561	0.99792	0.0033	0.0576	0.455	0.00387
	a	1.0023					
Midilli *et al.*	k	0.0841	0.99973	0.0028	0.0529	0.393	0.00652
	n	1.0626					
	b	0.00038					

©2026, Universidad Politécnica Salesiana, Ecuador.

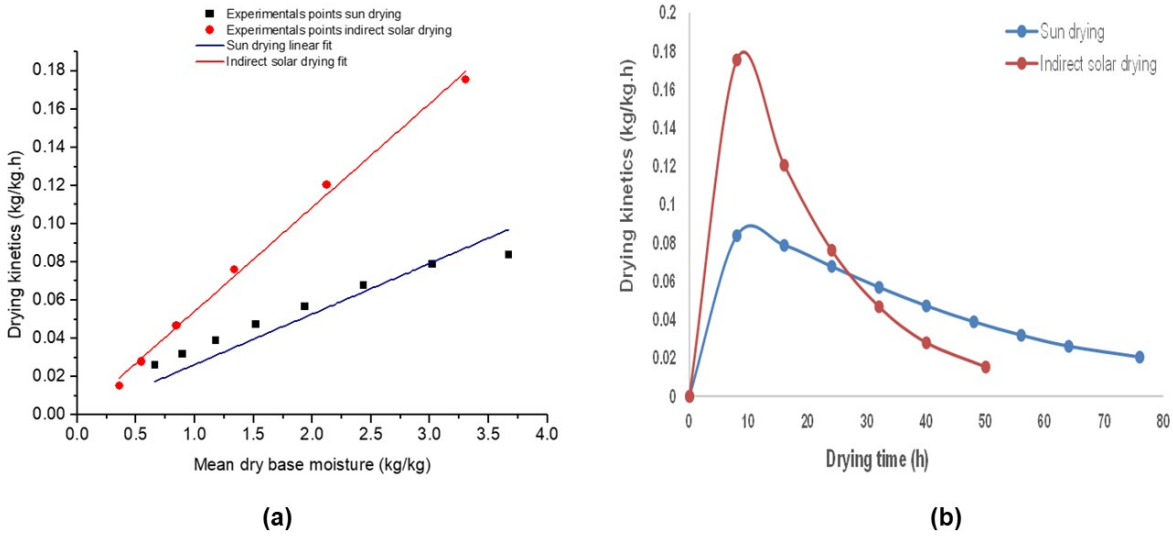


Figure 10. (a) Drying rate versus average moisture content in sun drying and indirect solar drying; (b) Drying rate versus drying time in sun drying and indirect solar drying of the Muscat of Alexandria grape variety

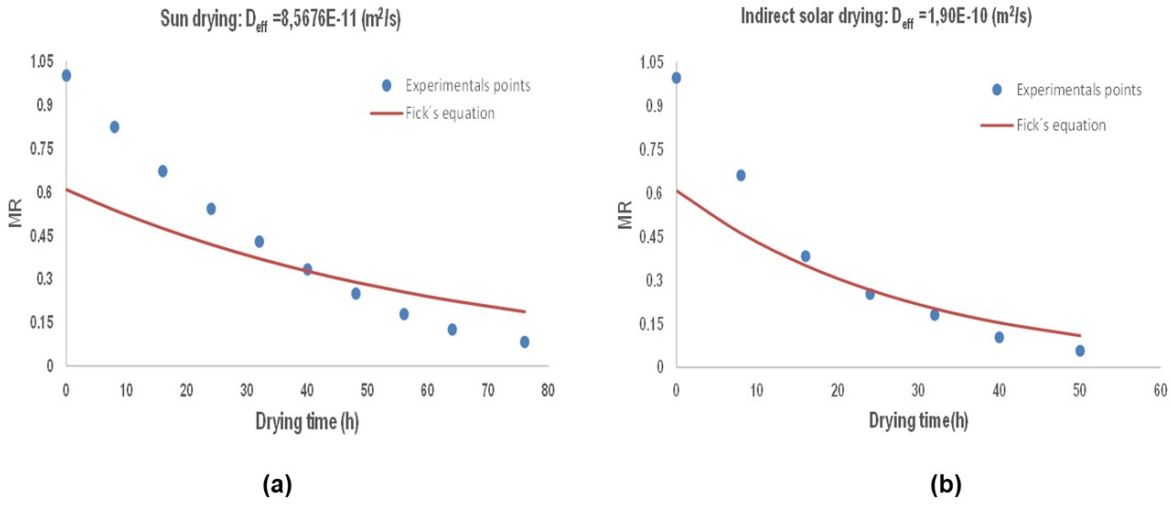


Figure 11. (a) Diffusional mathematical modeling of the sun-drying curve and (b) indirect solar drying curve for the Muscat of Alexandria grape variety

4 Conclusions

The drying of the Muscat of Alexandria grape variety (*Vitis vinifera*) was studied using two processes: sun drying and indirect solar drying using a dryer equipped with a large-surface-area solar collector. Prior to drying, an alkaline pretreatment was performed at temperatures ranging from 55–95 °C, with NaOH concentrations of 0.50–3.0 % and immersion times of 2–30 s. Sun drying and indirect solar drying were optimized, considering pretreatment conditions of 80 °C, 1.75 %, and 16 s to obtain approximate drying times of 75 h and 50 h, respectively, with a high overall product acceptance rate and a score above 8 points on the hedonic scale established for both processes.

©2026, Universidad Politécnica Salesiana, Ecuador.

Under optimal drying conditions, the mathematical model by Midilli et al. (2002) proved to be the model that best simulated the grape drying curve, as it presented the highest values for the coefficient of determination and the lowest values for the calculated relative errors. Effective water diffusivity values for the grapes were determined to be 8.57×10^{-11} and 1.90×10^{-10} m^2/s for direct sun drying and using an indirect solar dryer, respectively.

Acknowledgments

This research was conducted with the support of the Laboratory of Process Engineering and Unit Operations (LIPOU-FIPA) at the Faculty of Fisheries and Food Engineering, National University of Callao, Lima, Peru.

Declaration on the use of Artificial Intelligence

The authors DECLARE that, during the preparation of the manuscript titled "Application of a response surface Model for solar and indirect drying of muscat of alexandria grapes (*Vitis vinifera*)", no generative artificial intelligence tools or automated assistance systems were utilized for the drafting, analysis, data interpretation, content generation, translation, or editorial refinement of the text.

The authors assume full responsibility for the content, originality, integrity, and final approved version of the manuscript.

Author Contributions

D.V.P.: Conceptualization, Data curation, Formal analysis, Investigation, Methodology, Supervision. **H.R.N.:** Conceptualization, Data curation, Formal analysis, Investigation, Methodology. **R.S.J.:** Conceptualization, Data curation, Formal analysis, Investigation, Methodology. **D.C.R.:** Conceptualization, Data curation, Formal analysis, Investigation, Methodology.

References

Adiletta, G., Russo, P., Senadeera, W., and Di Matteo, M. (2016). Drying characteristics and quality of grape under physical pretreatment. *Journal of Food Engineering*, *172*, 9–18. Online: https://doi.org/10.1016/j.jfoodeng.2015.06.031

Atak, A., Göksel, Z., Tunçkal, C., and Yılmaz, Y. (2022). Comparison of important quality characteristics of some fungal disease resistance/tolerance grapes dried with energy-saving heat pump dryer. *Agronomy*, *12*(4), 909. Online: https://doi.org/10.3390/agronomy12040909

Azzouz, S., Guizani, A., Jomaa, W., and Belghith, A. (2002). Moisture diffusivity and drying kinetic equation of convective drying of grapes. *Journal of Food Engineering*, *55*(4), 323–330. Online: https://doi.org/10.1016/S0260-8774(02)00109-7

Barbosa de Lima, A. G., Delgado, J. M. P. Q., Neto, S. R. F., and Franco, C. M. R. (2016). Intermittent drying: Fundamentals, modeling and applications. En J. M. P. Q. Delgado and A. G. Barbosa de Lima (Eds.), *Drying and energy technologies* (pp. 19–41). Cham: Springer International Publishing. Online: https://doi.org/10.1007/978-3-319-19767-8_2

Bitaraf, M. S., Khodaiyan, F., Mohammadifar, M. A., and Mousavi, S. M. (2012). Application of response surface methodology to improve fermentation time and rheological properties of probiotic yogurt containing *Lactobacillus reuteri*. *Food and Bioprocess Technology*, *5*(4), 1394–1401. Online: https://doi.org/10.1007/s11947-010-0433-2

Bombana, V. B., Fischer, B., Oro, C. E. D., Rigo, D., Polina, C. C., Franco Denti, A., … others (2023). Drying kinetics of guabiju pulp (*Myrcianthes pungens*): Mass transfer parameters, mathematical modeling and evaluation of bioactive compounds. *Journal of Food Process Engineering*, *46*(1), e14205. Online: https://doi.org/10.1111/JFPE.14205

Castillo-Téllez, M., Pilatowsky-Figueroa, I., López-Vidaña, E. C., Sarracino-Martínez, O., and Hernández-Galvez, G. (2017). Dehydration of the red chilli (*Capsicum annuum L.*, costeño) using an indirect-type forced convection solar

©2026, Universidad Politécnica Salesiana, Ecuador.

dryer. *Applied Thermal Engineering*, *114*, 1137–1144. Online: https://doi.org/10.1016/J.APPLTHERMALENG.2016.08.114

Chen, K., Hu, Y., Chen, L., Zhang, J., Qiao, H., Li, W., ... others (2022). Role of dehydration temperature on flavonoids composition and free-form volatile profile of raisins during the drying process. *Food Chemistry*, *374*, 131747. Online: https://doi.org/10.1016/j.foodchem.2021.131747

Chopra, R., Rastogi, N. K., and Sambaiah, K. (2011). Enrichment of rice bran oil with α-linolenic acid by enzymatic acidolysis: Optimization of parameters by response surface methodology. *Food and Bioprocess Technology*, *4*(7), 1153–1163. Online: https://doi.org/10.1007/s11947-009-0191-1

Corona, O., Planeta, D., Bambina, P., Giacosa, S., Paissoni, M. A., Squadrito, M., ... others (2020). Influence of different dehydration levels on volatile profiles, phenolic contents and skin hardness of alkaline pre-treated grapes cv muscat of alexandria (*Vitis vinifera L.*). *Foods*, *9*(5), 666. Online: https://doi.org/10.3390/foods9050666

Corona, O., Torchio, F., Giacosa, S., Río Segade, S., Planeta, D., Gerbi, V., ... others (2016). Assessment of postharvest dehydration kinetics and skin mechanical properties of 'muscat of alexandria' grapes by response surface methodology. *Food and Bioprocess Technology*, *9*(6), 1060–1069. Online: https://doi.org/10.1007/s11947-016-1697-y

Crank, J. (1975). *The mathematics of diffusion* (2nd ed.). London, UK: Oxford University Press.

Deng, L.-Z., Mujumdar, A. S., Zhang, Q., Yang, X.-H., Wang, J., Zheng, Z.-A., ... Xiao, H.-W. (2019). Chemical and physical pretreatments of fruits and vegetables: Effects on drying characteristics and quality attributes – a comprehensive review. *Critical Reviews in Food Science and Nutrition*, *59*(9), 1408–1432. Online: https://doi.org/10.1080/10408398.2017.1409192

Di Matteo, M., Cinquanta, L., Galiero, G., and Crescitelli, S. (2000). Effect of a novel physical pretreatment process on the drying kinetics of seedless grapes. *Journal of Food Engineering*, *46*(2), 83–89. Online: https://doi.org/10.1016/S0260-8774(00)00071-6

Djebli, A., Hanini, S., Badaoui, O., Haddad, B., and Benhamou, A. (2020). Modeling and comparative analysis of solar drying behavior of potatoes. *Renewable Energy*, *145*, 1494–1506. Online: https://doi.org/10.1016/j.renene.2019.07.083

Doymaz, İ. (2004). Convective air drying characteristics of thin layer carrots. *Journal of Food Engineering*, *61*(3), 359–364. Online: https://doi.org/10.1016/S0260-8774(03)00142-0

Doymaz, İ. (2007). Air-drying characteristics of tomatoes. *Journal of Food Engineering*, *78*(4), 1291–1297. Online: https://doi.org/10.1016/j.jfoodeng.2005.12.047

EL-Mesery, H. S., EL-Seesy, A. I., Hu, Z., and Li, Y. (2022). Recent developments in solar drying technology of food and agricultural products: A review. *Renewable and Sustainable Energy Reviews*, *157*, 112070. Online: https://doi.org/10.1016/j.rser.2021.112070

FAO. (2020). *FaoStat database.* Online: http://www.fao.org/faostat/

Giordano, M., Rolle, L., Zeppa, G., and Gerbi, V. (2009). Chemical and volatile composition of three Italian sweet white Passito wines. *OENO One*, *43*(3), 159–170. Online: https://doi.org/10.20870/OENO-ONE.2009.43.3.796

Gopinath, G. R., Muthuvel, S., Muthukannan, M., Sudhakarapandian, R., Praveen Kumar, B., Santhan Kumar, C., and Thanikanti, S. B. (2022). Design, development, and performance testing of thermal energy storage based solar dryer system for seeded grapes. *Sustainable Energy Technologies and Assessments*, *51*, 101923. Online: https://doi.org/10.1016/j.seta.2021.101923

Gunasekaran, N., Manoj Kumar, P., Raja, S., Sharavanan, S., Avinas, K., Aakash Kannan, P., and Gokul, S. (2021). Investigation on ETC solar water heater using twisted tape inserts. *Materials Today: Proceedings*, *47*, 5011–5016. Online: https://doi.org/10.1016/J.MATPR.2021.04.586

Harutyunyan, M., Viana, R., Granja-Soares, J., Martins, M., Ribeiro, H., and Malfeito-Ferreira, M. (2022). Adaptation of ancient techniques to recreate 'wines' and 'beverages' using withered grapes of Muscat of Alexandria. *Fermentation*, *8*(2), 85. Online: https://doi.org/10.3390/fermentation8020085

©2026, Universidad Politécnica Salesiana, Ecuador.

Javed, H. U., Wang, D., Abdullah, Hasan, M., Zeng, L. Y., Lan, Y., ... others (2023). Interrogating raisin associated unsaturated fatty acid derived volatile compounds using HS–SPME with GC–MS. *Foods*, *12*(3), 428. Online: https://doi.org/10.3390/foods12030428

Kumar, P. M., Arunthathi, S., Jeevan Prasanth, S., Aswin, T., Anish Antony, A., Daniel, D., ... others (2021). Investigation on a desiccant based solar water recuperator for generating water from atmospheric air. *Materials Today: Proceedings*, *45*, 7881–7884. Online: https://doi.org/10.1016/J.MATPR.2020.12.506

Kusuma, H. S., Nasution, R. A., and Permatasari, D. (2023). Drying process on kaffir lime leaves using microwave: Evaluation of the drying performance and energy analysis of different microwave powers and sizes of leaves. *Applied Food Research*, 100317. Online: https://doi.org/10.1016/j.afres.2023.100317

Lara, I., Belge, B., and Goulao, L. F. (2014). The fruit cuticle as a modulator of postharvest quality. *Postharvest Biology and Technology*, *87*, 103–112. Online: https://doi.org/10.1016/j.postharvbio.2013.08.012

Leon Dharmadurai, P., Vasanthaseelan, S., Bharathwaaj, R., Dharmaraj, V., Gnanasekaran, K., Balaji, D., and Sathyamurthy, R. (2022). A comparative study on solar dryer using external reflector for drying grapes. *Materials Today: Proceedings*, *50*, 552–559. Online: https://doi.org/10.1016/j.matpr.2020.11.197

Martín-Gómez, J., Ángeles Varo, M., Mérida, J., and Serratosa, M. P. (2019). The influence of berry perforation on grape drying kinetics and total phenolic compounds. *Journal of the Science of Food and Agriculture*, *99*(9), 4260–4266. Online: https://doi.org/10.1002/jsfa.9657

Mehta, P. (2023). Drying kinetics with proposed model study for grapes drying in solar dryer—a case study. En S. Bhattacharyya and H. Chattopadhyay (Eds.), *Fluid mechanics and fluid power (vol. 1)* (pp. 13–18). Singapore: Springer Nature Singapore.

Midilli, A., Kucuk, H., and Yapar, Z. (2002). A NEW MODEL FOR SINGLE-LAYER DRYING. *Drying Technology*, *20*(7), 1503–1513. Online: https://doi.org/10.1081/DRT-120005864

Myers, R. H., Montgomery, D. C., and Anderson-Cook, C. M. (2016). *Response surface methodology: Process and product optimization using designed experiments*. John Wiley & Sons.

Naigam, A. P. V., Ridzuan, I. M. B., Tan, A. S. T., Abdullah, A., Wan Ismail, W. A. A. Z., and Janaun, J. (2021). Design, development and performance evaluation of a large-scale hybrid solar dryer. *IOP Conference Series: Materials Science and Engineering*, *1070*(1), 012016. Online: https://doi.org/10.1088/1757-899X/1070/1/012016

Patidar, A., Vishwakarma, S., and Meena, D. (2021). Traditional and recent development of pretreatment and drying process of grapes during raisin production: A review of novel pretreatment and drying methods of grapes. *Food Frontiers*, *2*(1), 46–61. Online: https://doi.org/10.1002/fft2.64

Pedrosa-López, M. d. C., Aragón-García, F., Ruíz-Rodríguez, A., Piñeiro, Z., Durán-Guerrero, E., and Palma, M. (2022). Effects from the freezing of either whole or crushed grapes on the volatile compounds contents in Muscat wines. *Foods*, *11*(12), 1782. Online: https://doi.org/10.3390/foods11121782

Pragati, S., and Preeti, B. (2012). Technological revolution in drying of fruit and vegetables. *International Journal of Science and Research (IJSR)*, *3*.

Ramos, I. N., Brandão, T. R. S., and Silva, C. L. M. (2015). Simulation of solar drying of grapes using an integrated heat and mass transfer model. *Renewable Energy*, *81*, 896–902. Online: https://doi.org/10.1016/j.renene.2015.04.011

Rizvi, S. S. H. (1986). *Engineering properties of foods*. New York, NY: Marcel Dekker.

Saravacos, G. D., and Maroulis, Z. B. (2001). *Transport properties of foods*. New York: Marcel Dekker Inc.

Serratosa, M. P., Lopez-Toledano, A., Medina, M., and Merida, J. (2008). Drying of Pedro Ximenez grapes in chamber at controlled temperature and with dipping pretreatments. changes in the color fraction. *Journal of Agricultural and Food Chemistry*, *56*(22), 10739–10746. Online: https://doi.org/10.1021/jf8021767

©2026, Universidad Politécnica Salesiana, Ecuador.

Shalaby, S. M., and Bek, M. A. (2014). Experimental investigation of a novel indirect solar dryer implementing PCM as energy storage medium. *Energy Conversion and Management*, *83*, 1–8. Online: https://doi.org/10.1016/j.enconman.2014.03.043

Singh, S. P., Jairaj, K. S., and Srikant, K. (2012). Universal drying rate constant of seedless grapes: A review. *Renewable and Sustainable Energy Reviews*, *16*(8), 6295–6302. Online: https://doi.org/10.1016/j.rser.2012.07.011

Srikiatden, J., and Roberts, J. S. (2006). Measuring moisture diffusivity of potato and carrot (core and cortex) during convective hot air and isothermal drying. *Journal of Food Engineering*, *74*(1), 143–152. Online: https://doi.org/10.1016/j.jfoodeng.2005.02.026

Srivastava, A., Anand, A., Shukla, A., Kumar, A., Buddhi, D., and Sharma, A. (2021). A comprehensive overview on solar grapes drying: Modeling, energy, environmental and economic analysis. *Sustainable Energy Technologies and Assessments*, *47*, 101513. Online: https://doi.org/10.1016/j.seta.2021.101513

Subbian, V., Murugavel, K. K., Raja, R. S., and Shanawaz, A. M. (2021). Experimental investigation and the performance evaluation of a mixed mode solar dryer for coconut. *Materials Today: Proceedings*, *45*, 3662–3665. Online: https://doi.org/10.1016/j.matpr.2021.01.157

Toğrul, İ. T. (2010). Modelling of heat and moisture transport during drying black grapes. *International Journal of Food Science & Technology*, *45*(6), 1146–1152. Online: https://doi.org/10.1111/J.1365-2621.2010.02246.X

Vázquez, G., Chenlo, F., Costoyas, R. M., and Costoyas, A. (2000). EFFECTS OF VARIOUS TREATMENTS ON THE DRYING KINETICS OF Muscatel GRAPES. *Drying Technology*, *18*(9), 2131–2144. Online: https://doi.org/10.1080/07373930008917830

Vigneshkumar, N., Venkatasudhahar, M., Manoj Kumar, P., Ramesh, A., Subbiah, R., Michael Joseph Stalin, P., … others (2021). Investigation on indirect solar dryer for drying sliced potatoes using phase change materials (PCM). *Materials Today: Proceedings*, *47*, 5233–5238. Online: https://doi.org/10.1016/j.matpr.2021.05.562

Wang, J., Mu, W.-S., Fang, X.-M., Mujumdar, A. S., Yang, X.-H., Xue, L.-Y., … others (2017). Pulsed vacuum drying of Thompson seedless grape: Effects of berry ripeness on physicochemical properties and drying characteristic. *Food and Bioproducts Processing*, *106*, 117–126. Online: https://doi.org/10.1016/j.fbp.2017.09.003

Yaldiz, O., Ertekin, C., and Uzun, H. I. (2001). Mathematical modeling of thin layer solar drying of sultana grapes. *Energy*, *26*(5), 457–465. Online: https://doi.org/10.1016/S0360-5442(01)00018-4

Zhao, D., Wei, J., Hao, J., Han, X., Ding, S., Yang, L., and Zhang, Z. (2019). Effect of sodium carbonate solution pretreatment on drying kinetics, antioxidant capacity changes, and final quality of wolfberry (*Lycium barbarum*) during drying. *LWT*, *99*, 254–261. Online: https://doi.org/10.1016/j.lwt.2018.09.066

©2026, Universidad Politécnica Salesiana, Ecuador.

La Granja: Revista de Ciencias de la Vida
pISSN:1390-3799; eISSN:1390-8596
https://doi.org/10.17163/lgr.n44.2026.08

Review / Reseña bibliográfica

Agricultural Sciences

CC BY NC SA

Integrated Management of *Zabrotes subfasciatus* in Common Bean (*Phaseolus vulgaris*), Challenges and Control Strategies for Food Security

Manejo integrado de *Zabrotes subfasciatus* en el frijol común (*Phaseolus vulgaris*), desafíos y estrategias de control para la seguridad alimentaria

Luis David Jarquín-Izaguirre*[1], Luisa Fernanda Correa Díaz[1] and Saul Alejandro Jarquín-Izaguirre[2]

[1]*Programa de Maestría en Agricultura Tropical Sostenible, Departamento de Posgrado, Universidad Zamorano, 04001, Tegucigalpa, Honduras. [https://ror.org/01kt2cx88]*
[2]*Departamento de Agroindustria, Universidad Nacional Autónoma de Honduras, 04001, El Paraíso, Honduras. [https://ror.org/03xyve152]*

*Corresponding author: luis.jarquin@est.zamorano.edu

Article received on November 14th, 2024. Accepted, after review, on October 24th, 2025. Published on September 1st, 2026.

Abstract

Integrated management of *Zabrotes subfasciatus* in common bean (*Phaseolus vulgaris*) is crucial due to its wide distribution and the significant damage it causes to stored grains. The goal of integrated management is to reduce losses and ensure food security. This review aimed to understand the biology of *Z. subfasciatus*, identify effective control methods, and propose an integrated model that minimizes the use of chemical insecticides. A systematic review of scientific literature published since 2000 was conducted, evaluating 653 initial studies, of which 61 met the inclusion criteria. Key aspects such as taxonomy, geographic distribution, life cycle, and pest control methods were addressed using information from databases such as ScienceDirect, Elsevier, and SciELO. The main findings showed that an integrated management approach combining cultural, physical, chemical, and genetic methods is effective in controlling the pest without relying solely on chemical insecticides, whose indiscriminate use poses risks to human health and the environment. Monitoring and the development of resistant bean varieties stand out as fundamental practices in pest management. In conclusion, integrated management of *Z. subfasciatus* significantly contributes to the protection of stored grains and, consequently, to the food security of farming communities. It is recommended to strengthen farmer training in sustainable control techniques and to promote research on alternative management methods.

Keywords: Storage, pest control, entomology, bean, insect.

©2026, Universidad Politécnica Salesiana, Ecuador.

Resumen

El manejo integrado del *Zabrotes subfasciatus* en frijol común (*Phaseolus vulgaris*) es crucial, debido a su amplia distribución y el daño significativo que causa en granos almacenados. Su manejo integrado busca reducir las pérdidas y garantizar la seguridad alimentaria. El objetivo de esta revisión es comprender la biología de *Z. subfasciatus*, identificar métodos de control eficaces y proponer un modelo integral que reduzca el uso de insecticidas químicos. Se realizó una revisión sistemática de literatura científica publicada a partir del año 2000, evaluando 653 estudios iniciales, de los cuales 61 cumplieron con los criterios de inclusión. Se abordaron aspectos como la taxonomía, distribución geográfica, ciclo de vida y métodos de control de la plaga, a partir de información recopilada en bases de datos como ScienceDirect, Elsevier y SciELO. Los resultados principales evidenciaron que un enfoque de manejo integrado, que combine métodos culturales, físicos, químicos y fitogenéticos, es eficaz para controlar la plaga sin depender exclusivamente de insecticidas químicos, cuyo uso indiscriminado representa un riesgo para la salud humana y el ambiente. El monitoreo y el desarrollo de variedades resistentes de frijol se destacan como prácticas fundamentales en el manejo de la plaga. En conclusión, el manejo integrado de *Z. subfasciatus* aporta significativamente a la protección de los granos almacenados y, por ende, a la seguridad alimentaria de las comunidades agrícolas. Se recomienda fortalecer la capacitación de los agricultores en técnicas sostenibles de control y promover la investigación en métodos alternativos de manejo.

Palabras clave: Almacenamiento, control de plaga, entomología, frijol, insecto.

Suggested citation: Jarquín, L., Correa, L. and Jarquín, S. (2026). Integrated Management of *Zabrotes subfasciatus* in Common Bean (*Phaseolus vulgaris*), Challenges and Control Strategies for Food Security. La Granja: Revista de Ciencias de la Vida. Vol. 44(2):136-150. https://doi.org/10.17163/lgr.n44.2026.08.

Orcid IDs:

Luis David Jarquín-Izaguirre: https://orcid.org/0009-0001-9970-8548
Luisa Fernanda Correa Díaz: https://orcid.org/0009-0001-3577-2399
Saul Alejandro Jarquín-Izaguirre: https://orcid.org/0009-0002-3819-099X

©2026, Universidad Politécnica Salesiana, Ecuador.

1 Introduction

The common bean (*Phaseolus vulgaris*) is the most important legume used for direct human consumption (Didinger et al., 2022). A member of the Fabaceae family, the common bean is a predominantly self-pollinating species native to Mesoamerica (Bitocchi et al., 2017). Due to its wide geographic distribution, this ancient legume split and evolved into two domesticated gene pools: the Mesoamerican and the Andean. The highest-quality varieties were developed and domesticated in South America, based on the Andean gene pool, while the lower-quality varieties originated in Mexico and Central America, with roots in the Mesoamerican gene pool (Wilker et al., 2020). Thanks to this genetic diversity and its adaptability, the common bean has established itself as one of the most important crops for human consumption worldwide (Refaay et al., 2021). Its high nutritional value makes it an essential food, especially in Latin America and developing countries (Hernández-Ochandía et al., 2018), where it constitutes an important source of protein, vitamins, and minerals. Dried beans contain approximately 22 % protein, complex carbohydrates (62 %), soluble fiber (15 %), and various micronutrients such as calcium, iron, magnesium, phosphorus, potassium, and folate, positioning them as a key food in balanced and healthy diets (Myers and Kmiecik, 2017).

In terms of production, *P. vulgaris* accounts for 85 % of global bean production, making it the most widely cultivated legume on the planet (Mamo et al., 2023). Annually, more than 27 million tons of beans are harvested on approximately 29 million hectares worldwide, feeding more than 300 million people who depend on agricultural economies in various regions of the world (Nasar et al., 2023). Latin America stands out as the region with the highest production and consumption, accounting for 45 % of global production (IICA / Proyecto Red SICTA, 2013). In this region, beans are not only a staple food but also a vital crop for the economy of smallholder farmers. Particularly in Central America, beans occupy a strategic position in food security and the rural economy. According to FAOSTAT data, in 2022 Honduras produced 130 906 tons of beans, with an average yield of 802 kg/ha, which highlights their importance within the region's agricultural economies (FAO, 2022).

Despite its importance of economic and food security, the crop faces various biotic and abiotic stresses that limit its productivity. Among biotic factors, the storage pests *Zabrotes subfasciatus* and *Acanthoscelides obtectus* stand out as the most destructive during the postharvest stage (Tigist et al., 2021). In particular, *Z. subfasciatus* represents one of the main threats to producers, causing significant losses that affect both commercialization and the availability of seeds for future plantings (Mukankusi et al., 2019). The management of these pests in stored grains has traditionally relied on the application of synthetic insecticides such as phosphine, pyrethroids, and organophosphate compounds. However, many of these products have limited availability to farmers in developing countries (Agrafioti et al., 2019; Gourgouta et al., 2019). Furthermore, the continued and indiscriminate use of pesticides has generated growing global concern due to the risks it poses to human health and the environment, highlighting the urgency of implementing more sustainable strategies for pest management in stored products (Souza et al., 2010).

Given its fundamental role in food security, the rural economy, and the nutrition of millions of people in developing countries, the common bean faces the challenge of maintaining its productivity in the face of threats such as *Zabrotes subfasciatus*, one of the main postharvest pests. Ensuring its sustainable management is key to reducing losses, preserving grain quality, and strengthening the livelihoods of smallholder farmers. In this context, this study aims to understand the biology of *Z. subfasciatus*, identify effective control methods, and propose an integrated management model that minimizes the use of chemical insecticides, thereby contributing to crop protection and the sustainability of agricultural systems.

2 Materials and Methods

2.1 Selection of Studies

Initially, a selection of inclusion criteria was carried out, identifying topics of interest within the field of bean pest control, with an emphasis on *Zabrotes subfasciatus*. Based on this identification, the key parameters for the literature search were defined. The inclusion criteria considered were: a) articles addressing the taxonomy of *Z. subfasciatus*, b) studies

©2026, Universidad Politécnica Salesiana, Ecuador.

on its biology and life cycle, c) research related to its geographic distribution, and d) control methods (cultural, phytogenetic, physical-mechanical, and chemical). In general, priority was given to literature published since 2000; however, for specific topics such as taxonomy, morphology, and physiology, earlier studies were included if they were relevant in terms of content and scientific validity.

2.2 Identification of Databases

The repositories used to identify scientific articles were ScienceDirect, Elsevier, and SciELO. Once an article met the inclusion criteria, the literature was analyzed and synthesized, involving a critical evaluation, the extraction of relevant data and scientific evidence, and the identification of trends and fundamental information about the species.

2.3 Analysis Structure

A basic structure was defined to organize the collected information, covering aspects such as taxonomy, morphology, geographic distribution, biology and life cycle, monitoring, as well as control methods in storage: cultural, phytogenetic, physical-mechanical, and chemical. This organization allowed for a comprehensive approach to the management of *Zabrotes subfasciatus* in *Phaseolus vulgaris*.

2.4 Final Selection of Studies for the Analysis

For the selection of articles, the PRISMA approach was used to guide the process of identifying, selecting, and documenting the studies included in this systematic review, following the methodology framework of Page et al. (2021), initially identifying 653 records through searches in scientific databases. Subsequently, the methodological quality of these studies was assessed using a checklist. This tool allowed us to identify potential biases and evaluate the internal validity, methodological clarity, and relevance of the studies. After removing duplicate articles, those that did not meet the thematic or methodological criteria were excluded, resulting in a total of 61 studies included for analysis (Figure 1).

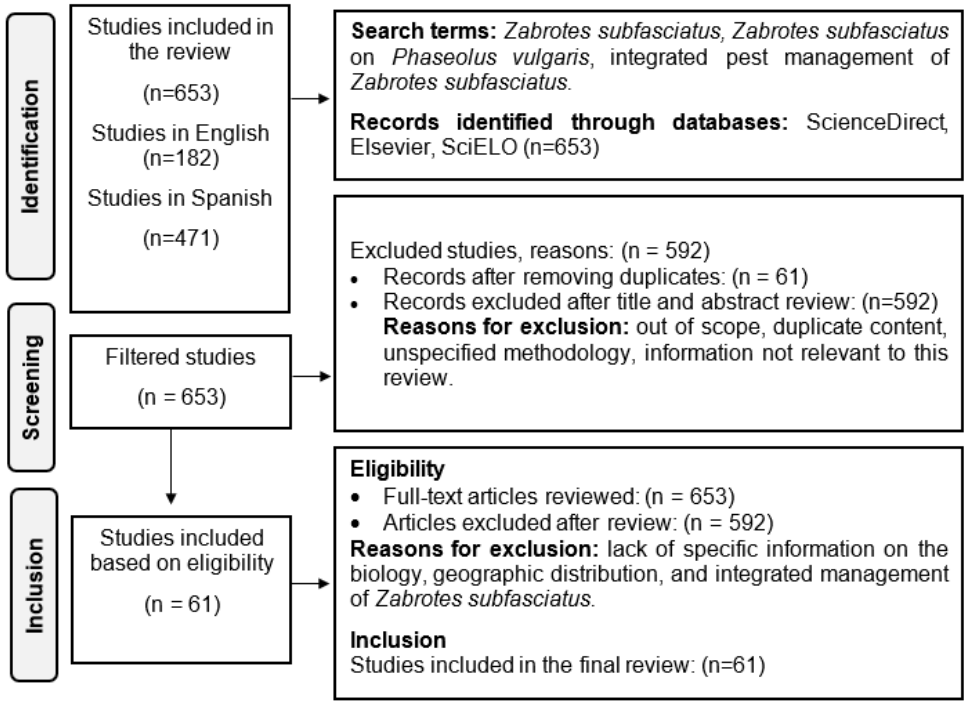


Figure 1. PRISMA flow diagram for the systematic review of *Zabrotes subfasciatus* in beans.

©2026, Universidad Politécnica Salesiana, Ecuador.

3 Results and Discussion

3.1 General characteristics of bean cultivation

The genus *Phaseolus* spp. consists of 76 species, 5 of which are domesticated species, including *P. vulgaris* (Kaplan, 2003). This genus is notable for its cultivated species, which occupy 90 % of the land dedicated to bean cultivation worldwide (Singh, 2013). It is a herbaceous plant that was independently domesticated in ancient Mesoamerica and the Andes (Kaplan, 1981). It is classified within the group of dicotyledonous plants (Katungi et al., 2009). The seeds can be consumed immature (tender), mature, fresh, or dried (Morales-Santos et al., 2017).

There are two bean planting cycles per year, but farmers mainly choose to plant during the late season (October–December). Planting during the early season (May–September) is less common, as it leads to grain losses due to germination or rot (Torres-Treminio and Mendoza-Montoya, 2002). Post-harvest handling of common beans is a critical stage in the agricultural production chain, where beans are exposed to various factors that can compromise their quality and quantity. In Central America and Mexico, losses of up to 35 % of stored beans are estimated (Espinal et al., 2021).

3.2 Taxonomy of *Zabrotes subfasciatus*

The Mexican bean weevil or bean beetle, *Zabrotes subfasciatus*, belongs to the order Coleoptera, a species of leaf beetle in the family Chrysomelidae. It is the primary phytosanitary problem affecting stored beans in areas below 1 500 meters in altitude (Cárdenas-Morales et al., 2019). It is characterized by complete metamorphosis and feeds exclusively on seeds (Dobie et al., 1991).

Members of this family are easily recognizable; the body, covered with small hairs, is compact and globular, the elytra are short, and the pygidium is exposed (Rees, 2018). Their primary host is *Phaseolus vulgaris* in its seed stage; however, they can also feed on other legume species under isolated conditions, such as *Vigna unguiculata* L. (Ramírez Cariño et al., 2017).

Table 1. Taxonomy of *Zabrotes subfasciatus*.

Taxonomic classification	
Taxonomic category	**Taxon to which it belongs**
Domain	Eukarya
Kingdom	Animalia
Phylum	Arthropoda
Class	Insecta
Order	Coleoptera
Suborder	Polyphaga
Superfamily	Chrysomeloidea
Family	Chrysomelidae
Genus	*Zabrotes*
Species	*Z. subfasciatus* (Boheman, 1833)
Common name	Mexican or pinto weevil

Source: Population increase of *Zabrotes subfasciatus* in common bean cultivars (Cárdenas-Morales et al., 2019).

©2026, Universidad Politécnica Salesiana, Ecuador.

3.3 Morphology of *Zabrotes subfasciatus*

This beetle exhibits distinctive characteristics in both males and females, which are crucial for its identification and study. The adult body is oval-shaped, thick, convex, and gray-brown or black in color, except for the base of the antennae and the tips of the tarsi. The body measures approximately 2 to 3 mm in length and 1 to 2 mm in width. Its antennae are long and can reach 1.45 mm in length; the segments are long and black, except for the first two, which are reddish (Dell'Orto and Arias-Velásquez, 1985). The elytra are short and relatively wide, square in shape, with the hind wings concealed (Dobie et al., 1991).

The female is larger than the male and is characterized by four white spots on the elytra (Figure 2) (Arnal and Ramos, 2006). The male is a uniform gray-brown color (Figure 3). Its hind femur is smooth, without protuberances or teeth. The part of the tibia near the femur has two movable spurs (Dobie et al., 1991). The larvae are robust, curved, and ivory-white. They are very voracious, and several may be found in a single grain (Figure 4) (Carrera-Rodríguez et al., 2009).



Figure 2. Dorsal and lateral view of the female *Zabrotes subfasciatus* (Johnson, 2019).



Figure 3. Dorsal and lateral views of the male *Zabrotes subfasciatus* (Johnson, 2019).

©2026, Universidad Politécnica Salesiana, Ecuador.



Figure 4. Larva of *Zabrotes subfasciatus* (Johnson, 2019).

3.4 Morphology of the Male

A beetle with a mostly black body, with some lighter areas in certain individuals. The head has white pubescence with a yellowish-brown spot on the *vertex*. The pronotum and elytra have small, scattered brown and yellow spots. The abdomen is mostly white, with brown patches on the sides. The head structure shows fine punctures, with a semicircular pronotum and uniformly punctured elytra. Measurements vary, but the beetle generally has a length of 1.56 to 2.16 mm and a width of 1.26 to 1.62 mm. Regarding the genitalia, the median lobe is wider at the base and has a subtriangular ventral valve. The lateral lobes are shorter and feature an apical cleft (Nápoles, 2018).

3.5 Morphology of the Female

Sexual dimorphism is present in this species, with females having a median band on the pronotum and a small white spot in each corner, as well as a transverse white band on the elytra. However, pubescence is generally similar to that of males. Antennal length is slightly shorter, ranging from 0.6 to 0.63 times body length. Typical measurements of length (pronotum-elytra) range from 2.28 to 2.46 mm, with a width of 1.74 to 1.86 mm and a maximum thoracic depth of 1.26 to 1.32 mm (Nápoles, 2018).

3.6 Geographic Distribution of *Zabrotes subfasciatus*

This species' ability to thrive under storage conditions has made it widely available worldwide (Del Obregón and Gómez-Gutiérrez, 2023). This insect is widely distributed in the tropical and subtropical regions of Africa, Madagascar, India, and the Americas, where it is believed to be native (Dobie et al., 1991). In the Americas, it is distributed from the United States to Brazil (Arnal and Ramos, 2006). It is mainly found in warm, humid climates at low elevations above sea level (Dell'Orto and Arias-Velásquez, 1985).

3.7 Reproductive Habits of *Zabrotes subfasciatus*

The female mates with the male, and this mating appears to be influenced by bean seeds. Upon contact with these, the number of sexual encounters increases, stimulating oogenesis (egg development) and oviposition activity. It has been documented that olfactory, gustatory, and tactile chemoreceptors regulate or control the reproductive activity of females (Pimbert and Pierre, 1983).

Females oviposite on the naked seed, never on the pods (Credland and Dendy, 1992). However, Pimbert and Pierre (1983) note that they are capable of reproducing on both parts in the field and in storage. When the pods of *P. vulgaris* and *P. lunatus* are partially or fully dehiscent, this allows the female to encounter the seeds to lay eggs. These same

©2026, Universidad Politécnica Salesiana, Ecuador.

authors note that *Z. subfasciatus* cannot pierce the pods to lay eggs on the seeds, nor can it lay eggs inside the pods as other members of the family can. If the female deposits the eggs on the walls of the pods, they adhere, and the larva can penetrate the walls but dies inside the pod since it cannot penetrate the seed (Del Obregón and Gómez-Gutiérrez, 2023).

3.8 Life Cycle of *Zabrotes subfasciatus*

3.8.1 Eggs

Females lay between 35 and 60 eggs and infest up to 36 grains during their reproductive cycle; the incubation period can range from four to eight days, followed by the larval stage (12 days). The eggs measure approximately 0.3 mm in diameter and are rounded. Two days after emerging, the female *Z. subfasciatus* usually begins to lay eggs (Credland and Dendy, 1992). Studies by Golob and Kilminster (1982) indicate that the female has a 1-day preoviposition period; subsequently, the female lays 50 eggs during her 13-day lifespan, with the majority laid after the fourth day. The egg is strongly attached to the grain's testa by a viscous, brightly colored, translucent substance that acts as glue. This glue or secretion that attaches the eggs is generally deposited a few seconds before oviposition (Credland and Dendy, 1992).

3.8.2 Larvae

They are vermiform and apodal, measuring 3 to 3.5 mm in length. Their body tends to be curved, with several folds, whitish in color, and a reduced head embedded in the prothorax (Ascencio-Alvarado, 2012). Newly emerged larvae penetrate the interior of the grain after consuming most of the cotyledon, constructing a tunnel and leaving only a covering over the grain's pericarp through which the adult subsequently emerges (Dell'Orto and Arias-Velásquez, 1985).

3.8.3 Pupae

They measure about 3 mm in length. They are of the exarate type, with appendages. The difference between the sexes can be noted at this stage by the shape of the last abdominal segment, which is straight in the female and arched in the male (Bonet et al., 2005; Ascencio-Alvarado, 2012). This stage lasts between four and nine days, after which the larva enters the adult stage and subsequently emerges through a hole it makes in the testa of the grain (González et al., 1984; Bonet et al., 2005).

3.8.4 Adults

Females, which are larger than males, can be easily distinguished by the presence of four light spots on the pronotum, which contrast with the dark, shiny color of the body. They have well-developed wings, and their body is oval-shaped with a free-standing head. The eyes are well-developed, and their antennae have 11 segments. The hind legs are thicker than the front ones (Bonet et al., 2005; Ascencio-Alvarado, 2012).

The exit point of the adult resembles a circular window on the seed surface (Rees, 2018). Emerging adults do not need to feed before or after mating, as they acquire all the necessary nutrients to complete their life cycle during their larval development. They are highly active, capable of running and flying quickly, and are frequently observed moving across the surface of infested seeds.



Figure 5. Life cycle of *Zabrotes subfasciatus* (CABI, 2019).

©2026, Universidad Politécnica Salesiana, Ecuador.

3.9 Infection Conditions

Its life cycle lasts 24 to 25 days under conditions of 32 °C and 70 % relative humidity (Dobie et al., 1991). However, other authors indicate that it takes more than 30 days from egg to adult (Golob and Kilminster, 1982; Credland and Dendy, 1992; Barbosa et al., 1999). The optimal temperature for development is 37–38 °C, with a minimum slightly below 20 °C (Dobie et al., 1991). Adults have a short lifespan. Various authors have determined the average lifespan of adults. For example, Dell'Orto and Arias-Velásquez (1985) indicated that the adult *Z. subfasciatus* lives for about 10 to 12 days, while Barbosa et al. (1999) argue that it lives for about 36 days.

3.10 Feeding and Damage

It is the most significant pest of stored common beans and lima beans (*P. lunatus*) (Dobie et al., 1991). It can also feed on other legume seeds, such as cowpeas, peas, lentils, and soybeans (Dell'Orto and Arias-Velásquez, 1985; Rees, 2018). The damage caused by this insect species results from the larvae invading and feeding inside the grains, leading to weight loss, reduced nutritional value, and compromised product hygiene due to the presence of excrement, eggs, and insects. Additionally, the germination capacity of the seeds may be reduced or completely lost (Barbosa et al., 1999).

3.11 Cultural Control

A traditional method used to control the population of *Z. subfasciatus* is to store bean seeds inside their own pods (Arnal and Ramos, 2006; Del Obregón and Gómez-Gutiérrez, 2023). This is because females can generally only lay eggs on bare seeds and very rarely on pods unless they are dehiscent (Pimbert and Pierre, 1983).

In many places, a mixture of local plants is used with stored grain. Information about which plants should be used for pest control and which parts of them should be mixed with the grain is passed down from generation to generation in rural areas (Carrera-Rodríguez et al., 2009). Plant-derived substances have been used for pest control since ancient times. However, their use declined with the advent of chemical insecticides, becoming limited to rural areas (Rodríguez Hernández and López Pérez, 2001).

In developing countries, it is common to mix plant-based products with stored beans to protect them during storage. Among the products that have been used are neem leaves (*Azadirachta indica*), *Ocimum canum* leaves, *Capsicum frutescens* fruits, and *Piper nigrum* fruits (Madueke-Onu et al., 2015; Perales-Aguilar et al., 2020; Okafor et al., 2024). Another method involves the use of vegetable oils, generally of local origin. Among the vegetable oils that have been found to be effective are those derived from the seeds of *Anthonomus grandis* (Perales-Aguilar et al., 2020). However, a disadvantage of using oils is that they impart a rancid and sticky appearance to the grains, which could reduce market acceptance (Álvarez Serrano et al., 2021).

The use of mineral powders as a cultural control method for stored grain insects, including *Z. subfasciatus*, has been widely employed (Lopez-Monzon et al., 2016). Mixing sand or ash with the grains is an alternative method for insect control. Sand or ash damages the insect's cuticle by scraping it, causing it to lose moisture. If the grain is dry, there will not be enough moisture for the insect to replenish what it has lost, so it will die from desiccation (Kalpna et al., 2022); ash creates a physical barrier for weevils.

Mixing lime with stored grains is a common practice in northwestern Mexico. Permuy-Abeleira et al. (2008) report that farmers in the region clean the storage area before harvests, removing any debris found, and wash the area with soap; after the grain is harvested, it is mixed with lime to prevent insect attacks.

The use of garlic (*Allium sativum*) extracts as a natural repellent and insecticide against *Zabrotes subfasciatus* in stored beans has also been documented. Studies conducted in El Salvador have shown that aqueous and hydroalcoholic garlic extracts, applied at concentrations between 5 % and 20 %, achieve significant effects on both adult mortality and infestation reduction, without compromising grain quality (Rámos-Archila and Santacruz-Jiménez, 2024).

Another method used is exposing the grains to the sun. The insects abandon the grain when it is exposed to sunlight due to the high temperatures (above 40–44 °C). However, sun exposure does not always kill the eggs and larvae that remain insi-

©2026, Universidad Politécnica Salesiana, Ecuador.

de the grain (Carrera-Rodríguez et al., 2009). This method only protects the outer layers of the grain, so it can only harm adult insects on the surface or larvae that are moving freely (Cuevas, 2006).

3.12 Phytogenetic Control

A wide variety of proteins found in the seeds of wild *P. vulgaris* plants (arcelin and α-amylase inhibitors) have been used to control *Z. subfasciatus* in stored beans (Goossens et al., 2000). Although bean seeds possess defense proteins such as enzyme inhibitors and secondary metabolites (alkaloids, saponins), they can still be attacked. This is because insects co-evolve with their food sources, and in the course of evolution, new insect strains emerge that allow them to defend themselves against the seeds' natural chemicals (Rodríguez-Sifuentes et al., 2020).

3.13 Physical-Mechanical Control

In the tropical regions of some Central American countries, as well as in Mexico, airtight storage of grains for human consumption is commonly used; under these conditions, insects experience stress due to reduced oxygen levels, creating an unfavorable environment for their survival (Moreno-Martinez et al., 2000). Low levels of O_2 and CO_2 cause metabolic stress in insects, generally increasing mortality and decreasing fecundity and development rate (Thompson and Suarez, 2009).

Another physical-mechanical treatment involves heat, which consists of heating a container to a specific temperature (50 to 55 °C) for 20 or 30 hours. This duration allows the container materials to expand and adjust to the change. Although storage insects die in less than an hour at these temperatures, such a long duration is necessary because the heat must penetrate to where the insects might be found. However, these control methods are not typically cost-effective, as the containers or heating equipment are often expensive.

3.14 Chemical Control

This is the most widely used method in grain warehouses; among the most commonly used are fumigantes (Perales-Aguilar et al., 2020). Phosphamine fumigants and methyl bromide are widely used in the control of stored grain insects (Dierksmeier-Corcuera, 2007). In highly technical warehouses, it is common to use insecticides to control pests that affect stored products. This approach involves the application of chemicals, which can take different forms, such as powder, liquid, or fumigants.

Powdered products are particularly used in warehouses where grain is stored in bulk or in bags, and their application can be both preventive and corrective. The most popular insecticides in this category include malathion, pirimiphos-methyl, and dichlorvos, among others. Although some of these products can also be used as sprays, the use of pyrethroid insecticides is widely preferred, with deltamethrin being particularly prominent. Additionally, many warehouses rely on fumigants, with aluminum phosphide being one of the most prominent (García-Lara et al., 2007).

Vázquez-Zamorano (2014) conducted a study to evaluate the effectiveness of permethrin, diazinon, and cypermethrin in controlling adult weevils. Permethrin was found to be the most effective insecticide, with a mortality rate exceeding 60 % when using the highest dose of 500 ppm. In a study conducted in Argentina to evaluate the efficacy of aluminum phosphide in the bag-in-silo storage system, it was observed that although there is some loss of the fumigant, by hermetically sealing the storage system, it is capable of retaining the adequate amount of fumigant to eliminate stored-product insects (Carpaneto et al., 2016).

The use of chemical control methods poses significant problems: risk of toxic residues in food, insect resistance, negative environmental impact, and increasing regulatory restrictions, in addition to the costs associated with their purchase, application, and specialized equipment (Cevallos-Taxi, 2020). From an economic standpoint, chemical control may be more effective in scenarios involving large volumes and mechanized storage facilities, but it is less accessible and viable in rural areas with limited resources (Raygoza-Martínez et al., 2025).

In contrast, cultural control has proven to be highly cost-effective in rural communities, especially when based on traditional knowledge and local resources. This effectiveness stems from the fact that it utilizes locally available inputs, requires

©2026, Universidad Politécnica Salesiana, Ecuador.

little initial investment, does not depend on external commercial products, and can be easily adopted by farming families, thereby reducing risks to human health and the environment.

4 Conclusions

The wide geographic distribution of *Zabrotes subfasciatus* and its ability to infest various legumes highlight the need for ongoing research and the implementation of monitoring and control practices adapted to different environmental and cultural contexts. The integrated management approach, which combines cultural, physical-mechanical, chemical, and phytogenetic methods, represents an effective and sustainable strategy for controlling this pest, minimizing dependence on chemical insecticides and their associated risks.

However, challenges remain, such as the limited adoption of sustainable practices, the lack of accessible technologies, and inadequate storage infrastructure. For this reason, it is recommended to deepen research into the development of resistant varieties as a key measure to ensure protein availability and contribute to food security. Similarly, efforts should be made to promote the development of new biological control alternatives and innovation in postharvest management technologies, incorporating participatory approaches that address the needs of smallholder farmers.

It is also crucial that public agricultural policies integrate post-harvest management and strengthen technical assistance programs with a focus on promoting sustainable practices as part of rural development and food security strategies. This involves promoting training programs, incentives for agroecological practices, and improvements in extension systems.

Declaration on the Use of Artificial Intelligence

The authors DECLARE that, during the preparation of the article entitled "Integrated Management of *Zabrotes subfasciatus* in Common Bean (*Phaseolus vulgaris*), Challenges and Control Strategies for Food Security", no generative artificial intelligence tools or automated assistance systems were used for the writing, analysis, data interpretation, content generation, translation, or editing of the manuscript.

The authors assume full responsibility for the content, originality, integrity, and final version of the article.

Author Contributions

L.D.J.I.: Conceptualization, Data curation, Investigation, Supervision, Writing – review and editing. **L.F.C.D.:** Investigation, Data curation, Methodology, Writing – original draft. **S.A.J.I.:** Conceptualization, Formal analysis, Validation, Writing – original draft.

References

Agrafioti, P., Athanassiou, C. G., and Nayak, M. K. (2019). Detection of phosphine resistance in major stored-product insects in greece and evaluation of a field resistance test kit. *Journal of Stored Products Research*, *82*, 40–47. Online: https://doi.org/10.1016/j.jspr.2019.02.004

Álvarez Serrano, A., Milan-Leyva, E., and Matos-Castillo, Y. (2021). Estudio del efecto de aceites vegetales en el control del gorgojo (*Callosobruchus maculatus* f) en la conservación de granos de frijol caupí. *Opuntia Brava*, *13*(3), 77–86. Online: https://shortlink.uk/1wIsu

Arnal, E. A., and Ramos, F. A. (2006). *Guía práctica sobre alternativas de control de insectos-plaga en los cultivos de caraota y frijol* (Inf. Téc. n.º 12). Publicación Especial (INIA). Online: https://shortlink.uk/1rhwg

Ascencio-Alvarado, J. I. (2012). *Evaluación de la actividad insecticida y repelente del extracto obtenido a partir de la semilla de Annona diversifolia (anona) sobre el Zabrotes subfasciatus (gorgojo común del frijol)* (Bachelor's thesis, Universidad de El Salvador). Online: https://shortlink.uk/1wIsx

Barbosa, F. R., Yokoyama, M., Arraes-Pereira, P. A., and Pfeilsticker-Zimmermann, F. J. (1999). Efeito da proteína arcelina na biologia de *Zabrotes subfasciatus* (Boheman 1833), em feijoeiro. *Pesquisa*

©2026, Universidad Politécnica Salesiana, Ecuador.

Agropecuária Brasileira, *34*(10), 1805–1810. Online: https://shortlink.uk/1wIsB2

Bitocchi, E., Rau, D., Bellucci, E., Rodriguez, M., Murgia, M. L., Gioia, T., … Papa, R. (2017). Beans (*Phaseolus* ssp.) as a model for understanding crop evolution. *Frontiers in Plant Science*, *8*, 722. Online: https://doi.org/10.3389/fpls.2017.00722

Bonet, A., Morales, C. O., and Rojas, C. V. (2005). El control biológico con parasitoides: una alternativa para limitar a los gorgojos en frijol almacenado. *Fitosanidad*, *9*(2), 35–42.

CABI. (2019). *Zabrotes subfasciatus (Mexican bean weevil). CABI Compendium.* Online Publication. Online: https://doi.org/10.1079/cabicompendium.57289

Cárdenas-Morales, M., Lavastida-Pérez, M., Valdés-Herrera, R., Pozo-Velazquez, E., and Rodríguez-Rojas, R. (2019). Incremento poblacional de *Zabrotes subfasciatus* en cultivares de frijol común. *Centro Agrícola*, *46*(2), 38–45. Online: https://shortlink.uk/1wIsH

Carpaneto, B., Bartosik, R., Cardoso, L., and Manetti, P. (2016). Pest control treatments with phosphine and controlled atmospheres in silo bags with different airtightness conditions. *Journal of Stored Products Research*, *69*, 143–151. Online: https://doi.org/10.1016/j.jspr.2016.07.007

Carrera-Rodríguez, M., Martínez-González, G. M., Navarrete-Bolaños, J. L., Botello-Alverez, J. E., Rico-Martínez, R., and Jiménez-Islas, H. (2009). Estudio numérico del efecto de la temperatura ambiental en la convección natural bidimensional en el almacenamiento de granos en silos cilíndricos. *Revista Mexicana de Ingeniería Química*, *8*(1), 77–91. Online: https://shortlink.uk/1wIsM

Cevallos-Taxi, S. F. (2020). *Evaluación del efecto de ozono (o_3) en el control de gorgojo Pagiocerus frontalis (f.), en granos almacenados de maíz suave (Zea mays l.) en la provincia Cotopaxi, campus experimental Salache, proyecto granos andinos 2020* (Bachelor's thesis, Universidad Técnica de Cotopaxi). Online: https://shortlink.uk/1wIsP

Credland, P. F., and Dendy, J. (1992). Comparison of seed consumption and the practical use of insect weight in determining effects of host seed on the Mexican bean weevil, *Zabrotes subfasciatus* (Boh.). *Journal of Stored Products Research*, *28*(4), 225–234. Online: https://doi.org/10.1016/0022-474x(92)90001-7

Cuevas, M. I. (2006). Insecticidas alternativos para el control de plagas en granos almacenados. *Inventio*, *2*(3), 55–60. Online: https://shortlink.uk/1wIsV

Dell'Orto, T. H., and Arias-Velásquez, C. J. (1985). *Insectos que dañan granos y productos almacenados* (Inf. Téc. n.º 4). Serie Tecnología Postcosecha (FAO/RLAC). Online: https://shortlink.uk/1wIsZ

Del Obregón, N. C., and Gómez-Gutiérrez, O. J. (2023). Tecnologías y prácticas que utilizan los productores en el manejo poscosecha de maíz y frijol en Estelí, Madriz y Nueva Segovia, Nicaragua. *La Calera*, *23*(41). Online: https://doi.org/10.5377/calera.v23i41.16739

Didinger, C., Foster, M. T., Bunning, M., and Thompson, H. J. (2022). Nutrition and human health benefits of dry beans and other pulses. En M. Siddiq and M. A. Uebersax (Eds.), *Dry beans and pulses* (pp. 481–504). Wiley. Online: https://doi.org/10.1002/9781119776802.ch19

Dierksmeier-Corcuera, G. (2007). Características y mecanismos de acción de algunos compuestos usados en el combate de plagas de almacén. *Fitosanidad*, *11*(2), 81–84.

Dobie, P., Haines, C. P., Prevett, P. F., and Rees, D. P. (1991). *Insects and arachnids of tropical stored products: their biology and identification*. Natural Resources Institute.

Espinal, J. R., Soto, O. J., Abrego, A. N., Pizarro, I. P., Rodriguez, I. Y., and Rosas-Sotomayor, J. C. (2021). Resistencia de genotipos de frijol común a los daños causados por el gorgojo mexicano *Zabrotes subfasciatus* (Boheman) en el almacenamiento. *CEIBA (Edición Zamorano Investiga)*, 112–121. Online: https://shortlink.uk/1wIt6

FAO. (2022). *FAOSTAT database: Dry Bean Yield.* Online: https://www.fao.org/faostat/en/#data/QCL

García-Lara, S., Espinosa-Carrillo, C., and Bergvinson, D. (2007). *Manual de plagas en granos almacenados y tecnologías alternas para su manejo y control*. México, D.F.: CIMMYT.

©2026, Universidad Politécnica Salesiana, Ecuador.

Golob, P., and Kilminster, A. (1982). The biology and control of *Zabrotes subfasciatus* (Boheman) (Coleoptera: Bruchidae) infesting red kidney beans. *Journal of Stored Products Research*, *18*(3), 95–101. Online: https://doi.org/10.1016/0022-474x(82)90008-x

González, M., Roche, R., and Simanca, M. E. (1984). Ciclo de vida de *Zabrotes subfasciatus* (Coleoptera: Bruchidae), plaga de granos almacenados. *Ciencias de la Agricultura*(21). Online: https://shortlink.uk/1wItb

Goossens, A., Quintero, C., Dillen, W., Rycke, R. d., Flower Valor, J., Clercq, J. d., … Angenon, G. (2000). Analysis of bruchid resistance in the wild common bean accession G02771: no evidence for insecticidal activity of arcelin 5. *Journal of Experimental Botany*, *51*(348), 1229–1236. Online: https://doi.org/10.1093/jexbot/51.348.1229

Gourgouta, M., Rumbos, C. I., and Athanassiou, C. G. (2019). Residual toxicity of a commercial cypermethrin formulation on grains against four major storage beetles. *Journal of Stored Products Research*, *83*, 103–109. Online: https://doi.org/10.1016/j.jspr.2019.05.001

Hernández-Ochandía, D., Rodríguez-Hernández, M. G., Miranda-Cabrera, I., Moreno-León, E., Castro-Lizazo, I., Delgado-Oramas, B. P., and Holgado, R. (2018). Reproducción y efecto nocivo de *Meloidogyne incognita* (Kofoid y White) Chitwood en *Phaseolus vulgaris* L. 'cuba-cueto-25-9'. *Revista de Protección Vegetal*, *33*(2). Online: https://shortlink.uk/1wIth

IICA / Proyecto Red SICTA. (2013). *Estudio de las cadenas de valor maíz blanco y frijol en Centroamérica* (Inf. Téc. n.º 115). Instituto Interamericano de Cooperación para la Agricultura. Online: https://shortlink.uk/1wItn

Johnson, A. (2019). *Zabrotes subfasciatus (Mexican bean weevil).* CABI Compendium. Online: https://doi.org/10.1079/cabicompendium.57289

Kalpna, Hajam, Y. A., and Kumar, R. (2022). Management of stored grain pest with special reference to *Callosobruchus maculatus*, a major pest of cowpea: A review. *Heliyon*, *8*(1), e08703. Online: https://doi.org/10.1016/j.heliyon.2021.e08703

Kaplan, L. (1981). What is the origin of the common bean? *Economic Botany*, *35*(2), 240–254. Online: https://doi.org/10.1007/bf02858692

Kaplan, L. (2003). Taxonomy, Distribution, and Ecology of the Genus *Phaseolus* (Leguminosae–Papilionoideae) in North America, Mexico, and Central America. *Economic Botany*, *57*(3), 421. Online: https://shortlink.uk/1wItr

Katungi, E., Farrow, A., Chianu, J., and Beebe, S. (2009). *Common bean in Eastern and Southern Africa: A situation and outlook analysis* (Inf. Téc.). CIAT. Online: https://shortlink.uk/1wItw

Lopez-Monzon, C. E., Tobar-Tomas, W. V., and Ventura-Gomez, A. G. (2016). Controles alternativos para el gorgojo del frijol (*Acanthoscelides obtectus* Say) en granos almacenados a partir de materiales naturales y minerales. *Ciencia, Tecnología y Salud*, *3*(2), 149–156. Online: https://doi.org/10.36829/63CTS.v3i2.196

Madueke-Onu, F., Ogu, E., and Ikehi, M. (2015). Use of neem and garlic dried plant powders for controlling. *Egyptian Journal of Biological Pest Control*, *25*(2), 507–512.

Mamo, T., Singh, A., Singh, A., Mahama, A. A., and Suza, W. (2023). Common bean breeding. En *Crop improvement*. Iowa State University Digital Press. Online: https://shortlink.uk/1rhxk

Morales-Santos, M. E., Peña Valdivia, C. B., García-Esteva, A., Aguilar-Benítez, G., and Kohashi-Shibata, J. (2017). Características físicas y de germinación en semillas y plántulas de frijol (*Phaseolus vulgaris* L.) silvestre, domesticado y su progenie. *Agrociencia*, *51*(1), 43–62. Online: https://shortlink.uk/1rhxn

Moreno-Martinez, E., Jiménez, S., and Vázquez, M. E. (2000). Effect of *Sitophilus zeamays* and *Aspergillus chevalieri* on the oxygen level in maize stored hermetically. *Journal of Stored Products Research*, *36*(1), 25–36. Online: https://doi.org/10.1016/s0022-474x(99)00023-5

Mukankusi, C., Raatz, B., Nkalubo, S., Berhanu, F., Binagwa, P., Kilango, M., … Beebe, S. (2019). Genomics, genetics and breeding of common bean in Africa: A review of tropical legume project. *Plant Breeding*, *138*(4), 401–414. Online: https://doi.org/10.1111/pbr.12573

©2026, Universidad Politécnica Salesiana, Ecuador.

Myers, J. R., and Kmiecik, K. (2017). Common bean: Economic importance and relevance to biological science research. En J. R. Myers and K. Ken (Eds.), *Compendium of plant genomes* (pp. 1–20). Springer International Publishing. Online: https://doi.org/10.1007/978-3-319-63526-2_1

Nápoles, J. R. (2018). *Revisión del género Zabrotes para México (Coleoptera: Bruchidae)* (Master's thesis, Colegio de Postgraduados). Online: https://shortlink.uk/1rhxp

Nasar, S., Shaheen, H., Murtaza, G., Tinghong, T., Arfan, M., and Idrees, M. (2023). Socioeconomic evaluation of common bean (*Phaseolus vulgaris* L.) cultivation in providing sustainable livelihood to the mountain populations of Kashmir Himalayas. *Plants*, *12*(1). Online: https://doi.org/10.3390/plants12010213

Okafor, K. P., Akunne, C. E., Nwaoke, A. J., Nlemchi, C. J., Okeke, T. E., Chidi, C. A., … Offor, V. O. (2024). Evaluation of insecticidal potentials of chilli pepper (*Capsicum frutescens* L.) and guinea pepper (*Xylopia aethiopica* Dun. A. Rich.) in the control of bean weevil (*Callosobruchus maculatus* L. Fabricus). *Multidiscience: Journal of Multidisciplinary Science*, *1*(2), 51–66. Online: https://doi.org/10.59631/multidiscience.v1i2.202

Page, M. J., McKenzie, J. E., Bossuyt, P. M., Boutron, I., Hoffmann, T. C., Mulrow, C. D., … Moher, D. (2021). The PRISMA 2020 statement: An updated guideline for reporting systematic reviews. *BMJ (Clinical Research Ed.)*, *372*, n71. Online: https://doi.org/10.1136/bmj.n71

Perales-Aguilar, L., Chávez-Servia, J. L., Perales-Aguilar, L., Tafoya, F., and Perales-Segovia, C. (2020). Manejo del gorgojo de frijol almacenado, con extractos de plantas asociadas al cultivo. *Revista Mexicana de Agroecosistemas*, *7*(2), 76–84.

Permuy-Abeleira, N., Chaveco-Pérez, O., González-Ferrer, E., J. y García-Sánchez, and Hidalgo-Figueroa, N. (2008). Pérdidas de grano de frijol común en un sistema de almacenamiento tradicional. *Agricultura Técnica en México*, *34*(1), 91–100.

Pimbert, M. P., and Pierre, D. (1983). Ecophysiological aspects of bruchid reproduction. I. The influence of pod maturity and seeds of *Phaseolus vulgaris* and the influence of insemination on the reproductive activity of *Zabrotes subfasciatus*. *Ecological Entomology*, *8*(1), 87–94. Online: https://shortlink.uk/1rhxu

Ramírez Cariño, R. N., Romero Nápoles, J., Vera Graziano, J., Equihua Martínez, A., Bautista Martínez, N., Hernández Morales, J., and Aragón García, A. (2017). Demografía de brúquidos (Coleoptera: Bruchidae) asociados con *Vigna unguiculata* (L.) Walp (Fabaceae). *Acta Zoológica Mexicana*, *33*(1), 9–17.

Rámos-Archila, N. E., and Santacruz-Jiménez, S. F. (2024). *Evaluación de tres diluciones de un extracto de Allium sativum (ajo) y su posible uso como insecticida natural contra el Zabrotes subfasciatus (gorgojo)* (Bachelor's thesis). Universidad de El Salvador.

Raygoza-Martínez, A. P., Rodríguez-Herrera, S. A., Cervantes-Ortiz, F., García-Rodríguez, J. G., Rodríguez-Mercado, D., and Mendoza Elos, M. (2025). Bioinsecticidas para el control de *Zabrotes subfasciatus* Boheman y la calidad de semilla en frijol. *Revista Mexicana de Ciencias Agrícolas*, *16*(1). Online: https://doi.org/10.29312/remexca.v16i1.3086

Rees, D. P. (2018). Coleoptera. En *Integrated management of insects in stored products* (pp. 1–39). CRC Press. Online: https://doi.org/10.1201/9780203750612-1

Refaay, D. A., El-Marzoki, E. M., Abdel-Hamid, M. I., and Haroun, S. A. (2021). Effect of foliar application with *Chlorella vulgaris*, *Tetradesmus dimorphus*, and *Arthrospira platensis* as biostimulants for common bean. *Journal of Applied Phycology*, *33*(6), 3807–3815. Online: https://doi.org/10.1007/s10811-021-02584-z

Rodríguez-Sifuentes, L., Marszalek, J. E., Chuck-Hernández, C., and Serna-Saldívar, S. O. (2020). Legumes protease inhibitors as biopesticides and their defense mechanisms against biotic factors. *International Journal of Molecular Sciences*, *21*(9). Online: https://doi.org/10.3390/ijms21093322

Rodríguez Hernández, C., and López Pérez, E. (2001). Actividad insecticida e insectistática de la chilca (*Senecio salignus*) sobre *Zabrotes subfasciatus*. *Manejo Integrado de Plagas*, *62*, 45–52. Online: https://shortlink.uk/1rhxz

©2026, Universidad Politécnica Salesiana, Ecuador.

Singh, S. P. (2013). *Common bean improvement in the twenty-first century* (Vol. 7). Springer Netherlands.

Souza, S. M., Uchôa, A. F., Silva, J. R., Samuels, R. I., Oliveira, A. E. A., Oliveira, E. M., … Silva, C. P. (2010). The fate of vicilins, 7S storage globulins, in larvae and adult *Callosobruchus maculatus* (Coleoptera: Chrysomelidae: Bruchinae). *Journal of Insect Physiology*, *56*(9), 1130–1138. Online: https://doi.org/10.1016/j.jinsphys.2010.03.009

Thompson, S. N., and Suarez, R. K. (Eds.). (2009). *Encyclopedia of insects*. London, UK: Academic Press.

Tigist, S. G., Raatz, B., Assefa, A., Melis, R., Sibiya, J., Keneni, G., … Tsegaye, D. (2021). Introgression of bruchid (*Zabrotes subfasciatus*) resistance into small red common bean (*Phaseolus vulgaris*) background and validation of the BRU_00261 (snpPV0007) resistance marker. *Plant Breeding*, *140*(6), 1081–1089. Online: https://doi.org/10.1111/pbr.12969

Torres-Treminio, J. A., and Mendoza-Montoya, J. (2002). *Efecto de la fertilización mineral, orgánica y control de malezas sobre crecimiento y rendimiento en frijol común (Phaseolus vulgaris L.) en condiciones de ladera, establecido bajo dos sistemas de labranza, Ticuantepe, postrera dos mil* (Bachelor's thesis, Universidad Nacional Agraria, Managua, Nicaragua). Online: https://shortlink.uk/1wItV

Vázquez-Zamorano, R. L. (2014). *Evaluación de tres insecticidas para el control del gorgojo del maíz Sitophilus zeamays Motschulsky, bajo condiciones de laboratorio* (Bachelor's thesis, Universidad Autónoma Agraria Antonio Narro, Saltillo, Coahuila, México). Online: https://shortlink.uk/1wItZ

Wilker, J., Humphries, S., Rosas-Sotomayor, J. C., Cerna, M. G., Torkamaneh, D., Edwards, M., … Pauls, K. P. (2020). Genetic diversity, nitrogen fixation, and water use efficiency in a panel of Honduran common bean (*Phaseolus vulgaris* L.) landraces and modern genotypes. *Plants*, *9*(9). Online: https://doi.org/10.3390/plants9091238

©2026, Universidad Politécnica Salesiana, Ecuador.

La Granja: Revista de Ciencias de la Vida
pISSN:1390-3799; eISSN:1390-8596
https://doi.org/10.17163/lgr.n44.2026.09

Scientific paper / Artículo científico

Conservation

CC BY NC SA

Land cover and land use factors associated with the risk of vegetation degradation in the Arenillas Ecological Reserve

Factores de cobertura y uso del suelo asociados al riesgo de degradación de la vegetación en la Reserva Ecológica Arenillas

Jaime Enrique Maza Maza*, Hugo Enrique Añazco Loaiza, Darwin Amable Poma Luna and Alex Dumany Luna Florin

Universidad Técnica de Machala. Machala, Ecuador. [https://ror.org/036zk8k10]

*Corresponding author: jemaza@utmachala.edu.ec

Article received on March 29th, 2023. Accepted, after review, on September 7th, 2023. Published on September 1st, 2026.

Abstract

Protected areas are priority zones for the conservation of natural and cultural biodiversity, allowing the assurance of goods and services for society. This study evaluates land cover and land adoption factors associated with vegetation criteria risks in the Arenillas Ecological Reserve (REAR) (southern Ecuador), using the Normalized Difference Vegetation Index (NDVI) and anthropic variables to which the vegetation is elucidated as indicators. The analysis procedure was applied using SENTINEL-B2 satellite images based on the Reserve's four ecosystems and the six soil types found. Through multiple linear regression, a risk probability model was determined in relation to the threat variables of agricultural, aquaculture, livestock, population and road zones. The results revealed a higher NDVI value in Flooded Grassland and Mangrove, followed by the Deciduous Shrubland and Deciduous Forest. Correspondingly, 18.7 % of vegetation cover is at high risk throughout the REAR, with the greatest disturbance and threat on the northwestern and northeastern edges of the deciduous shrub forest and southwestern edges of the deciduous forest, and the identical pattern is present at the entrances to the main and secondary roads. On the other hand, for the Mangrove ecosystem, the areas with the greatest variability are those bordering the shrimp aquaculture activity. It is essential to note that if the areas adjacent to the REAR are not protected, the little remaining forest will disappear, limiting connectivity with other natural forests.

Keywords: NDVI, risk factors, dry forest, Arenillas Ecological Reserve, land use.

©2026, Universidad Politécnica Salesiana, Ecuador.

Resumen

Las áreas protegidas constituyen zonas prioritarias para conservar la biodiversidad natural y cultural, permitiendo el aseguramiento de los bienes y servicios para la sociedad. El presente estudio evalúa los factores de cobertura y uso de suelo asociados a los riesgos del estado de la vegetación en la Reserva Ecológica Arenillas (REAR) (sur de Ecuador), usando como indicador el Índice de Vegetación de Diferencia Normalizada (NDVI en inglés) y variables antrópicas a las que está expuesta la vegetación. El proceso de análisis se efectuó con el uso de imágenes satelitales SENTINEL-B2 con base en los cuatro ecosistemas de la Reserva y los seis tipos de suelo encontrados. A través de regresión lineal múltiple se estableció un modelo de probabilidad de riesgo en relación a las variables de amenaza de zonas: agrícolas, acuícolas, pecuarias, de población y vías. Los resultados revelaron un mayor valor de NDVI en el Herbazal Inundable y Manglar, seguidos del Bosque Arbustal deciduo y Bosque deciduo. Así mismo, 18.7 % de cobertura vegetal se encuentra en alto riesgo en toda la REAR, situándose la mayor perturbación y amenaza en los bordes noroeste y noreste del Bosque Arbustal deciduo y bordes suroeste del Bosque deciduo, y bajo el mismo patrón se presentan en las entradas de las Vías principal y secundarias. En cambio, para el ecosistema Manglar las zonas de mayor variabilidad se ubican en aquellas que limitan con la actividad acuícola camaronera. Es importante indicar que, si no se protegen las áreas adyacentes a la REAR, el poco bosque remanente desaparecerá, limitando la conectividad con otros bosques naturales.

Palabras clave: NDVI, factores de riesgo, bosque seco, Reserva Ecológica Arenillas, uso de suelos.

Suggested citation: Maza, J., Añazco, H., Poma, D. and Luna, A. (2026). Land cover and land use factors associated with the risk of vegetation degradation in the Arenillas Ecological Reserve. La Granja: Revista de Ciencias de la Vida. Vol. 44(2):151-166. https://doi.org/10.17163/lgr.n44.2026.09.

Orcid IDs:

Jaime Enrique Maza Maza: https://orcid.org/0000-0002-4845-5165
Hugo Enrique Añazco Loaiza: https://orcid.org/0000-0001-6090-7155
Darwin Amable Poma Luna: https://orcid.org/0000-0002-6761-7430
Alex Dumany Luna Florin: https://orcid.org/0000-0003-4975-405X

©2026, Universidad Politécnica Salesiana, Ecuador.

1 Introduction

Currently, protected areas (PAs) constitute priority zones for environmental conservation, enabling the proper functioning and safeguarding of biotic and abiotic resources, as well as the maintenance of the goods and services provided by each ecosystem (Union Internacional para la Conservacion de la Naturaleza IUCN, 2005). Globally, PAs encompass a vast expanse of tropical dry forests. Recent studies conducted by the Organización de las Naciones Unidas para la Agricultura y la Alimentación FAO (2020) indicate that of the 218 million hectares of existing forests, 26.7 % are protected. However, unlike rainforests, governments have paid little attention to dry forests, resulting in a lack of protection and a higher risk of human impact (Ramírez et al., 2018); a problem arising from inexperience and a lack of information that has compromised conservation principles (Carey et al., 2000), and which is consequently cause for concern due to the level of threat and vulnerability these ecosystems face (Wright and Muller-Landau, 2006).

In Ecuador, the tropical dry forest, located on the Pacific coast, belongs to one of the 35 biodiversity hotspots (Mittermeier et al., 2011), known as Tumbes–Chocó–Magdalena. Its ecological importance has been the determining factor for the regulation and provision of ecosystem services that are used by society. However, due to their abundant endemic natural wealth, tropical dry forests are the most prone to deforestation and degradation, without a clear understanding of the factors driving the shift to other land uses in these ecosystems. According to Armenteras and Rodríguez (2014), the problem of deforestation in these areas is due to biophysical and social factors such as: the establishment of settlements, easy accessibility due to road construction, proximity to water bodies, as well as inadequate land management and climate change. However, studies conducted by Tapia-Armijos et al. (2015) in the tropical forests of southern Ecuador revealed that the increase in roads in the year 2000 intensified access to previously inaccessible sites, resulting in approximately 46 % of natural forest being converted by 2008 into grassland, agricultural land, and other types of human activity.

According to public data from Ecuador's Ministry of the Environment, Water, and Ecological Transition (MAAE), there are 21 000 ha of dry deciduous forest registered within the National System of Protected Areas (SNAP), equivalent to nearly 50 % of the country's total forest area (41 000 ha) (Riofrío, 2018). Part of this national system is the Arenillas Ecological Reserve (REAR), located in the province of El Oro, which since its creation has faced intense pressure from surrounding communities seeking to carry out agricultural and livestock activities within and around the forest, as well as other human threats such as hunting, logging, and the establishment of aquaculture activities, all of which are direct causes that have impeded the natural regeneration of native species (Ministerio del Ambiente del Ecuador MAE, 2015). According to Ruiz (2018), these types of forests are at high risk, especially due to the human activities taking place within them and in their area of influence. On the other hand, climatic pressures such as rising temperatures and decreasing rainfall are likely to affect the ecological communities of dry forests (Maza-Maza et al., 2021), which means a reduction in ecosystem services related to habitat provision, important for soil conservation and biodiversity (Qian et al., 2022).

Given the great importance of dry forests, and the scarcity of scientific information in the REAR and other areas of Ecuador's Southern Coast, it is necessary to use Geographic Information Systems (GIS) and satellite imagery to gather data on the region. These tools are of great importance and precision for assessing the condition and quality of vegetation, as well as the anthropogenic risks to which ecosystems are exposed. Furthermore, these technologies offer the possibility of conducting analyses at the continental level and over specific time periods (Sudmanns et al., 2020), thereby enabling the timely identification of the most vulnerable areas, the evaluation of land cover and land use transformation processes and their adjacent areas (Faruque et al., 2022), and to assist decision-makers in establishing socioeconomic measures for improved forest conservation management (Baig et al., 2022).

Therefore, the objective of this study is to evaluate the land cover and land use factors associated with vegetation condition risks in the REAR, using the Normalized Difference Vegetation Index (NDVI) as an indicator and considering various anthropogenic variables to which the area is exposed. Ac-

©2026, Universidad Politécnica Salesiana, Ecuador.

cording to Gonzaga-Aguilar (2015) and Mesa-Sierra et al. (2022), the NDVI is an indicator of active photosynthetic biomass related to crop behavior, condition, and the health of natural vegetation. The study began with the hypothesis that changes in vegetation cover within the reserve are due to the socioeconomic pressure of productive activities carried out in its area of influence. Thus, the results obtained will allow for greater precision and interpretation of information regarding the REAR's area of influence, which will lead to sound decision-making in the proposal and implementation of public policies and restoration and conservation programs in each of the protected area's ecosystems.

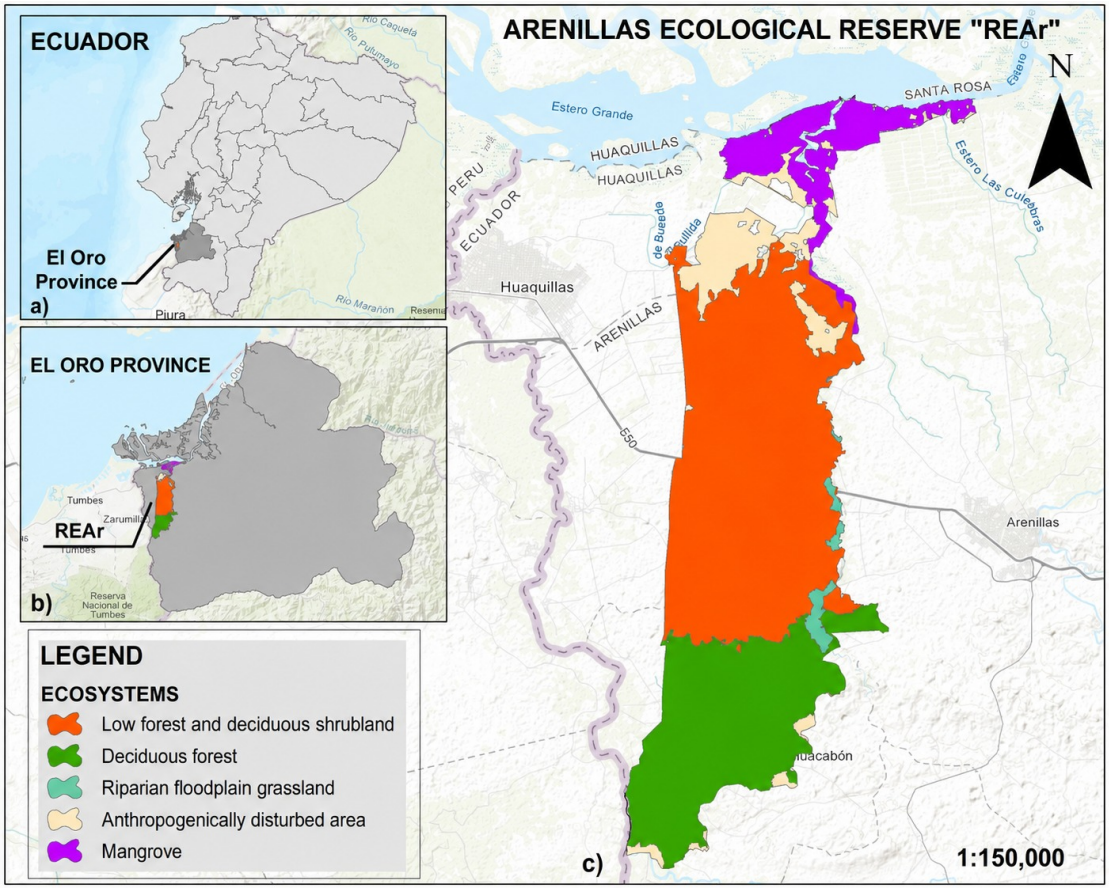


Figure 1. Study area and ecosystems. a) El Oro Province, Ecuador; b) the REAR in El Oro Province; and c) Ecosystems of the REAR.

2 Materials and Methods

This study was conducted in the REAR, located in southwestern Ecuador, in the Zarumilla River basin of El Oro Province (see Figure 1). According to the Reserve's management plan, this area covers 13 170.025 ha (Ministerio del Ambiente del Ecuador MAE, 2015). The climate varies by zone, characterized by a warm, arid climate in the lower zone, with annual precipitation of up to 350 mm; a very dry, warm climate in the middle zone; and a warm, dry climate in the upper zone, with annual precipitation ranging from 500 to 1 000 mm (Instituto de Ecología Aplicada ECOLAP and Ministerio del Ambiente del Ecuador MAE, 2007). The elevation ranges from 0 to 300 meters above sea level (masl) and the average temperature is 24 °C. It is the country's most important protected area of xerophytic vegetation, with a recorded 111 plant species, mostly native and endemic, with the *Mimosaceae* family being the most prominent, followed by the *Cactaceae* and *Bromeliaceae*. As for the fauna, the record consists of 159 species,

©2026, Universidad Politécnica Salesiana, Ecuador.

with birds being the most prominent group, comprising around 79 species (Union Internacional para la Conservacion de la Naturaleza IUCN, 2020). Due to its large size, the area also includes mangrove and floodplain grassland vegetation zones.

2.1 Analysis of vegetation status

For this analysis, the Normalized Difference Vegetation Index (NDVI) was applied, which is calculated by combining the reflectance values captured in the spectral range from red to near-infrared (Gonzaga-Aguilar, 2015), as explained in the following equation:

$$\mathrm{NDVI} = \frac{\mathrm{NIR} - \mathrm{R}}{\mathrm{NIR} + \mathrm{R}} \quad (1)$$

Where NIR is the atmospherically corrected reflectance corresponding to the near infrared; R is the atmospherically corrected reflectance corresponding to the red. SENTINEL-2B images were used for the months with the highest precipitation: January, February, March, April, May, and June 2018; the remaining months were excluded due to their seasonal dryness and the high percentage of cloud cover in the images. The NDVI was calculated for each image scene based on the satellite's bands 4 and 8. Using the various available satellite images and the quality mosaicking method—which involves spatially linking a set of image data (Eraso et al., 2022)—a monthly composite was generated for the months of January through June, and each pixel was assigned the maximum NDVI value. This process was carried out by adapting a specific script (available at http://www.gisandbeers.com/RRSS/Engine/Script-GEE-lista-indices-vegetacion.txt) on the Google Earth Engine (GEE) platform (see Figure 2). This tool stands out for its high processing capacity, which allows for the addition of more resources in parallel when analyzing the data (Gomes et al., 2020).

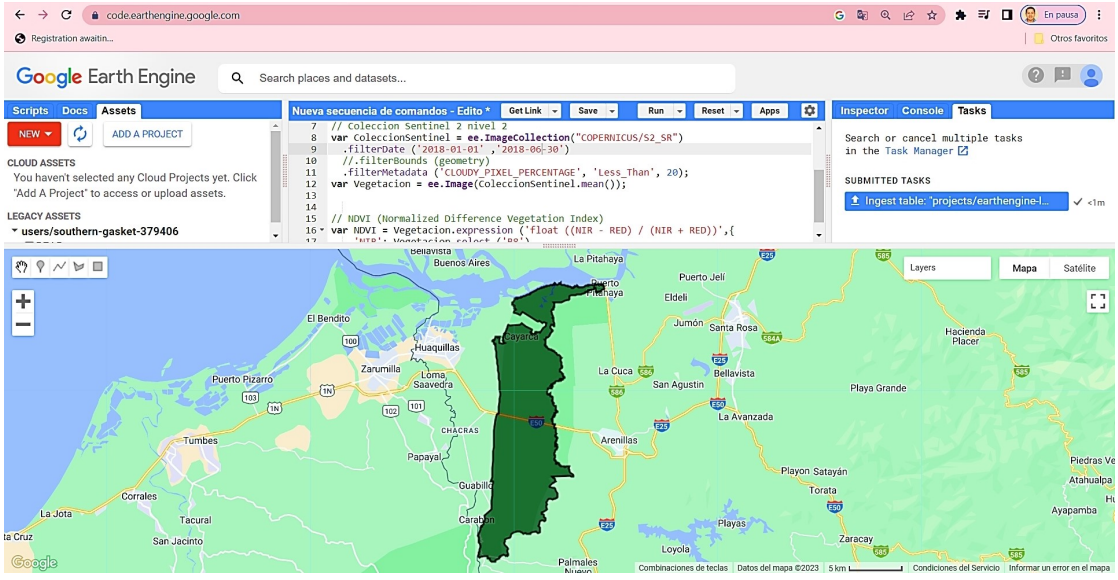


Figure 2. GEE platform interface, identifying the study area and NDVI processing.

Once the six monthly NDVI composites were obtained, the mean (average value) and maximum statistics were calculated; the latter was used to analyze the data range and find the largest value per cell across multiple rasters, resulting in two sets of new raster files (mean; January to June; and maximum; January to June). A zonal statistical operation was performed on each raster for the different ecosystems in the study area, creating four raster files for each statistic.

The defined ecosystem types correspond to: (1) Jama-Zapotillo lowland deciduous forest (Deciduous forest), (2) Jama-Zapotillo low forest and

©2026, Universidad Politécnica Salesiana, Ecuador.

deciduous shrubland (Deciduous shrub forest), (3) Jama-Zapotillo mangrove (Mangrove), and (4) Jama-Zapotillo lowland riparian floodplain grassland (Floodplain Grassland) (Ministerio del Ambiente del Ecuador MAE, 2013).

Finally, the created files were merged using the "Mosaic to New Raster" tool, determining the average NDVI of the mean and maximum values for each identified ecosystem. This process was carried out in ArcGIS version 10.2.

2.2 Analysis of vegetation risk factors

As established in the REAR Management Plan (Ministerio del Ambiente del Ecuador MAE, 2015), the main threats affecting the conservation of the dry forest are anthropogenic in origin: land tenure disputes; encroachment into the ecological reserve area; extraction of forest species; and increased pressures due to agricultural and aquaculture activities. Therefore, based on this criterion, a 1-km buffer zone was established outside the reserve, and five land cover and land use categories were considered as risk variables for vegetation, as follows: (1) Aquaculture zone, (2) Agricultural zone, (3) Livestock zone, (4) Population, and (5) Access roads, in accordance with the findings of Barber et al. (2014), who state that the factors most conducive to deforestation are the growth of settlements, the expansion of agricultural and aquaculture activities, proximity to roads and rivers, and soil capacity.

Population and road data were obtained from the National Information System (SNI) platform (Secretaría Nacional de Planificación, 2014). For roads, the following categories were considered: paved two-lane or wider roads, narrow unpaved roads, and summer roads; while for aquaculture, agriculture, and livestock land cover, Google Earth images were used, and each of the areas was digitized using QGIS 3.10 software. These were then cross-referenced with the Ministry of the Environment's (Ministerio del Ambiente del Ecuador MAE, 2018) land cover and land use map and reclassified in ArcGIS 10.2 software, resulting in a binary map. Subsequently, using the cost distance tool, the shortest weighted distance was determined for each land cover variable (De Smith et al., 2007), yielding distance rasters to the following zones: aquaculture, agriculture, livestock, population, and roads.

2.3 Statistical analysis

Based on the monthly NDVI composites, the average index was estimated for the entire vegetation cover of the REAR. As an initial statistical analysis, considering that different soil types and their characteristics are not always conducive to producing the nutrients necessary for healthy vegetation growth (Moreno et al., 2018), analysis of variance (one-way ANOVA) was used to analyze the potential disturbance effect on vegetation caused by different soil types and ecosystems (Cantón et al., 2020). This developed model allows for comparing the variances among the means of different groups (Liu and Wang, 2021). In this case, it explains whether the quadratic model is significant among the independent variables of ecosystems and soil order based on the dependent variable of NDVI response. Soil information was obtained from the geopedological mapping on the Ecuadorian Agriculture Portal (Ministry of Agriculture and Livestock–MAG, 2016). To analyze whether more than one variable influences or is correlated with the value of a third variable, the multiple linear regression model was applied to fit linear models, which allow us to determine in which of the REAR ecosystems vegetation is at greatest risk of disturbance in relation to independent threat variables such as distances to: (1) agricultural areas, (2) aquaculture, (3) livestock, (4) population, and (5) roads (Cayuela, 2010).

3 Results and Discussion

3.1 Vegetation status in the ecosystems and soil types of the REAR

Based on the results of this analysis, it was determined that within the REAR Ecological Reserve, the average NDVI for each of the ecosystems present ((1) Deciduous Forest, (2) Deciduous Shrub Forest, (3) Mangrove, and (4) Flooded Grassland), as defined by Ministerio del Ambiente del Ecuador MAE (2013), fluctuates within a range of -0.19568 to 0.85521, where values with an NDVI < 0 correspond to non-vegetation cover, and values close to the lower range (below 0) correspond to areas with greater anthropogenic pressure, causing degradation of the ecosystems' natural vegetation, while values close to the upper range indicate dense vegetation cover with low levels of anthropogenic pressure.

©2026, Universidad Politécnica Salesiana, Ecuador.

Research conducted in forests with characteristics similar to the REAR, such as the Cerro Blanco protective forest located in the Guayaquil canton, where NDVI values exceed 0.50—equivalent to dense and well-developed vegetation—has demonstrated the importance of its ecosystem services and the need to implement conservation measures, due to the anthropogenic threat surrounding it (Cervantes et al., 2022). In fact, most of the vegetation cover within the REAR (see Figure 3a) is an indicator of the effective conservation monitoring work carried out by its park rangers. This pattern is not unique to this region; globally, lower rates of deforestation are also observed within protected areas (Figueroa and Sánchez-Cordero, 2011).

Based on a study of the spatial dynamics of the REAR, with the aim of examining the behavior of outlier data points related to NDVI values in conjunction with variables from the four ecosystem types ((1) Deciduous forest, (2) Deciduous shrub forest, (3) Mangrove, and (4) Flooded grassland), and the six soil orders ((1) Miscellaneous soils, (2) Vertisol, (3) Entisol, (4) Alfisol, (5) Inceptisol, and (6) Aridisol) of the REAR, box plots were created. Figures 3b and 3c compile these graphs, where it was observed that most outliers (vertical lines) lie below the median (2nd quartile), i.e., they are values that are distant from the third quartile and first quartile, 1.5 times greater than the interquartile range (Montealegre, 2017). Likewise, an asymmetric distribution toward high values was observed between the NDVI response factor and the variables of the four ecosystem types, as well as an asymmetric distribution of the NDVI toward medium to high values across the six soil orders.

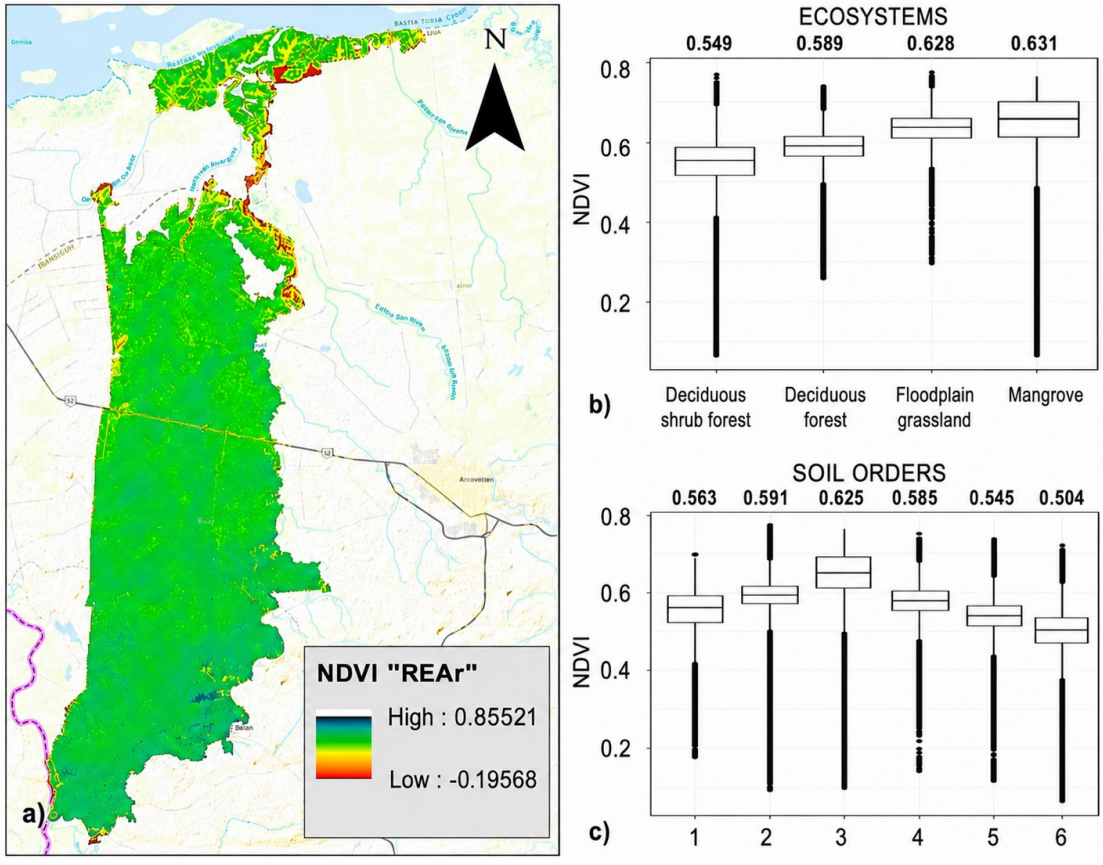


Figure 3. Vegetation status: a) Spatial distribution of the REAR's NDVI, b) box plot with NDVI averages by ecosystem, and c) box plot with NDVI averages by soil order

©2026, Universidad Politécnica Salesiana, Ecuador.

In Figure 3b, the size of the boxes reveals that the highest NDVI value had a median of 0.631 in the Mangrove ecosystem, covering an area of 1 239 ha, accepting small areas located in the northeast at the edges of the forest patches, a sector adjacent to aquaculture activities, where the lowest NDVI values (NDVI < 0.1) are recorded, indicating a higher level of disturbance and poor vegetation condition. According to Torres et al. (2014), this phenomenon is caused by the proximity of certain patches to disturbed areas, directly impacting the ecological conditions of the vegetation. On the other hand, vegetation with high NDVI values, with medians above 0.628, is also located in the floodplain grassland ecosystem, suggesting that the 184-hectare area comprises vigorous natural vegetation, such that various threats—including population growth, deforestation, and the establishment of agricultural and livestock activities (Aldás, 2019)—do not have a significant influence on the area.

Regarding the NDVI values for the Deciduous Forest and Deciduous Shrub Forest, the size of the median boxes was smaller, corresponding to averages of 0.589 and 0.549, respectively, implying that anthropogenic pressure on the natural vegetation in these ecosystems is significant in certain sectors. For example, for the Deciduous Forest, with an area of 3 597 ha, the areas with the highest degree of disturbance are located at the edges of the remaining vegetation patches in the southwestern sector. In contrast, for the largest ecosystem (6 773 ha), the Deciduous Shrub Forest, the areas under the greatest threat are concentrated at the edges of the remaining vegetation patches in the northern, eastern, and western sectors. This is due to direct contact with areas of agricultural and aquaculture activity, as well as the areas adjacent to the main road and trails that crisscross the zone.

In Figure 3c, for the soil types ((1) Miscellaneous soils, (2) Vertisol, (3) Entisol, (4) Alfisol, (5) Inceptisol, and (6) Aridisol), the highest median NDVI value was dominant for Entisol, with an average of 0.625, followed by Vertisol and Alfisol, with values of 0.591 and 0.585, respectively. In contrast, median values in the moderate range were found in Miscellaneous soils, with an average of 0.563, followed by Inceptisol, with 0.545; for the Aridisol soil type, the average NDVI was the lowest at 0.504. Across the entire study area, 72 % of Entisol soils were located in the mangrove ecosystem, specifically covering 92 % of its surface area, followed by 8 % of Vertisol and Miscellaneous soils. Leiva et al. (2009), in their research in Costa Rica, argue that Entisols, being in a chronosequence of physicochemical changes, could cause water stress in plants.

For the Deciduous Forest, the soils with the greatest coverage were: Alfisol at 56 % and Vertisol at 32 %, followed by Entisol and Inceptisol at 9 % and 3 %, respectively. Meanwhile, in the Deciduous Shrub Forest, due to its extent and geographic location, the area was mostly covered by Inceptisol and Alfisol soils (38 % and 28 %, respectively), followed by Aridisol (18 %), Vertisol (14 %), and 2 % between Entisol and Miscellaneous soils. The Flooded Grassland consisted of 58 % Vertisol and 42 % Alfisol. The diversity of soils present in the Reserve may be due to certain factors such as slope; in flat areas, the process of localized accumulation of water and nutrients is more effective than on steep slopes (Clark, 2002). The seasonal climate in areas with very low precipitation and high temperatures would favor aridisols (Botta et al., 2019). The likely presence of volcanic rocks would be the formers of vertisols and entisols, whereas inceptisols and alfisols are more conducive to undulating and mountainous landscapes (Hartemink and Bockheim, 2013).

Table 1. ANOVA of interaction between NDVI and ecosystem variables and soil orders

Variables	Degrees of freedom	Mean squares	Sum of squares	F-value	Pr (>F) (*p*-value)
Ecosystems	3	869.5	289.83	107 470	<2e-16 ***
Soil order	5	1 313.2	218.86	81 154	<2e-16 ***
Two-factor interaction	5	78.2	13.04	4 834	<2e-16 ***

Significance codes: 0 '***' 0.001 '**' 0.01 '*' 0.05 '.'.

©2026, Universidad Politécnica Salesiana, Ecuador.

Through the calculation of the means in the ANOVA (see Table 1), significant differences were found between the NDVI response factor and the ecosystem and soil order variables. It was shown that the *F*-value for the two study variables was significant at the $\alpha = 0.05$ significance level, since Pr $> F$ (probability greater than the calculated F) is equal to $< 2 \times 10^{-16}$, the latter value being less than 0.05. The interaction variable of the two factors showed the same level of significance, thus determining that both soil and ecosystem, as well as their interactions, are highly significant; i.e., the ecosystem and soil condition the NDVI response, and the effect of each depends on the other. In this case, soil has the greatest influence; all ecosystems exhibit a nearly identical response with minor differences in the Flooded Grassland and Mangrove ecosystems, and their productivity is highly conditioned by soil (see Figure 4), relative to the results obtained by Mesa-Sierra et al. (2022), where NDVI and soil fertility values were uniformly distributed between 0.21 and 0.34, considered unhealthy vegetation due to its location in regions with high anthropogenic impact and ecological degradation.

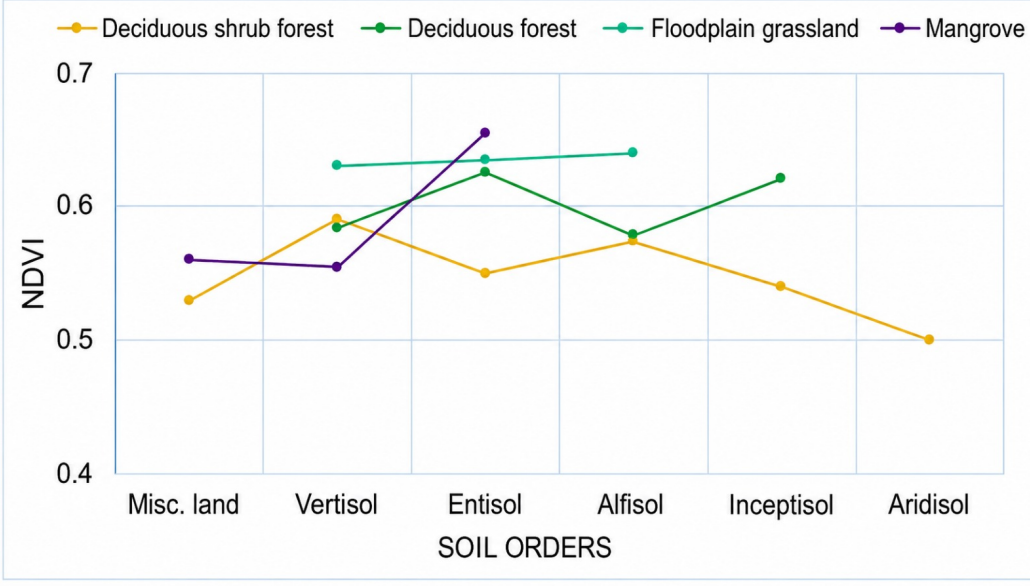


Figure 4. Interaction of NDVI averages with ecosystems and soil orders in the REAR

3.2 Factors and degree of risk to vegetation in the REAR

The data obtained in this analysis highlighted the influence of the different ecosystems within the REAR on the interactions and relationships between the various land covers and land uses located in the area of influence—i.e., factors that jeopardize the condition and quality of the vegetation.

The analysis revealed that of the total area of the four ecosystems studied ((1) Deciduous forest, (2) Deciduous shrub forest, (3) Mangrove, and (4) Flooded Grassland), 18.7 % of the vegetation cover is at high risk, with the greatest disturbance and threat occurring along the northwest and northeast edges of the Deciduous Shrub Forest and the southwest edge of the Deciduous Forest; a similar pattern is observed at the entrances to the main and secondary roads. The at-risk areas for the two ecosystems were 2 438 and 950 ha, equivalent to 36 % and 26.4 %, respectively. In contrast, for the Mangrove ecosystem, the areas of greatest variability are located where the ecosystem borders shrimp aquaculture activity, with a low-risk area of 126 ha, corresponding to 10.2 %. The ecosystem that did not present a significant risk was the floodplain grassland, whose value reached 2 %, equivalent to 4 ha (see Figure 5).

©2026, Universidad Politécnica Salesiana, Ecuador.

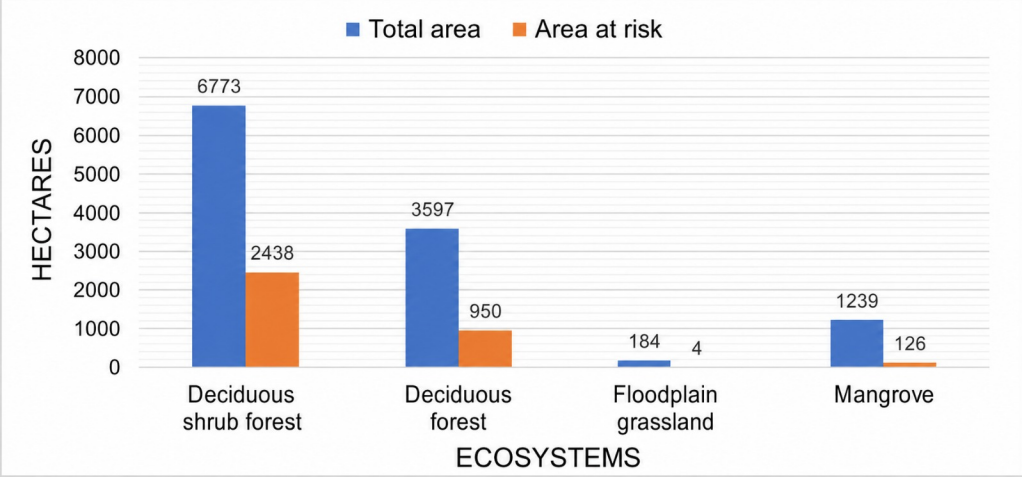


Figure 5. Degree of risk to the vegetation of the REAR ecosystems

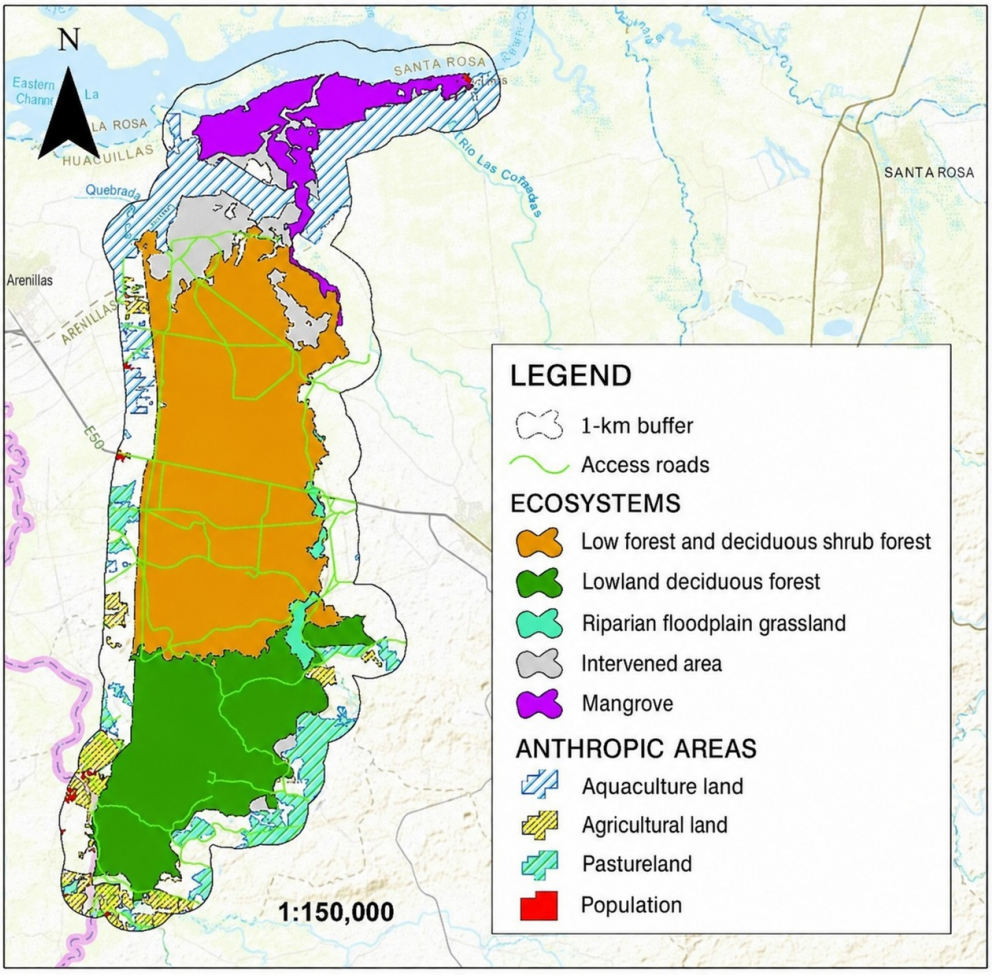


Figure 6. Land cover and land use in the REAR's area of influence

©2026, Universidad Politécnica Salesiana, Ecuador.

Figure 6 shows that the dominant land cover in the REAR's area of influence corresponds to aquaculture zones, covering 1 994 ha, followed by livestock farming, covering 1,137 ha, and agriculture, covering 657 ha. The land cover with the smallest area corresponds to population settlements, covering 46 ha. The main access roads within and outside the REAR covered a total length of 148 km.

Table 2. Coefficients obtained from the multiple linear regression model

Distance of variables	**Shrubland deciduous**		**Forest deciduous**		**Grassland floodplain**		**Mangrove**	
	Beta	*p*-value	Beta	*p*-value	Beta	*p*-value	Beta	*p*-value
Aquaculture	**0.596**	0.000	0.017	0.000	0.030	0.000	**0.234**	0.000
Agricultural	**0.221**	0.000	**0.345**	0.000	**0.188**	0.000	**-0.553**	0.000
Livestock	**0.151**	0.000	**0.145**	0.000	**-0.334**	0.000	**-0.480**	0.000
Population	**0.123**	0.000	0.083	0.000	-0.060	0.160	**0.180**	0.000
Roads	0.016	0.000	**0.106**	0.000	0.056	0.000	0.040	0.000
R^2	**0.360**		**0.264**		**0.020**		**0.102**	

In Table 2, based on the model established by Sierra (2013), we sought to estimate the risk of change in vegetation cover for each deforestation factor, such as distances to aquaculture, agricultural, livestock, population, and road areas. These deforestation variables showed the same level of significance, excepting the population variable in the Flooded Grassland ecosystem, where the p-value $= 0.000$ is less than the significance level $\alpha = 0.05$; i.e., the distances of the variables influence the response of vegetation status in the study ecosystems to a greater or lesser degree. The Beta values corresponded to the model coefficients, which represent the elasticity of the tendency for the vegetation cover of a site with coordinates to be converted to another land use. In contrast, R^2 as a coefficient of determination explains how much of a factor's variability can be attributed to its relationship with another related factor; i.e., it quantifies the model's goodness of fit, allowing an approximation of the deforested fraction of each REAR ecosystem. This means that R^2 values for 100 % of the cells with that value indicate a risk of threat to vegetation cover in 36 % of Deciduous Shrub Forest, 26.4 % of Deciduous Forest, 2 % of Flooded Grassland, and 10.2 % of Mangrove.

It was found that the variable for aquaculture zones exhibited positive beta coefficients in all four ecosystems, indicating a higher probability of change in vegetation in the deciduous shrub forest, followed by a moderate probability of change in the mangrove ecosystem. Its values of 0.596 and 0.234 demonstrated that the variable for distance from aquaculture zones is related to the condition and health of the vegetation in the two ecosystems, a pattern that does not occur with the same intensity in the Deciduous Forest and Flooded Grassland (see Figure 6). The increase in intensive aquaculture activity in recent years in the northwestern part of the Reserve has occupied large areas, where market forces and deficient agricultural policy have contributed to this productive growth (Agila and Lalangui, 2019). A similar finding is revealed in the research by Faruque et al. (2022), which notes an increase in aquaculture area relative to agricultural area during the 1990–2020 period, a transformation that could negatively impact the mangrove forests in southwestern Bangladesh.

Regarding the agricultural area variable, positive beta coefficients were found in the Deciduous Forest, Deciduous Shrub Forest, and Flooded Grassland ecosystems; their values of 0.345, 0.221, and 0.188 indicate a moderate to low probability of forest change, respectively, i.e. the greater the distance from agricultural activities, the lower the forest loss will be. In the case of the Deciduous Shrub Forest ecosystem, the probability of change could be contradictory, since despite the proximity of agricultural areas, this activity is regulated under a sustaina-

©2026, Universidad Politécnica Salesiana, Ecuador.

ble production plan, resulting from the concession of nearly 3 800 ha of land granted in 2014 by the State to producer groups in the area (Ministerio del Ambiente del Ecuador MAE, 2015). For the Mangrove ecosystem, the coefficient value was negative (-0.553), indicating an uncertain probability of vegetation change due to agricultural activities.

For the livestock area variable, the analysis reveals an average Beta coefficient value of 0.148 for the Deciduous Forest and Deciduous Shrub Forest ecosystems, indicating a moderate probability of change in their forest cover. According to Hidalgo et al. (2020), the increase in livestock activity depends on the geography and climate, particularly in the Deciduous Forest, with approximately 95 % of livestock farming occurring in the border area of the southeastern sector of the REAR. On the other hand, for the Flooded Grassland and Mangrove ecosystems, the Beta coefficient values were negative at -0.334 and -0.480, respectively, indicating an indirect relationship that suggests the vegetation in these areas faces no significant risk from grazing activities.

The variable of distance to settlements also influenced risk, particularly in the Deciduous Shrub Forest and Mangrove ecosystems. Their Beta coefficient values of 0.123 and 0.180, respectively, indicate a moderate probability of localized landscape change along the edges of remaining forest patches. The socioeconomic status of the population, linked to illiteracy and low wages, could be the cause of these changes (Cruz et al., 2017; Pineda et al., 2009). According to Figure 6, the settlement closest to the mangrove ecosystem is Pitahaya in the north. In contrast, for the lowland forest and deciduous shrubland, the villages of Cooperativa Valdivia, El Cruce, El Telégrafo, El Mango, and Carcabón are located in the south. The soil suitability characteristics of these populated areas have served as attractions for progressive human settlement. It is important to note that the Reserve contains no residential settlements within its boundaries; i.e., there is no human impact within the Reserve. In line with the findings of Baig et al. (2022), the persistent degradation of unprotected forest cover in Selangor, Malaysia, is closely linked to the expansion of human settlements and land conversion for agricultural purposes, identified as the determining factors in land-use transition.

The beta coefficient for the variable "distance to roads" was positive in all four ecosystems (see Table 2); however, the values for the Deciduous Shrub Forest, Flooded Grassland, and Mangrove ecosystems revealed a very low probability of change in vegetation. In contrast, for the Deciduous Forest ecosystem, the probability of change is significant, with a value of 0.106. The construction of main roads allows people from neighboring communities to enter the forest, creating new trails for the purpose of logging or clearing land to establish agricultural areas (Delgado, 2012; García-Villacorta, 2009). This pattern is largely located in the southwest of the Reserve, while in the eastern sector, disturbance and threats have not been significant due to limited accessibility caused by steep slopes and high altitude. According to the findings of Qian et al. (2022) derived from their impact model, ecological risks at the landscape level are conditioned by a multivariate interaction. In this regard, distance from anthropogenic elements, land use, slope, and precipitation emerge as the primary determinants of these dynamics. Conversely, our study did not consider the latter two factors because they have no direct connection to human-induced changes; however, we deemed it important to relate slope and precipitation to aspects of other ecosystem services, such as water quality.

4 Conclusions

The analysis of vegetation indices (NDVI) using Sentinel-2B satellite imagery allowed us to estimate the condition and health of natural vegetation in the four ecosystems (deciduous forest, deciduous shrubland, mangrove, and floodplain grassland) that make up the REAR. The average values of the indices obtained differed for each zone. The highest values were recorded in the Flooded Grassland and Mangrove ecosystems, while the Deciduous Shrub Forest and Deciduous Forest ecosystems had low values, indicating greater disturbance and threat to vegetation cover. This could be due to the optimal fertility conditions of their soils, as well as atmospheric conditions and the progressive human settlement that seeks to establish agricultural and aquaculture activities in the area every day.

©2026, Universidad Politécnica Salesiana, Ecuador.

The statistical interaction of the average NDVI with ecosystem variables and soil suitability allowed us to establish that these variables condition the NDVI response, determining that the effect of each depends on the other. This pattern resembles the reality of the disturbed ecosystem within the REAR, particularly in the northwestern sector bordering the Deciduous Shrub Forest, where progressive soil degradation caused by intensive aquaculture and agricultural activity is altering its physical, chemical, and biological properties—aspects critical for healthy vegetation development.

Regarding the analysis of risk factors and levels, it was found that the eastern and western edges of the Deciduous Shrub Forest and Deciduous Forest ecosystems present high probabilities of landscape change. This increased risk is related to the ease with which people can establish productive activities within the buffer zone. Specifically, the buffer zone—despite being regulated by the state—does not comply with the stipulated requirement to protect the natural resources of protected areas.

It is important to note that if the areas adjacent to the REAR are not protected, the little remaining forest will disappear, limiting connectivity with other natural forests; for this reason, it is important that the Reserve's management plan take high-risk zones into account through the efficient implementation of good agricultural, livestock, and aquaculture practices within its area of influence, since ensuring their proper functioning could contribute to the creation of biological corridors linking the municipal conservation area "El Conchal" in the northern sector and the "Río Arenillas-Presa Tahuín" protective forest on the southeastern side.

Acknowledgments

To the Vice-Rectorate for Research at the Technical University of Machala for the funding awarded to the Research Group for Conservation (INCON). Likewise, we thank the Provincial Directorate of the Environment of El Oro, especially the REAR park rangers, for the support provided to the project "Estimation of the physical and chemical properties of soils with an ecosystem-based approach in the restoration area of the Arenillas Ecological Reserve," which, under authorization No. 007-2017-IC-S-DPAEO-MAE, dated August 14, 2017, allowed us to carry out and conclude the research in a meaningful manner.

Declaration on the use of Artificial Intelligence

The authors DECLARE that, during the preparation of the manuscript entitled "Land cover and land use factors associated with the risk of vegetation degradation in the Arenillas Ecological Reserve", no generative artificial intelligence tools or automated assistance systems were used for writing, data analysis, interpretation of results, content generation, translation, or manuscript editing.

The authors assume full responsibility for the content, originality, integrity, and final version of the manuscript.

Author Contributions

J.E.M.M.: Conceptualization, Data curation, Investigation, Methodology, Project administration, Software, and Writing – original draft. **H.E.A.L.:** Formal analysis, Supervision, and Writing – review & editing. **D.A.P.L.:** Investigation, Resources, Validation, and Visualization. **A.D.L.F.:** Data curation, Formal analysis, and Writing – review & editing.

References

Agila, R., and Lalangui, M. (2019, octubre). Análisis de los factores estratégicos que inciden en la producción camaronera ecuatoriana. En *Xxiv congreso internacional de contaduría, administración e informática* (pp. 1–29). Ciudad Universitaria, Ciudad de México, México.

Aldás, A. (2019). *Análisis de la dinámica temporal del índice de vegetación de diferencia normalizada (NDVI) para los años 1986, 2001 y 2017 en la reserva ecológica cotacachi cayapas, imbabura, mediante el uso de google earth engine* (Tesis de grado). Pontificia Universidad Católica del Ecuador, Quito, Ecuador.

Armenteras, D., and Rodríguez, N. (2014). Dinámicas y causas de deforestación en bosques de latino

©2026, Universidad Politécnica Salesiana, Ecuador.

américa: una revisión desde 1990. *Colombia Forestal*, *17*(2), 233–246. Online: https://shortlink.uk/1rmld

Baig, M. F., Mustafa, M. R. U., Baig, I., Takaijudin, H. B., and Zeshan, M. T. (2022). Assessment of land use land cover changes and future predictions using CA-ANN simulation for selangor, malaysia. *Water*, *14*(3), 402. Online: https://doi.org/10.3390/w14030402

Barber, C. P., Cochrane, M. A., Souza, C. M., and Laurance, W. F. (2014). Roads, deforestation, and the mitigating effect of protected areas in the amazon. *Biological Conservation*, *177*, 203–209. Online: http://dx.doi.org/10.1016/j.biocon.2014.07.004

Botta, G. F., Bienvenido, J. F., Antille, D. L., Rivero, E. R. D., Contessotto, E. E., Ghelfi, D. G., … Pelizzari, F. M. (2019). Effect of traffic with a light-weight tractor on physical properties of an aridisol soil in almeria, spain. *Revista de la Facultad de Ciencias Agrarias*, *51*(2), 270–279. Online: https://shortlink.uk/1wNro

Cantón, Y., Chamizo, S., Rodriguez-Caballero, E., Lázaro, R., Roncero-Ramos, B., Román, J. R., and Solé-Benet, A. (2020). Water regulation in cyanobacterial biocrusts from drylands: Negative impacts of anthropogenic disturbance. *Water*, *12*(3), 720. Online: https://doi.org/10.3390/w12030720

Carey, C., Dudley, N., and Stolton, S. (2000). *Squandering paradise?: The importance and vulnerability of the world's protected areas*. Gland, Switzerland: WWF-World Wide Fund For Nature International.

Cayuela, L. (2010). *Modelos lineales generalizados (GLM)*. Granada, España: EcoLab, Centro Andaluz de Medio Ambiente, Universidad de Granada.

Cervantes, F., Imbaquingo, J., and Leon, D. (2022). Valoración económica de los servicios ecosistémicos del bosque protector cerro blanco, guayaquil ecuador. *Revista Geoespacial*, *19*(1), 50–63. Online: https://shortlink.uk/1wNrr

Clark, D. B. (2002). *Los factores edáficos y la distribución de las plantas*. Cártago, Costa Rica: LUR.

Cruz, M. A., Rodríguez, D. A., Villanueva, A., and Santillán, J. (2017). Factores sociales de uso del suelo y vegetación asociados a los incendios forestales en hidalgo. *Revista Mexicana de Ciencias Forestales*, *8*(41), 139–163. Online: https://shortlink.uk/1wNru

Delgado, V. (2012). La responsabilidad civil extracontractual por el daño ambiental causado en la construcción u operación de las carreteras. *Revista de Derecho (Valdivia)*, *25*(1), 47–76. Online: https://dx.doi.org/10.4067/S0718-09502012000100003

De Smith, M., Goodchild, M., and Longley, P. (2007). *Geospatial analysis: A comprehensive guide to principles, techniques and software tools* (2nd ed.). Troubador Publishing Ltd.

Eraso, O., Badia, A., and Gisbert, M. (2022). Google earth engine aplicado al monitoreo de superficies quemadas y cambios de coberturas y usos del suelo. *GeoFocus: Revista Internacional de Ciencia y Tecnología de la Información Geográfica*, *29*, 89–113. Online: https://dx.doi.org/10.21138/GF.764

Faruque, M. J., Vekerdy, Z., Hasan, M. Y., Islam, K. Z., Young, B., Ahmed, M. T., … Kundu, P. (2022). Monitoring of land use and land cover changes by using remote sensing and GIS techniques at human-induced mangrove forests areas in bangladesh. *Remote Sensing Applications: Society and Environment*, *25*, 100699. Online: https://doi.org/10.1016/j.rsase.2022.100699

Figueroa, F., and Sánchez-Cordero, V. (2011). Evaluación de la efectividad de las áreas protegidas para contener procesos de cambio en el uso del suelo y la vegetación. ¿un índice es suficiente? *Revista Mexicana de Biodiversidad*, *82*(3), 951–963. Online: https://shortlink.uk/1rmln

García-Villacorta, R. (2009). Diversidad, composición y estructura de un hábitat altamente amenazado: los bosques estacionalmente secos de tarapoto, perú. *Revista Peruana de Biología*, *16*(1), 81–92. Online: https://shortlink.uk/1wNry

Gomes, V., Queiroz, G., and Ferreira, K. (2020). An overview of platforms for big earth observation data management and analysis. *Remote Sensing*, *12*(8), 1253. Online: https://doi.org/10.3390/rs12081253

©2026, Universidad Politécnica Salesiana, Ecuador.

Gonzaga-Aguilar, C. (2015). Aplicación de índices de vegetación derivados de imágenes satelitales para análisis de coberturas vegetales en la provincia de loja, ecuador. *Revista CEDAMAZ*, *5*(1), 30–41. Online: https://shortlink.uk/1rmlt

Hartemink, A., and Bockheim, J. (2013). Soil genesis and classification. *Catena*, *104*, 251–256. Online: https://doi.org/10.1016/j.catena.2012.12.001

Hidalgo, M., Vargas, O., and Vite, H. (2020). Análisis situacional de la actividad ganadera en la parroquia palmales del cantón arenillas. *Revista Metropolitana de Ciencias Aplicadas*, *3*(2), 124–130. Online: https://shortlink.uk/1wNrF

Instituto de Ecología Aplicada ECOLAP, and Ministerio del Ambiente del Ecuador MAE. (2007). *Guía del patrimonio de Áreas naturales protegidas del ecuador*. Quito, Ecuador: ECOFUND, FAN, DarwinNet, IGM.

Leiva, J., Rocha, O. J., Mata, R., and Gutiérrez, M. (2009). Cronología de la regeneración del bosque tropical seco en santa rosa, guanacaste, costa rica: II. la vegetación en relación con el suelo. *Revista de Biología Tropical*, *57*(3), 817–836. Online: https://shortlink.uk/1wNrJ

Liu, Q., and Wang, L. (2021). t-test and ANOVA for data with ceiling and/or floor effects. *Behavior Research Methods*, *53*(1), 264–277. Online: https://doi.org/10.3758/s13428-020-01407-2

Maza-Maza, J. E., Sánchez-Asanza, A. W., Añazco Loaiza, H. E., and García-Ochoa, J. A. (2021). Estudio de las características físico-químicas del suelo en áreas prioritarias de la reserva ecológica arenillas. *Revista Científica Agroecosistemas*, *9*(3), 30–40. Online: https://shortlink.uk/1rmlB

Mesa-Sierra, N., de la Peña Domene, M., Campo, J., and Giardina, C. (2022). Restauración de bosques secos tropicales mexicanos: una revisión nacional. *Sustentabilidad*, *14*, 3937. Online: https://doi.org/10.3390/su14073937

Ministerio del Ambiente del Ecuador MAE. (2013). *Sistema de clasificación de los ecosistemas del ecuador continental*. Quito, Ecuador: Ministerio del Ambiente del Ecuador.

Ministerio del Ambiente del Ecuador MAE. (2015). *Plan de manejo de la reserva ecológica arenillas* (Inf. Téc.). Quito, Ecuador: Ministerio del Ambiente del Ecuador.

Ministerio del Ambiente del Ecuador MAE. (2018). *Capa cartográfica de cobertura y uso de la tierra 2018 del ecuador continental [shapefile].* Sistema Nacional de Monitoreo de Bosques. Online: http://ide.ambiente.gob.ec/mapainteractivo/

Mittermeier, R. A., Turner, W. R., Larsen, F. W., Brooks, T. M., and Gascon, C. (2011). Global biodiversity conservation: The critical role of hotspots. En F. E. Zachos and J. C. Habel (Eds.), *Biodiversity hotspots: Distribution and protection of conservation priority areas* (pp. 3–22). Berlin, Heidelberg: Springer Berlin Heidelberg. Online: https://doi.org/10.1007/978-3-642-20992-5_1

Montealegre, F. (2017). *Evaluación espacio temporal de la productividad agrícola con índices de vegetación de diferencias normalizadas (NDVI) como herramienta para el ordenamiento territorial. caso de estudio: cuenca alta del arroyo napaleofú, provincia de buenos aires, argentina* (Tesis de Grado). Universidad Nacional de la Plata, La Plata, Argentina.

Moreno, A., Carda, V., Reyes, J. L., and Cano, P. (2018). Rizobacterias promotoras del crecimiento vegetal: una alternativa de biofertilización para la agricultura sustentable. *Revista Colombiana de Biotecnología*, *20*(1), 68–83. Online: https://doi.org/10.15446/rev.colomb.biote.v20n1.73707

Organización de las Naciones Unidas para la Agricultura y la Alimentación FAO. (2020). *El estado de los bosques del mundo 2020: Los bosques, la biodiversidad y las personas*. Roma, Italia: FAO.

Pineda, N. B., Bosque, J., Gómez, M., and Plata, W. (2009). Análisis de cambio del uso del suelo en el estado de méxico mediante sistemas de información geográfica y técnicas de regresión multivariantes: Una aproximación a los procesos de deforestación. *Investigaciones Geográficas*, *69*, 33–52. Online: https://shortlink.uk/1wNrV

Qian, Y., Dong, Z., Yan, Y., and Tang, L. (2022). Ecological risk assessment models for simulating impacts of land use and landscape pattern on ecosystem services. *The Science of the Total Environment*, *833*, 155218. Online: https://doi.org/10.1016/j.scitotenv.2022.155218

©2026, Universidad Politécnica Salesiana, Ecuador.

Ramírez, V., Aranda, L., and Rico-Gray, V. (2018). La resiliencia del bosque seco tropical: un seguro de vida para su conservación. CONABIO. *Biodiversitas*, *137*, 12–16. Online: https://shortlink.uk/1rmlN

Riofrío, I. (2018). *El bosque seco, una joya amenazada en el ecuador.* Mongabay. Online: https://es .mongabay .com / 2018 / 07 / ecuador -bosque -seco/ (Publicado el 05 de julio de 2018)

Ruiz, M. (2018). *Evaluación de la calidad y riesgo de la vegetación del bosque protector la ceiba y su área de influencia* (Tesis de grado). Universidad Técnica Particular de Loja, Loja, Ecuador.

Secretaría Nacional de Planificación. (2014). *Archivos de información geográfica.* Sistema Nacional de Información. Online: https://sni.gob.ec/coberturas (Accedido el 31 de diciembre de 2014)

Sierra, R. (2013). *Patrones y factores de deforestación en el ecuador continental, 1990-2010. y un acercamiento a los próximos 10 años*. Quito, Ecuador: Conservación Internacional Ecuador y Forest Trends.

Sudmanns, M., Tiede, D., Lang, S., Bergstedt, T., Trost, G., and Augustin, H. (2020). Big earth data: disruptive changes in earth observation data management and analysis? *International Journal of Digital Earth*, *13*(7), 832–850. Online: https://doi.org/10.1080/17538947.2019.1585976

Tapia-Armijos, M., Homeier, J., Espinosa, C., Leuschner, C., and de la Cruz, M. (2015). Deforestation and forest fragmentation in south ecuador since the 1970s – losing a hotspot of biodiversity. *PLoS ONE*, *10*(9), e0133701. Online: https://doi.org/10.1371/journal.pone.0142359

Torres, R. C., Giorgis, M. A., Trillo, C., Volkmann, L., Demaio, P., Heredia, J., and Renison, D. (2014). Post-fire recovery occurs overwhelmingly by resprouting in the chaco serrano forest of central argentina. *Austral Ecology*, *39*(3), 346–354. Online: https://doi.org/10.1111/aec.12084

Union Internacional para la Conservacion de la Naturaleza IUCN. (2005). Benefits beyond boundaries: Proceedings of the vth IUCN world parks congress. En *The vth iucn world parks congress.* Durban, South Africa.

Union Internacional para la Conservacion de la Naturaleza IUCN. (2020). *Red list quadrennial report 2017-2020* (Inf. Téc.). IUCN.

Wright, S. J., and Muller-Landau, H. C. (2006). The future of tropical forest species. *Biotropica*, *38*(3), 287–301. Online: https://doi.org/10.1111/j.1744-7429.2006.00154.x

©2026, Universidad Politécnica Salesiana, Ecuador.

La Granja: Revista de Ciencias de la Vida
pISSN:1390-3799; eISSN:1390-8596
https://doi.org/10.17163/lgr.n44.2026.10

Artículo científico / Scientific paper

Environmental Sciences

CC BY NC SA

Evaluation of the Composition of Settleable Aerosols in the Urban Area of Espíndola Canton, Loja Province, Ecuador

Evaluación de la composición de aerosoles sedimentables en el área urbana del cantón Espíndola, provincia de Loja, Ecuador

David Emmanuel del Pozo, María de los Angeles Alvarez* and Bryan Gabriel Valle

Universidad Técnica Particular de Loja, Ecuador. [https://ror.org/04dvbth24]

*Corresponding author: mdalvarez8@utpl.edu.ec, mddel@utpl.edu.ec

Article received on April 16th, 2025. Accepted, after review, on July 9th, 2025. Published on September 1st, 2026.

Abstract

The present study analyzes the composition and concentration of settleable particulate matter (SPM) in the urban area of the Espíndola canton. It is based on the limited information available regarding air quality in small rural communities, where vehicular emissions and material extraction represent sources of pollution. The objective is to determine the concentration and chemical composition of SPM, specifically the presence of heavy metals such as cadmium (Cd), chromium (Cr), lead (Pb), and copper (Cu), comparing the SPM concentration results with Ecuador's environmental regulation (Ministerial Agreement 097-A), which establishes a limit value of 1 mg/cm^2 over 30 days. The methodology involved systematic sampling over five months at five points within the urban area. Using gravimetric methods and chemical analyses, results were obtained based on SPM concentrations. Although levels were below the maximum permissible limit, the presence of heavy metals was identified in the SPM samples. The distribution of these metals showed a stronger correlation with monthly variations than with land use. It is concluded that, while SPM levels comply with environmental regulations, the presence of heavy metals cannot be ruled out. These findings highlight the importance of continuously monitoring air quality in rural regions such as Espíndola, where human activities, although limited, may contribute to atmospheric pollution and the dispersion of toxic elements.

Keywords: Settleable particulate matter, heavy metals, air pollution, gravimetric methods.

©2026, Universidad Politécnica Salesiana, Ecuador.

Resumen

El presente trabajo analiza la composición y concentración del material particulado sedimentable (MPS) en el área urbana del cantón Espíndola, con base en la limitada información sobre la calidad del aire en pequeñas comunidades rurales donde las emisiones vehiculares y la extracción de materiales representan fuentes de contaminación. Se planteó como objetivo determinar la concentración y composición química del MPS, específicamente la presencia de metales pesados como el cadmio (Cd), cromo (Cr), plomo (Pb) y cobre (Cu), comparando los resultados de las concentraciones de MPS con la normativa ambiental del Ecuador (Acuerdo Ministerial 097-A), que establece un valor límite de 1 mg/cm^2 por 30 días. La metodología empleó un muestreo sistemático durante cinco meses en cinco puntos del área urbana; por medio de métodos gravimétricos y análisis químicos se obtuvieron los resultados con base en las concentraciones de MPS, los cuales, pese a encontrarse por debajo del límite máximo permisible, identificaron la presencia de metales pesados en las muestras. La distribución de estos metales mostró mayor correlación con las variaciones mensuales que con el uso del suelo. Se concluye que, si bien los niveles de MPS cumplen con la normativa ambiental, no se exime la presencia de metales pesados. Estos hallazgos resaltan la relevancia de monitorear continuamente la calidad del aire en regiones rurales como Espíndola, donde las actividades humanas, aunque limitadas, pueden contribuir a la contaminación atmosférica y a la dispersión de elementos tóxicos.

Palabras clave: Material particulado sedimentable, metales pesados, contaminación atmosférica, métodos gravimétricos.

Suggested citation: del Pozo, D. E., Álvarez, M. A. and Valle, B. G. (2026). Evaluation of the Composition of Settleable Aerosols in the Urban Area of Espíndola Canton, Loja Province, Ecuador. La Granja: Revista de Ciencias de la Vida. Vol. 44(2):167-180. https://doi.org/10.17163/lgr.n44.2026.10.

Orcid IDs:

David Emmanuel del Pozo Meza: https://orcid.org/0009-0008-9162-7410
María de los Angeles Alvarez Correa: https://orcid.org/0009-0008-5236-9498
Bryan Gabriel Valle Esparza: https://orcid.org/0009-0002-0689-7640

©2026, Universidad Politécnica Salesiana, Ecuador.

1 Introduction

Air quality is a global issue that is not limited to a specific region, as air knows no geographical boundaries (Pérez Cárdenas, 2017). Air pollutants, such as settleable particulate matter (SPM), can be carried by the wind and affect less polluted areas, causing adverse effects on human health, ecosystems, and food security (OPS, 2018). SPM is defined, according to Annex 4 of Ministerial Agreement 097-A, as solid or liquid particles that, due to the force of gravity, settle on a horizontal surface, and whose size allows them to be collected in static devices over a specific period.

These particles are associated with various sources, both natural and anthropogenic. Among the former are pollen, spores, wildfires, and volcanic eruptions (Suárez and Vásquez, 2017). However, human activities, such as the combustion of fossil fuels, industrial activities, and vehicular transportation, generate the largest number of pollutants (Morocho, 2024).

Settleable particulate matter (SPM) is an important component of air pollution (P. Santillán et al., 2021). This includes particles with an aerodynamic diameter greater than 10 micrometers ($PM_{>10}$), which, due to their size, do not remain suspended in the air for long, quickly settling on the ground and other surfaces (Suárez and Vásquez, 2017). Its chemical composition includes both heavy metals (Cd, Cr, Pb, Cu, Mg, Zn, Al, Ni, Mn) and anions (chlorides, nitrates, and sulfates), which pose a significant risk to human health and the environment due to their toxicity and ability to accumulate in the food chain (Reyes et al., 2016; Mejía et al., 2018).

In Ecuador, air quality issues affect both large cities and rural areas with less industrial development (López et al., 2022). Cities such as Quito and Cuenca have stood out for their investment in resources dedicated to monitoring atmospheric pollutants, including settleable particulate matter, which has allowed for the identification of concentrations of up to $2.86\ \mathrm{mg/cm^2}$ over 30 days in the city of Quito, according to the 2013 environmental quality report (Municipio del Distrito Metropolitano de Quito, 2015). On the other hand, in the city of Cuenca, lower concentrations of settleable particulate matter have been recorded, ranging from 0.28 to $0.35\ \mathrm{mg/cm^2}$ over 30 days (EMOV EP, 2021), reflecting the presence of variable concentrations of SPM, even in areas with more intensive monitoring.

Some studies have shown that factors such as wind-blown resuspension of urban dust and vehicular traffic are significant sources of settleable particulate matter, especially in areas with poor road infrastructure or slow-moving traffic, which, in combination with seasonal factors, contribute significantly to the distribution and concentration of SPM and its components in the air (Valencia et al., 2019; Villacis, 2023). Despite this, studies on air pollution in small rural areas are limited or nonexistent, highlighting the importance of research evaluating the composition and effects of settleable particles in these locations (Solórzano, 2023).

The Espíndola canton, in the province of Loja, presents a unique context as it is a border area with constant heavy transport traffic, compounded by the presence of extractive activities that could contribute to the emission of air pollutants affecting the health of the 1388 inhabitants residing in its urban area (INEC, 2001). For this reason, the main objective of this study is to evaluate the composition of settleable aerosols in the urban area of the Espíndola canton, with an emphasis on identifying the concentration of settleable particulate matter and assessing the presence of heavy metals in its composition.

2 Materials and Methods

2.1 Study Area

The study was conducted in the urban area of the Espíndola canton, in the Amaluza parish, where five representative areas were selected using stratified random sampling.

©2026, Universidad Politécnica Salesiana, Ecuador.

Table 1. Distribution of sampling areas

Sector	Point	Land Use	Description
Center	1	CM	Urban center with heavy vehicle traffic.
Terminal	2	EQ2	Characterized by a continuous flow of vehicles.
River	3	IND	Presence of auto repair shops, spas, and nearby aggregate mining.
Dolorosa	4	R1	Close to unpaved roads.
School	5	EQ1	High traffic volume associated with school hours.

Sampling points and distribution based on land use. Commercial (CM), Social Services Facilities (EQ1), Public Services Facilities (EQ2), Industrial (IND), Residential (R1).

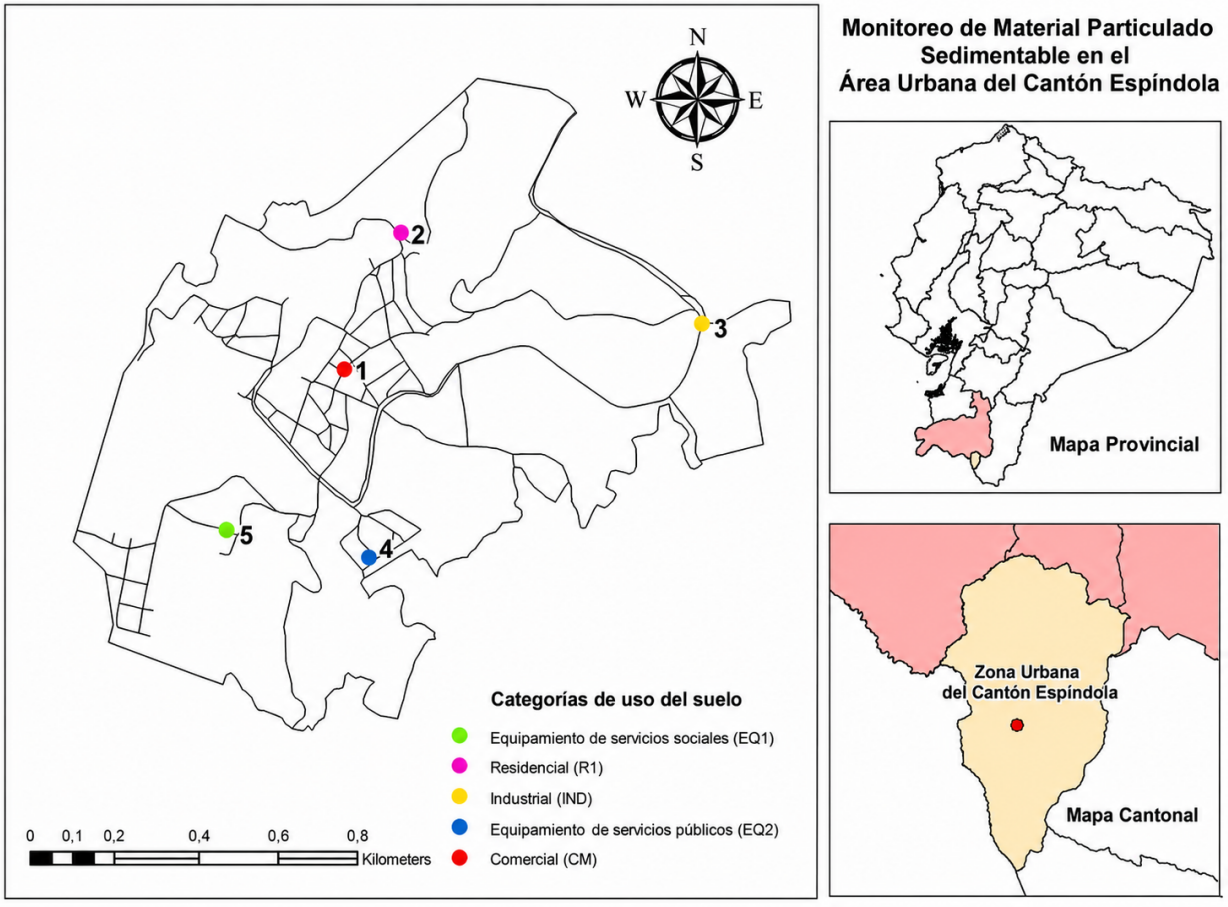


Figure 1. Map showing the location of sampling areas.

©2026, Universidad Politécnica Salesiana, Ecuador.

2.2 Meteorological information for the Espíndola canton

To complement the SPM sampling, available information on the prevailing meteorological conditions in the Espíndola canton during the sampling period was compiled. According to historical data from the National Institute of Meteorology and Hydrology (Instituto Nacional de Meteorología e Hidrología (INAMHI), 2024) and the Decentralized Autonomous Municipal Government of Espíndola (Gobierno Autónomo Descentralizado (GAD) Municipal de Espíndola, 2015), during this period (March–July), there is a marked transition between the rainy and dry seasons in the region. Therefore, variables such as precipitation, wind speed, and wind direction were collected and considered in the analysis of results, with the aim of relating them to the dynamics of settleable particulate matter.

2.3 Design and installation of samplers

The settleable particulate matter (SPM) collectors were designed in accordance with Method 502 of the *Methods of Air Sampling and Analysis* (Intersociety Committee, 1988) and in compliance with Ministerial Agreement 097-A. They are made of 15.24 cm diameter PVC pipe and a funnel of the same size, connected to a one-gallon plastic container. The top features an electro-welded mesh that filters out coarse contaminants, ensuring representative samples. The collectors were installed more than 2.5 meters above ground level.



Figure 2. Settleable Particulate Matter Collector.

2.4 Sample Collection

The sampling period lasted five consecutive months, covering two seasonal periods between March and July 2024. Samples were collected every 30 days in accordance with the guidelines established in Annex 4 of Ministerial Agreement 097-A. Once this period had elapsed, the samples were removed, after first washing them with distilled water to dislodge the particles adhering to both the walls of the collector tube and the funnel, directing them into the collection container. Finally, a new container was installed for collecting the following month's sample.

The samples taken to the laboratory were separated into soluble and insoluble fractions using the gravimetric method.

2.5 Gravimetric Analysis

To quantify settleable particulate matter (SPM), 47 mm quartz filters and porcelain capsules were used, dried at 105 °C in an oven to be weighed before and after filtration. The vacuum filtration equipment allowed for the efficient retention of particles on the filters. The SPM concentration was calculated in $\mathrm{mg/cm^2}$ over 30 days, using the difference in weight between the filters and capsules before and after the process, by applying the following formulas in Microsoft Excel:

©2026, Universidad Politécnica Salesiana, Ecuador.

The settling rate of insoluble particles was determined using the equation (1):

$$Cf = \frac{Pf - Pi}{AT} \quad (1)$$

Where: Cf is the concentration of insoluble particles; Pi is the initial weight of the filter before filtration; Pf is the final weight of the filter after filtration; A represents the cross-sectional area of the particle precipitation vessel, expressed in m^2; and T is the duration of the monitoring period (30 days).

The equation was used to calculate the settling rates of soluble particles (2):

$$Cs = \frac{(Mfs - Mis)}{AT}\frac{V1}{V2} \quad (2)$$

Where: Cs is the concentration of soluble particles; Mis is the initial weight of the capsule before filtration; Mfs is the final weight of the capsule after filtration; A is the cross-sectional area of the particle precipitation vessel in m^2; T denotes the duration of the monitoring period (30 days); $V1$ corresponds to the volume of all the filtered liquid expressed in litres; and $V2$ is equivalent to the volume of all the extracted liquid converted to litres.

Finally, the total particle fallout rate was calculated using the equation (3):

$$Ct = Cu + Cs \quad (3)$$

Where: Ct represents the total particle deposition rate expressed in g/m^2 per month; Cu is the deposition rate of insoluble particles in g/m^2 per month; and Cs is the deposition rate of soluble particles, also expressed in g/m^2 per month.

2.6 Comparison with established limits for SPM

To determine whether particulate matter concentrations exceed the recommended limits, the values stipulated in Annex 4 of Ministerial Agreement 097-A were used as a reference, as detailed in Table 2.

Table 2. Maximum permissible limit for SPM

Ecuadorian Environmental Legislation TULSMA AM - 097 Annex 4
1 mg/cm^2 for 30 days

The reference value corresponds to a concentration accumulated over 30 days.

2.7 Acid digestion and metal analysis

To assess heavy metals in settleable particulate matter (SPM), microwave-assisted acid digestion was performed. The samples were incinerated at 500 °C for three hours to remove organic matter, then treated with 9 ml of nitric acid (HNO3) and 3 ml of hydrofluoric acid (HF). The mixture was digested in a microwave following US EPA Method 3052, cooled, filtered, and diluted to 25 ml with distilled water.

Heavy metal concentrations were determined by atomic absorption spectroscopy (AA), using certified standards to ensure the accuracy of the analysis. Four metals were selected: copper (Cu), lead (Pb), cadmium (Cd), and chromium (Cr), due to their high toxicity and common presence in anthropogenic sources associated with transportation and extractive activities (Morales Tates et al., 2024; Dall'Osto et al., 2014). Furthermore, this selection was based on the availability of supplies and reagents and on the main objective of the study, which aimed to identify the presence or absence of heavy metals in settleable particulate matter.

3 Results and Discussion

The climatic conditions recorded in the Espíndola Canton are described in Table 3. During the five months of monitoring, the canton underwent a seasonal transition characteristic of Ecuador's southern Andean region, shifting from a rainy season to a dry season, as reflected in the decrease in precipitation and the increase in wind speed beginning in May.

©2026, Universidad Politécnica Salesiana, Ecuador.

Table 3. Climatic conditions in the Espíndola Canton

Month	Average Precipitation (mm)	Average Wind Speed (km/h)	Predominant Direction
March	160–200	8–12	East — Northeast
April	130–170	9–14	East — Northeast
May	60–90	11–16	East — Northeast
June	25–45	14–20	East — Northeast
July	10–25	15–22	East — Northeast

Precipitation intervals, wind speed and prevailing wind direction.

Table 4. Chemical characterization of SPM

Land Use	Point	Month	SPM (mg/cm^2 × 30 days)	Cd (μg/L)	Cu (μg/L)	Pb (μg/L)	Cr (μg/L)
CM	1	March	0.17	51.4	262.3	696.5	5.7
EQ1	2		0.22	217.4	282.1	1 042.2	21
IND	3		0.43	49.3	310.7	919.9	100.5
R1	4		0.28	41.2	234.1	872	7
EQ2	5		0.3	28.3	150.4	563.5	0
EQ1	2	April	0.39	31.4	157.2	662.5	69
IND	3		0.42	28.8	180.1	777.2	0
R1	4		0.22	25.1	131.8	580	0
EQ2	5		0.28	684	176.3	910.2	95.1
CM	1	May	0.3	46.3	320	908.7	8.3
EQ1	2		0.31	67.1	277.6	837.6	89
IND	3		0.35	81.7	257.6	836.3	87.1
R1	4		0.27	108	213.7	758.3	72.5
EQ2	5		0.38	130.9	353.6	1 235.2	163.1
CM	1	June	0.25	38	242.6	769.9	0
EQ1	2		0.27	39.2	192.9	771.3	76.9
IND	3		0.51	43.8	350.3	910.5	95.5
R1	4		0.33	41.3	365.1	1 075.2	38
EQ2	5		0.25	19	130.5	538.6	0.3
CM	1	July	0.21	20.1	116	538.5	0
EQ1	2		0.3	17.7	112.8	536.8	0
IND	3		0.33	9.2	111.8	537.3	0
R1	4		0.27	19	216.6	703	68
EQ2	5		0.23	19.3	109.6	509.8	29

SPM is expressed in mg/cm^2 over 30 days, and Cd, Cu, Pb and Cr in μg/L. No SPM concentrations exceeding the regulatory limit of 1 mg/cm^2 over 30 days were recorded.

©2026, Universidad Politécnica Salesiana, Ecuador.

The concentrations of settleable particulate matter (SPM) and heavy metals (Cd, Cu, Pb, Cr) obtained during five months of continuous monitoring across different land uses are presented in Table 4. Although SPM concentrations remained within the maximum permissible limits set by Ecuadorian environmental regulations, the analysis revealed the presence of heavy metals, with lead being the most abundant element. Although Ecuador phased out lead in gasoline in 1998 (Ministerio de Energía y Minas, 1998), its effects persist due to the historical accumulation of this metal in soils and sediments, which can be released back into the environment (Tong et al., 2016). In Latin America, the combination of agricultural sources, residues from leaded fuels, and deteriorated construction materials generates complex atmospheric profiles (Bergametti et al., 2020; Iglesias et al., 2012). This presence of heavy metals is consistent with reports in the literature, where they are associated with industrial processes, vehicle wear, and abrasion of their metal components (Huang et al., 2022).

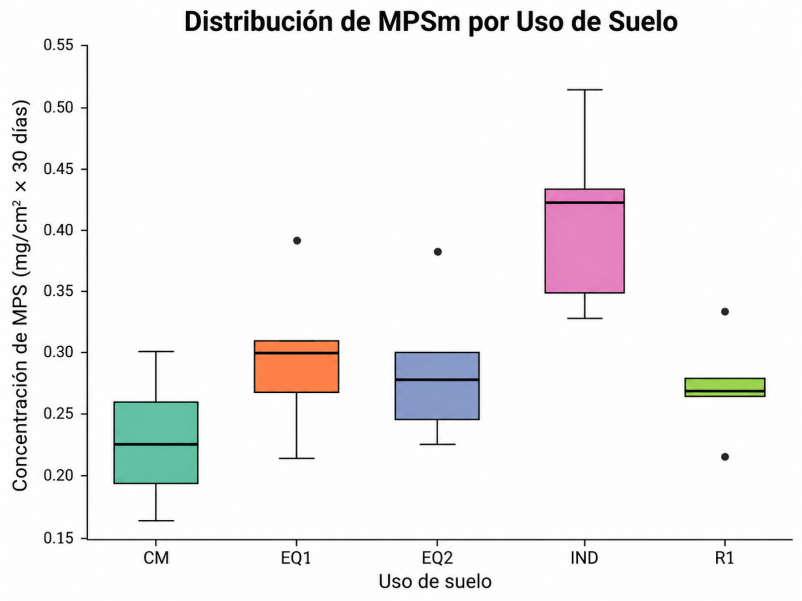


Figure 3. Box plot showing concentrations of settleable particulate matter by land use.

Figure 3 shows the concentrations of settleable particulate matter (SPM) at each sampling point, highlighting sampling point number 3 (IND), located in an industrial area, as the one with the highest concentrations, with an average of $0.41\ \mathrm{mg/cm^2}$ over 30 days and a maximum peak of $0.51\ \mathrm{mg/cm^2}$ over 30 days. These values could suggest the combined influence of stationary and mobile sources in the industrial zone, such as aggregate extraction and heavy vehicle traffic, factors that contribute to the release and dispersion of particles in the area (Alloway, 2013; Muñoz P. et al., 2021). Similarly, in industrial areas, other sources may be involved, such as auto repair shops and local aggregate processing activities, which, although not always formally registered, can emit particles enriched with metals such as Cu and Cr. These sectors, by generating resuspended dust and wear on metallic materials, represent a significant source of atmospheric pollutants in unregulated urban and industrial environments (Huang et al., 2022; BaLich et al., 2024). On the other hand, point 1 (CM), associated with commercial land use, had the lowest concentrations, with an average of $0.23\ \mathrm{mg/cm^2}$ over 30 days.

Figure 4 shows the SPM concentrations over the five-month monitoring period, revealing relative stability in the monthly averages, which range from 0.27 to $0.33\ \mathrm{mg/cm^2}$ over 30 days. Although this period experimented a climatic transition marked by a gradual decrease in rainfall and an increase in wind speed from May onward (Table 3), no signifi-

©2026, Universidad Politécnica Salesiana, Ecuador.

cant differences were observed in average SPM concentrations between months, indicating that meteorological conditions alone do not fully explain the variability of settleable particulate matter. The decrease in precipitation could reduce the atmospheric washing of particles, while the increase in wind speed favors the resuspension of previously deposited particles, facilitating particle transport—an effect that can be amplified on unpaved surfaces, dry agricultural areas, and industrial areas with low vegetation cover (Zhao et al., 2018).

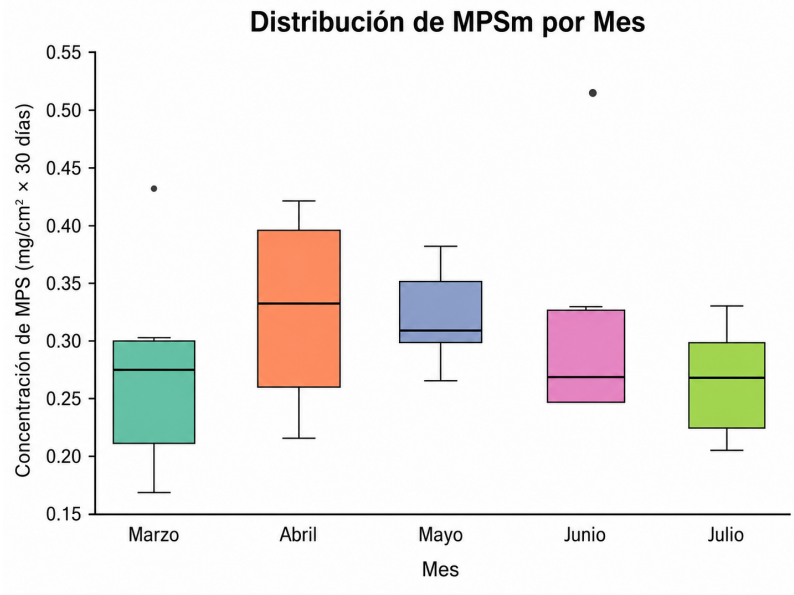


Figure 4. Box plot showing concentrations of settleable particulate matter by month.

Furthermore, when analyzing the dispersion of the data, it can be observed that concentration ranges tend to be narrower in the driest months, which could be due to factors such as land use type, traffic intensity, and local activities that exert a greater influence on SPM concentrations. This can be observed during the month of June, when the highest concentration of the study ($0.51\,\mathrm{mg/cm^2}$ over 30 days) was recorded in the industrial use zone (IND).

Figure 5 shows the results of the nonparametric Kruskal-Wallis test, revealing significant differences in SPM concentrations according to land use ($p = 0.020$), suggesting that levels of settleable particulate matter vary depending on the activities and environmental characteristics specific to each zone.

Similarly, the Kruskal-Wallis test applied to monthly concentrations (Figure 6) shows statistically significant differences for Cd, Cu, and Pb ($p = 0.006$, 0.015 and 0.038, respectively). These monthly fluctuations could be attributed to factors such as the topography of Espíndola and atmospheric transport dynamics, which could facilitate the transport of pollutants from other areas depending on weather conditions, as well as the seasonality of agricultural activities.

©2026, Universidad Politécnica Salesiana, Ecuador.

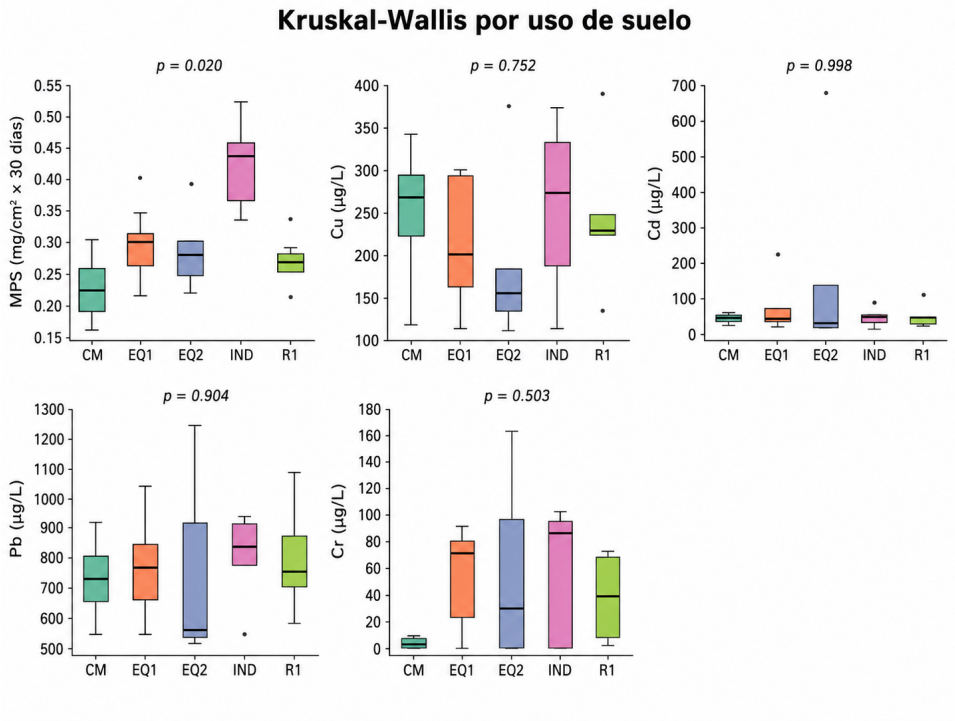


Figure 5. Kruskal-Wallis test for differences in means between SPM and metal concentrations by land use.

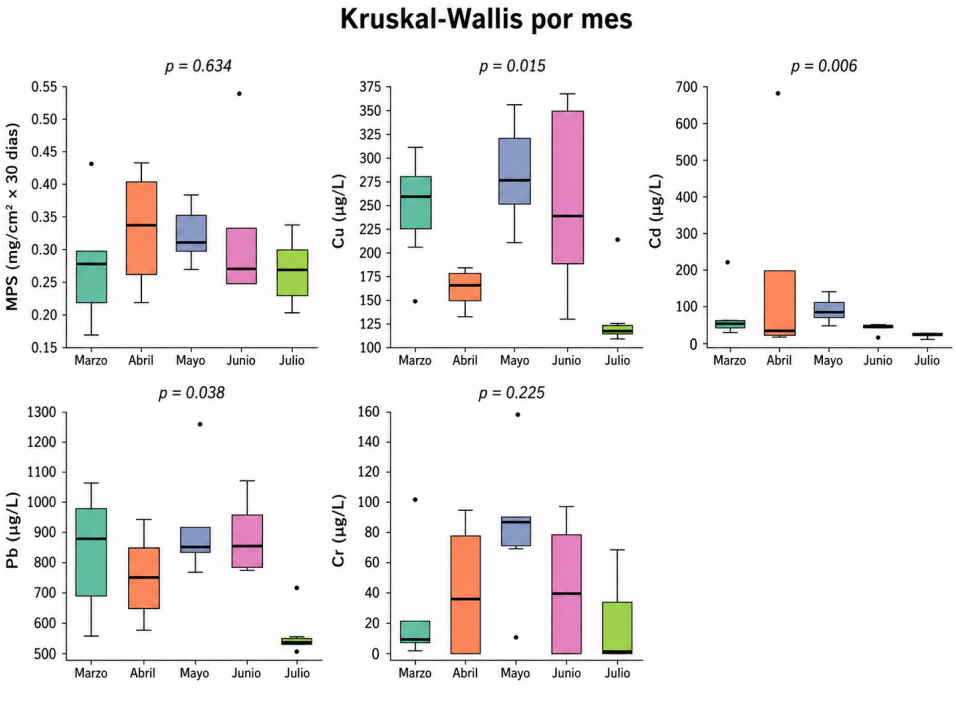


Figure 6. Kruskal-Wallis test for differences in means between monthly SPM concentrations.

©2026, Universidad Politécnica Salesiana, Ecuador.

Spearman's correlation analysis, the results of which are summarized in Figure 7, revealed a significant positive correlation between Pb and SPM ($r = 0.421$, $p = 0.040$), as well as between Cr and SPM ($r = 0.435$, $p = 0.033$), suggesting that these metals tend to accumulate or be transported together with settleable particulate matter, possibly due to their affinity for solid particles present in the air and soil (Guo et al., 2021; Zhao et al., 2018). In addition, significant correlations were observed between the metals Cd, Cu, Pb, and Cr, with a particularly strong relationship between Pb and Cu ($r = 0.893$, $p = 0.000$), pointing to the possibility of a geochemical interaction or a common emission source caused by vehicular traffic, tire abrasion, brakes, and fuels, as well as resuspended dust in unpaved urban areas (BaLich et al., 2024; Cesari et al., 2012; Huang et al., 2022).

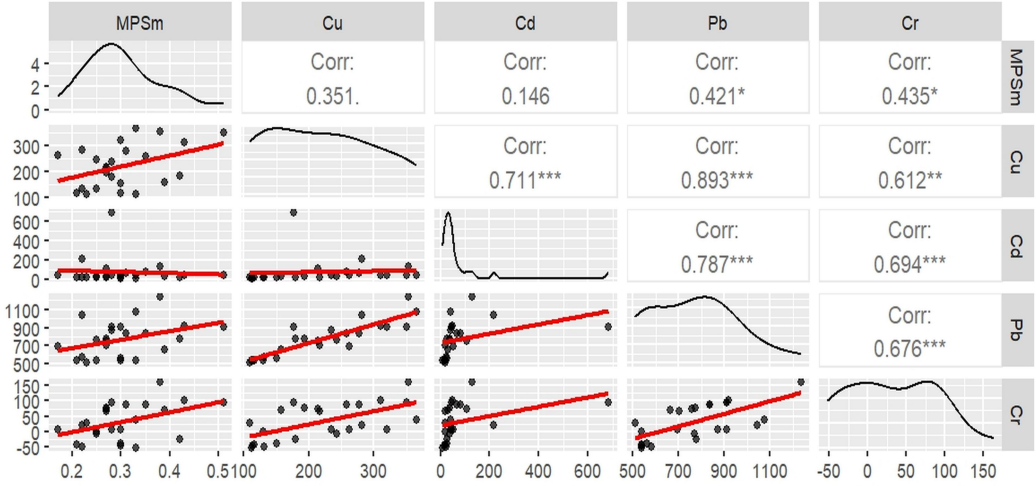


Figure 7. Spearman's correlation matrix between settleable particulate matter and the metals analysed.

These correlations among metals could be influenced by agro-environmental conditions and soil management in Espíndola. Specifically, the application of phosphate fertilizers and pesticides on crops such as coffee and sugarcane—common practices in the region—could explain the presence of Cd, as noted by Alloway (2013), who identifies these agricultural inputs as a significant source of this metal in the soil. Additionally, the persistence of Pb and Cu in organic and mineral particles, as has been documented in areas impacted by agricultural activities (Zhang et al., 2020; Wang et al., 2022), could contribute to the strong correlation observed between these two metals.

The observed correlation between heavy metals such as cadmium (Cd), chromium (Cr), lead (Pb), and copper (Cu) in settleable particulate matter is more influenced by monthly factors than by land use in the studied area. These metals can adhere to solid particles present in the air and soil, such as minerals (silicates and iron oxides) and organic matter, which act as vectors for their transport and accumulation in different areas (Saeedi et al., 2015). This behavior is due to the interaction of the metals with the surfaces of these particles, where they become trapped and protected from leaching processes, especially under windy conditions or mechanical disturbances caused by human activities (Guo et al., 2021; Zhao et al., 2018).

Pb and Cu tend to accumulate in areas impacted by agricultural activities, as their persistence in organic and mineral particles facilitates their accumulation in soils and sediments (Valdivieso et al., 2024). These associations are closely linked to the use of fertilizers and pesticides containing metal compounds, which intensify their presence in the environment (Villacis, 2023). In contrast, the mobility of metals such as Cr and Cd is higher in acidic environments, which is common in agricultural soils disturbed using fertilizers, pesticides, and tillage activities. According to Abad (2014), these compounds, when solubilized, can adhere to fi-

©2026, Universidad Politécnica Salesiana, Ecuador.

ne particles and facilitate their airborne transport, especially under dry and windy conditions. This can be observed particularly during dry seasons, when reduced soil moisture and increased wind activity favor the dispersion of contaminated particles (Zhang et al., 2020; Wang et al., 2022).

This correlation pattern reflects the intrinsic properties of metals, such as their affinity for mineral and organic particles, as well as the possible influence of the specific climatic conditions of the study area (Zegarra et al., 2020). Seasonal variations, especially during dry periods, could intensify the mobility of metal-laden particles (Lara, 2022). Wind action during these seasons promotes the resuspension and transport of settleable particulate matter over long distances, redistributing metals in the environment (G. Santillán et al., 2025). This highlights how potential local climatic dynamics may contribute to the dispersion and accumulation of Cd, Cr, Pb, and Cu, resulting in concentration patterns marked by monthly variations (Wang et al., 2022; Zhang et al., 2020).

4 Conclusions

Specific increases were detected during certain periods, associated with possible local and seasonal factors. Furthermore, chemical characterization revealed the presence of heavy metals such as Cd, Cr, Pb, and Cu in the samples, even in areas with low total SPM concentrations. These findings highlight that, although SPM complies with established standards, its chemical composition may pose risks to the environment and human health.

Statistical correlations suggest that factors such as wind intensity, terrain topography, proximity to specific emission sources, and the mobilization of particles by human activities play a crucial role in the dispersion and accumulation of these elements. It was observed that local climatic dynamics, such as dry periods and particle resuspension, increase the presence of metals in the air.

Overall, the results indicate that the dynamics of settleable particulate matter in Espíndola are primarily determined by specific local conditions and the nature of emission sources, while climatic influence, although present, does not appear to be the predominant factor in the variability of SPM concentrations; however, an influence of climatic variation on metals (Cd, Pb, Cu) was found over the course of the months.

Acknowledgments

We thank Universidad Técnica Particular de Loja for the support and funding provided for conducting this research. Their support was key to carrying out the study and analyzing the data.

Declaration on the use of artificial intelligence

The authors DECLARE that, during the preparation of the article entitled "Evaluation of the Composition of Settleable Aerosols in the Urban Area of Espíndola Canton, Loja Province, Ecuador", generative artificial intelligence tools were used exclusively to assist with the translation and improvement of the wording of specific sections of the manuscript. These tools were not used for data analysis, interpretation, the generation of results, the drawing of conclusions, or to replace the authors' academic and scientific judgement.

The authors assume full responsibility for the content, originality, integrity, and final version of the article.

Author's contributions

M.A.A.C.: Conceptualisation, data analysis, sampling. **B.G.V.E.:** Statistics, sampling. **D.E.P.M.:** Experimental design, data analysis.

References

Abad, M. (2014). *Fitotoxicidad del material particulado sedimentable (MPS) generado en la zona urbana del cantón Cuenca.* Online: https://short-url.cc/1yHlV (Disponible en línea)

Alloway, B. J. (2013). *Heavy metals in soils: Trace metals and metalloids in soils and their bioavailability*. Springer. Online: https://short-url.cc/1taxP

©2026, Universidad Politécnica Salesiana, Ecuador.

BaLich, P., Anh Duc, T., Huy Thong, V., and Van Linh, N. (2024). Geochemical speciation, pollution assessment, and source identification of heavy metals in sediment cores of the Cau River basin, Hai Duong province, Vietnam. *RSC Sustainability*. Online: https://short-url.cc/1taxY

Bergametti, G., Formenti, P., Desboeufs, K., and Triquet, S. (2020). Trace elements in atmospheric aerosols: Sources and implications. *Elements*, 339–344.

Cesari, D., Contini, D., Genga, A., Siciliano, M., Elefante, C., Baglivi, F., and Daniele, L. (2012). Analysis of raw soils and their re-suspended PM10 fractions: Characterisation of source profiles and enrichment factors. *Applied Geochemistry*, *27*(6), 1238–1246. Online: https://doi.org/10.1016/j.apgeochem.2012.01.006

Dall'Osto, M., Beddows, D. C. S., Gietl, J. K., Olatunbosun, O. A., Yang, X., and Harrison, R. M. (2014). Characteristics of tyre dust in polluted air: Studies by single particle mass spectrometry (ATOFMS). *Atmospheric Environment*, *94*, 224–230. Online: https://doi.org/10.1016/j.atmosenv.2014.05.033

EMOV EP. (2021). *Informe de calidad del aire Cuenca 2020-2021* (Inf. Téc.). Cuenca, Ecuador: Empresa Pública de Movilidad, Tránsito y Transporte de Cuenca. Online: https://short-url.cc/1yHmj

Gobierno Autónomo Descentralizado (GAD) Municipal de Espíndola. (2015). *Plan de Desarrollo y Ordenamiento Territorial de Espíndola 2014-2019* (Inf. Téc.). Espíndola, Loja, Ecuador: GAD Municipal de Espíndola. Online: https://short-url.cc/1yHmn

Guo, J., Li, X., Wang, Y., and Zhao, L. (2021). Adsorption of heavy metals onto soil minerals: A review of recent advances. *Journal of Hazardous Materials*.

Huang, L., Zhang, X., Meng, Y., Yu, Y., and Qi, M. (2022). Sources and formation mechanisms of heavy metals in road dust: A review. *Environmental Pollution*, *303*.

Iglesias, V., Carreras, H., Pongrac, C., Alvarez, L., and Mateos, A. (2012). Atmospheric lead deposition in the Argentine Pampas: Historical trends from c. 1995–2006 in a fast-developing agricultural region. *Environmental Pollution*, 140–147.

INEC. (2001). *Instituto Nacional de Estadística y Censos.* Online: https://goo.gl/iczP53

Instituto Nacional de Meteorología e Hidrología (INAMHI). (2024). *Datos históricos meteorológicos.* Quito, Ecuador. Online: https://geoservicios.inamhi.gob.ec/#/

Intersociety Committee. (1988). *Methods of air sampling and analysis*. Lewis Publishers. Online: https://short-url.cc/1yHmu

Lara, R. (2022). *Material particulado en suspensión y depósitos en la zona oeste de la aglomeración de Gijón* (Tesis Doctoral, Universidad de Oviedo). Online: https://short-url.cc/1yHmz

López, J., Correa, J., Cano, Y., and Bermúdez, J. (2022). Evaluación de los gases de combustión y material particulado en el aire de parqueaderos del distrito metropolitano de Quito, Ecuador. *Revista Científica ECOCIENCIA*, *19*.

Mejía, D., Zegarra, R., Astudillo, A., and Moscoso, D. (2018). Análisis de partículas sedimentables y niveles de presión sonora en el área urbana y periférica de Cuenca. *Revista de la Facultad de Ciencias Químicas*, *19*.

Ministerio de Energía y Minas. (1998). *Acuerdo Ministerial No. 112: Autorización para la producción y comercialización a nivel nacional de gasolinas extra y súper sin plomo.* Registro Oficial No. 308 del 30 de abril de 1998. Quito, Ecuador.

Morales Tates, J., Morocho, L., Garzón, L., and Cepeda, M. (2024). Evaluación de la concentración de material particulado sedimentable en Fertisa Sur de Guayaquil. *Polo del Conocimiento*, *9*(3), 9–24. Online: https://doi.org/10.23887/pc.v9i3.6697

Morocho, D. (2024). Fuentes de contaminación atmosférica en zonas rurales. *Ciencia y Desarrollo Ambiental*, 27–39.

Municipio del Distrito Metropolitano de Quito. (2015). *Informe de calidad del aire Quito* (Inf. Téc.). Quito, Ecuador: Dirección Metropolitana de Ambiente. Online: https://short-url.cc/1yHmE

Muñoz P., S., Salcedo R., J., and Sotomayor M., A. (2021). *Contaminación ambiental producida por el tránsito vehicular y sus efectos en la salud humana: revisión de literatura.* Online: https://goo.gl/abcd12

©2026, Universidad Politécnica Salesiana, Ecuador.

OPS. (2018). *Organización Panamericana de la Salud.* Online: https://short-url.cc/1yHmH

Pérez Cárdenas, A. (2017). Contaminación atmosférica: Una amenaza global. *Revista Internacional de Ciencias Ambientales*, 25–38.

Reyes, P., Morales, H., and Gómez, F. (2016). Impacto de los metales pesados en el ambiente y la salud humana. *Ciencia y Salud Ambiental*, 18–34.

Saeedi, M., Daneshvar, S., and Karbassi, A. (2015). Role of riverine sediment and particulate matter in adsorption of heavy metals. *International Journal of Environmental Science & Technology*. Online: https://www.bioline.org.br/pdf?st04017

Santillán, G., Rodríguez, M., Orozco, J., Paredes, M., Maldonado, C., and Rivadeneira, J. (2025). Determinación de la concentración de material particulado sedimentable en el barrio Juan Montalvo en el Cantón Riobamba. *TESLA Revista Científica*, *18*.

Santillán, P., Rodríguez, M., Orozco, J., Ríos, I., and Bayas, K. (2021). Evaluación de la concentración y distribución espacial de material particulado en los campus de la UNACH - Riobamba. *Scielo*. Online: https://short-url.cc/1yHmL (1 de diciembre)

Solórzano, P. (2023). *Monitoreo de material particulado sedimentable en la parroquia Coronel Marcelino Maridueña, provincia del Guayas durante el período 2023.* Online: https://short-url.cc/1yHmR

Suárez, L., and Vásquez, M. (2017). Composición y riesgos del material particulado. *Journal of Environmental Studies*, *10*(2), 56–67.

Tong, Y., Liu, X., and Zhang, Z. (2016). Status and phases of lead in typical garden soils from Beijing urban area. *Environmental Science and Pollution Research*.

Valdivieso, J., Coral, K., and Esteban, J. (2024). Determinación de la concentración de metales pesados mediante la caracterización de material particulado sedimentable en la reserva biológica Limoncocha, Ecuador. *Atena Editora*. Online: https://short-url.cc/1tayK (1 de abril)

Valencia, P., Sánchez, F., Tigua, M., and Mena, S. (2019). Cálculo referencial de material particulado en el aire como factor de contaminación en Pujilí. *Revista Científica Cienciamerica*, *8*(2), 15–24.

Villacis, O. (2023). *Plomo en material particulado sedimentable aledañas en terminales de transporte masivo, Guayaquil-Ecuador.* Online: https://short-url.cc/1tayN (Agosto)

Wang, F., Qiao, H., and Zhao, J. (2022). The influence of climatic variability on the resuspension and transport of sediment-bound heavy metals. *Environmental Research*.

Zegarra, R., Andrade, S., Parra, M., Mejía, D., and Rodas, C. (2020). Análisis espacial de PM10 en el aire y su composición de metales con relación a factores ambientales alrededor de centros de educación preescolar en Cuenca. *Maskana*. Online: https://short-url.cc/1yHn4 (29 de abril)

Zhang, Z., Chen, Y., and Xiao, H. (2020). High-efficiency solar evaporator prepared by one-step carbon nanotubes loading on cotton fabric toward water purification. *Science of the Total Environment*. Online: https://short-url.cc/1yHn9

Zhao, Y., Shao, M., and Zhang, Z. (2018). Heavy metals in agricultural soils from a typical mining region in China: Spatial distribution, risk assessment, and sources. *Ecotoxicology and Environmental Safety*.

©2026, Universidad Politécnica Salesiana, Ecuador.

Guidelines for Authors

This manual describes the steps that must be taken into account to successfully submit your manuscript. Please take the necessary time to read this document carefully.

1 General Information

"La Revista de Ciencias de la Vida, La Granja" is a bilingual scientific journal of the Universidad Politécnica Salesiana of Ecuador. It has been published continuously since January 2002, with a fixed semiannual periodicity, and specializes in Life Sciences, Environmental Sciences, and their transdisciplinary areas, such as Earth Sciences, Biotechnology, Agricultural Sciences, and Sustainable Local Development, among others.

It is a peer-reviewed scientific journal that uses an external expert evaluation system (*peer review*) under a blind peer-review methodology (*double-blind review*), in accordance with Harvard citation style standards. Compliance with this system ensures authors an objective, impartial, and transparent review process, thereby facilitating the journal's inclusion in international databases, repositories, and indexing systems of reference.

"La Revista de Ciencias de la Vida, La Granja" is indexed in SCOPUS, in the Emerging Sources Citation Index ESCI of Web of Science, in the directory and selective catalogue of the Regional Online Information System for Scientific Journals from Latin America, the Caribbean, Spain, and Portugal (Latindex), in the REDALYC Scientific Information System, in the Directory of Open Access Journals DOAJ, in the Integrated Classification System of Scientific Journals CIRC, in BaseSearch, the Academic Search Engine of *Bielefeld*, and in more than 42 repositories, libraries, and specialized catalogues in Ibero-America.

The journal is published in two versions: print (ISSN: 1390-3799) and electronic (e-ISSN: 1390-8596), in Spanish and English. In addition, each published work is identified with a DOI (Digital Object Identifier System).

All articles are published under open access, allowing unrestricted access to their content without economic barriers during the submission, review, publication, and integrated translation stages of the manuscripts.

2 Scope and Policy

2.1 Subject Areas

Original contributions in the fields of Life Sciences, Environmental Sciences, and their transdisciplinary areas, such as Earth Sciences, Biotechnology, Agricultural Sciences, Sustainable Local Development, and all disciplines interdisciplinarily related to the journal's central thematic scope, are accepted.

2.2 Contributions

"La Revista de Ciencias de la Vida, La Granja" preferably publishes results of empirical, theoretical, or experimental research (*Scientific Articles*), written in Spanish and/or English. Select bibliographic reviews (*Reviews*) are also admissible.

All submissions must be original, must not have been published in any medium, and must not be under review or publication elsewhere.

Accordingly, the journal accepts the following types of contributions:

a. Scientific Research Articles (*Scientific Articles*):

5,000 to 6,500 words of text, including title, abstracts, introduction, materials and methods, results, conclusions, tables, figures, and references. References must be cited, current, and selective, comprising approximately 40 works.

b. Reviews (*Reviews*):

Suggested maximum length: 7,000 words of text,

©2026, Universidad Politécnica Salesiana, Ecuador.

including tables and references. Special consideration will be given to justified, current, and selective

«La Revista de Ciencias de la Vida, La Granja» tiene periodicidad semestral (20 artículos por año), publicada en los meses de marzo y septiembre.

2.3 Política económica abierta

«La Revista de Ciencias de la Vida, La Granja», es una revista abierta, donde todos los artículos son publicados para poder acceder a su contenido de manera abierta sin restricciones de contenido o económicas, tanto en el proceso de revisión como de publicación y traducción integra de los manuscritos. La revista es publicada por el Editorial Abya-Yala, en Quito, Ecuador.

2.4 Copyright

Las obras que se publican en «La Revista de Ciencias de la Vida, La Granja» están sujetas a los siguientes términos:

1. La Universidad Politécnica Salesiana (RUC: 0190151530001) conserva los derechos patrimoniales (copyright) de las obras publicadas, y favorece y permite la reutilización de las mismas bajo la licencia *Creative Commons* Reconocimiento-No-Comercial-Sin Obra Derivada 3.0 Ecuador, por lo cual se pueden copiar, usar, difundir, transmitir y exponer públicamente, siempre que:
    - Se cite la autoría y fuente original de su publicación (revista, editorial, URL y DOI de la obra).
    - No se usen para fines comerciales u onerosos.
    - Se mencione la existencia y especificaciones de esta licencia de uso.
2. La publicación otorgará a cada artículo un *Digital Object Identifier* (DOI). Ejemplo: Navarrete, Bernardo, Oswaldo Valarezo, Ernesto Cañarte y Ramón Solórzano. 2017. Efecto del nim (*Azadirachta indica Juss.*) sobre Bemisia tabaci Gennadius (*Hemiptera: Aleyrodidae*) y controladores biológicos en el cultivo

references, comprising approximately 50 works.

del melón *Cucumis melo* L. La Granja: Revista de Ciencias de la Vida. Vol. 25(1):33-4. https://doi.org/10.17163/ret.n12.2016.05

"La Revista de Ciencias de la Vida, La Granja" has a semiannual periodicity, with 20 articles published per year, in March and September.

2.3 Open Economic Policy

"La Revista de Ciencias de la Vida, La Granja" is an open-access journal in which all articles are published to provide open access to their content without content-related or economic restrictions, both during the review process and throughout publication and the full translation of manuscripts. The journal is published by Editorial Abya-Yala, in Quito, Ecuador.

2.4 Copyright

The works published in "La Revista de Ciencias de la Vida, La Granja" are subject to the following terms:

1. Universidad Politécnica Salesiana (RUC: 0190151530001) retains the patrimonial rights (copyright) of the published works and promotes and permits their reuse under the *Creative Commons* Attribution-NonCommercial-NoDerivatives 3.0 Ecuador license. Therefore, the works may be copied, used, disseminated, transmitted, and publicly displayed, provided that:
    - The authorship and original source of publication are cited, including the journal, publisher, URL, and DOI of the work.
    - They are not used for commercial or profit-making purposes.
    - The existence and specifications of this license of use are mentioned.
2. Each article will be assigned a *Digital Object Identifier* (DOI). Example: Navarrete, Bernardo, Oswaldo Valarezo, Ernesto Cañarte and Ramón Solórzano. 2017. Effect of

©2026, Universidad Politécnica Salesiana, Ecuador.

neem (*Azadirachta indica Juss.*) on *Bemisia tabaci* Gennadius (*Hemiptera: Aleyrodidae*) and biological controllers in melon cultivation *Cucumis melo* L. La Granja: Revista de Ciencias de la Vida. Vol. 25(1):33-4. https://doi.org/10.17163/ret.n12.2016.05

2.5 Use of Artificial Intelligence (AI)

La Revista de Ciencias de la Vida, La Granja allows the use of artificial intelligence tools only as support for writing, language editing, statistical analysis, or data processing, provided that such tools do not replace the academic judgment or intellectual authorship of the researchers.

The use of AI must be explicitly declared and/or included in the Methodology section if it forms part of the scientific methodology of the results presented. The tool used and the purpose of its application must be indicated. At all times, the use of AI must remain under human supervision, and full responsibility for the content, accuracy, and originality of the manuscript rests exclusively with the authors. AI systems may not be credited as authors, nor may they be used to generate false, manipulated, or scientifically unverified results.

3 Manuscript Presentation, Structure, and Submission

All authors must register their credits, institutional affiliations, country, and ORCID identifier in the OJS platform; however, only one of them shall be designated as the corresponding author. No author may submit or have two manuscripts under review simultaneously, with a required waiting period of one consecutive issue, equivalent to one year.

When submitting the article, authors should not attempt to design the manuscript, justify the document, center titles, or use a two-column format. The only required formatting is that the Latin names of organisms must be written in italics.

Manuscripts must be submitted in Arial font, size 10, double-spaced, except for table and figure titles, fully justified, and without tabs or blank spaces between paragraphs. All lines must be automatically numbered: Word >Layout >Line Numbers >Continuous. Only the main sections should be separated by a blank space: title, authors, abstract, introduction, materials and methods, results, conclusions, and references.

The page must have 2-centimeter margins on all sides. Authors should download the "anonymized manuscript" template. Manuscripts must be submitted as Microsoft Word documents (.doc or .docx) or LaTeX files (.tex), including references in .bib format. The file must be anonymized in File Properties so that author identification does not appear.

Manuscripts must be submitted exclusively through the OJS (Open Journal System), where all authors must previously register. Original manuscripts sent by email or through any other interface will not be accepted.

To improve the visibility and impact of publications, all authors must have an ORCID number <https://orcid.org/>, and it is suggested that at least one of the authors have a ResearchGate account <https://www.researchgate.net/home>.

3.1 Manuscript Structure

For scientific research articles, manuscripts must follow the IMRDC structure: Introduction, Materials and Methods, Results, Discussion, and Conclusions. Any annexes must be submitted as a separate Word or LaTeX document and will be classified as supplementary material. Authors should download the "anonymized manuscript" template.

For review articles, the structure may be more flexible, especially in the Materials and Methods, Results, and Discussion sections. In all types of manuscripts, References are mandatory and, whenever possible, should include an electronic reference link. In any case, manuscripts must include the following sections:

a. Title Spanish / *Title* English:

The title must be concise but informative, with the Spanish title on the first line and the English title on the second. A maximum of 25 words, including spaces, is accepted. The title is not solely the responsibility of the authors, and changes may be

©2026, Universidad Politécnica Salesiana, Ecuador.

proposed by the Editorial Board.

It must be written using uppercase and lowercase letters and centered. If it contains scientific names of taxa, these must be italicized, without including the taxon author.

b. Names and affiliation of the authors:

The first name(s) and surname(s) of each author must be listed in order of authorship. The names must be followed by institutional affiliation, address, city, country, email address of each author, and ORCID number. In addition, the corresponding author must be identified with an asterisk (*). This information must be included only in the file model entitled "cover presentation" or "presentation-portada".

c. Abstract Spanish / *Abstract* English:

The abstract must have a maximum length of 250 words, first in Spanish and then in English. It must concisely describe, either explicitly or implicitly and in the following order: rationale of the topic, objectives, methodology and sample, main results, and main conclusions. It must be written impersonally, for example: "The present study analyzes...". In the case of the English abstract, do not use automatic translators; take proper care when translating the abstract, as it is the first impression the reviewer will have.

d. Keywords Spanish / *Keywords* English:

Four to six descriptors must be provided for each language version, directly related to the topic of the manuscript. Try not to repeat the same words used in the title. Keywords must be included in both Spanish and English.

e. Introduction:

The use of the SPPR system is suggested: Situation, Problem, Question, and Response. Thus, the updated state of the art of the study, the problem statement, the context of the problem, the justification, foundations, and purpose of the study must be clearly presented, using the most significant and current literature on the topic.

f. Materials and Methods:

This section must be written in such a way that the reader can easily understand the development of the research. It must chronologically describe the methodology, sample, sampling method, and the type of statistical analysis used. The replicability of the experiment must be ensured at all times by explaining the experimental design, laboratory equipment used, computer programs, among others. For every methodology used, the reasons for its use must be stated, and its possible limitations must be described.

g. Results and Discussion:

The most important observations should be highlighted. This section must include the quantitative or qualitative information supporting the final conclusions. The information must appear in a logical sequence in the text and in essential tables, figures, and equations, avoiding data duplication. Every table, figure, or equation must be cited in the text and numbered sequentially.

In the case of equations, authors should use the Word equation editor or LaTeX programming, numbering equations consecutively with a number in parentheses, for example (1). For better understanding, see the "anonymized manuscript" document.

Photographs, illustrations, and graphs must be presented only as figures; these, like tables, must include an explanatory description for each one. See the anonymized manuscript.

In the text, every table and figure must be named, analyzed, and discussed, highlighting the most representative findings and/or limitations of the study. Cite them in the text as Figure 6 or Table 1, for example. Do not abbreviate the words figure or table.

Figures may be line drawings, maps, or halftone photographs in black and white or color, with a resolution of 300 dpi; that is, the figure size must be large and appropriate for publication-quality format. Each figure must be attached upon submission in TIFF, PNG, or JPG format and numbered according to its order of appearance. Authors must ensure that figure captions and axes are perfectly

©2026, Universidad Politécnica Salesiana, Ecuador.

j. References:

Bibliographic citations must be presented as references to the text. Under no circumstances should references not cited in the text be included, nor should citations be included only in the text without their corresponding reference. The number of references must be sufficient to contextualize the theoretical framework using criteria of currency and relevance.

References must be presented alphabetically by the first author's surname, following the Harvard style, as described below and/or as generated by the citation manager of the word processor used.

3.2 Reference Guidelines

3.2.1 In-text Citation

Harvard is a citation style that allows the use of both surnames of the author, often separated by a hyphen, if they are provided. Otherwise, only one surname is used, as is customary in the Anglo-Saxon tradition.

One author: Samaniego (2012); (Samaniego, 2012); Valdés-Pérez (2016); (Valdés-Pérez, 2016); (Valdés Pérez, 2016); Valdés Pérez (2016).

Up to three authors: Samaniego, Vásquez and Torres (2010); (Samaniego, Vásquez and Torres, 2010).

More than three authors: Samaniego *et al*. (2010); (Samaniego *et al*., 2010).

3.2.2 References

a. Journal article always include the article DOI or, whenever possible, the electronic URL of the article:

Arnold, M. and Osorio, F. (1998) Introduction to the Basic Concepts of General Systems Theory. Revista Cinta de Moebio [online], (3). Universidad de Chile. Available at <https://goo.gl/FwjAqo>[accessed: 20 January 2005].

Dhillon, B. (2004) Should Doctors Wear Ties? Medical Monthly [online], 3 (1), 55-88. Available at <https://goo.gl/pHzUxJ>[accessed: 20 April 2006].

b. Complete books:

One author:
Holt, DH 1997, Management principles and practices, Prentice Hall, Sydney.

Two authors:
McCarthy, EJ, William, DP & Pascale, GQ 1997, Basic marketing, Irwin, Sydney.

Three or more authors:
Bond, WR, Smith, JT, Brown, KL & George, M 1996, Management of small firms, McGraw-Hill, Sydney.

c. Electronic sources:

Reed, S 2015, 'Shift to lower-carbon energy is too slow, report warns', New York Times, 9 November. Available from: https://goo.gl/iczP53. [10 November 2015].

It is mandatory that all citations with a DOI (Digital Object Identifier System) include it in the References section. DOIs may be obtained at https://goo.gl/gfruh1. All journals and books without a DOI must include their link, in the online version if available, shortened using Google Shortener: https://goo.gl.

Journal articles must be presented in English, except those written in their original language, in which case both versions must be provided using brackets.

All web addresses included in the manuscript must be shortened, except DOI links, which must follow the indicated format: https://doi.org/XXX.

3.3 Headings

The headings in the body of the article must be numbered using Arabic numerals. They must not be written entirely in uppercase, underlined, or bold. Numbering must have a maximum of three levels: 1. / 1.1. / 1.1.1.

©2026, Universidad Politécnica Salesiana, Ecuador.

A space must be inserted at the end of each numbered heading.

4 Submission Process

The following files must be submitted through the OJS system, after registering at the journal website <https://revistas.ups.edu.ec/index.php/granja/user/register>:

File No. 1: Cover Letter, Copyright Transfer, and Conflict of Interest Statement:
Download the "cover letter" template.

File No. 2: Cover Presentation:
This file, in Word or LaTeX format, must contain three clearly identifiable sections:

a) Title in Spanish and English, standardized names and surnames of the authors with ORCID number, affiliation, and academic degree.

b) Abstract, resumen, keywords, and palabras clave.

c) A declaration stating that the manuscript is an original contribution, has not been submitted to or is not under evaluation by another journal, confirmation of the listed authorship, acceptance, where applicable, of formal changes to the manuscript in accordance with the journal guidelines, and partial transfer of rights to the publisher. Authors should download the "cover presentation" template.

File No. 3: Fully anonymized manuscript, in accordance with the aforementioned guidelines.

File No. 4: The corresponding author must submit a list of five potential reviewers for the manuscript who meet the following criteria. Authors should download the "suggested reviewers" template:

- They must not be from the same country as the corresponding author. For example, if the corresponding author works in Brazil, the proposed reviewer must NOT be affiliated with institutions from the same country as the corresponding author, that is, "Brazil".

This file may be prepared using any Word or LaTeX word processor and must include the following information for each potential reviewer:

- First and last names
- Affiliation
- Academic degree
- Email address
- Corresponding ORCID code

Briefly indicate the relevance of each reviewer for the evaluation of the manuscript.

Failure to comply with any of the requirements of these guidelines
may result in the AUTOMATIC rejection of the manuscript.
Please take the necessary time to complete the submission process correctly.

©2026, Universidad Politécnica Salesiana, Ecuador.

LA GRANJA:
REVISTA DE CIENCIAS DE LA VIDA

SPECIAL ISSUE
Chirality across scales



"Geometries of Life"

This photograph seeks to capture the geometry that naturally emerges in living organisms. The butterflies' wings reveal patterns, lines, colors, and forms that appear to repeat and mirror one another, yet, upon closer observation, display subtle differences. Each individual also occupies a distinct position and orientation within the scene. The image thus invites us to contemplate life through its spatial organization: between symmetries and asymmetries, similarities and differences, order and variation. In the context of chirality, these butterflies become a visual metaphor for a fundamental characteristic of nature: geometry is not only about form, but also about orientation, relationship, and organization.
Autor: ©Jonathan González Chuqui (2026)

UNIVERSIDAD POLITÉCNICA SALESIANA DEL ECUADOR
Juan Cárdenas Tapia, sdb
Rector

©Universidad Politécnica Salesiana
Turuhuayco 3-69 y Calle Vieja, Cuenca, Ecuador
Telephone: (+593 7) 205 00 00 Fax: (+593 7) 408 89 58 Post office box 2074
e-mail: srector@ups.edu.ec
Web: www.ups.edu.ec

Fortalezas

La Granja, Revista de Ciencias de la Vida es la primera revista científica del Ecuador que aborda las temáticas de Ciencias Ambientales, de la Tierra y sus líneas transdisciplinares como Biotecnología, Ciencias Agropecuarias y Desarrollo Rural Sostenible, entre otras. Publicada por la Universidad Politécnica Salesiana en doble formato: impreso y on-line con periodicidad semestral, todos sus artículos se presentan en español e inglés. 24 años de edición y 320 artículos científicos publicados; editada por Abya-Yala con más de 48 años de experiencia en Ecuador.

La Granja tiene presencia en 96 bases de datos internacionales, plataformas de evaluación de revistas, directorios selectivos, portales especializados, catálogos hemerográficos, como: SCOPUS, ESCI, Emerging Sources Citation Index ESCI de la Web of Science, MIAR, EBSCO, LATINDEX, DOAJ, REDIB, DIALNET, REDALYC, BASE, entre otros.

Trabaja con un riguroso y transparente sistema peer review doble ciego de evaluación de manuscritos, sin costo, realizado por un consejo de revisión con 280 reconocidos investigadores de países de todo el mundo.

La administración de manuscritos se realiza a través del Sistema OJS 3, de la Fundación de Ciencia y Tecnología, con compromisos éticos publicados para la comunidad científica de transparencia y puntualidad; revisión de antiplagio realizada a través de Ithenticat y Similarity Check.

Alto nivel de visibilización con múltiples sistemas de búsqueda, DOI, ORCID, PDF dinámicos, xml jats, epub, con conexión a gestores documentales como Mendeley, RefWorks, EndNote y redes sociales científicas como Academia.edu y ResearchGate. Accesible digitalmente a texto completo, de forma gratuita, para toda la comunidad científica e investigadores de todo el mundo en apoyo a la política de Open Access y Early Access.

